Metal Additive Manufacturing Conference

Industrial perspectives in Additive Technologies

November 24-25, 2016
voestalpine Stahlwelt Linz, Austria

voestalpine
ONE STEP AHEAD.

www.mamc2016.org

organised by ASMET®
THE AUSTRIAN SOCIETY FOR METALLURGY AND MATERIALS

Metal Additive Manufacturing Conference

PROGRAMME

November 24-25, 2016
voestalpine Stahlwelt Linz, Austria

organised by ASMET®
THE AUSTRIAN SOCIETY FOR METALLURGY AND MATERIALS

CONFERENCE CHAIRMAN

Franz Rotter
Member of the Mangagement Board of voestalpine AG

SCIENTIFIC COMMITTEE

Bruno Buchmayr, Montanuniversität Leoben
Bruno Hribernik, ASMET
Wilhelm Meiners, Fraunhofer ILT
Jürgen Stampfl, TU Wien

ORGANISING COMMITTEE

Yvonne Dworak, ASMET
Ursula Müller, voestalpine Edelstahl GmbH
Armin Wiedenegger,
voestalpine Additive Manufacturing Center GmbH

INDUSTRIAL PERSPECTIVES IN ADDITIVE TECHNOLOGIES

ASMET, the Austrian Society for Metallurgy and Materials and voestalpine, invite decision-makers, engineers, developers, industry experts, scientists and students to the second **M**etal **A**dditive **M**anufacturing Conference with exclusive focus on the processing of metals.

TOPICS

- Powder for MAM
- Systems & Equipments for MAM
- Additive Design & Engineering
- Laser Melting,
  Electron Beam Melting & Direct Energy Deposition Processes
- AM Process- and Qualitiy Control
- Post- processing of AM parts
- Tools, Space and Aircraft, Automotive, Medical and others
- Recent Research Topics

Thursday, 24th November 2016

ROOM B	ROOM A	Time
	Registration	8:00
	Opening Rotter, voestalpine Edelstahl GmbH	09:30
	Keynote Poprawe, RWTH Aachen	09:45
	Blitz SMR Premium GmbH	10:25
	Wallner Böhler Edelstahl GmbH & Co KG	10:45
	Coffee Break	11:05
	Heino Uddeholms AB	11:30
	Giedenbacher University of Applied Sciences	11:50
	Junker Institute of Manufacturing Technology	12:10
	Panzl Montanuniversität Leoben	12:30
	Lunch	12:50
	Keynote, Niendorf, University of Kassel	14:10
	Bremen RWTH Aachen University -ILT	14:50
	Zielinski RWTH Aachen University -ILT	15:10
	Hollaus CADFEM GmbH	15:30
ROOM B	**Coffee Break**	15:50
Kitzmantel RHP-Technology GmbH	**Gradinger** LKR Ranshofen GmbH	16:20
Motzarzadeh University of Warwick	**Leung** University of Manchester	16:40
Stockinger Graz University of Technology	**Leitz** Plansee SE	17:00
Nutal CRM Group	**Pichler** Graz University of Technology	17:20
	Conference Dinner	18.30

Metal Additive Manufacturing Conference

voestalpine Stahlwelt Linz, Austria

Friday, 25th November 2016

Time	ROOM A	
08:30	**Wu, Leuders** voestalpine Additive Manufacturing Center GmbH	
08:50	**Mayer** RENISHAW GmbH	
09:10	**Schäfer** FIT Production GmbH	
09:30	**Hatos** Szechenyi Istvan University	
09:50	**Hughes** University of Warwick	
10:10	**Coffee Break**	**ROOM B**
10:40	**Wallis** Montanuniversität Leoben	**Revilla Castillo** Vrije Universiteit Brussel
11:00	**Brillinger** Graz University of Technology	**Yazheng**, University of Science and Technology Beijing
11:20	**Ziegler** RWTH Aachen University -ILT	**Prashanth**, Erich Schmid Institute of Materials Science
11:40	**Walzl** Montanuniversität Leoben	**Krakhmalev** Karlstad University
12:00	**Coffee Break**	
12:30	**Keynote Pirklbauer Airbus**	
13:10	**Neulinger** AIM Sweden AB	
13:30	**Huskiz** University of Applied Sciences	
13:50	**Lunch**	
15:00	**End of conference**	

Thursday, 24th November 2016

09.30 – 10.05 Room A

Time	Topic
09.30	**Opening Lecture** **F. Rotter** voestalpine Edelstahl GmbH, AT
09.45	**Keynote** **R. Poprawe** RWTH Aachen University, LLT, DE
10.25	**The world market for metal powders & steels, status quo and outlook** **B. Blitz** SMR Premium GmbH, DE
10.45	**Comparison of characterization technologies for properties of metal powders used in additive manufacturing** **S. Wallner** BÖHLER Edelstahl GmbH & Co KG, AT
10.05	**Coffee Break**

Thursday, 24th November 2016

11.30 – 12.50 Room A

Time	Topic
11.30	**Material properties and quality considerations for tools made with AM technology** **S. Heino** Uddeholms AB, SE
11.50	**Processing and material properties of hot work tool steels manufactured by selective laser melting** **J. Giedenbacher[1], S. Wallner[2], A. Huskic[2], C. Sommitsch[4]** [1] Forschungs- und Entwicklungs GmbH, AT [2] BÖHLER Edelstahl GmbH & Co KG, AT [3] University of Applied Sciences Upper Austria, AT [4] Graz University of Technology, AT
12.10	**Tribological properties of tools manufactured and polished by using laser metal deposition machine setup** **D. Junker, A. Fedorov, M. Schmidt, M. Merklein** Institute of Manufacturing Technology, DE
12.30	**Investigation of usability of plastic mould steels for the laser metal fusion process** **G. Panzl[1], S. Wallner[2], B. Buchmayr[1]** [1] Montanuniversität Leoben, Chair of Metal Forming, AT [2] BÖHLER Edelstahl GmbH & Co KG, AT
12.50	**Lunch**

Thursday, 24th November 2016

14.10 – 15.50 Room A

Time	Topic
14.10	**Keynote** **Ni- and Fe-based alloys processed by AM – From microstructure to fatigue damage** **T. Niendorf[1], Riemer[2], Leuders[3], Aydinoez[2], Brenne[1]** [1] Universität Kassel [2] DMRC [3] voestalpine Additive Manufacturing Center GmbH
14.50	**Material properties of IN718 processed with high power selective laser melting** **S. Bremen, W. Meiners, K. Wissenbach** Fraunhofer Institute for Laser Technology ILT, DE
15.10	**Influence of powder bed characteristics on material quality in additive manufacturing** **J. Zielinski[1], H.-W. Mindt[2], M. Megahed[2]** [1] Fraunhofer Institute for Laser Technology ILT, DE [2] ESI - CFD & Multiphysics Center of Excellence, DE
15.30	**Design and Engineering by Topology Optimization for an Additive Manufactured Jump Robotic leg** **F. Hollaus[1], M. Kellermeyer[1], K. Führer[2], M. Knaak[3]** [1] CADFEM GmbH, DE [2] Deutsches Zentrum für Luft- und Raumfahrt, DE [3] Stratasys GmbH; DE
15.50	**Coffee Break**

Thursday, 24th November 2016

16.20 – 18.30 Room A

Time	Topic
16.20	**Alloy development methodology for new aluminium MAM powder variants** **R. Gradinger[1], S. Bozorgi[1], E. Wolfsgruber[2], F. Palm[3],** [1] LKR Leichtmetallkompetenzzentrum Ranshofen, AT [2] Mepura Metallpulvergesellschaft m.b.H., AT [3] Airbus Group Innovations, Airbus Defence and Space GmbH, DE
16.40	**Three dimensional characterization on effects of preheating conditions on sintered Ti-6Al-4V powders in Electron Beam Melting (EBM) process** **C. L. A. Leung[1], R. Tosi[2], D. Wimpenny[2], P. Withers[1], P. D. Lee[2]** [1] University of Manchester, Manchester X-ray imaging facility, UK [2] University of Birmingham, the Manufacturing Technology Centre, UK
17.00	**Thermo-fluiddynamical simulation of layer buildup by selsctive laser melting of molybdenum and steel** **K.-H. Leitz, P. Singer, A. Plankensteiner, B. Tabernig, H. Kestler, L. Sigl** Plansee SE, AT
17.20	**Full job quality assurance in laser melting processes for parts with high reliability requirements** **R. Pichler, C. Höller** Graz University of Technology, Institute of Production Engineering, AT
18.30	**Conference Dinner**

Thursday, 24th November 2016

16.20 – 18.30 Room B

Time	Topic
16.20	**Challenges for XXL components by powder and wire metal deposition** **M. Kitzmantel, L. Vály, D. Grech, E. Neubauer, L. Baca, N. Stelzer** RHP-Technology GmbH, AT
16.40	**The effect of process parameters on residual stress evolution in plasma transferred arc cladding (PTA) of Ti-6Al-4V** **H. Moztarzadeh[1], D. Hughes[1], S. Seth[1], G. Gibbons[1], H. Amel[2], R. Dashwood[1]** [1] University of Warwick, UK, [2] University of Sheffield, UK
17.00	**Additive manufacturing via CMT Process** **J. Stockinger[1], C. Wiednig[1], N. Enzinger[1], C. Sommitsch[1] D. Huber[2], M. Stockinger[2]** [1] Graz University of Technology, Institute of Materials Science and Welding, AT [2] BÖHLER Schmiedetechnik GmbH & Co KG, AT
17.20	**Surface processing for metal parts made by additive manufacturing** **N. Nutal[1], J. Crahay[1], M. Larnicol[1], J.-F. Vanhumbeeck[1], J.-P. Collette[2], H. Jochem[3], C. Masse[3], J. Magnien[4], O. Rigo[4], L. Pambaguian[5]** [1] CRM Group, BE [2] Walopt scrl, BE [3] Thales Alenia Space France, FR [4] Sirris, BE [5] ESA, FR
18.30	**Conference Dinner**

Friday, 25th November 2016

08.30 – 10.10 Room A

Time	Topic
08.30	**The meaning of process parameter for LBM– multi target optimization for different length scales** **L. Wu, S. Leuders**, voestalpine Additive Manufacturing Center GmbH, DE
08.50	**Additive Manufacturing with maraging steel** **R. Mayer**, RENISHAW GmbH, DE
09.10	**Additive Design & Manufacturing - Products of tomorrow** **D. Schäfer**, FIT Production GmbH, DE
09.30	**Advanced conformal cooling by heat-conducting pins** **I. Hatos**, Szechenyi Istvan University, HU
09.50	**The potential of central facilities to improve understanding of metal additive processes** **D. J. Hughes, H. Moztarzadeh, G. Gibbons, R. Dashwood** University of Warwick, UK
10.10	**Coffee Break**

10.40 – 12.00 Room A

Time	Topic
10.40	**Additive manufacturing of maraging steel on a copper substrate using selective laser melting** **C. Wallis[1], B. Buchmayr[1], M. Kitzmantel[2], E. Brandstätter[3]** [1] Montanuniversität Leoben, Chair of Metal Forming, AT [2] RHP Technology GmbH, AT, [3] Joanneum Research Materials Leoben, AT
11.00	**Basic characterisation of 17-4PH structure manufactured by selecitve laser melting** **M. Brillinger[1], F. Haas[1]; N. Enzinger[1], S. Pfanner[2]** [1] Graz University of Technology, AT, [2] Anton Paar GmbH

Friday, 25th November 2016

10.40 – 12.00 Room A

Time	Topic
11.20	**Lightweight construction by lattice structures made out of steel - mechanical properties and freedom of design** **S. Ziegler[1], J. Bültmann[1], S. Merkt[2]** [1] RWTH Aachen University, Chair of Laster Technology ILT, DE [2] Trumpf Laser- und Systemtechnik GmbH, DE
11.40	**Topology optimization - Design Tool for future manufacturing methods** A. Walzl, B. Buchmayr Montanuniversität Leoben, Chair of Metal Forming, AT
12.00	**Coffee Break**

12.30 – 13.50 Room A

Time	Topic
12.30	**Keynote** **3D printing in civil aircraft construction: A manufactoring revolution takes off** **P. Pirklbauer**, Airbus
13.10	**Additive Manufacturing on the border of crossing the chasm to a mainstream market – case studies from the north** **K. Neulinger, M. Cronskär, A. Bergström**, AIM Sweden AB, SE
13.30	**Use of selective laser melting and laser cladding for the manufacturing for hot stamping tools** **A. Huskiz[1], N. Wild[2]** [1] University of Applied Sciences Upper Austria, AT [2] Forschungs- und Entwicklungs GmbH, AT
13.50	**Lunch**
15.00	**End of Conference**

Friday, 25th November 2016

10.40 – 12.00 Room B

Time	Topic
10.40	**Understanding the local corrosion mechanism of additive manufactured AlSi10Mg specimens** R. I. Revilla Castillo[1], J. Liang[1], S. Godet[2], I. de Graeve[1] [1] Vrije Universiteit Brussel, BE [2] Université Libre de Bruxelles, BE
11.00	**Effect of retained austenite on mechanical properties of bearing roller steel for large size shield tunnelling machine** **L. Yazheng, J. Bo, Z. Dan, H. Chao, Z. Chaolei** University of Science and Technology Beijing, CH
11.20	**Tuning of Tensile Properties in Nano-Structured Alloys Processed by Selective Laser Melting** K. G. Prashanth[1], J. Eckert[1,2] [1] Erich Schmid Institute of Materials Science, AT [2] Montanuniversität Leoben, AT
11.40	**Solidification microstructure and texture in SLM of metallic material** P. Krakhmalev, Karlstad University, SE
12.00	**Coffee Break**

CSM – CENTER FOR SMART MANUFACTURING

The CSM belongs to the area of "Production Technology" at the FH OÖ and is headed by Prof. (FH) Dr.-Ing. Aziz Huskic. The CSM is an industry oriented teaching and research laboratory. It consists of the following areas:

- **Cutting and forming technology**
- **3D printing, additive manufacturing, and generative tooling**
- **Robotics, automation, digital factory, and simulation**

The CSM was founded in 1998 and was expanded to a size of about 800 m^2 in 2005.

3D PRINTING, ADDITIVE MANUFACTURING, AND GENERATIVE TOOLING

In this laboratory, Austria's first machine for generative processing of metals has been in use since 2005. Therefore the laboratory has the longest experience with this technology. Since 2014, a second metal technology has been in use in addition to FDM addition and 3D printing.

In numerous research projects, the generative processing of material with higher carbon content is being developed. Additionally, research projects are carried out in the fields of topology optimization, medical technology, and hydraulics. Furthermore, plants are developed further and new plant concepts and procedures for the generative production are examined with a view to increase productivity. Currently, tool steels (for example, 1.2709, 1.2344, HTCS150), stainless steel, Inconel, Al and Ti-based alloys, and bronze can be processed.

During the excursion, a visit to the laboratory with a live presentation of both of the selective laser melting equipment (M1 and M2 from Concept Laser) and LASERTEC 65 3D (5-axis milling machine with integrated laser cladding) is offered. Here, in addition to component manufacturing and the CSM their newest development, such as automated powder suction, can be seen.

www.csm-3d-druck.at

Date: 23 November 2016
Departure: 13.00 in front of the voestalpine Stahlwelt – Conference Location
Return: appr. 17.00
Costs: Euro 100,- (including bus transfer, guided tour and coffee break)

SOCIAL PROGRAMME

Conference Dinner
Date: 24 November 2016
When: 18.30
Where: voestalpine Stahlwelt 2nd Floor (the way will be signed)

After the conference dinner, a bus shuttle will be provided to the following hotels:

- Ibis Styles Hotel Linz
- Arcotel Nike Linz
- Courtyard by Marriott Linz

CONFERENCE VENUE

LINZ

The new slogan of the city is programme: “Linz changes”

Linz is where you can find beautiful stucco facades from earlier times side by side with interesting new buildings of appealing architectural styles with futuristic lighting.

Linz, the city on the Danube, has become the pulsating centre between East and West during the last decades.

No other Austrian city has experienced such a tremendous change like the capital of Upper Austria. The result is a modern city which offers its inhabitants and its visitors a perfect place to be, with large green areas and good air quality.

VOESTALPINE STAHLWELT LINZ

Discover a new world.

Our world relies on steel. From cutlery to cars, from razor blades to skyscrapers, from tools to rocket ships, from railway tracks to highway bridges – steel shapes our every day lives, makes life easier for us, moves us forward. Steel connects continents, countries and people. Yet so many possibilities and potential uses of high-grade steel products have yet to be tapped.

The adventure of steel

Around the world, voestalpine produces, processes and develops steel to make high-quality products and innovative solutions. Be our guest – come and visit voestalpine’s world of discovery, where you can learn more about steel and the countless ways it can be used. Discover the fascinating world of steel. Discover the voestalpine Stahlwelt.

GENERAL INFORMATION

Badges .... All officially registered participants and sponsors/exhibitors wearing their official congress badge. Please wear your name badge at all times in order to obtain admittance to the areas of the voestalpine Stahlwelt.

Congress Venue .... voestalpine-Straße 4, 4020 Linz, Austria

Official Language . The congress language is English.

Parking .... There is a free underground car park provided next to the congress venue.

Publications .... The publications are provided on a USB Stick

Mobile Phone .... Please keep your mobile phone turned off or in silent mode in all congress rooms.

Photographs .... The organizer ASMET will take photographs of this event. Please note that you are not allowed to take pictures yourself.

SPONSORS

Platin Sponsor

voestalpine
ONE STEP AHEAD.

Gold Sponsor

eco plus cluster niederösterreich · Europäische Union · EFRE

pankl RACING

Silver Sponsor

SIEMENS

Bronze Sponsor

RHP TECHNOLOGY

Thermo-Calc Software

AIR LIQUIDE

CONFERENCE ORGANISATION

ASMET
Austrian Society for Metallurgy and Materials

Franz-Josef-Str. 18, 8700 Leoben, Austria
Phone: +43 3842 402 2291
Email: asmet@asmet.at

ASMET®
THE AUSTRIAN SOCIETY FOR METALLURGY AND MATERIALS


www.mamc2016.org

Presentation Abstract

Benedikt BLITZ - SMR Premium GmbH

The World Market for Metal Powders & Steels, Status Quo and Outlook

The Production of Metal Powders and Powder Metallurgical Steels and especially its associated production technologies like HIP, MIM and AM are and will become key future core technologies for a number of demanding products and thus for the usage in different associated industries. This presentation will highlight the actual supply and demand situation of metal powders and the manufactured metal powder steels, will introduce leading manufacturers of both powders and steels, and summarizes installed capacity and new capacity that are on the way. Finally this presentation also compares regional demand dynamics as well as highlights endues structures of today and the near future.

About the Author

Benedikt BLITZ, Managing Director SMR Premium

Benedikt BLITZ graduated from the University of Applied Sciences, Innsbruck, Austria and holds a degree in Process Technology and Environmental Technology.

Benedikt started to be active in the metal industry in 1998 followed by a number of internships during his education. In 2007, he joined SMR as a Market Analyst, specializing in the field of the stainless and specialty steel industry on a global scale and became Senior Market Analyst in 2012. He primarily worked on projects with a focus on specialty industry segments, special products (forgings, remelted steels, etc.) and raw materials (STS scrap, Cr, Ni, Mo, Nb, etc.) of the stainless and specialty steel industry as well as a focus on process technology for global leading players.

In April 2015, Benedikt BLITZ and Markus MOLL established a new company named SMR Premium GmbH, to grow and focus on market research for the world of High Value Metals. Benedikt became Partner and Managing Director of SMR Premium GmbH.

Wallner Stefan [1]

COMPARISON OF CHARACTERIZATION TECHNOLOGIES FOR PROPERTIES OF METAL POWDERS USED IN ADDITIVE MANUFACTURING

Abstract

Current methods used in evaluating the properties of metal powder show that there exists already several international, consensus based standards. They cover some of the relevant properties for metal powder used for additive manufacturing processes.
Determination of the powder properties used for metal additive manufacturing is required for industry to be able to confidently select powder and produce consistent parts with known and predictable properties. Due to the fact that hardly any standards for required powder properties exist, the comparison of different powder batches is difficult.
The most important properties of metal powders are size and size distribution, morphology, chemical composition, flow ability and density. Different investigation methods and procedures for powder material characterization are available, but not all of them are useable for testing metal powder used for additive manufacturing.
Aim of this work is an assessment of the current state-of-the-art testing methods for determining properties of metal powder materials. In addition, also some new developed testing methods which showed their applicability for qualification of metal powders are presented. These methods will be evaluated with respect to applicability and enhanced for use on additively manufactured parts and powder used as raw material for powder bed additive manufacturing processes.

Keywords

Powder characterisation, particle size distribution, flowability

1. Introduction

The more a technology grows and is established in the market, the greater the need becomes for a common understanding of process details. Today AM has reached a status were it is stepping into industrialisation. The number of printing devices in operation grows significantly since the last 5 years. As the technology made its way from university to industry also the need for robustness of the printing device as well as the feedstock increased. There are still many challenges ahead in order to make this technology a sustained success. Particularly, the strong links between manufacturing process parameters and the material properties require much more attention compared to conventional metal manufacturing processes. At the moment, standardisation of process or pre-material parameters is a blank area. As shown in Figure 1, standardisation committees over the world are working on AM standards since some years. The work of these committees is important for the improvement of quality assurance of AM parts especially for critical applications in aerospace or motorsport.

[1]Böhler Edelstahl GmbH & Co KG

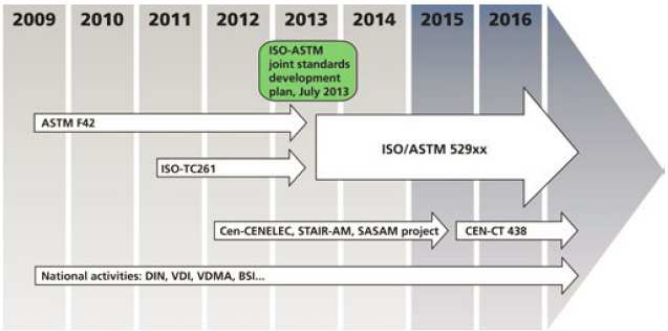

Figure 1: International standardisation activities on Additive Manufacturing [1]

Due to restrictions in powder usability in different available AM powder bed printers, the characterisation of the powder feedstock is coming more and more in focus. The used characterisation techniques are still common for powder classification over the last decades. In this paper Chapter 2 will deal with these technologies. In chapter 3 some additional methods for powder evaluation are shown. Some of them are still partially used in academic field application.

2. Common measurement methods for powder used in AM

To make sure that measurements lead to reproducible results, the powder sampling is a key issue. Due to segregation effects within powder packages, taken samples have to be sub-divided in order to make the taken powder size manageable and to guarantee a homogenous grain size distribution within the different samples. Some of these samplers are shown in Figure 2. Powder from the feedstock is feed into the sampler and divided into a defined amount of powder samples.

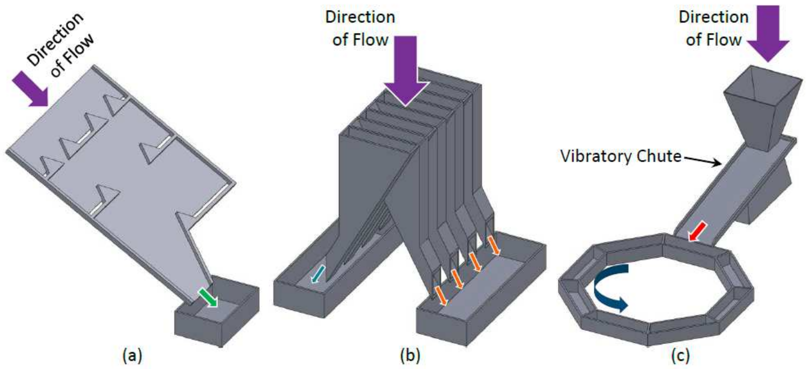

Figure 2: Some examples for powder sample preparation: (a) table sampler, (b) chute splitter, (c) spin riffler [2].

2.1 Chemical composition

For the measurement of the chemical composition of metal powders well established techniques like ICP OES, XRD etc. are used for the analysation of the primary chemical elements. Interstitial elements like Oxygen, Carbon, Nitrogen and Sulphur are analysed using combustion and fusion techniques, respectively. The control of the chemical composition is on the one hand side necessary to guarantee that the virgin powder is within the expected limits

[1]Böhler Edelstahl GmbH & Co KG

according to the standard. On the other side it’s necessary to control possible changes in chemistry after multiple powder usage within several additive manufacturing processes.

2.2. Particle size distribution

The particle size distribution can be determined using different measurement devices. Easiest and cheapest way is a sieve analysis. Therefore, a defined quantity of powder is placed at the top of a stack of calibrated sieves with decreasing mesh size. The stack is oscillated, causing the smaller particles to pass through the meshes (Figure 3). After stopped oscillation the weight of powder retained on each mesh is weighted so the proportions can be calculated and dedicated to the used sieve meshes. Lack of this method is the restricted availability of sieve meshes (with 25µm as smallest one) as well as the potential of falsified measurement values due to not sufficient oscillating time (high amount of smaller particles remaining in the larger sieve mesh). Relevant standards are ISO 4497 (Metallic powders, determination on particle size by dry sieving) and ASTM B814 (Test method for sieve analysis of metal powders).

Sieve	Powder	
[µm]	[g]	[%]
36	120	60
45	76	38
60	2	1
90	0.6	0.3
120	1.4	0.7
total	200	100

Figure 3: Stack of calibrated sieves on an oscillating table; particle distribution result after sieve analysis.

A more sufficient way is an automatically analysis using either dynamic image analysis or laser diffraction. For both technologies a powder sample is suspended in either a liquid (water) or a gas (air) and irradiated by a laser beam (laser diffraction) or by a double optical camera system (dynamic image analysis – Figure 4). Relevant standards are ISO 13320 (Particle size analysis – Laser diffraction), ASTM B822 (Test method for particle size distribution of metal powders by light scattering), ISO 9276-6 (Particle shape), etc. One additional benefit of the dynamic image analysis is the simultaneous investigation and record of the particle morphology via an evaluation of the powder pictures taken during the process.

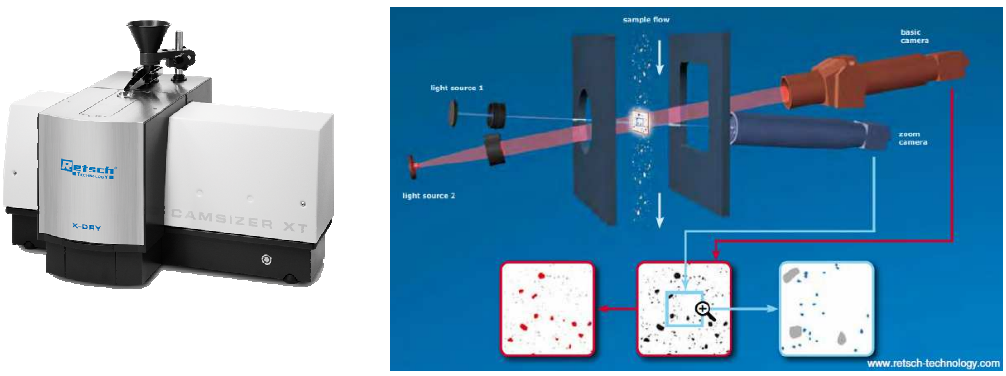

Figure 4: Example for a dynamic image analysis equipment (Retsch Camsizer XT) [3].

[1]Böhler Edelstahl GmbH & Co KG

Result of the process is a continuous particle size distribution diagram which can be evaluated in accordance to the measured particle dimensions as shown in Figure 5. The particle size distribution is strongly influenced from the taken measurements values – minimum particle length, maximum particle length or adequate area calculated from the irregular particle. Most comparable with the results from the sieve analysis are the results from the minimum particle length measurements.

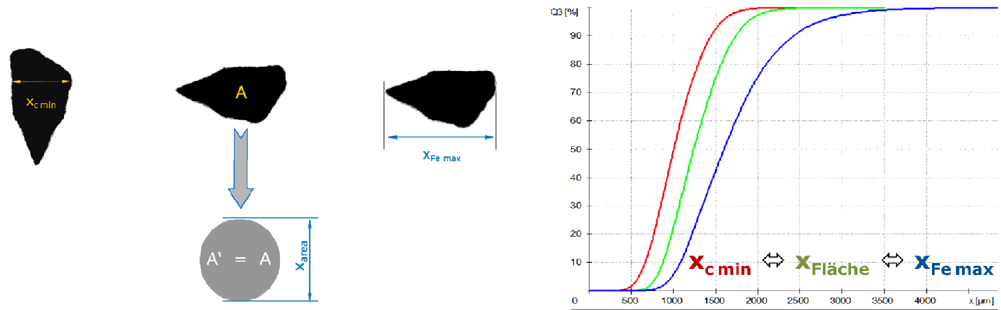

Figure 5: Calculated particle size distributions as a function of the measurement values minimum-, maximum particle length and adequate area of the particle [3].

2.3. Particle morphology

Due to the fact that spherical particles are preferred for AM the morphology has to be investigated. As mentioned before, one technique is using a dynamic image analysis. Advantage of this evaluation is the rather high amount of investigated particle. Figure 6 exemplarily shows a result from a Camsizer XT measurement with rather spherical particles.

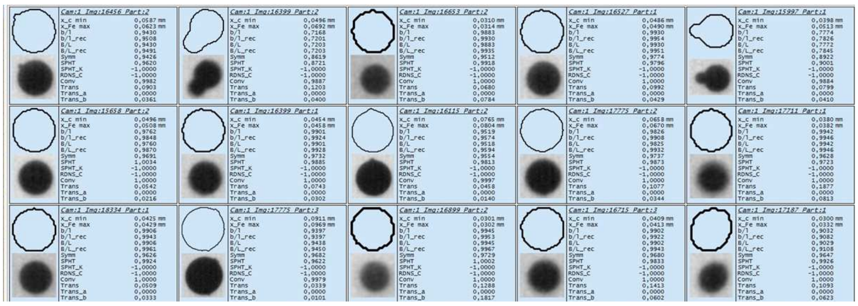

Figure 6: Particle shape recorded from the Camsizer XT particle distribution measurement.

Most common method for powder morphology measurement is using a light optical microscope or a scanning electron microscope (SEM). Here, only some powder particles are either embedded or loose positioned and optical investigated. However, the advantage is that embedded powders can be grinded and polished to check the internal porosity too.

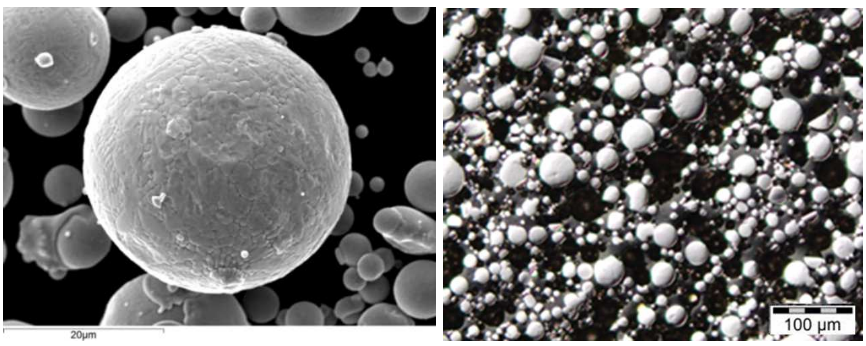

Figure 7: SEM picture of a spherical IN718 particle and metallographic specimen with sliced powder for investigation of the internal porosity.

[1]Böhler Edelstahl GmbH & Co KG

2.4. Powder flow

The rheological properties of metal powders used in additive manufacturing are important for the formation of consistent layers in powder bed systems. Measurement of powder flow is a rather complex topic. There are some standard test methods available like the evaluation of the tap or apparent density, the flow rate through standard funnel (Figure 8) or the angle of response. All these measurement methods used due to the fact that they are most common in powder testing for different applications are and so best practice. Some relevant standards are ISO 3923 and ASTM B213 (Hall Flowmeter), ASTM B703-10 (Arnold meter), ISO 3953 and ASTM B527 (Tap density), ISO 4324 (angle of response).

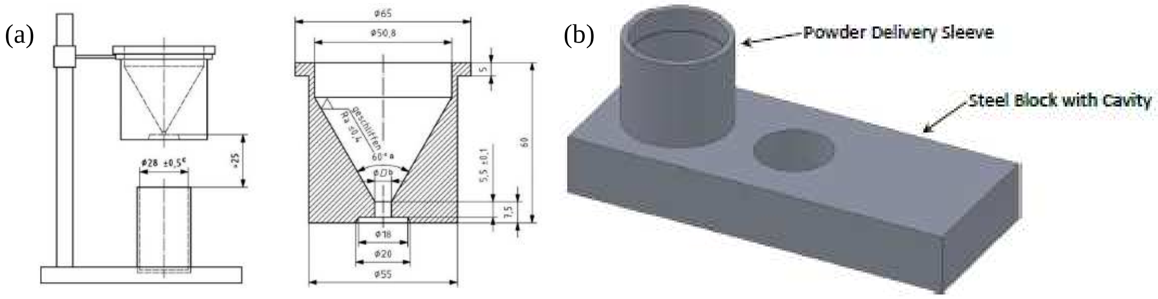

Figure 8: (a) Hall Flowmeter according to ISO 3923[4] , (b) Arnold meter according to ASTM B703-10 [5].

Exemplarily two methods for the powder flowability measurement are shown in Figure 8. In the case of the Hall Flowmeter powder is filled in the funnel and, the hole in the bottom of the funnel is closed by the operator (using his finger!). A cup with a defined volume is placed under the funnel and the powder is released. When the cup is totally filled the powder cone on its top is flattened and the powder is weighted. In the case of the Arnold meter, the powder is filled in the powder delivery sleeve. This sleeve is slipped over a hole with a defined volume in a steel block. After slipping the powder is weighted and as for the Hall Flowmeter, the apparent density is calculated. A comparison of the results for the apparent density using both measurement methods for three different powder grades is shown in Figure 9. The apparent density values calculated from the Arnold meter are in all investigated cases higher than the values from the Hall Flowmeter.

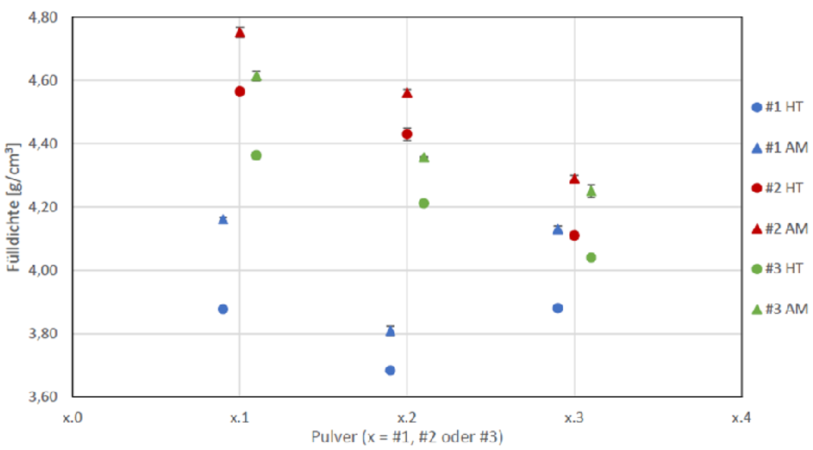

Figure 9: Comparison of the measurement of apparent density using Hall Flowmeter (HT) and Arnold meter (AM) for three different powder grades [6].

3. Alternative measurement methods for powder used in AM

[1]Böhler Edelstahl GmbH & Co KG

As mentioned in chapter 2.4, the powder flow can be measured using different equipment. Due to the fact that none of them realistically depicts the layer process in powder bed systems some new methods have been evolved. One of them is a test from the TU Vienna (Figure 10). This equipment consists of a steel block where two cavities are milled in. Powder is squeegeed using a scoop and the surface condition is investigated using a 3D optical microscope. Using this is rather simple and leads to a fast result if a powder can be easily used in the AM powder bed equipment.

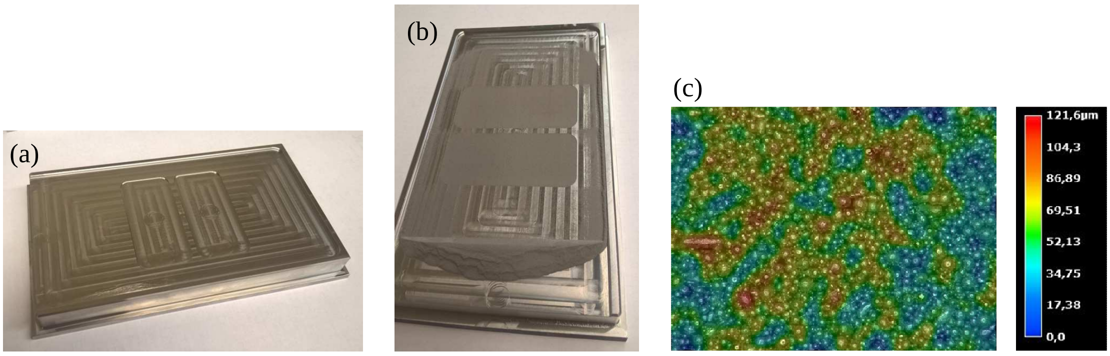

Figure 10: Squeegee test (a) without powder, (b) powder coated, (c) 3D optical image of the surface.

Figure 11 shows a similar method than the above mentioned. Powder is filled in a defined geometry and the powder hopper is spread over a plate. The length and the surface quality of the powder layer are investigated.

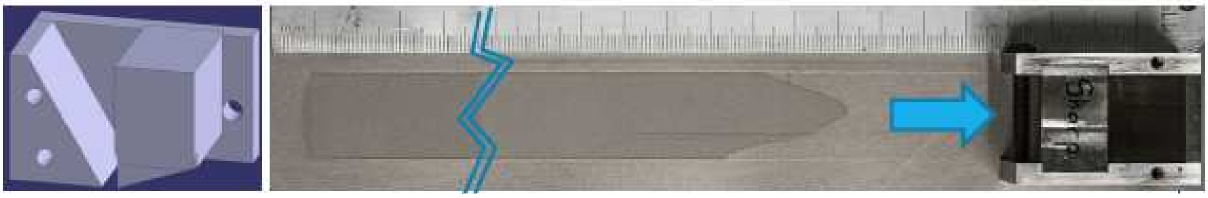

Figure 11: Equipment for powder testing for its usability in powder bed AM processes [7].

To test the flowability in a more quantitative way a powder rheometer can be used. Therefore, 25ml powder is filled into a glass. A special designed curl is moving downwards while rotating and the torque is measured. Using this measurement the flowability can be depicted as a function of torque or force as shown in the results in Figure 12 for a perfect spherical and a satellite afflicted powder.

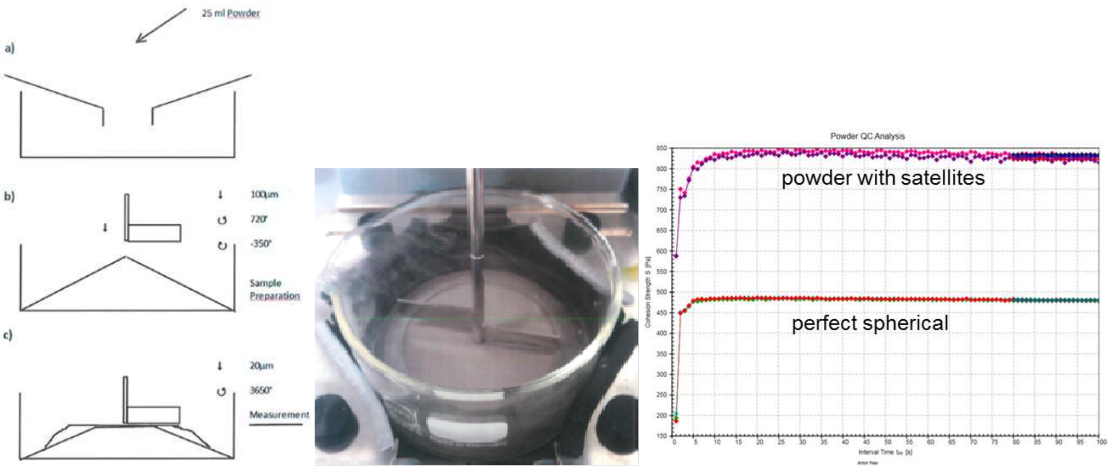

Figure 12: Schematic picture of a powder rheometer for testing the flowability of metal powder as well as results from the measurement [8].

[1]Böhler Edelstahl GmbH & Co KG

4. Summary

Additive Manufacturing is a technology which enables new innovations. The market growth is fast, with enormous investments being made worldwide. Nevertheless, the application of AM is just on beginning and users will explore the many possibilities of this technology. To exploit full potential it is necessary to gain knowledge on the process and on the feedstock. Therefore, common measurement methods are used for characterisation of powder properties. Due to increasing standardisation work these techniques are now deeper investigated if they can describe the process related parameters in a proper way. New measurement technologies will be implemented and maybe replace some which are now state of the art. For quality assurance it is a key factor of the whole AM process to keep an eye on the feedstock not only before the first printing job started, but also while the whole lifetime of powder use and reuse.

References

[1] C. Aumund-Kopp, F. Petzoldt, Standards for metal Additive Manufacturing: A global perspective, Metall AM (Summer 2016, Volume 2), p.45
[2] A. Cooke, J. Slotwinski, Properties of Metal Powders for Additive Manufacturing, NIST, NISTR 7873, 2012
[3] Retsch Technology, internal presentation on powder characterization.
[4] ISO 3923 standard
[5] ASTM B703-10 standard
[6] M. Mitterlehner, Untersuchungen des Lagerverhaltens inertagsverdüster Metallpulver für die Anwendung im Bereich Additive Manufacturing, Diploma Thesis, TU Vienna, 2016.
[7] Marc de Smit, Quality assurance in Additive Manufacturing, presentation during the MAMTeC, Cologne, EASA, 2016.

[8] Anton Paar, internal document.

[1]Böhler Edelstahl GmbH & Co KG

STEFAN HEINO [1], CHRISTOS OIKONOMOU [1], SESHENDRA KARAMCHEDU [1], JOHNNY SJÖSTRÖM [1]

MATERIAL PROPERTIES AND QUALITY CONSIDERATIONS FOR TOOLS MADE WITH AM TECHNOLOGY

Abstract

The expectation on Additive Manufacturing (AM) is growing rapidly and there is growing interest for using this technology for advanced tooling applications. However, developing a tool using the AM technique is different and requires that the tool manufacturer and the designer fully understand the possibilities, as well as the limitations of an AM produced part. The aim of this study was to compare the properties and microstructure of conventionally produced tool steels with tool steels manufactured using Selective Laser Melting (SLM) technology. The tool steel investigated was a precipitation hardening tool steel manufactured with two different SLM systems, using the same starting material and powder production route for both systems. The results are discussed from the material, quality and application perspective and highlight important material and processing considerations for the use of AM technology in tooling applications.

Keywords

Tool steels, maraging steels, mechanical properties, microstructure, retained austenite, SLM, Uddeholm Corrax®

1. Introduction

In recent years the growth of the Additive Manufacturing (AM) technology has also seen an increasing interest for using this process in tooling applications, especially via the Selective Laser Melting (SLM) route.

The AM technology has been extensively used in producing plastic moulding tools for improved cooling conditions in the tool e.g. minimizing hot spots. By doing so, more efficient temperature profiles can be realized, thus achieving shorter process cycle times [1] [2]. It can also be used to handle very complex geometric features, in e.g. cores, and other tool components [3].

Currently the types of tool steels available are limited and the most common grades on the market are of the stainless maraging type. Compared to conventional tool steels with higher carbon content, the maraging steels are relative insensitive to cracking from thermal stresses built up during the AM process and do not require any complex post processing heat treatments. Usually, only solution annealing followed by a precipitation hardening step is sufficient to achieve a useful result [4].

Although the processing of the maraging stainless steels is rather straightforward in AM, several factors dependent on the process may still affect the tool performance. Local variations in the melting and remelting steps during building an AM component can influence the amount of retained austenite in the material [5]. This austenite can transform to martensite

[1] Uddeholms AB, SE-683 85 Hagfors, Sweden

to various degrees during subsequent heat treatment [6], which in turn may influence the microstructural stability of the material during service.

The AM process also introduces defects in the material, such as pores, inclusions and other artefacts [7], which may or may not have an impact on the intended application. For these reasons, the effect of the process to the quality of the final components needs to be understood and taken well into consideration when utilizing the technology. For instance, the expected result from polishing might be affected by porosity, and it is therefore desirable to achieve a consistent structure after printing in order to establish an optimum post treatment.

With wider use of the AM technology for tooling it is important to understand the possible differences in microstructure and properties of AM produced tools, which today may also vary between systems from different manufacturers. Naturally, as the technology finds more use, tool makers will be operating several systems using the same starting powder.

In that context, the purpose of the current investigations was to evaluate the quality and properties of parts produced with AM from two different SLM systems and with two separately developed sets of parameters. The aim was to better understand the variability in the process, as well as to point out important considerations for the tool maker using AM in tool manufacturing.

The material of the present study, Uddeholm Corrax®, is one of the most common grades used today for plastic moulding applications. This alloy is a precipitation hardening stainless martensitic tool steel [8], reaching hardness levels of about 50 HRC. The high hardness is achieved through precipitation of intermetallic phases during tempering (ageing), which is done in the range 525 °C – 600 °C, depending on the desired combination of hardness and toughness.

2. Material and Experimental Procedure

For this investigation, metal AM powder was produced from Uddeholm Corrax® through atomization. Closed coupled gas atomization processing method assisted by vacuum melting was utilized in order to acquire fine, high purity and well spheroidized powder for the needs of AM processing. The chemical composition of the alloy is shown in

Table 1. The morphology and size distribution of the metal AM powder were evaluated using both Scanning Electron Microscopy (SEM), (FEI Quanta 600F equipped with both secondary and back-scattered electron detectors), as well as with a particle size and shape analyser based on dynamic imaging processing (ISO 13322-2) (CamsizerX2, Retsch Technology). Elemental chemical analysis for both metal powder and AM produced specimens was performed using combustion and reduction extraction method utilizing a LECO system.

The two different SLM systems used in the present study were the TruPrint 1000 from TRUMPF and an EOS M290, equipped with a 200W and 400W fibre laser sources respectively. To benchmark the results from the process high relative specimen's density, in respect to the known density of Uddeholm Corrax® material, was chosen as key physical property along with indentation hardness. For that purpose, cubes of 10x10x10mm in dimensions were built based on a developed Design of Experiments (DoE) method, taking into account core process parameters such as laser power, scan speed, layer thickness and hatch distance which determine the energy input on the material under processing. Moreover,

[1] Uddeholms AB, SE-683 85 Hagfors, Sweden

different hatch modes were implemented in both SLM systems with the TruPrint 1000 following a checkerboard pattern while the EOS M290 a striped one. The density of the produced cubes based on the DoE was measured based on Archimedes principle method and the hardness with a Rockwell indenter.

For phase identification of the produced specimens, X-ray Diffraction (XRD) analysis was performed using a Seifert XRD 3003 PTS system with PSD detector and a Cr source at angle of rotation φ at 360 degrees and oscillation angle χ at 130 degrees. Angular speed for both cases was set at 12 degrees per minute. Additionally, microstructural and phase identification analyses on the produced AM specimens were performed with SEM at 20keV acceleration voltage, coupled to Energy Dispersive X-ray Spectroscopy (EDS) and Electron Backscattered Diffraction (EBSD) techniques with an SSD X-Max^N and NordlysNano detectors from Oxford Instruments, respectively. For the EBSD analysis, maps of 1200x1200 pixels with a step size of 0,05μm were acquired and evaluated with CHANNEL5 software package from Oxford Instruments HKL.

Finally, AM produced mechanical testing specimens from both SLM systems were built and post heat treated first at 850°C for 30min in vacuum, as solution treatment, while subsequently aged at 525°C for 4 hours and air cooled to room temperature. The samples were finally subjected to impact toughness and uniaxial tensile testing.

Table 1: Nominal chemical composition in wt% of Uddeholm Corrax®

C	Si	Mn	Cr	Ni	Mo	Al
0,03	0,3	0,3	12,0	9,2	1,4	1,6

3. Results

Two different AM metal powder lots were produced from Uddeholm Corrax®, specifically aiming for the two different SLM systems in this study, the TruPrint 1000 and the EOS M290. The elemental chemical analysis of those AM metal powders is given in *Table 2* for oxygen, carbon, nitrogen and sulphur content. Additionally, the results from the particle size and shape analysis based on the dynamic image processing technique are shown in *Table 3*. There, the D10, D50 and D90 values from the cumulative size distribution of the two powder lots are presented. Both AM metal powders have very similar values with the lot used for the EOS M290 system having a slightly increased fraction of finer particles. Moreover, the mean values from powder particles sphericity and aspect ratio, which evaluate their shape characteristics, are given with values of 1 for both cases to be considered for the case of perfect spherical particles.

Table 2: Elemental composition analysis in wt% of materials investigated in the present study

	C	S	N	O
Uddeholm Corrax®	0,03	0,023	0,005	0,001
Corrax® AM powder (TruPrint1000)	0,028	0,026	0,015	0,0190
Corrax® AM powder (EOS M290)	0,028	0,024	0,013	0,0210
Corrax® AM specimens	0,025	0,021	0,017	0,0103

[1] Uddeholms AB, SE-683 85 Hagfors, Sweden

(TruPrint1000)				
Corrax® AM specimens (EOS M290)	0,027	0,023	0,017	0,0109

Table 3: Particle size and shape analysis with CamsizerXT for Uddeholm AM Corrax® powder for two different SLM systems

	D10 (µm)	**D50 (µm)**	**D90 (µm)**	**Sphericity (Mean)**	**Aspect Ratio (Mean)**
Uddeholm AM Corrax® (TruPrint1000)	27,6	39,6	52,2	0,94	0,90
Uddeholm AM Corrax® (EOS M290)	22,5	33,9	48,9	0,95	0,93

In *Fig. 1* the SEM analysis of the AM metal powder is shown, where representative images from the surface of both coarse and fine powder particles within the defined size distributions are depicted. The powder lot utilized in the EOS M290 system exhibited slightly improved sphericity and aspect ratio according to *Table 3*. This is probably due to the presence of higher fraction of fine particles as shown in the size distribution values, which as seen here from the SEM investigations have excellent morphology

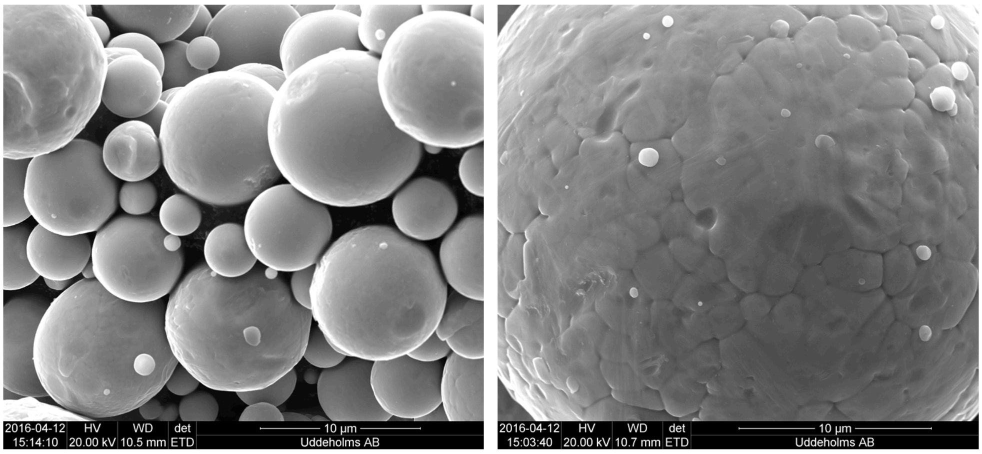

Fig. 1: SEM analysis of the morphology of the Uddeholm AM Corrax® powder

The process parameters used in the two different SLM systems are shown in *Table 4*. These values represent the parameters used for processing the inner core of an AM built part with the SLM process. For the development of the process parameters a DoE method was used. The procedure followed in determining the optimum set of parameters was to first test various boundary conditions, which subsequently allowed the prediction of the response of all the intermediate conditions. These were in turn tested in terms of relative density and indentation hardness from the cubed samples.

The density measurements on the specimens produced with the aforementioned process parameters showed that it was possible to reach average density values of 7,608 g/cm^3 with the TruPrint 1000 system and 7,624 g/cm^3 with the SLM M290 in as-built state.

[1] Uddeholms AB, SE-683 85 Hagfors, Sweden

Table 4: Process inner core parameters for two different SLM systems for Corrax® AM powder

	TruPrint1000	EOS M290
Layer thickness	20 µm	30 µm
Laser power	175 W	170 W
Scan speed	800 mm/sec	1250 mm/sec
Hatch distance	0,05 mm	0,10 mm
Hatch mode	Checkerboard	Stripes

Moreover, the indentation hardness measurements showed that for the specimens produced with both SLM systems, average values of 35 HRC were achieved in as-built condition and 50 HRC after solution treatment and ageing at 525°C for 4 hours.

Specimens built with both SLM systems in as-built and heat treated conditions were subjected to XRD analysis for phase identification and determination of the amount of retained austenite through the whole process. The results with respect to condition of the sample and to SLM system from which they originate are shown in *Table 5*. Three conditions were measured; as-built, aged after build and solution treated with subsequent ageing after build. The amount of retained austenite for the specimens in as-built state from both SLM systems were quite high and similar reaching up to 22,5%. Subsequent ageing of those samples reduced the amount down to about 10,5% in the case of the TruPrint 1000 and 16% for the samples produced with the EOS M290 system. In order to avoid the deleterious effects of high amount of retained austenite in a tool under service, a subsequent solution treatment after the as-built state followed by an ageing post treatment was performed, in order to minimize its content. The amount of the austenite was in that case reduced significantly to 7% for the specimens produced with the TruPrint 1000 and to 4% with the EOS M290.

Table 5: Amount of retained austenite measured by XRD analysis

		Retained austenite %	Std. error %
Uddeholm AM Corrax® specimens (TruPrint1000)	As-built	22,25	2,5
	Aged	10,5	1
	Solution treated and aged	7	2
Uddeholm AM Corrax® specimens (EOS M290)	As-built	22,5	2,5
	Aged	16	1
	Solution treated and aged	4	2

In *Fig. 2* SEM imaging along with EDS point analysis of cross sections of samples in as-built state from both SLM systems are shown. There, representative types of defects encountered from both systems are depicted, together with local chemical microanalysis from matrix and defects. It was observed that the inclusions appear to vary in size and shape with the ones from the EOS M290 to be significantly smaller in size and more round-shaped, while for the case of the TruPrint 1000 they could reach up to more than 100 µm in one direction.

Furthermore, in *Fig. 3* an EBSD map is shown from a specimen in as-built condition from the EOS M290 system. The map shows the distribution of austenitic grains in the bcc matrix,

[1] Uddeholms AB, SE-683 85 Hagfors, Sweden

overlaid with band contrast information that exhibits the quality of the diffraction patterns, revealing in this manner the local microstructure at the areas of interest.

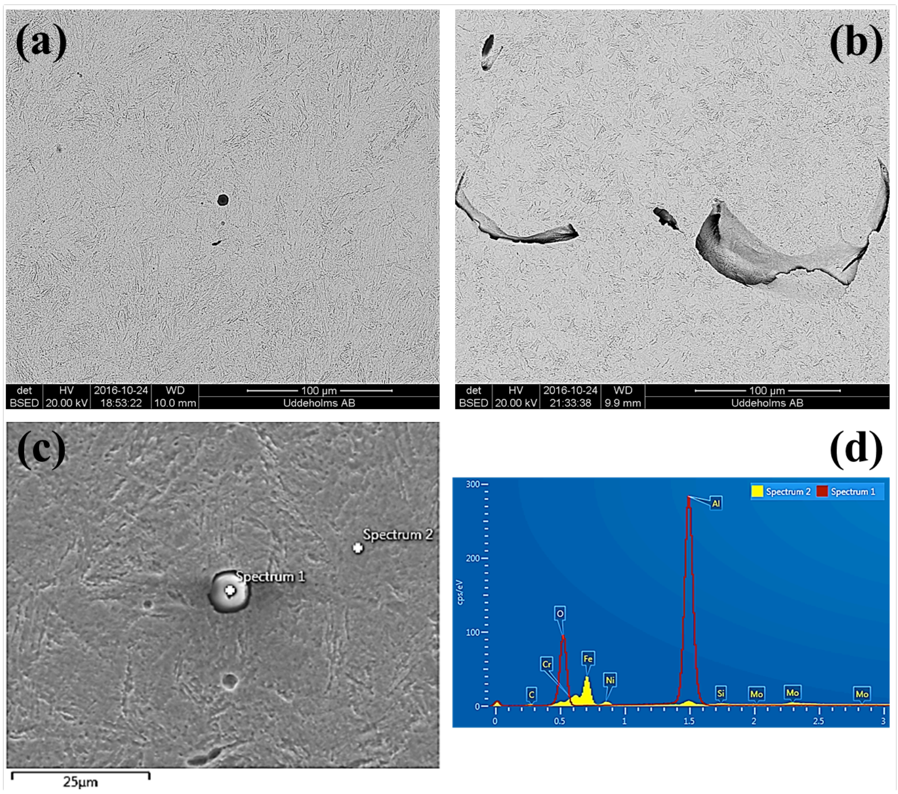

Fig. 2: (a) and (b) SEM analysis on specimens build with EOS M290 and TruPrint 1000 respectively, (c) and (d) EDS point analysis on specimens built with EOS M290

In *Table* 6 are given the results from the mechanical testing of specimens produced from both SLM systems, in all cases after solution heat treatment at 850°C for 30min and ageing at 525°C for 4 hours. In this study, samples prepared both parallel (horizontally) and perpendicular (vertically) to the base build plate were measured for both impact toughness and uniaxial tensile testing. For both of the SLM systems used the impact toughness and A5 values were lower in the vertical build direction. The strength levels, Rm and $Rp_{0,2}$ were also on a similar level for both SLM systems, while slightly higher values were observed in the vertical build direction in all cases. The main difference between specimens produced with the two different systems was for the impact toughness and elongation tests, where the values from the TruPrint 1000 were considerably lower.

[1] Uddeholms AB, SE-683 85 Hagfors, Sweden

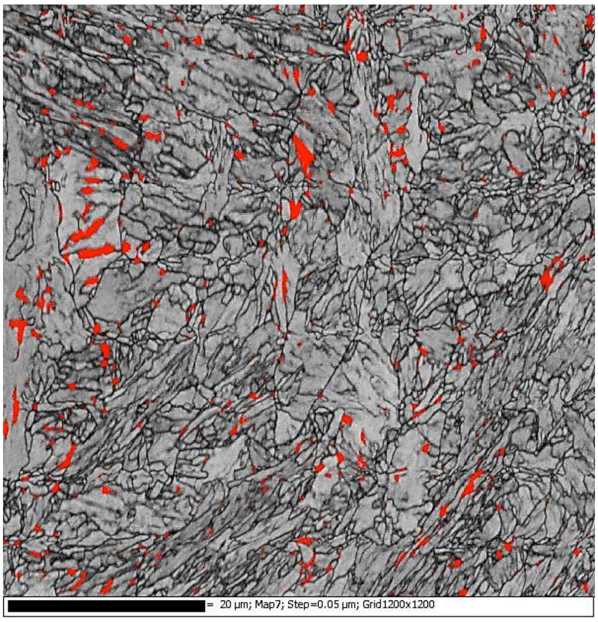

Fig. 3: EBSD map overlaying band contrast information and austenite grains (red coloured) for specimen in as-built condition (EOS M290)

Table 6: Mechanical testing on Uddeholm AM Corrax® produced test specimens, after solution treatment at 850°C for 30min and ageing at 525°C for 4 hours

		Impact toughness (J) / stdv.	Modulus (MPa) / stdv.	Rm (MPa) / stdv.	$Rp_{0,2}$ (MPa) / stdv.	Elongation A5 (%) / stdv.
Uddeholm AM Corrax® specimens (TruPrint1000)	Built vertically	6,22 / 0,53	197723 / 1118	1667 / 7	1595 / 12	1,7 / 0,6
	Built horizontally	11,17 / 0,68	191796 / 3356	1624 / 13,7	1518 / 14,2	3,68 / 1,3
Uddeholm AM Corrax® specimens (EOS M290)	Built vertically	18,70 / 2,16	199867 / 3231	1701 / 4	1640 / 12	8,6 / 0,3
	Built horizontally	22,06 / 2,54	197992 / 12667	1653 / 6	1560 / 18	9,7 / 0,3

4. Discussion

The analysis with both the SEM and CamsizerX2 techniques (*Fig. 1* and *Table 3*) showed that the Uddeholm AM Corrax® metal powder exhibits excellent morphological attributes, with minimum amount of satellites present on the particles and a clean surface free from particulates and oxide scale. Larger particles have a more distinct dendritic structure due to the lower cooling rates while the fine fractions tend to have superior sphericity and cleaner surfaces. These aspects suggest that the Uddeholm AM Corrax® metal powder produced in this manner should yield good packing bed density, thus rendering it suitable for AM powder bed processes [9].

The elemental chemical analysis of the AM produced specimens (*Table 2*) showed that the amount of oxygen present is half from the one existing on the metal powder and it is for both SLM systems very similar. Comparing those levels with the ones acquired from conventional

[1] Uddeholms AB, SE-683 85 Hagfors, Sweden

Uddeholm Corrax®, it can be seen that the oxygen content in AM produced samples has a tenfold increase. In that context, oxide inclusions enriched in aluminium content were clearly visible in the microstructural investigations of the AM produced samples, as shown from the point EDS analysis in *Fig. 2*. These results point out on the fact that SLM process is not to be considered as a clean process. Similar results have been observed on other studies on maraging steels processed in SLM systems[7]. It is obvious that a number of contributions for oxygen uptake are available, such as the native oxide layer from the metal powder, the impurities from the shielding gas used and vacuum levels in the AM systems, which all should be well considered and tackled before achieving optimum results.

In relationship to the presence of defects in the microstructure and the development of the latter in an AM produced specimen, the process parameters need to be also taken under consideration. It is possible to calculate the volume energy based density E (J/mm^3) introduced locally to the material during the AM process based on the following formula:

$$E = \frac{P}{v * h * t}$$

where P is the laser power in Watts, v is the laser speed in mm/sec, h is the hatch distance in mm and t is the layer thickness in mm. By taking this formula into account based on the values from *Table 4*, the volume energy density for the case of TruPrint 1000 can be evaluated at 218 J/mm^3 while for the case of the EOS M290 at 45 J/mm^3. Furthermore, the building strategies (hatch mode) followed between the two SLM systems were different, which can be considered as an additional factor to the already mentioned for the development of the microstructure and defects. The effect of all those aforementioned process parameters to the latter can be assessed indirectly by the microstructural investigations and mechanical performance testing.

In that context, the XRD analysis of the AM produced specimens gave interesting results that point out to the differences in the thermal history of a sample, which is developed during building, depending on the local variation under the selected processing conditions. In order to understand the origin of such high amount of austenitic phase in the AM produced specimens, up to 22,5% in the present study, one could investigate the favourable thermodynamic equilibrium phases present in different temperature regimes. In *Fig. 4* it is shown the phase diagram calculated from the Thermo-Calc software based on the chemical composition of the Uddeholm Corrax® alloy. There it can be seen that a stable fcc phase can be present down to 350°C to about 11%. As shown in the present study the microstructure of samples processed in the SLM systems differ significantly from those acquired according to the conventional production route. In particular, the MnS inclusions which are frequently observed in the case of the conventional Uddeholm Corrax® were not present in the SLM produced specimens. In addition, a significant amount of aluminium oxide inclusions were observed in the latter case. Moreover, local variations in the distribution of alloying elements and the complex thermal history that the SLM processed samples are subjected to could contribute further to the high concentration of retained austenite [5] [9].

In respect to the presence of the austenitic phase in the as-built condition of the AM specimens the EBSD investigations also yielded interesting results. There, the austenitic grains appear to be fine in size and dispersed at the boundaries of the martensitic blocks and laths. EBSD technique though in this case seems to significantly underestimating the amount of austenite, up to about 2% was detected, compared to the XRD measurements. A source of

[1] Uddeholms AB, SE-683 85 Hagfors, Sweden

such discrepancy can of course be the smaller area investigated with EBSD as opposed to a more bulk analysis with XRD and the sensitivity limits of the technique. Nevertheless, the fact that the austenitic phase does not appear to segregate into large bulky configurations seems to have a contribution to the high hardness observed in this condition, despite the high content when compared to the conventional Uddeholm Corrax®.

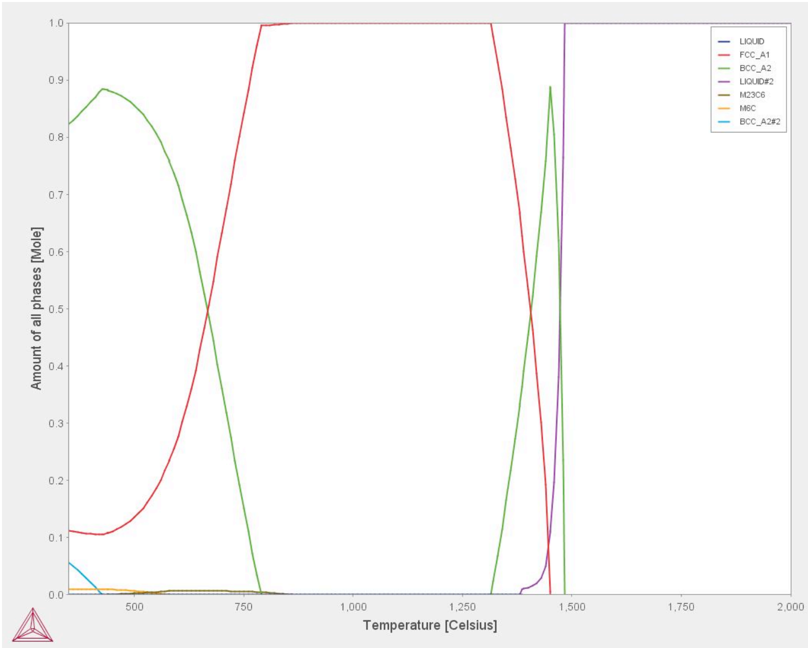

Fig. 4: Phase diagram for Uddeholm Corrax® composition with Thermo-Calc Software

The mechanical performance of the AM produced specimens was also evaluated in this study and it appears that there is a direct relationship to the developed process parameters through the resulting microstructure of the built samples. To achieve optimum quality in an AM produced tool the resulting strength level, elongation values and inclusion content also need to be considered. It was shown with the present investigations that although the density, hardness and strength reaches similar levels between the two different SLM systems, as well as in comparison to the conventional material [8], the elongation and impact toughness values can still differ and be lowered as a consequence of larger microstructural defects present, as in the case of the TruPrint 1000. These may in turn impact the tool lifetime due to cracking and fatigue, as well as its polishability and corrosion resistance, along with other surface related damages. Such findings raise the question of proper benchmarking the material properties which can be related to the optimization of the AM process.

Further investigations thus should be conducted for more in-depth studies on to the influence of the consistency and quality of the base material to the AM process, as well as to the optimum processing conditions and process parameter development in respect to the material performance. A tool maker using several different systems could possibly benefit from using the starting powder from the same source, with the same and verified characteristics for the process.

5. Conclusions

[1] Uddeholms AB, SE-683 85 Hagfors, Sweden

A precipitation hardening stainless tool steel developed for AM applications, Uddeholm AM Corrax®, has been successfully processed in two different SLM systems. The SLM processed material exhibited high densities and hardness values corresponding to those of conventionally processed Uddeholm Corrax® in the delivery condition. The microstructure of the samples produced from the SLM systems was characterized by the presence of significant amounts of inclusions and high amounts of retained austenite. After solution treatment and subsequent ageing, the amount of retained austenite was considerably reduced. The tensile and yield strength of the SLM processed samples after heat treatment were comparable to those corresponding to conventional Uddeholm Corrax®. The samples processed in the different SLM systems exhibited differences in defect density which consequently resulted in differences in the impact toughness and elongation values in spite of their similar density and hardness values. Higher amounts of defects had a negative impact on the impact toughness and elongation values while strength levels were rather insensitive to the defects. It is suggested that the defect density, impact toughness and elongation values are to be considered important in order to achieve the expected quality in a tool manufacturing setting.

References

[1] S. Kitayama, H. Miyakawa, M. Takano, and S. Aiba, "Multi-objective optimization of injection molding process parameters for short cycle time and warpage reduction using conformal cooling channel," *Int. J. Adv. Manuf. Technol.*, pp. 1–10, 2016.

[2] EOS, "EOS 3D Printing for Tooling," *https://www.eos.info/tooling*. .

[3] R. Hölker, M. Haase, N. Ben Khalifa, and A. E. Tekkaya, *Hot Extrusion Dies with Conformal Cooling Channels Produced by Additive Manufacturing*, vol. 2, no. 10. Elsevier Ltd., 2015.

[4] K. Kempen, E. Yasa, L. Thijs, J. P. Kruth, and J. Van Humbeeck, "Microstructure and mechanical properties of selective laser melted 18Ni-300 steel," *Phys. Procedia*, vol. 12, no. PART 1, pp. 255–263, 2011.

[5] E. A. Jägle, P.-P. Choi, J. Van Humbeeck, and D. Raabe, "Precipitation and austenite reversion behavior of a maraging steel produced by selective laser melting," 2014.

[6] S. Höring, D. Abou-Ras, N. Wanderka, H. Leitner, H. Clemens, and J. Banhart, "Characterization of Reverted Austenite during Prolonged Ageing of Maraging Steel CORRAX," *Steel Res. Int.*, vol. 80, no. 1, pp. 84–88, 2009.

[7] L. Thijs, J. Van Humbeeck, K. Kempen, E. Yasa, J. P. Kruth, and M. Rombouts, "Investigation on the Inclusions in Maraging Steel Produced by Selective Laser Melting," in *Innovative Developments in Virtual and Physical Prototyping: Proceedings of the 5th International Conference on Advanced Research in Virtual and Rapid Prototyping*.

[8] "Uddeholm Corrax Brochure." [Online]. Available: http://uddeholm.com/products/plastic-applications-tool-steel/uddeholm-corrax.

[9] D. Herzog, V. Seyda, E. Wycisk, and C. Emmelmann, "Additive manufacturing of metals," *Acta Mater.*, vol. 117, pp. 371–392, 2016.

[1] Uddeholms AB, SE-683 85 Hagfors, Sweden

Giedenbacher Jochen[1], Huskic Aziz[1], Wallner Stefan[2], Sommitsch Christof[3]

PROCESSING AND MATERIAL PROPERTIES OF HOT WORK TOOL STEELS MANUFACTURED BY SELECTIVE LASER MELTING

Abstract

Selective Laser Melting (SLM), an additive manufacturing technology, has established rapidly in recent years to produce metallic prototypes and complex component geometries. At present the commercial production of steel components, using this technology, is limited to steel powder with very low carbon content.

The aim of this study is to characterize the selective laser melting process by using a metal powder alloy, which is commonly used for manufacturing hot-working tools. In the future these alloys will be utilised to manufacture moulds and inserts for hot working applications such as forging, press hardening, hot stamping and die-casting processes.

In this paper the processing of a hot work tool steel alloy with a powder preheating built-platform for SLM is investigated. The results of this study show that an elevated built-platform temperature of 500 °C is necessary to reduce the temperature gradient between the built-platform and the laser-melted powder. The experiments indicate low risks of defects at higher temperatures. Consequently, alloys with a higher content of carbon show a major influence on residual stresses. These stresses lead to distortions and cracking and consequently to failure of the produced parts. In addition, the physical and mechanical properties are determined for these powder materials. A homogeneous microstructure is achieved by optimizing the process parameters. Metallographic examinations illustrate that the parameters lead to a minimum level of porosity and a limited number of defects.

Keywords

Selective Laser Melting, SLM, Hot Work Steel, Preheated Powder Bed, High Density, Higher Carbon Content, Residual Stresses

1. Introduction

Additive manufacturing (AM) of metallic components allows a direct fabrication of complex geometries for many technical applications. Selective Laser Melting (SLM), a layer by layer manufacturing process, offers a customized production of parts with functional structures. So far a small range of powder materials are available for SLM to produce parts for hot work tooling applications. The most common SLM powder alloy for manufacturing moulds and dies is X3NiCoMoTi18-9-5 (18% Ni Maraging 300) [1][2]. This established iron-based powder alloy is distributed from the manufacturer of SLM-machines and contains a very low carbon content of less than 0.03 wt.-% and a high percentage of nickel and cobalt [3][4]. The weldability and processing of this maraging steel is under control. After ageing a hardness up to 52 HRC can be achieved [3]. SLM-produced tools for injection moulding applications correspond to the state of the art. The procedure is particularly useful to manufacture complex geometries with functional features such as individual conformal cooling channels [5].

[1] University of Applied Sciences Upper Austria, Stelzhamerstraße 23, 4600 Wels, Austria
[2] BÖHLER Edelstahl GmbH & Co KG, Mariazeller Straße 25, 8605 Kapfenberg, Austria
[3] Institute of Materials Science and Welding, Kopernikusgasse 24/I, 8010 Graz, Austria

In comparison to a conventional produced hot work steel (X38CrMoV5-3) this established maraging alloy shows no sufficient wear behaviour under series-production conditions. High mechanical and thermal loads lead to an increased material abrasion during the press hardening process by using a selective laser melted tool (X3NiCoMoTi18-9-5) [6].

In order to meet the requirements of tool steels for dies and punches in warm and hot forming processes it is necessary to combine a high hardness, a good toughness and a high tempering resistance. These properties are important to increase the life-time of such tools. In the future these steels manufactured by Selective Laser Melting should have the same characteristics like conventional produced hot work steels.

Generally, hot work steel alloys contain a carbon content of 0.3 – 0.6 wt.-%. These steels also include further alloying elements such as silicon, manganese, chromium, molybdenum, vanadium, cobalt and tungsten to increase the hardness and tempering resistance. So far these steel grades are characterised by a limited weldability without preheating [7]. Limited weldability is caused by a hardening effect in the heat-affected zones. A phase transformation (martensitic structure) leads to induced residual stresses in the welded zone. From previous studies it can be seen that residual stresses lead to crack initiation during the SLM process [8]. Figure 1 shows cracks in an SLM-produced cube by using X40CrMoV5-1 powder without preheating. To reduce the residual stresses a preheating built-platform is used. As a result, a lower thermal gradient can be achieved.

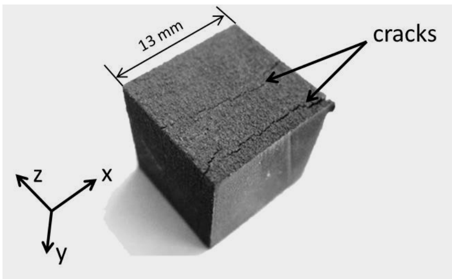

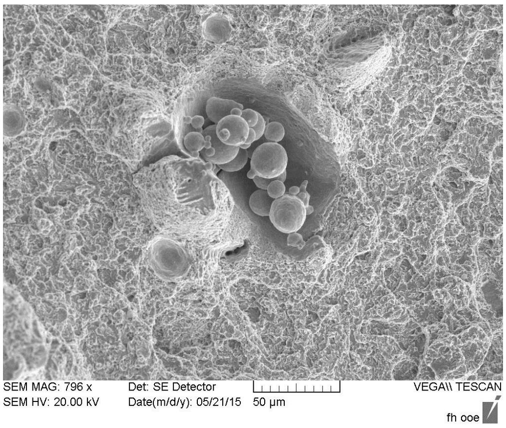

Fig. 1: Hot work steel samples produced by SLM, incorrect SLM-parameters (left), unmelted powder particles on a fracture surface (right).

In the last years it has been observed that the processability of further tool steel alloys by using the SLM-technology is possible. It can be seen that producing complex shapes for forming applications will be a future trend [6]. Research activities indicate that the successful processing of tool steel powders depends on the optimisation of SLM-parameters. Some publications focus on this issue to expand the range of iron-based powder materials (e.g. HS6-5-2C, X40CrMoV5-1, X110CrMoVAl8-2) for SLM applications [6][9][10][11][12].

In this study a hot work steel grade Böhler W360 was manufactured at different preheating temperatures to produce accurate SLM-samples without cracks.

2. Experimental

2.1 Material

[1] University of Applied Sciences Upper Austria, Stelzhamerstraße 23, 4600 Wels, Austria
[2] BÖHLER Edelstahl GmbH & Co KG, Mariazeller Straße 25, 8605 Kapfenberg, Austria
[3] Institute of Materials Science and Welding, Kopernikusgasse 24/I, 8010 Graz, Austria

In this research, the steel powder alloy was developed by BÖHLER Edelstahl GmbH & Co KG for hot work tooling applications. This steel grade offers a variety of properties such as high toughness, hardness and an excellent thermal conductivity. The particle size of gas atomized powder material is between 10 to 45 µm. The particle size determination shows an average grain size d_{50} of 22.1 µm. The main part of the powder particles shows a spherical shape, which consequently leads to an excellent flowability. Figure 2 illustrates the formation of the powder particles (SEM) and the particle size analysis (PSA) of the used hot work steel powder.

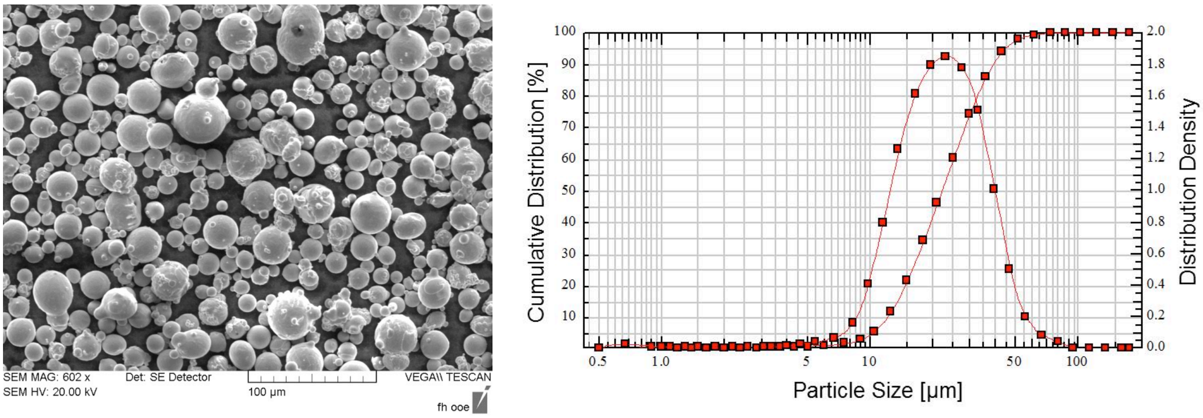

Fig. 2: SEM picture (left) and particle size analysis (right) of gas atomized Böhler W360.

Before starting the experimental series, a re-drying of the steel powder is carried out in a climatic chamber at a constant temperature of 130 °C and relative humidity (rh) of 0% for 12 hours to achieve the optimum processing properties. Low humidity guarantees an excellent application of powder layer by layer and a high quality of the laser welding process. The chemical composition of the hot work steel W360 is given in Table 1.

Table 1: Chemical composition of the hot work steel Böhler W360 (wt.-%).

Fe	C	Si	V	Cr	Mn	Mo
bal.	0.48	0.15	0.58	4.77	0.34	2.46

2.2 SLM-machine and process parameters

The investigated samples were manufactured by using a M1 SLM-machine from Concept Laser GmbH. The SLM-machine is equipped with a single 200 W fibre laser. To preheat the powder bed during the SLM-process, an internally developed heating system was implemented. All samples were produced in protective nitrogen atmosphere. The concentration of oxygen in the building chamber was measured and kept below 1% during the whole SLM-process. The selected process parameters for this study are given in Table 2.

[1] University of Applied Sciences Upper Austria, Stelzhamerstraße 23, 4600 Wels, Austria
[2] BÖHLER Edelstahl GmbH & Co KG, Mariazeller Straße 25, 8605 Kapfenberg, Austria
[3] Institute of Materials Science and Welding, Kopernikusgasse 24/I, 8010 Graz, Austria

Table 2: Used process parameters for the hot work steel Böhler W360.

Process Parameter	Sign	Setting	
Laser Power	P	180	W
Laser Scan Speed	v	600	mm/s
Hatch Distance	a	105	µm
Laser Beam Diameter	d	150	µm
Layer Thickness	h	30	µm
Preheating Temperature	T	none–560	°C

Previous parameter studies for further tool steels show that applying island scanning strategy leads to higher density values by using these determined parameters settings. In this study it was possible to produce small SLM-samples (13x13x13 mm) with a relative density of more than 99%.

3. Results and Discussion

The investigations were performed in order to determine the quality of the produced samples (11x9x56 mm) using the hot work steel Böhler W360 for SLM-processes. SLM-samples manufactured at powder preheating temperatures up to 200 °C show a crack-free processing. Cross-sections of one of these samples are given in Figure 3. The black spots represent the formation of micro pores within the laser welded material at a preheating temperature of 560 °C. In this case image analyses (LOM) show an average porosity of about 0.24%. Additionally, microstructural investigations indicate a distributed fine-grained welding structure due to process-related cooling rate.

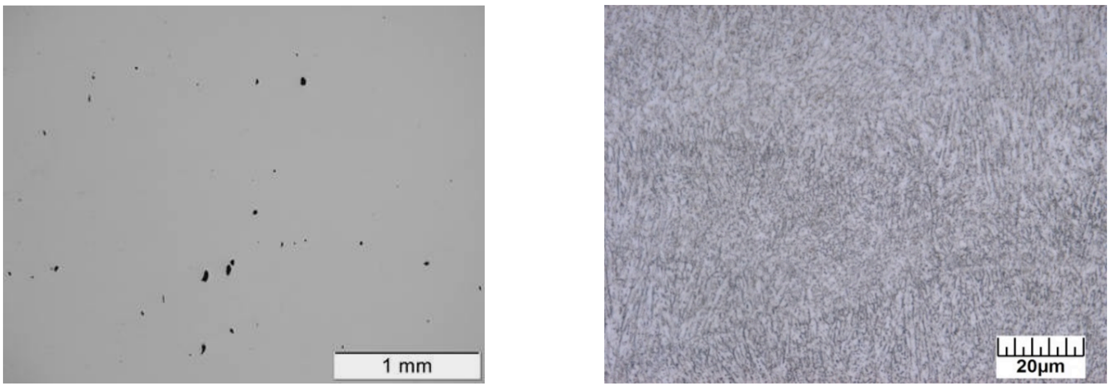

Fig 3: Cross-section of W360 samples produced by SLM at T = 560 °C.

The results of density (volumetric mass and relative density) and micro hardness measurements at different powder preheating temperatures are given in Fig. 4. Volumetric mass density of several samples was calculated using the Archimedes principle. Samples produced without powder preheating indicate the highest volumetric mass density. In this case a relative density of 99.75% was achieved. A preheating temperature of 300 °C shows lower values. Preheating temperatures above 300 °C indicate a rise of the volumetric mass density.

Microhardness measurements indicate a relatively high hardness for SLM produced W360-samples at different preheating temperatures. In this investigation a hardness up to 560

[1] University of Applied Sciences Upper Austria, Stelzhamerstraße 23, 4600 Wels, Austria
[2] BÖHLER Edelstahl GmbH & Co KG, Mariazeller Straße 25, 8605 Kapfenberg, Austria
[3] Institute of Materials Science and Welding, Kopernikusgasse 24/I, 8010 Graz, Austria

HV1 has been reached. A decrease in hardness was measured at preheating temperatures of 300 °C and 560 °C. Generally, high hardness indicates a martensitic microstructure. In this case the SLM-process also induces the phases retained austenite and carbides. To verify this result an exact quantitative phase analysis is planned to be done as a next step.

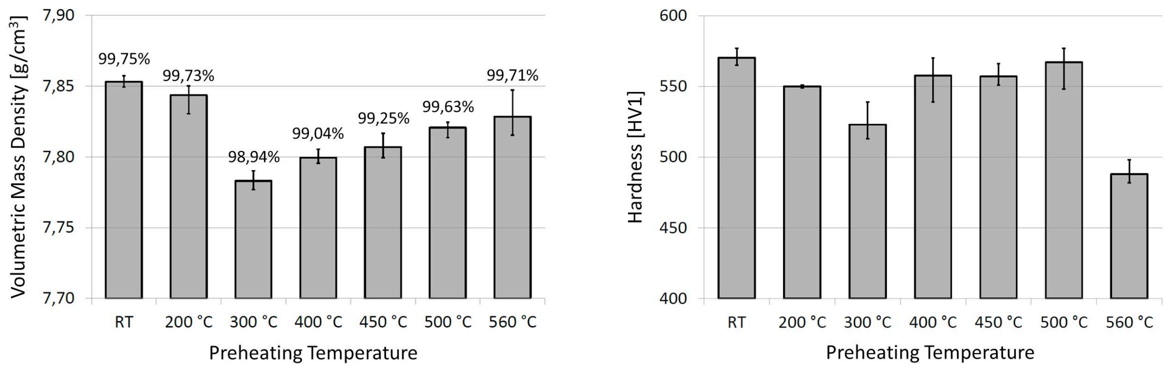

Fig. 4: Volumetric mass density (left) and hardness (right) of W360 at different preheating temperatures.

Additionally, residual stress measurements are carried out with manufactured twin-cantilever for different preheating temperatures. Figure 5 illustrates the effect of residual stresses in SLM-parts. It can be observed that lower preheating temperatures lead to a significant increase of residual stresses within the test parts. In general, distortions lead to unsatisfying results during the manufacturing of fine structures. The dimensional accuracy and compliance with specified tolerances were not achieved. Subsequently, complex SLM-parts with supports could not be realized. In addition, high residual stresses induce cracks and cause an abort of the process.

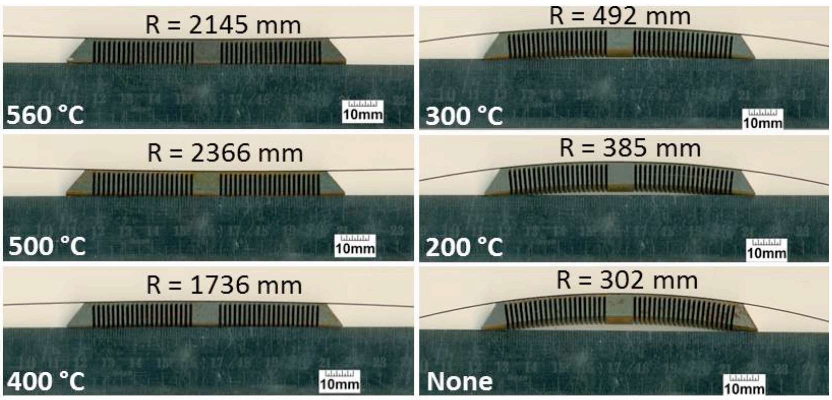

Fig. 5: Twin-cantilever measurements - residual stresses as a function of the preheating temperature.

For comparison, chemical analysis shows a decarburization of the preheated powder after the selective laser melting process at elevated preheating temperatures. Further C-analysis results indicate that the carbon content significantly decreases from 0.49 wt.% of the powder to 0.29 wt.% of the SLM-part at a preheating temperature of 560 °C.

4. Conclusion and Outlook

[1] University of Applied Sciences Upper Austria, Stelzhamerstraße 23, 4600 Wels, Austria
[2] BÖHLER Edelstahl GmbH & Co KG, Mariazeller Straße 25, 8605 Kapfenberg, Austria
[3] Institute of Materials Science and Welding, Kopernikusgasse 24/I, 8010 Graz, Austria

Preliminary studies showed that an insufficient selection of SLM process parameters lead to a risk of cracking. In this research SLM-samples of a hot work steel powder with a carbon content of 0.49 wt.% have been successfully manufactured without visible cracks and delamination.

Small samples produced without preheating or lower preheating temperatures (less than 200 °C) indicate a high relative density and a high hardness. However, the measurement of twin-cantilever-samples show that a low preheating temperature leads to an increased propensity to induce residual stresses. A reduction of thermal gradient reduces the residual stresses of the fabricated hot work tool steel samples. A preheating temperature of 500 °C shows a comparatively high hardness of 560 HV1, a low porosity and moderate residual stresses.

In future studies, the influence of decarburization at elevated preheating temperatures shall be investigated. Furthermore, the quantity and size of phase segregation will be determined depending on the preheating temperatures. In comparison with conventional produced hot work tool steels, the physical and mechanical properties will be investigated. In addition, the heat treatment process will be optimized to balance hardness and toughness for selective laser melted W360-parts.

The reutilization and processing of preheated powder particles will be an important aspect for an efficient production of SLM-parts entailing optimum material utilisation. Chemical and physical analysis of the preheated powder particles will be carried out for achieving the research objectives. Finally, the quality of the manufactured parts depends on the processability of the powder materials.

5. Acknowledgements

The authors gratefully acknowledge the financial support of this project by Böhler Edelstahl GmbH & Co KG. Furthermore, thanks are directed to the Institute of Materials Science and Welding at Graz University of Technology and the Center for Smart Manufacturing for their technical and scientific support.

6. References

[1] T.H. Becker, D. Dimitrov, The achievable mechanical properties of SLM produced Maraging Steel 300 components, Rapid Prototyping Journal (2016, Volume 22/3), p.487

[2] K. Kempen, E. Yasa, L. Thijs, J.-P. Kruth, J. Van Humbeeck, Microstructure and mechanical properties of Selective Laser Melted 18Ni-300 steel, Physics Procedia (2011, Volume 12), p. 256

[3] Concept Laser GmbH, Data Sheet: CL 50WS, http://www.conceptlaserinc.com (2016)

[4] LPW Technology Inc., Data Sheet: LPW M300, http://www.lpwtechnology.com (2016)

[5] S. Jansen, Generative Fertigung von konturnah temperierten Werkzeugen mittels Selective Laser Melting, Apprimus Verlag, Aachen (2014)

[6] R. Stache, Application-oriented usage of tool steels in 3D-Printing, Rapid.Tech, Conference for Additive Manufacturing, Erfurt (2016), p.380

[7] L.A. Poznyak, S.I. Tishaev, Effect of alloying elements on the properties of steels for hot working dies, Metal Science and Heat Treatment (1969, Volume 11), p.59

[8] A. Huskic, Additive processing of materials with higher carbon content, International Conference on Processing & Manufacturing of Advanced Materials, Graz (2016)

[1] University of Applied Sciences Upper Austria, Stelzhamerstraße 23, 4600 Wels, Austria
[2] BÖHLER Edelstahl GmbH & Co KG, Mariazeller Straße 25, 8605 Kapfenberg, Austria
[3] Institute of Materials Science and Welding, Kopernikusgasse 24/I, 8010 Graz, Austria

[9] J. Sander, J. Hufenbach, L. Giebeler, H. Wendrock, U. Kühn, J. Eckert, Microstructure and properties of FeCrMoVC tool steel produced by selective laser melting, Materials and Design (2016, Volume 89), p.335
[10] M.J. Holzweissig, A. Taube, F. Brenne, M. Schaper, T. Niendorf, Microstructural characterization and mechanical performance of hot work tool steel processed by Selective Laser Melting, Metallurgical and Materials Transactions B (2015, Volume 46B), p.545
[11] F. Feuerhahn, A. Schulz, T. Seefeld, F. Vollertsen, Microstructure and properties of selective laser melted high hardness tool steel, Physics Procedia (2013, Volume 41), p. 843
[12] K. Kempen, B. Vrancken, S. Buls, L. Thijs, E. Yasa, J. Van-Humbeeck, J.P. Kruth, Selective Laser Melting of Crack-Free High Density M2 High Speed Steel Parts by Baseplate Preheating, Journal of Manufacturing Science and Engineering (2014, Volume 136)

[1] University of Applied Sciences Upper Austria, Stelzhamerstraße 23, 4600 Wels, Austria
[2] BÖHLER Edelstahl GmbH & Co KG, Mariazeller Straße 25, 8605 Kapfenberg, Austria
[3] Institute of Materials Science and Welding, Kopernikusgasse 24/I, 8010 Graz, Austria

Daniel Junker[1], Aleksandr Feorov, Michael Schmidt, Marion Merklein

Tribological properties of tools manufactured and polished by using Laser Metal Deposition machine setup

Abstract

In industry the variety of products is increasing and product life cycles are getting shorter. For parts made by forging processes this trend leads to very high prizes, as the tool costs have to be assimilated with only few parts. To reduce the tool costs new, flexible processes have to be established in tool manufacturing. Laser based additive manufacturing is noted for its high flexibility and especially laser metal deposition (LMD) is already used for coating and repairing of forming tools, therefore investigations are made to qualify this process for the production of forging tools. Recent investigations showed the possibility to build three dimensional, volumetric structures with the high carbon hot work tool steel 1.2343. The mechanical properties of additively manufactured tool structures are similar to those of conventional produced 1.2343. One special feature of the LMD process is the possibility to use the machine setup for a post-processing to polish the surface with the defocused laser. As the surface of additively built parts is very rough this process combination within one machine could have the potential to replace a post-machining process.
Within the present work tools for ring compression tests will be manufactured and polished with the described setup by using different parameters. Afterwards the surface roughness and waviness are measured by using a laser scanning microscope. Furthermore residual stresses will be identified by an x-Ray inspection. To qualify the friction, ring compression tests are made with the additively manufactured and polished tools as well as with conventionally milled and polished tools. For an exact investigation the ring tests will be made with two different, in the industry established lubricants like molybdenum disulphid or Beruforge 120D.

1 Institute of Manufacturing Technology, Friedrich-Alexander-Universität Erlangen-Nürnberg, Egerlandst. 13, 91058 Erlangen, DE

GERHARD PANZL [1], BRUNO BUCHMAYR [1], STEFAN WALLNER [2]

INVESTIGATION OF USABILITY OF PLASTIC MOULD STEELS FOR THE LASER POWDER BED FUSION PROCESS

Abstract

This work is focussed on the usability of pulverized plastic mould steel alloys for the laser powder bed fusion process. Therefore, the steel grades M130 (1.2764) and M368 (trade names of Böhler Edelstahl GmbH&Co KG) were investigated. At first, parameter studies were performed to find proper parameter combinations for laser power and scan speed (for constant hatch distance and stripe width). The focus was laid on the formation of consistent welding beads with only marginally vertical exaggerations of the built surface. With appropriate parameter combinations cylindrical specimens for metallographic analysis (porosity, microstructure) were manufactured. In addition, material tests like tensile tests, hardness measurements and charpy impact tests were performed and the results compared to conventionally produced materials.

Keywords
Additive manufacturing, laser powder bed fusion (L-PBF), selective laser melting (SLM), plastic mould steel, parameter study

1. Introduction

The laser powder bed fusion process (L-PBF) is the main technology for additive manufacturing of metallic components. One of the main applications is the manufacturing of injection mould tools and inserts with complex geometries and internal cooling systems [1]. The possibility of an adjustable cooling leads to a reduction of cycle time, improved part quality and longer tool life [2]. At present, the variety of available metal powder materials for the laser powder bed fusion process is limited to very few commercial available alloys. The most common steel powder materials for tooling applications such as tools for injection moulding or die casting are stainless steels and tool steels like 1.2709 (X3NiCoMoTi18-9-5), 1.4404 (X2CrNiMo17-12-2), 1.4542 (X5CrNiCuNb16-4)[2] and 1.2344 (H13, X40CrMoV5-1) [3,4].
Steel metal powders for additive manufacturing have in common, that the carbon content is very low. The carbon content, respectively the hardness of a powder material reached during the L-PBF process, is an important indicator for the usability of a particular steel grade. The formation of cracks or delamination, due to the presence of residual stresses, determine the suitability of metal powders. Mercelis and Kruth [5] describe two main mechanisms which cause residual stresses. The first mechanism is called the temperature gradient mechanism (TGM, Figure 1) and stems from the large thermal gradients that occur around the laser spot. Due to the rapid heating of the upper layers and the low heat conduction of the bulk material, a steep temperature gradient develops. The upper layers with high temperature tend to expand, while the underlying colder layers impede this expansion. This leads to compressive stresses (σ_{comp}) in the upper layers. If these stresses exceed the yield strength of the material, plastic deformations (ε_{pl}) in the upper layers occur. When the layers cool down, the compressive stresses are converted in residual tensile stresses (σ_{tens}), which may induce cracking of the part.

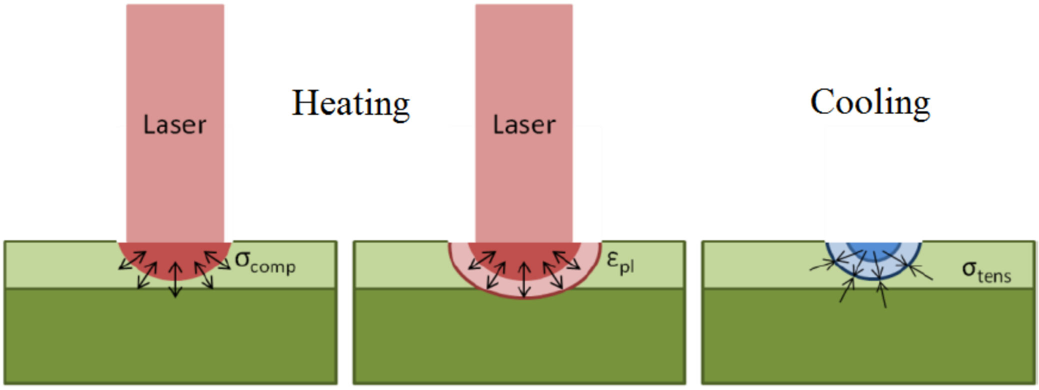

Fig 1: Temperature Gradient Mechanism (TGM) [5]

The second mechanism occurs during the cool-down phase of the molten welding pools. The top layers tend to shrink due to the thermal contraction, which is inhibited by the underlying material. This causes tensile stress in the top layers and compressive stress below [5]. If the material shows transformations of the microstructure during the cool down phase, a further contribution to the amount of residual stresses has to be taken in account [6]. A superposition of these mechanisms can result in distortion or crack formation [5]. A possibility to reduce residual stresses is to raise the temperature within the building chamber. The pre-heating temperature should be based on the martensite start temperature (the beginning of the austenite-martensite transformation) of the material. For welding of tool steels, a pre-heating temperature of 50 to 100 °C above the martensite start temperature is proposed [6,7]. Currently available L-PBF systems only offer the possibility to pre-heat the substrate plate to 200 °C, which is insufficient to avoid cracking in materials with as-built hardness level above 50 HRC. The frequently used maraging steel 1.2709 has the advantage, that the hardness level in as-built condition reaches 33 to 37 HRC. After a subsequent heat treatment the hardness can be increased above 50 HRC. Typical plastic mould steel materials show a different behaviour. In case of M130 alloy, the samples manufactured by the L-PBF process show a hardness level which is almost near to their maximum hardness values (without any additional hardening treatments).
For the fabrication of plastic moulds for highly abrasive plastics, high hardness as well as wear- and corrosion-resistance of the tool materials are necessary [8]. Available metal powders often cannot meet the full requirements. In this work, two steel grades, usually applied for the fabrication of plastic moulds, were under investigation.

2. Materials and methods

M130 (1.2764), a Ni-Cr-Mo case hardening steel for plastic moulds and grade M368, a martensitic chromium steel, were gas atomized and separated to a particle size range of 10 to 45 µm. Table 1 shows the nominal chemical compositions of the alloys.

Tab. 1: Nominal chemical compositions of the M130 and M368 alloys

	C [%]	Si [%]	Mn [%]	Cr [%]	Mo [%]	Ni [%]	V [%]	
M130	0,19	0,25	0,30	1,30	0,20	4,10	-	
M368	0,54	0,45	0,40	17,30	1,10	-	0,10	+N

L-PBF experiments were carried out using an EOSINT M280 (by EOS, Germany) equipped with a 400 W Ytterbium fibre laser with a focussed spot size of 100 µm. Nitrogen was used as protective gas.

Parameter studies

The first stage of parameter studies is the fabrication of multi-layered test structures (2x30x1 mm^3). For constant layer thickness (t), hatch distance (d_H) and stripe width combinations of laser power (P) and scan speed (v), covering a wide range of values (P: 100-300 W, v: 200-1000 mm/s), are tested. Fig. 3 shows the tested P-v combinations for the steel grade M130.

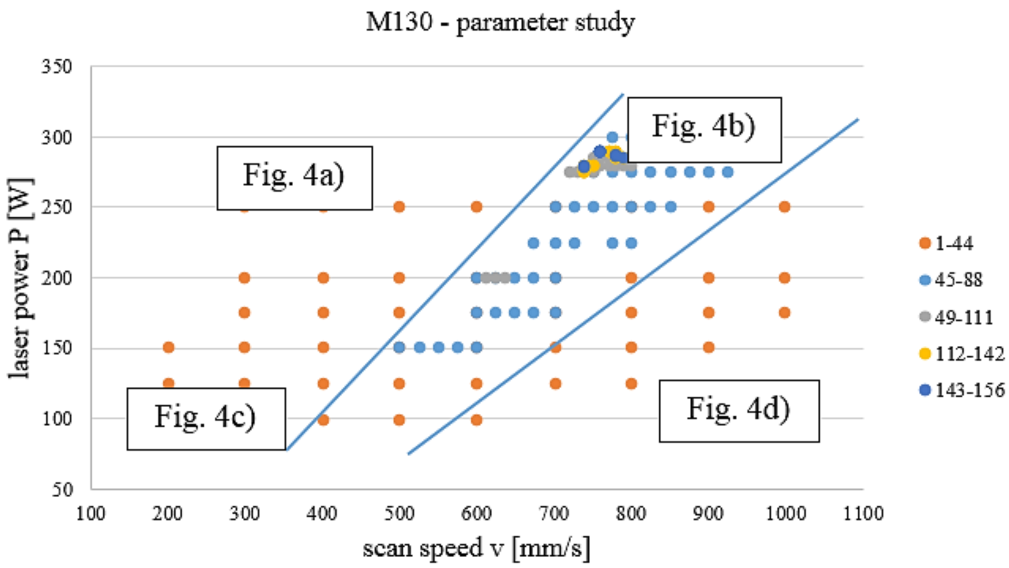

Fig. 3: Development of a parameter study (here M130). The labels Fig. 4a to 4c correspond to the shown micrographs of Fig. 4

The volume-based energy density E (J/mm³, Eq. 1) can be used to categorize the energy input for different parameter combinations.

$$E\left[\frac{J}{mm^3}\right] = \frac{P}{v*d_H*t} \qquad \text{Eq. 1}$$

The top surface of the test structures were analysed using a ZEISS KL 1500 LCD stereomicroscope (see Fig. 4).

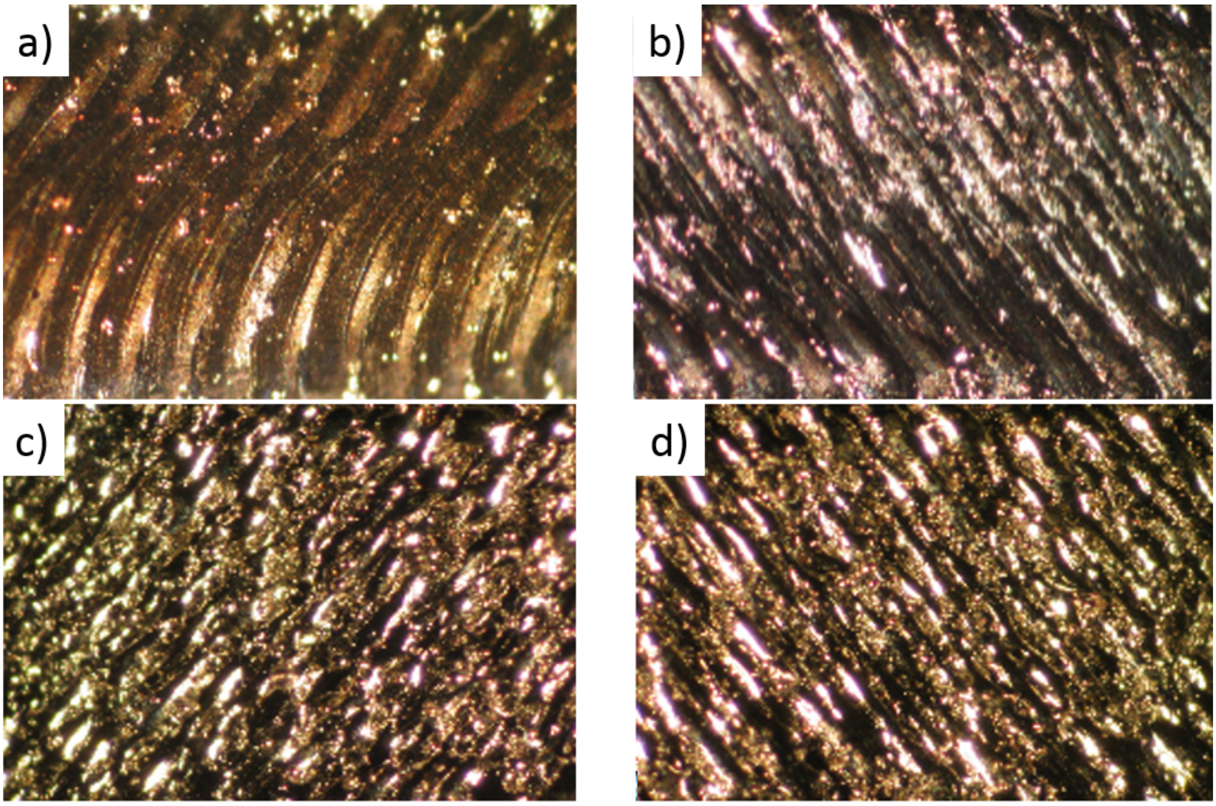

Fig. 4: Micrograph of the top surfaces of the test structures

The focus lies on the formation of continuous welding beads with only marginally vertical exaggerations of the built surface and minimal annealing colours. Fig. 4a shows the top surface of a parameter combination with a high energy input. The surface is convex and annealing colours are clearly evident. The surfaces of Fig. 4c and 4d are a result of a low energy input, whereby Fig. 4c is dominated by low laser power while Fig. 4d is characteristic for too high scan speed. In both cases, the amount of energy input is insufficient to melt enough metal powder to form continuous welding lines. The surface in Fig. 4b is an example for a good P- v combination. The surface shows a flat shape and continuous welding lines. The parameter sets which meet the requirements were used to build cylindrical test specimens (20 mm diameter, 20 mm height) to analyse presence and amount of porosities or cracks. For this, cross-sections of the cylindrical test specimens are subjected to a standard metallographic procedure such as grinding with 180, 320, 500, 800, and 1200 abrasive papers as well as polishing with 3 µm and 1 µm diamond suspension. For the analysis of the microstructures, the samples are etched. M130 was etched using 3 % Nital and M368 in V2A etchant.

For the analysis of porosities, cracks and microstructures an inverse light microscope (Olympus GX51) was used. To obtain almost non-porous samples (density ratio >99 %), the parameter combinations for M130 had to be adjusted in several iterations. Because the microstructures of the M368 samples showed cracks for all parameter combinations no further investigations were done. For the alloy M130 hardness tests of samples in as-built and heat treated conditions were performed. Therefore the hardness testing machine EMCO-TEST M1C 010 was used. For M130 charpy impact tests (Zwick RKP 450) and tensile tests (Zwick Z250) were performed. The fracture surfaces of the impact tests were analysed using a scanning electron microscope (JEOL JSM-6460 LV).

For the two steel grades the chemical composition was quantified. The carbon content was measured by a LECO CS844 element analyser. The nitrogen content (M368) was measured with a LECO TCH600 Nitrogen/Oxygen/Hydrogen determinator. Other elements were detected by a Perkin Elmer Optima 3300DV ICP-OES spectrometer.

3. Results and discussion

3.1. M130

The parameter studies for M130 led to crack free test specimens with a density of >99.6 %. Fig. 5 shows etched cross sections of a M130 sample.

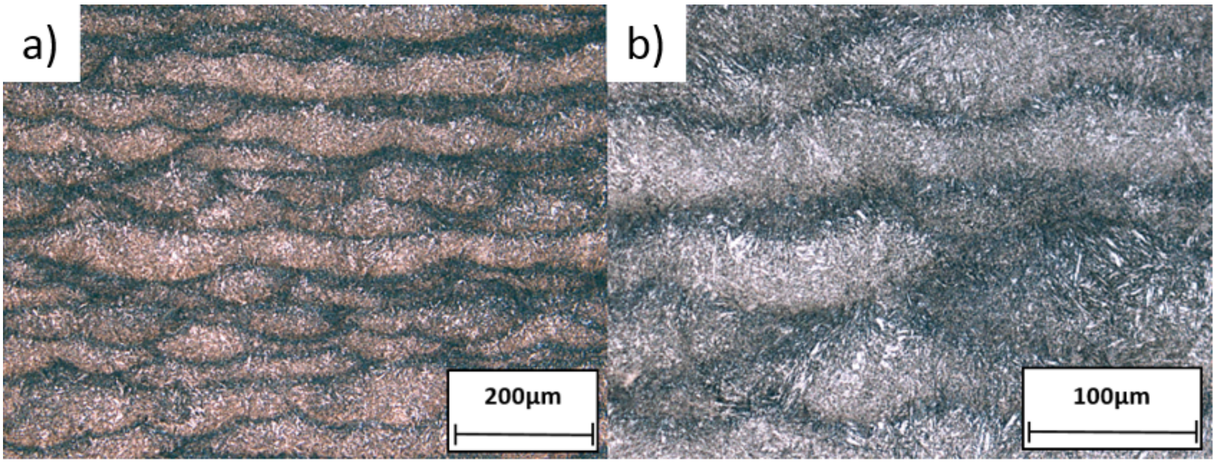

Fig. 5: Etched cross-sections of printed M130 material

Three testing series were carried out and compared to the properties of conventional fabricated material. For the first testing series samples with an energy density of 73.3 J/mm³ (P = 250 W, v = 750 mm/s, t = 40 µm, d_H = 0.11 mm) were fabricated and heat treated. The heat treatment of the standard material is a 40 minutes hardening process at 800 °C followed by furnace cooling and three annealing procedures at 200 °C for 2 hours. The measurements of the hardness values after the heat treatment showed increased hardness values of the printed samples of 48 HRC compared to 44 HRC for the reference material. Also the values of the impact testing specimens reached 45 J compared to 92 J. For the second testing series, the same process parameter combinations were chosen. The annealing procedure was changed to three two-hour treatments at 200 °C, 220 °C and 250 °C. This led to a reduction of the hardness to 46.5 HRC but similar impact testing values (46 J). The third testing series was performed with a slightly higher energy density of 78.7 J/mm³ (P = 270 W, v = 780 mm/s, t = 40 µm, d_H = 0.11 mm). In addition, the annealing process was changed to two annealing stages at 250 °C and at 350 °C (holding period 2 hours), respectively. Under these conditions a hardness level of 44 HRC and charpy impact testing values of 64 J were reached. The tensile tests for the third testing series (Fig.6, R_m = 1350 MPa, $R_{p0,2}$ = 1180 MPa, A_g = 3 %) showed comparable values to the conventional fabricated material (R_m = 1420 MPa, $R_{p0,2}$ = 1135 MPa, A_g = 3.6 %).

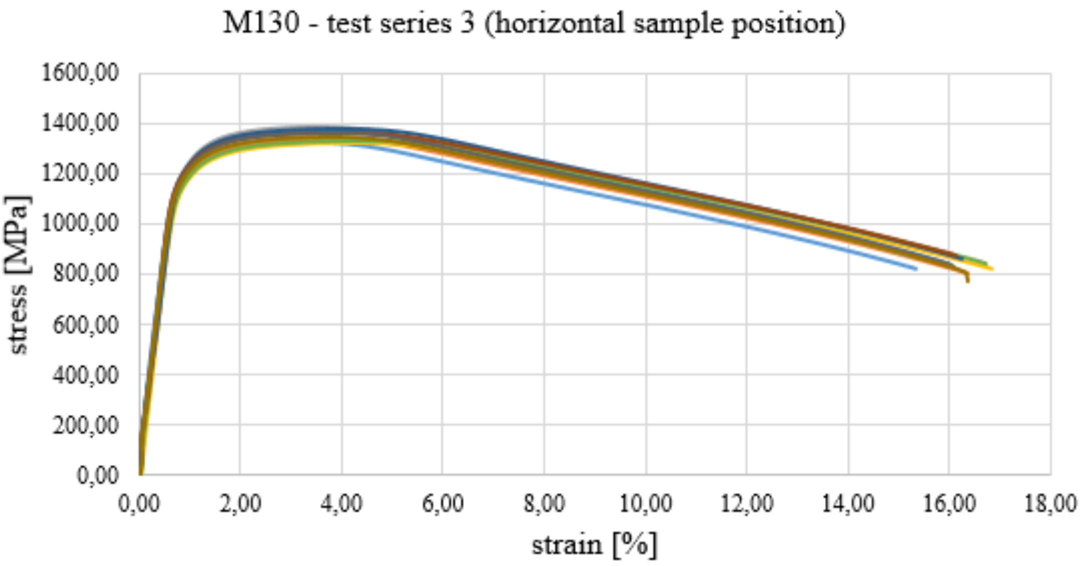

Fig. 6: Stress-strain curves of in horizontal position built M130 specimens of test series 3

The tensile tests for test series 1 and 2 were performed on samples which were printed in horizontal and vertical direction. It has to be noted, that the distinctive anisotropy of printed samples has no influence after a heat treatment. The chemical composition of the printed specimens showed no differences compared to conventional fabricated test specimens and the initial powder material. Fig. 7 shows a fracture surface of a charpy impact test specimen of test series 3.

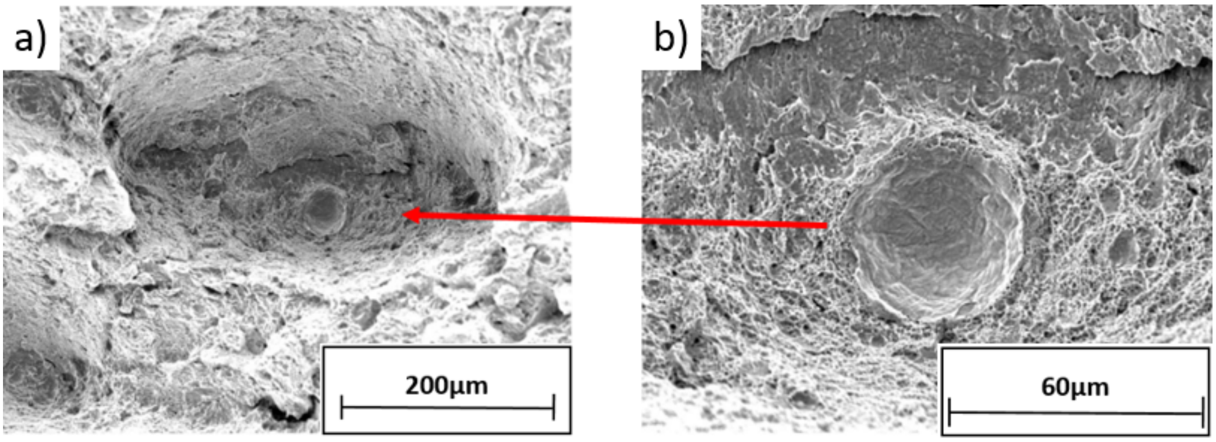

Fig. 7: REM image of a comb-like area in an impact test specimen of test series 3

The fracture surfaces show a ductile behaviour without localised origins of fracture. In some areas round combs with a smooth inner surface are visible. These combs could have their origins in porosities. But the amount and size of these combs should have no influence on the results of the impact tests.

3.2. M368 steel grade

For M368 a parameter study in the energy density range of 48.7 J/mm³ (P = 150 W, v = 700 mm/s, t = 40 µm, d_H = 0.11 mm) to 73.5 J/mm³ (P = 275 W, v = 850 mm/s, t = 40 µm, d_H = 0.11 mm) was carried out. The analysis of the cross-sections showed a high number of cracks within the microstructure for all samples (Fig. 8).

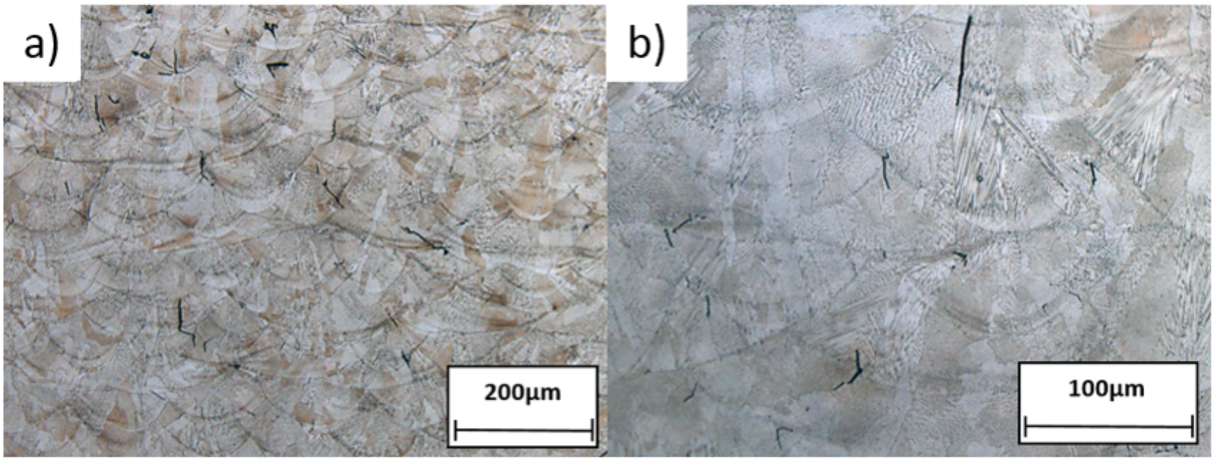

Fig. 8: Etched cross-sections of printed M368 material

The chemical composition of the printed test specimen is very close to the initial composition. In addition to the parameter studies with single melting of each layer, remelting experiments were done. Each layer of a test cube (20 x20 x20 mm³) was remelted directly after the first exposure of the powder layer. Due to the fact of the high C-content of this alloy (0,54 % C) and the lack of preheating possibilities of the printing device no parameter combinations could be found which lead to crack free printed samples.

4. Conclusions

The investigation of two plastic mould steel grades showed two different behaviours. Printed M130 specimens can be produced crack free and achieve similar material properties to conventionally produced material, if the heat treatment is adapted. For the steel grade M368the production of crack free samples was not possible within the used printing device. Both alloys show no differences between the chemical composition of powder material and printed specimens.

References

[1] R. Pacurar, A. Pacurar, N. Balc, in *Recent Advances in Engineering Mechanics, Structures & Urban Planning*, Proceedings of the 6th International Conference on Engineering Mechanics, Structures, Engineering Geology - EMESEG `13 (EDS: E. Scutelnicu, F. Rotondo, H. Varum), WSEAS Press, Cambridge (2013), pp. 81-86.
[2] T. Wohlers, *Wohlers Report 2010*, Additive Manufacturing, State of the Industry, Annual Worldwide Progress Report, Wohlers Associates (2010).
[3] M. Mazur, M. Leary, M. McMillan, J. Elambasseril, M. Brandt, *Rapid Prototyping Journal* (2016, Vol. 22), pp. 504-518.
[4] R. Cottam, J. Wang, *J. Mater. Res.* (2014, Vol. 29, No. 17), pp. 1978-1986.
[5] P. Mercelis, J.P. Kruth, *Rapid Prototyping Journal* (2006, Vol. 12, No. 5), pp. 254-265.
[6] C. Over, Generative Fertigung von Bauteilen aus Werkzeugstahl X38CrMoV5-1 und Titan TiAl6V4 mit „Selective Laser Melting“, Dissertation RWTH Aachen, Shaker Verlag (2003).
[7] http://www.bohler-edelstahl.com/media/BW140D_Schweissbrosch.pdf, accessed June 2016.

[8] K. Kempen, L. Thijs, B. Vrancken, S. Buls, J. Van Humbeeck, J.P. Kruth, *Proceedings of the 24th Solid Freeform Fabrication Symposium* (2013), pp. 131-139.

Sebastian Bremen[1]
Tel: +49 (0) 241 8906-537
Mail: Sebastian.bremen@ilt.fraunhofer.de
Wilhelm Meiners[1]
Tel: +49 (0) 241 8906-301
Mail: Wilhelm.meiners@ilt.fraunhofer.de
Konrad Wissenbach[1]
Reinhard Poprawe[1]

Material properties of IN718 processed with High-Power Selective Laser Melting

Abstract

For SLM to become suitable for series production, its productivity and, thereby, process speed have to be increased. One possibility to achieve this is by increasing laser power and adapting the process parameters (beam diameter, laser power, scanning velocity etc.) accordingly (High Power SLM). This adaption of the process parameters, however, leads to a significant change in the cooling and solidification conditions in the melt pool: The microstructure and the resulting mechanical properties are significantly changed. For this reason, it is necessary to investigate the influence of the HP-SLM process on the resulting material properties. The results show the investigation of a process window with up to 2kW laser power for the nickel-based alloy IN718, which is a material frequently used for high temperature applications in the turbomachinery branch. Here, the extent to which different process parameters influence the achievable productivity is analysed. Afterwards, the microstructure (grain size and orientation) and the mechanical properties (tensile tests) are examined for selected process windows. In the end a correlation between process parameters, microstructure and mechanical properties is conducted.

Keywords

Selective Laser Melting (SLM), High Power Selective Laser Melting (HP SLM), Productivity, Process efficiency, Inconel 718 (IN718), Theoretical build-up rate, Material properties IN718

1. Introduction

During the last few years, the additive manufacturing technology Selective Laser Melting (SLM), developed at Fraunhofer ILT, has evolved from a manufacturing technology for prototypes and small batches into a production technology for functional parts [1]. The metal AM sector and, especially, the powder metal-based AM technology SLM has grown in size significantly, which can be seen in the considerable increase from approx. 202 metal AM systems sold to industry and research entities in 2012 to 808 in 2015 [2].

In particular, the turbomachinery branch can make good use of the geometrical freedom the SLM technology offers, which is based on layer-by-layer production to produce parts with additional integrated functions, lower weight or monolithic design. Examples for these applications, used to manufacture components out of high temperature alloys such as Inconel

[1] Fraunhofer Insitute for Laser Technology ILT, Steinbachstraße 15, 52070 Aachen, Germany

718 (IN718), titanium alloys (e.g. Ti6Al4V) or cobalt-chromium alloys, can be found at companies such as General Electric, MTU or Airbus [3] [4] [5]. These applications show the increasing demand for high temperature alloys that can be processed by SLM.

Additionally, increasing productivity is one of the most important ways to enable SLM technology to reach series production with higher lot sizes. According to the current state of the art, there are two principles commonly applied in commercial SLM machines that can increase the theoretical build-up rate for the SLM process. [6]

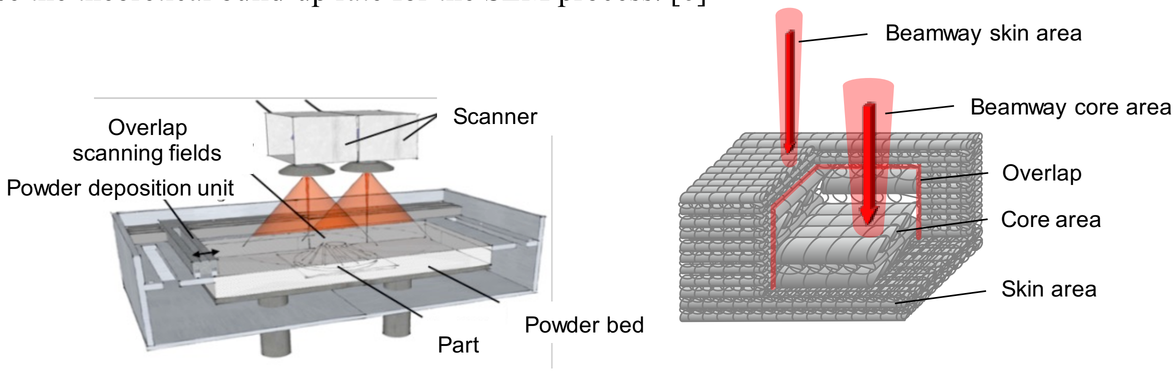

Figure 1: Principles to increase the theoretical build-up rate of the SLM process (Right: Parallelization | Left: High Power SLM with skin-core strategy)

The first principle, called "Parallelisation", uses up to four fibre-laser sources in parallel within the SLM process. When this principle is applied, the theoretical build-up rate can be increased linearly by the number of laser sources used (Figure 1 left). The second principle to increase the theoretical build-up rate, called High-Power SLM, uses increased laser power (P_L ≤1 kW) and adapts the following process parameters accordingly: laser beam diameter d_s, hatch distance Δy_s, layer thickness D_s and scanning velocity v_{scan} (Figure 1 right). Increasing the laser power and keeping the beam diameter stable increases the intensity in the interaction zone between powder material and laser. In particular, materials with lower heat conductivity, such as IN718 ($\lambda \approx 11.2$ W/mK), show evaporation, spattering and deep welding effects when the intensity is increased. Here a stable and reproducible process is not possible. In order to prevent these effects, the beam diameter must be increased to decrease the intensity in the interaction zone. [7] [8]

The increased beam diameter, however, impairs both the surface roughness and detail resolution. To rectify this, the skin-core strategy can be employed, whereby two different laser beam diameters are used, one for the skin and one for the core of a component. [9]

An increased beam diameter can be used to lower, especially the scanning velocity, which results in a significant change of the cooling and solidification behaviour in the SLM process. This behaviour directly influences the component's microstructure and the mechanical properties. Currently, there are no fundamental studies on the extent to which HP SLM influences the resulting microstructure and the mechanical properties for the nickel-based alloy IN718. Since there is a great demand from the industry to process high temperature alloys, e.g. IN718, with SLM and an increased theoretical build-up rate, it is necessary to investigate the influence of the HP-SLM process on the resulting material properties for the nickel-based alloy IN718.

2. State of the art

To date, there are a limited number of research activities exploring the use of higher laser power to increase the theoretical build-up rate, which is calculated as the product of hatch distance Δy_s, layer thickness D_s and scanning velocity v_{scan}. [16]

[1] Fraunhofer Insitute for Laser Technology ILT, Steinbachstraße 15, 52070 Aachen, Germany

Initial investigations dealing with the use of increased laser power for SLM were carried out by Schleifenbaum [1]. In his work, a laboratory system with an integrated 1kW laser source was designed and built. Based on this laboratory machine, Schleifenbaum developed the process for the austenitic steel 1.4404 (X2CrNiMo17-12-2) and the hot-working steel 1.2343 (X37CrMoV5-1). It could be observed that, when the beam diameter ($d_s \approx 1100 \mu m$) was increased and the process parameters adapted, the theoretical build-up rate could be increased by up to $V_{th}=21 mm^3/s$ to manufacture test samples with an average density > 99%. [9]

Further research in the field of HP SLM was done by Buchbinder, who investigated the influence of increased laser power by up to $P_L \leq 1kW$ on the material properties of the aluminium casting alloy AlSi10Mg [10]. The results show that $P_L=1kW$ laser power can significantly increase the theoretical build-up rate ($V_{th}=20 mm^3/s$) without needing to increase the beam diameter ($d_s \approx 200 \mu m$). Furthermore, the mechanical properties at static load (tensile test) were investigated for HP-SLM generated test samples. In terms of tensile strength and yield strength, the mechanical properties only show marginal differences in contrast to SLM-manufactured test samples at $P_L=400W$. However, the breaking elongation for HP-SLM manufactured test samples was slightly higher in comparison to that of conventionally manufactured test samples, which is explained by the different size and orientation of the grains. [11]

There are a great deal of investigations dealing with the process development for the nickel-based alloy IN718 and with the resulting material properties [12] [13 [14]. Amato et al. examined the influence of different heat treatment strategies on the microstructure and the mechanical properties at static load for IN718 processed with a maximum laser power of $P_L \leq 400W$. The investigations show that the test specimens have columnar grains with preferred orientation in the build-up direction. These results can also be observed from the other investigations carried out by Wang et al. and Jia et al. [13] [14]. During solidification in the SLM process, the heat flow is directed from the interaction zone between powder and laser to the substrate (parallel to the build-up direction), which can explain these results.

The mechanical properties in these investigations were determined with tensile tests according to different heat treatment strategies. The heat treatment strategies differ in the temperature and time cycles as well as in the number of annealing steps. For selected test specimens, a hot isostatic pressing (HIP) was done before solution annealing. The mechanical properties show that the SLM-manufactured test specimen ($P_L \leq 400W$) has tensile strengths of R_m = 1120 - 1148N/mm². After heat treatment the tensile strength can be increased by up to R_m = 1280 - 1358N/mm² according to the build-up direction. Typically, test specimens with a build-up angle of 90° to the substrate show lower values in comparison to a build-up angle of 0°. The breaking elongation is measured to be 19 - 26% after the SLM process. After heat treatment the breaking elongation varies between A = 10 - 22%, depending on the heat treatment strategy employed. [12] [13 [14]

The analysis show that there currently are no investigations for processing IN718 with increased laser power and adapted process parameters with respect to achievable theoretical build-up rate. In addition, no investigations exist which examine how increased laser power and adapted process parameters influence the resulting material properties.

[1] Fraunhofer Insitute for Laser Technology ILT, Steinbachstraße 15, 52070 Aachen, Germany

3. Methodology

The investigations were conducted using the SLM machine SLM280HL (SLM Solutions). The machine is equipped with two laser sources, a single-mode fibre laser with a maximum laser power $P_L \leq 400W$ (beamway 1) and a multimode fibre laser with a maximum laser power $P_L \leq 2kW$. The beam diameter for beamway 1 is d_{s1} = 80µm and d_{s2}=730µm for beamway 2. The machine allows the active fibre to be changed during the process by using a beam-switching unit.[15]

For the tests, powder material from a commercial supplier was used. The grain size is 15 - 45µm. A chemical analysis was done and shows that the alloy composition is within the specifications for IN718.

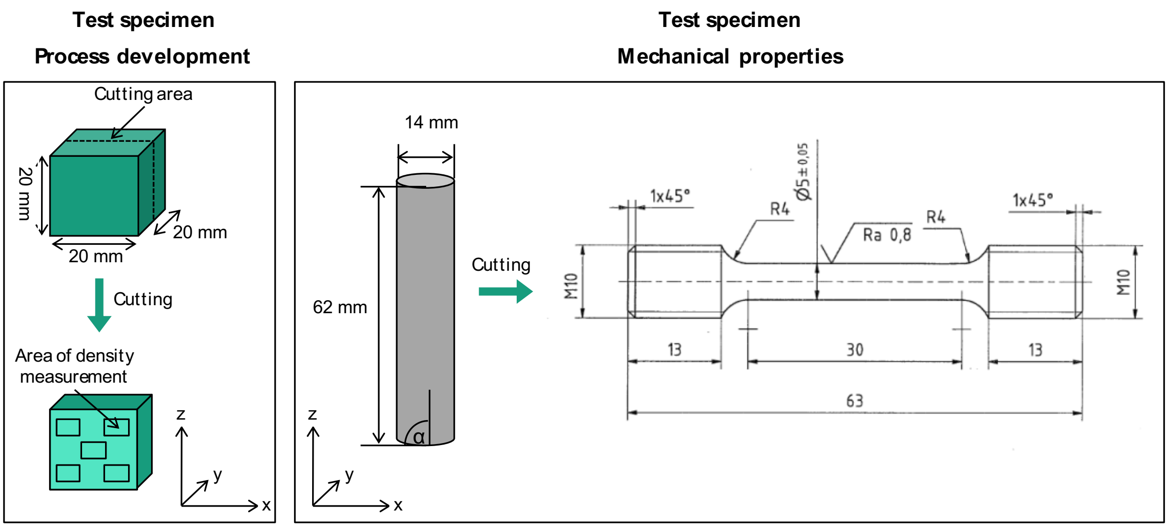

Figure 2: Dimension and shape of test samples used for process development and testing of mechanical properties

The density of the test samples (20x20x20mm³) was measured by light microscopy. After the SLM process, the test samples were purified from powder material and separated from the substrate. Afterwards the test samples were cut into two pieces and embedded, ground and finally polished. The density measurement was done by light microscopy in order to compare black areas (pores and defects) and white areas (dense material). For each test sample, five density measurements were made and the values averaged (see Figure 2). Additionally, the standard deviation has been calculated.

So that the process windows can be evaluated, the theoretical build-up rate and the volume energy is calculated. The theoretical build-up rate is an estimation of the manufactured volume per time by the use of the values independent of a machine: scanning velocity, hatch distance and layer thickness, as seen in Equation 1. The theoretical build-up rate V_{th} can be used as a reference value of the productivity of the SLM process.

Equation 1: $$V_{th} = v_{csan} \cdot \Delta y_s \cdot D_s \, [mm^3/s]$$

Equation 2: $$E_V = P_L / (v_{csan} \cdot \Delta y_s \cdot D_s) \, [J/mm^3]$$

In order to quantify the efficiency of the SLM process, one uses the volume energy, calculated by the product of employed laser power and theoretical build-up rate (Equation 2). This value describes how efficient the laser power used is transferred into an increased theoretical build-up rate.

[1] Fraunhofer Institute for Laser Technology ILT, Steinbachstraße 15, 52070 Aachen, Germany

Scanning electron microscopy (SEM) with an Electron Backscatter Diffraction (EBSD) probe head was used to measure the grain size and orientation. The test cubes were ion-beam polished in order to prevent contamination on the surface. The mechanical properties at static load are measured according to DIN EN ISO 6892-1:2009 at room temperature with the tensile test machine Zwick type 1466. The geometry of the tensile test specimen is illustrated in Figure 2. For each parameter set, five test specimens were manufactured in the form of a cylinder. After being separated from the substrate, the cylinder was finished to final dimension. The tensile test specimen were manufactured in a vertical orientation with an inclination angle of α=90° to the substrate.

4. Results

4.1 Process development

The average density of the test cubes has to be ≥99.5%, a limiting condition for parts manufactured with SLM. First, beamway 1 (d_s≈80µm) was used to manufacture test parts with laser power P_L=200 - 400W at a constant layer thickness of D_s=30µm. The scanning velocity was varied between v_{scan}=1200 - 2000mm/s. The cross sections of the test samples are illustrated in Figure 3. When the scanning velocity was increased, the density of test samples decreased due to the lower input of volume energy E_V. For a laser power P_L = 200W up to a scanning velocity of v_{scan}=1200mm/s an average density ≥99.5% can be achieved (V_{th}=2.88mm³/s). When the laser power was increased up to P_L = 300W, the scanning velocity could be increased to v_{scan}=1600mm/s, which resulted in a theoretical build-up rate of V_{th}=3.8mm³/s. A further increase of laser power (P_L=400W) generated an increase in the number of spatters and enabled the scanning velocity to be increased to v_{scan}=1700mm³/s (V_{th} =4.1mm³/s).

With respect to the volume energy (Equation 2), an increase of the laser power leads to increased values for volume energy, which means that the laser power employed is converted poorly into an increased theoretical build-up rate. For this reason the process window at P_L=300W at a scanning velocity of v_{scan}=1600mm/s was chosen as a reference for the following investigations in order to develop a process window for High-Power SLM (HP SLM).

[1] Fraunhofer Insitute for Laser Technology ILT, Steinbachstraße 15, 52070 Aachen, Germany

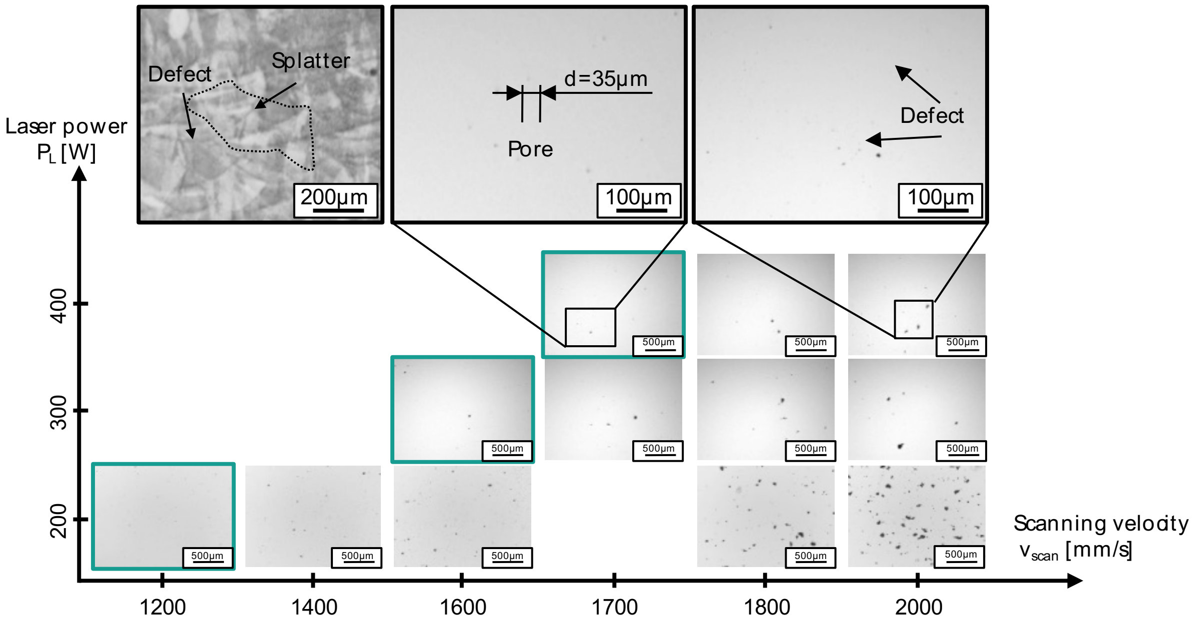

Figure 3: Cross-sections of the manufactured test samples for beamway 1 ($d_s \approx 80\mu m$) according to scanning velocity and laser power at Ds = 30 µm

In the next step, beamway 2 with a beam diameter $d_s \approx 730\mu m$ and increased laser power ($P_L \leq 2kW$) was employed to manufacture test samples as seen in Figure 2. For a laser power of P_L=1kW cubic test cubes with a density ≥99.5% can be produced with a layer thickness of D_s=90µm (v_{scan}=350mm/s) and D_s=150µm (v_{scan}=250mm/s). The theoretical build-up rate can be calculated to V_{th}=15.75mm³/s (D_s=90µm) and V_{th}=18.75mm³/s, which is a significant increase compared to the theoretical build-up rate achieved for the conventional SLM process: P_L=300W (V_{th}=3.8mm³/s). When the volume energy for the two process windows is taken into account, an increase of the layer thickness and a reduction of the scanning velocity leads to an increased theoretical build-up rate, and a lower volume energy is needed ($E_{V,Ds=90\mu m}$=63,5J/mm³ | $E_{V,Ds=150\mu m}$=53.3J/mm³). These results will be analysed by means of melt pool depth according to scanning velocity in Chapter 4.2.

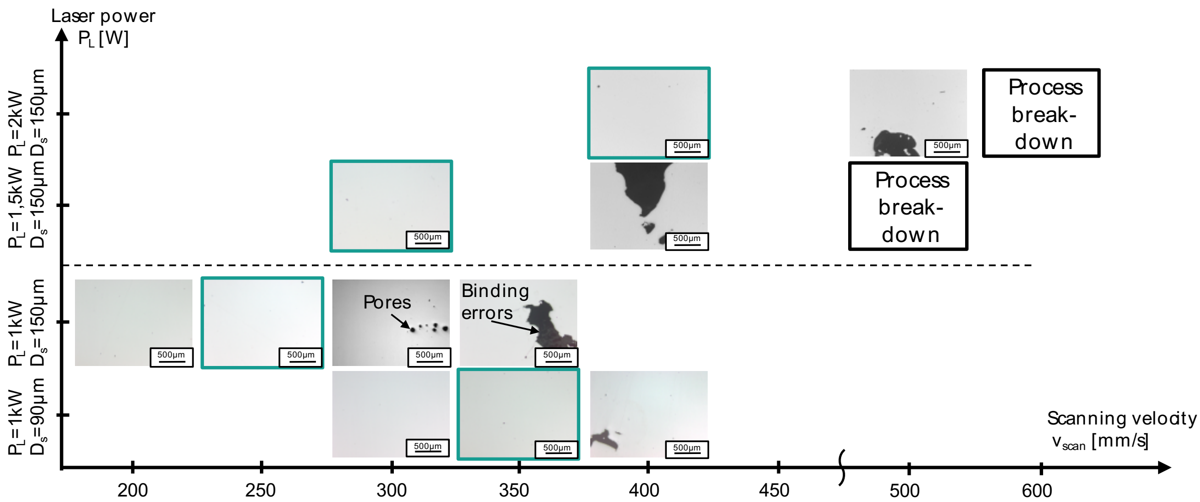

Figure 4: Cross-sections of test cubes manufactured by HP SLM according to scanning velocity (beamway 2 | D_s=90+150µm | P_L=1-2kW)

Subsequently, the laser power was increased up to P_L=1.5kW and P_L=2kW and the layer thickness was constant at D_s=150µm. The results show that when the laser power is increased,

[1] Fraunhofer Insitute for Laser Technology ILT, Steinbachstraße 15, 52070 Aachen, Germany

the scanning velocity can be increased by up to v_{scan}=300mm/s (P_L=1.5kW) and v_{scan}=400mm/s (P_L=2kW), which, in turn, leads to theoretical build-up rates of V_{th}=22.5mm³/s and V_{th}=30mm³/s (see Figure 5). The volume energy is calculated to E_v= 66.7J/mm³ for a laser power of P_L=1.5kW and P_L=2kW. In comparison to P_L=1kW at D_s=150µm, the theoretical build-up rate can be increased, but the volume energy decreases, which means that the increased laser power cannot be transferred proportionally into an increased theoretical build-up rate.

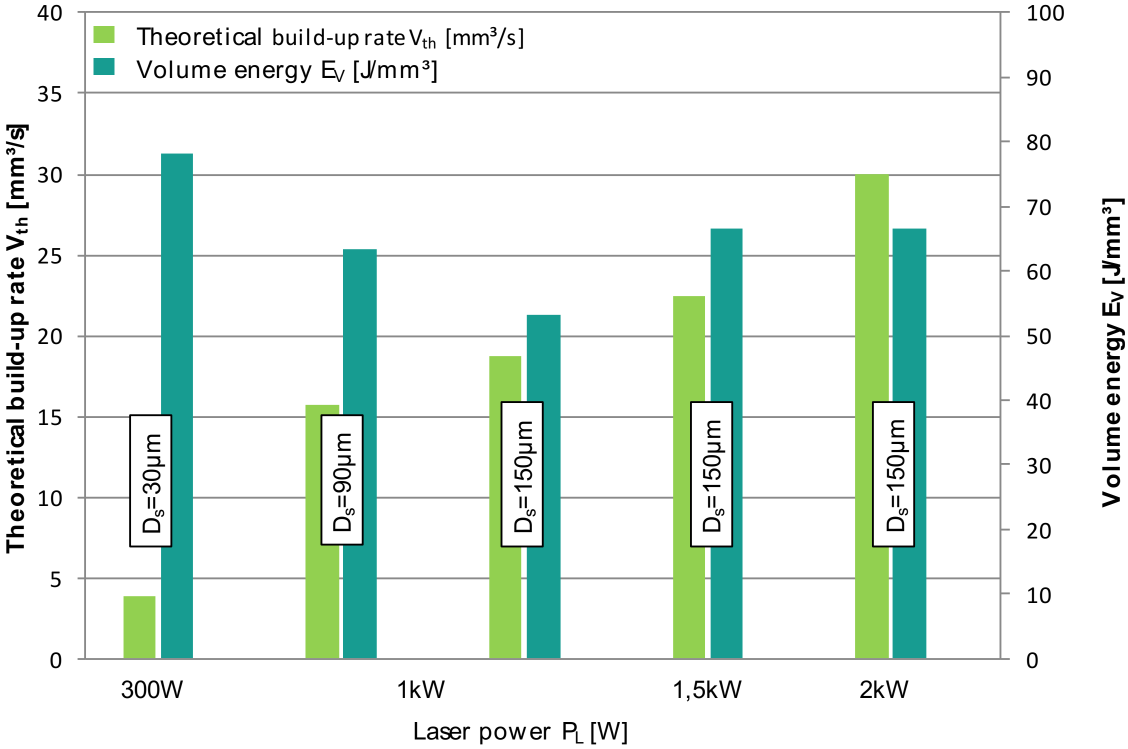

Figure 5: Theoretical build-up rate and volume energy for process windows 1 - 3

These results could be explained by the appearance of spatters from the increased laser power. Due to the increased beam diameter and the reduced scanning velocity, the interaction time between laser and powder material is significantly increased, although the intensity for beamway 2 at P_L=1kW ($I_{1kW,\ BW2}$= $2{,}46 \cdot 10^3$ W/mm² is an order of magnitude smaller in comparison to beamway 1 at P_L=300W ($I_{300W,\ BW1}$=$5{,}41 \cdot 10^4$ W/mm²). Nevertheless, the number of spatters and the size of spatters increase. These spatters are deposited on the molten layer and have a size between 50 - 200µm. Therefore, these spatters are not completely melted in the following scanning step, thus resulting in bonding errors. Nevertheless, increased laser power and adaption of the process parameters scanning velocity v_{scan} as well as layer thickness D_s can be used to significantly increase the theoretical build-up rate for IN718.

4.2 Microstructure

After process windows for HP SLM were developed, the microstructure and the melt pool shape was investigated. To do this, the melt pool size and shape (melt pool depth t_s, melt pool width b_s and melt pool shape b_s/t_s) were examined. The etched cross section of the test samples was analysed in order to investigate the last unremolten layer. The scanning direction is perpendicular to the plane of the cross-section in order to prevent the melt pool from

[1] Fraunhofer Insitute for Laser Technology ILT, Steinbachstraße 15, 52070 Aachen, Germany

deforming in the cross section (see figure 6). To quantify the size of the melt pool for each parameter set, nine measurements were taken and averaged.

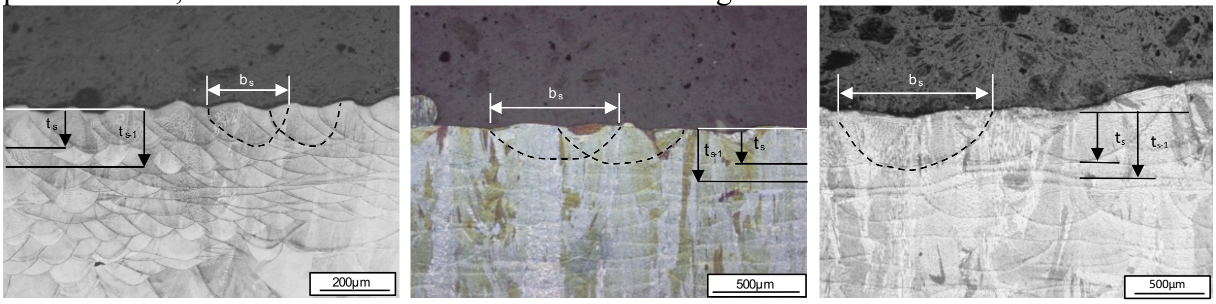

Figure 6: Melt pool size and shape for process window 1 (left), process window 2 (middle) and process window 3 (right)

The results in Figure 6 show that a melt pool forms similar to an elongated parabola with $t_s \approx 112µm$ and $b_s \approx 208µm$ for conventional SLM that uses a laser power of $P_L=300W$ at $D_s=30µm$ layer thickness and a scanning velocity of $v_{scan}=1600mm/s$ (process window 1). By contrast, the melt pool for HP SLM at $P_L=1kW$ and $D_s=90µm$ (process window 2) is significantly higher, at $t_s \approx 195µm$ and $b_s \approx 846µm$. The shape of the melt pool is flatter in comparison to that of the process window at $P_L=300W$ ($b_s/t_s=1.9$), which clearly shows the ratio between melt pool width and depth of $b_s/t_s=4.3$.

Increasing the layer thickness for HP SLM up to $D_s=150µm$ (process window 3) and reducing the scanning velocity result in an increased melt pool depth of $t_s \approx 244µm$. The melt pool does not change significantly in comparison to that of the process window at $D_s=90µm$ and is measured to be $b_s \approx 835µm$. For this reason the shape of the melt pool looks more like a compressed parabola and the ratio is calculated to be $b_s/t_s=3,4$.

The results show that the HP-SLM process with increased beam diameter and laser power leads to a significant increase of the melt pool size and shape. When the scanning velocity is reduced by an increase of layer thickness, the melt pool depth is not influenced linearly. For this reason it can be assumed that the reduction of the scanning velocity by a factor of two, for example, leads to an increase of the melt pool depth by a factor >2. Therefore, the scanning velocity does not have to be reduced by a factor of two in order to achieve an increased melt pool depth by a factor of two, which is necessary to completely melt the powder material of one deposited layer. This possibly explains the results in Chapter 4.1: the fact that an increase of the layer thickness and a reduction of the scanning velocity lead to an increased theoretical build-up rate.

In the next step the grain size, shape and orientation for the process windows were investigated by EBSD. The results are illustrated in Figure 7. It can be observed that small grains exist with a diameter of $d_K= 25µm$ for beamway 1 with $P_L=300W$ at $Ds=30µm$. These grains grow over two to ten layers and are elongated in the build-up direction. Most of the grains have an angle of 35 - 40° according to build-up direction. In comparison, for test cubes generated with HP SLM at $P_L=1kW$ at $D_s=90µm$, the EBSD shows grains with a diameter of $d_K=97µm$. The grains grow over the whole height of the test cube and are strictly directed in the build-up direction.

[1] Fraunhofer Insitute for Laser Technology ILT, Steinbachstraße 15, 52070 Aachen, Germany

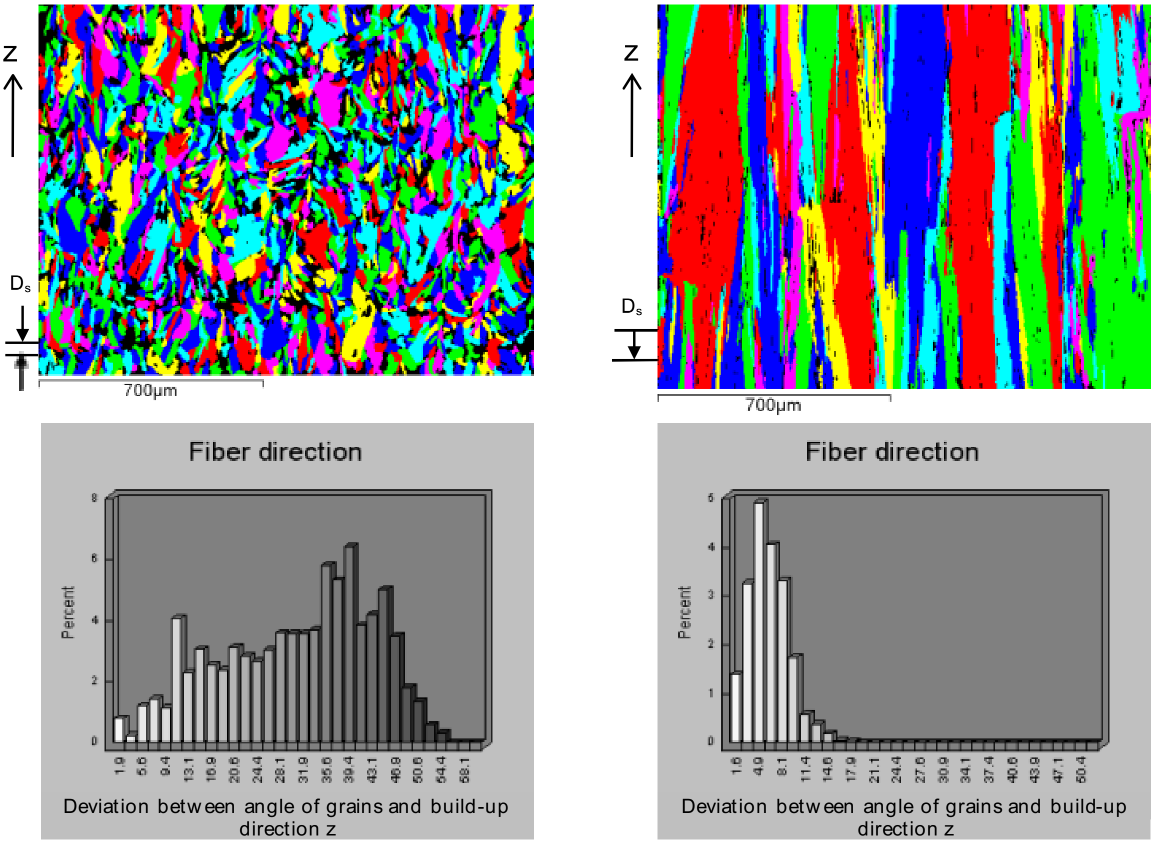

Figure 7: Results of the EBSD analysis for process window 1 (P_L=300W| D_s=30µm|v_{scan}=1600mm/s) and process window 2 (P_L=1kW| D_s=90µm|v_{scan}=350mm/s)

These results can be explained by the cooling and solidification conditions. For conventional SLM at PL=300W, the scanning velocity is much higher (v_{scan}=1600mm/s) than with HP SLM (v_{scan}=300-600mm/s). In addition, the melt pool shape differs significantly between conventional SLM and HP SLM. Both facts have are direct influenced by the cooling and solidification rates, both of which directly influence the refinement and the morphology of the microstructure [11]. In order to prove these assumptions, temperature field calculations for these process windows were necessary.

4.3 Mechanical properties

After the microstructure was examined, the mechanical properties at static load were investigated for the two process windows (P_L=300W, D_s=30µm | P_L=1kW, D_s=90µm). Therefore, ten bars per process window with cylindrical shape, as seen in Figure 2, were manufactured with an inclination angle of 90° to the substrate and then cut to final dimensions. Afterwards, half of the test specimens were heat treated according to AMS 5662 with an additional hipping process before the solution annealing (T=965°C, t=1h, p=2000bar). The results for the tensile tests are shown in Figure 8.

[1] Fraunhofer Insitute for Laser Technology ILT, Steinbachstraße 15, 52070 Aachen, Germany

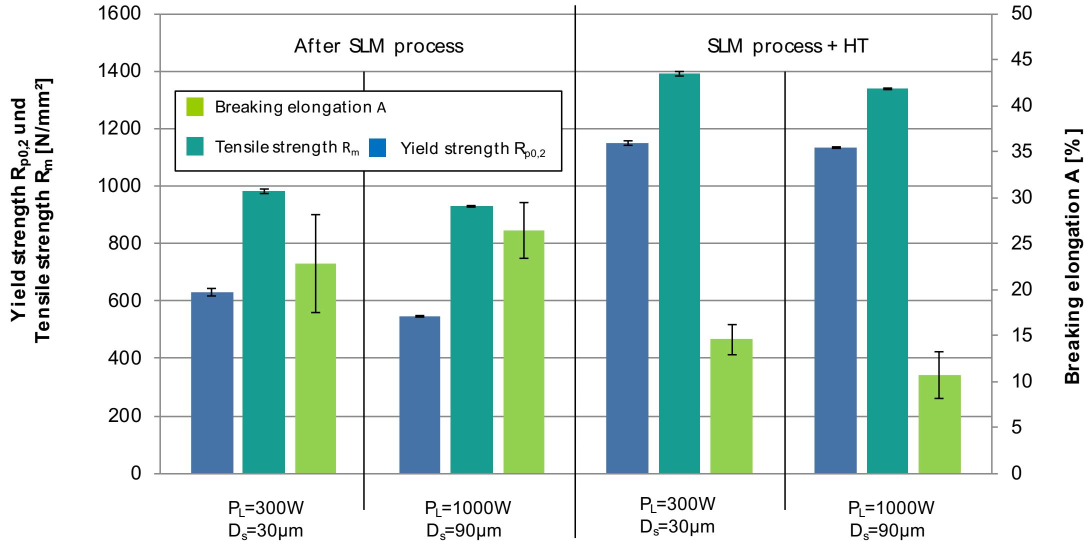

Figure 8: Mechanical properties for SLM-manufactured test specimens according to employed process parameters and heat treatment

The mechanical properties for process window 1 after SLM process (P_L=300W, D_s=30µm, v_{scan}=1600mm/s) show a tensile strength of R_m= 983N/mm² and a yield strength $R_{p0.2}$=632N/mm² with a breaking elongation of A=22.8%. In contrast the mechanical properties for HP SLM (P_L=1kW, D_s=90µm) show slightly reduced tensile strength of R_m= 930N/mm² and yield strength $R_{p0.2}$=549N/mm². But the breaking elongation (A=26.4%) is higher in comparison to conventional SLM (A=22.8%).

After heat treatment, the tensile strength and yield strength had increased and the breaking elongation was lower. For conventional SLM a tensile strength of R_m=1391N/mm², a yield strength of $R_{p0.2}$=1150N/mm² at A=14.9% can be observed. For HP-SLM manufactured tensile specimens (P_L=1kW, D_s=90µm), the tensile strength is in the same range (R_m=1340N/mm²) as well as the yield strength ($R_{p0.2}$=1136N/mm²). Thus, both process windows show values that exceed the requirements for heat-treated and forged IN718 [17]. The requirements demand a tensile strength of R_m=241 - 1275N/mm², a yield strength of $R_{p0.2}$=862N/mm² and a breaking elongation of A=6 - 12%. Only the breaking elongation for the HP-SLM manufactured test specimen does not exceed the requirements, but is within the given range between A=6 - 12%.

These results show that the nickel-based alloy IN718 can be manufactured by HP SLM with increased laser power P_L≤2kW and that the resulting mechanical properties are comparable to conventionally manufactured IN718. Furthermore, for process window 1 (P_L=300W, D_s=30µm) the mechanical properties are higher than for conventionally manufactured IN718.

5. Summary and conclusion

Initial investigations for HP SLM with laser power P_L≤2kW have been presented above and contain the process development, analysis of the microstructure and the mechanical properties for the nickel-based alloy IN718. The results prove that the theoretical build-up rate can be significantly increased from V_{th}=3.84mm³/s to V_{th}=30mm³/s by using increased laser power and adapted process parameters such as scanning velocity and layer thickness.

[1] Fraunhofer Insitute for Laser Technology ILT, Steinbachstraße 15, 52070 Aachen, Germany

Furthermore, the volume energy is used to quantify the process efficiency of the SLM process. The results for HP SLM show that an increase of the layer thickness and a reduction of the scanning velocity decrease process efficiency. The melt pool size and especially the melting depth give an initial explanation for this observation.

In addition, the melt pool size and shape is directly influenced by HP SLM. In combination with the reduction of the scanning velocity with HP SLM, the grain size, shape and orientation show significant differences between conventional SLM and HP SLM.

The mechanical properties according to heat treatment were investigated for conventional SLM and HP SLM. When HP SLM is used along with heat treatment, tensile strengths, yield strengths and breaking elongations can be achieved that fulfill the requirements for conventionally manufactured IN718.

6. Outlook

The investigations show that IN718 can be processed by HP SLM with increased theoretical build-up rates. In the next step, the individual influence of the process parameters (layer thickness, scanning velocity, laser power etc.) on the theoretical build-up rate and the volume energy has to be investigated in detail. Based on these investigations, a correlation needs to be found between the resulting microstructure and the process parameters.

Furthermore, the mechanical properties have be examined and correlated with the process parameters and the resulting microstructure. In order investigate the part behaviour for HP SLM manufactured IN718 at realistic usage loads, the mechanical properties at dynamic load have to be investigated.

Finally, temperature field calculations for selected process windows have to be done. Based on these results, the differences in microstructure, especially in grain size, shape and orientation can be explained.

Acknowledgement

The authors would like to thank the European Commission for the support of the research described here within the project AMAZE “Additive Manufacturing Aiming Towards Zero Waste & Efficient Production of High-Tech Metal Products”, which is part of the 7th Framework Programme of the European Commission (FP7-FoF.NMP.2012-4).

References

[1] J. H. Schleifenbaum, Verfahren und Maschine zur individualisierten Produktion mit High Power Selective Laser Melting, Dissertation RWTH Aachen, Shaker Verlag, 2011

[2] Wohlers, T.: Wohlers Report 2016 –3D Printing and Additve Manufacturing – State of the industry – Annual worldwide progress report, Fort Collins, Colorado (USA), Wohlers Associate INC. (2016)

[3] Dusel, K., H.: Einsatz von RP-Technologien im Workflow bei der MTU Aero Engines, MTU Aero Engi-nes, Informationsblatt der MTU Aero Engines (2013)

[1] Fraunhofer Insitute for Laser Technology ILT, Steinbachstraße 15, 52070 Aachen, Germany

[4] EOS GmbH Electro Optical Systems: Information auf der Hompage: http://www.eos.info/presse/kundenreferenzen/siemens (Stand 26.06.2015)

[5] GE Aviation: Information auf der Homepage: http://www.gereports.com/post/91763815095/worlds-first-plant-to-print-jet-engine-nozzles-in/ (Stand 26.06.2015)

[6] Poprawe, R.; Hinke, C.; Bremen, S.; Meiners, W.; Schrage, J. und Merkt, S.: SLM Production Systems: Recent Developments in Process Development, Machine Concepts and Component Design, Advances in Production Technology, S. 49-65, Springer Verlag

[7] Schleifenbaum, J. H.: Individualized production by means of high power Selective Laser Melting. CIRP Journal of Manufacturing Science and Technology, vol 2 (3), pp. 161-169 (2010)

[8] Bremen, S.; Buchbinder, D.; Meiners, W. und Wissenbach, K.: Selective Laser Melting – A Manufacturing Method for Series Production?, Proceedings DDMC 2012

[9] Schleifenbaum, H.; Diatlov, A.; Hinke, C.; Bültmann und Voswinckel H.: Direct Photonic Production: Towards High Speed Additive Manufacturing of Individual-ized Goods, Production Engineering – Research and Development 2011, Vol. 5, No. 4, pp. 359-371

[10] Buchbinder, D.; Schleifenbaum, H.; Heidrich, S.; Meiners, W. und Bültmann, J.: High Power Selective Laser Melting (HP-SLM) of aluminium parts, Proceedings of LIM conference, 2011

[11] Buchbinder, D.: Selective Laser Melting von Aluminiumgusslegierungen, Dissertation RWTH Aachen, Shaker Verlag (2013)

[12] Amato, K.N.; Gaytan, S.M.; Murr, L.E.; Martinez, E. Shindo, P.W. Hernan-dez, J.; Collins, S. und Medina, F.: Microstructures and mechanical behavior of Inconel 718 fabricated by selective laser melting. Journal Acta Materialia, 2012, Vol. 60, pp. 2229 – 2239.

[13] Jia, Q.; Gu, Dongdong: Selective laser melting additive manufacturing of Inconel 718 superalloy parts: Densification, microstructure and properties. Journal of Alloys and Compounds, 2014, Vol. 585, pp. 713 – 721.

[14] Wang, Z.; Guan, K.; Gao, M.; Li, X.; Chen, X. und Zheng, X.: The microstructure and mechanical properties of deposited-IN718 by se-lective laser melting. Journal of Alloys and Compounds, 2012, Vol. 513, pp. 518 – 523.

[15] SLM Solutions GmbH: Information auf der Hompage: http://slm-solutions.de/produkte/maschinen/slmr280hl (Stand 27.06.2016)

[16] Meiners, W.: Direktes selektives Laser-Sintern einkomponentiger metallischer Werkstoffe. Dissertation RWTH Aachen, Shaker Verlag (1999)

[17] Special Metals Coporation, Datenblatt Inconel 718: www.specialmetals.com%2Fdocuments%2 FInconel%2520alloy%2520718.pdf&ei=wYuzVbe4J8SiyAPvyYIg&usg=AFQjCNE7hNV66K_peXVtanAQg5J3zJMZrw (Stand 11.07.2016)

[1] Fraunhofer Insitute for Laser Technology ILT, Steinbachstraße 15, 52070 Aachen, Germany

Jonas Zielinski[1], Hans-Wilfried Mindt[2], Mustafa Megahed[2], Simon Vervoort[1]

Influence of Powder Bed Characteristics on Material Quality in Additive Manufacturing

Abstract

In powder bed based Additive Manufacturing (AM) processes like Selective Laser Melting (SLM) or Electron Beam Melting (EBM) the spatial distribution of the individual powder particles is typically unknown. Nevertheless, the distribution of particles in the heat affected zone defines the thermophysical properties of the region being processed by the heat source and therefore plays a crucial role in the heat transfer conditions.
In this work, the spatial distribution of individual particles and their influence on the AM process SLM is numerically investigated.
Two different methods are used to approach this problem. Firstly, the powder coating process is modelled using a discrete element method (DEM). The modelled distribution is compared with an experimentally obtained distribution. In a second step, the two distributions are used as input for a Volume-of-fluid (VOF) method driven simulation of the whole AM process (melting of the powder particles and solidification to a solid). From the VOF-simulation other parameters, like melt pool depth and width are compared with experimentally determined values.
Particle size distributions are measured using a MorphologiG3 analyzer and used as an input to the DEM powder bed simulation. The results provide insights on how the powder bed packing density affects the AM process and eventually affects the final product quality.

Keywords

Selective Laser melting; powder bed characteristics; CFD simulation; particle distribution; powder packing

1. Introduction

In powder bed based Additive Manufacturing (AM) processes, like Selective Laser Melting (SLM), a large number of variables that influence the quality of the built-up specimen exist. Some of them can be set and measured directly (e.g. Laser power, scanning velocity and coater arm speed), some are machine based and can only be controlled indirectly (e.g. shielding gas velocity over the powder bed is only controlled via the volume flow rate setting of the machine). Others are hard to measure or control, yet could have a significant influence on the process; like the spatial arrangement of the particles in the powder bed and their size- and shape-distribution.

In the context of this work, the influence of the powder bed characteristics (particle size distribution and spatial arrangement) on the SLM process is investigated. Since in an experiment it is hard to setup up, or measure, the spatial arrangement of the particles in the powder bed, therefore for the investigation of the impact of those parameters on the SLM process is investigated numerically.

[1] RWTH Aachen University – Chair for Laser Technology
[2] CFD & Multiphysics Centre of Excellence; ESI-Software GmbH

2. Proceeding

As an input for the coating process the particle size distribution was measured using a “morphologi” system. The measured particles are normally not perfect spheres (or since a 2D projection is measured; circles) but irregular shaped. After determining the area of each particle a circle equivalence diameter and sphere equivalent volume is calculated and is used to generate the diameter vs. volume fraction distribution for spheres matching the measured data.

The temperature-dependet material properties of the hot work steel 1.2367, the particle size distribution of the steel powder (measured with a “morphologi G3” system) and the laser- and process parameters serve as input for the two simulations.

The first simulation by Mindt et al. uses discrete element methods (DEM) to study powder spreading and the distribution of powder on the processing table [5]. Every powder particle is treated as an individual, with its own properties, which interacts with other particles that are in range to be affected by it. DEM is a Lagrangian approach where the modelled region considers the particles inside their own point of reference describing Newton’s laws of motion for conservation of momentum.

The second simulation utilizes the predicted particle distribution on the powder bed as input to analyse the laser interaction with the feed stock providing more insight about the phase changes and solidification behaviour of the material [1].

3. Powder spreading simulation

From a given particle size distribution, the particles are binned in a subset of (seven, eight or nine) classes depending on the diameter. The used DEM code creates a random powder bed particle distribution consisting of spherical particles, using that particle class distribution (see Figure 1).

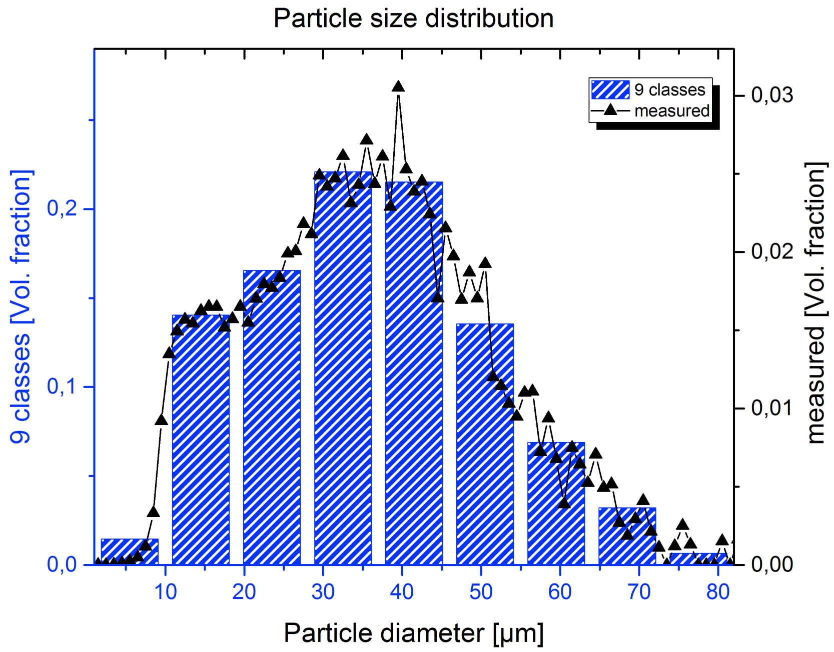

Figure 1 Conversion of a particle size distribution in its nine corresponding subclasses

[1] RWTH Aachen University – Chair for Laser Technology
[2] CFD & Multiphysics Centre of Excellence; ESI-Software GmbH

In this study two different powder distributions with seven classes are considered, since the impact of the class with the largest, respectively the smallest diameter is expected to be negligible (both classes together only combine less than 3% of the Volume/mass fraction). Another reason to ignore the smallest particle class is that its impact on the SLM process is not significant but the computational effort to calculate the large amount of light weighted particles during the spreading is enormous.

During the powder spreading process we observe a segregation of particles leading to a different powder size distribution on the processing table as compared to the input distribution. This is in agreement with observation made for other powders [5]

In Figure 2 a test particle size distribution is compared to the simulated after-spreading particle size distribution in the welding domain for spreader-substrate distances of 35 µm and 50 µm. The distance corresponds to the gap between the coater arm lower edge and the substrate.

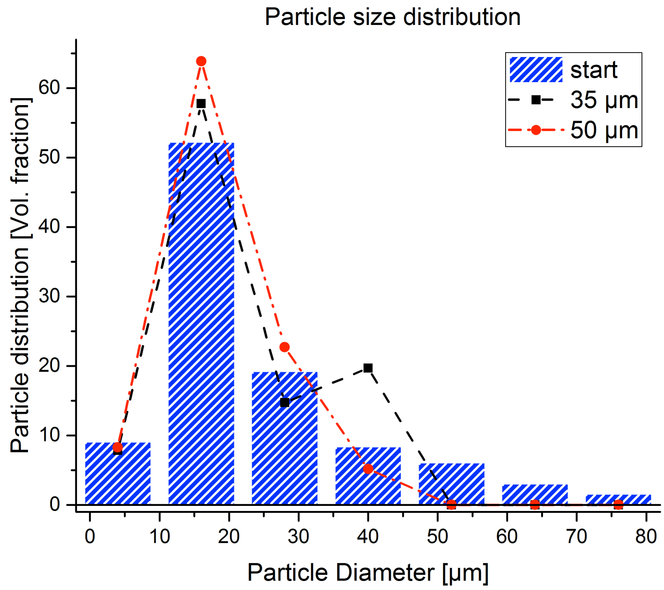

Figure 2 Change of the particle distribution through the spreading process for different spreader-substrate distances

The two classes with the biggest diameters are not present in the welding domain because the particles belonging to these classes are wiped off the platform for the reason that the gap between spreader and substrate is too small.

In the case of 35 µm some particles slightly larger than the gap size are observed on the processing table. These particles are compressed slightly allowing them to pass through the gap. Since the model does not account for particle crushing or compression of the particles in a partially solidified substrate, this behaviour is not expected to happen in the same manner in reality. In reality particles larger than the gap will either be pushed away from the substrate or will interact with coater blade in some manner (e.g. crushing, denting the coater arm …etc.)

[1] RWTH Aachen University – Chair for Laser Technology
[2] CFD & Multiphysics Centre of Excellence; ESI-Software GmbH

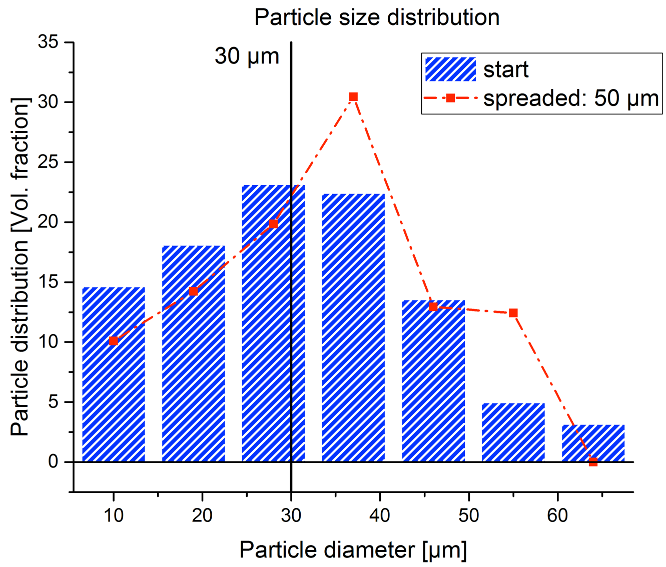

Figure 3 Particle size distribution before and after the spreading process, line: manual particle packing diameter

The gap size of 50 µm was chosen to model a process with a platform lowering of 30 µm with each layer and an assumed volume shrinkage of 40% from powder to fully remelted solid. As in the previous study, the highest particle class is not present in the welding domain. The calculated domain serves as input for the SLM process calculation, see chapter 3 and Figure 4.

Figure 4 shows the powder distribution on the substrate. The particles are coloured by their sizes. The shaded area indicates the domain used for the melting simulation

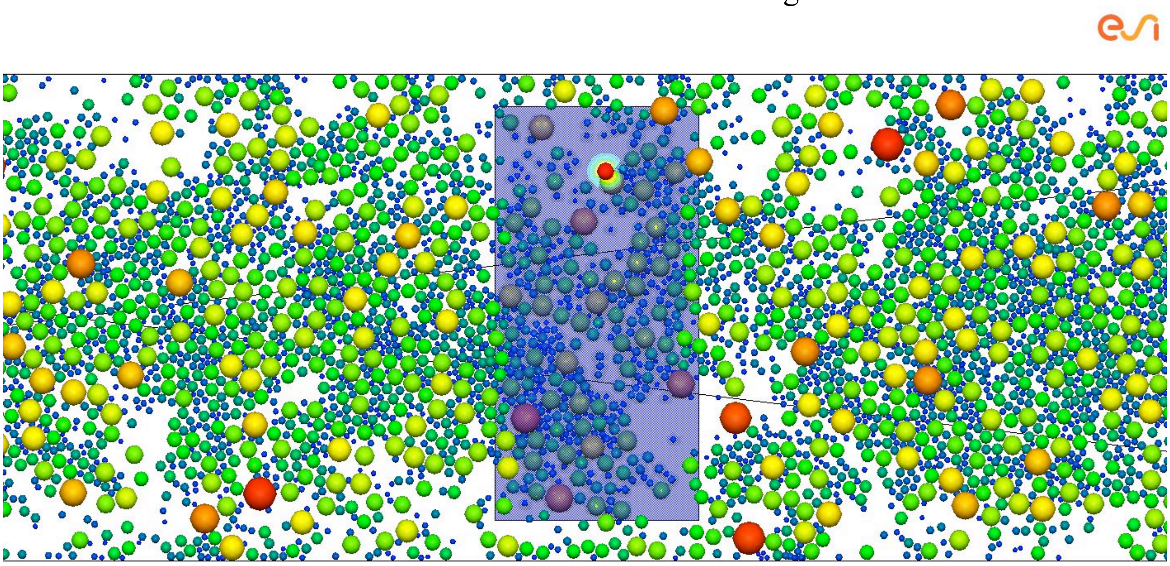

Figure 4 Calculated spatial particle distribution and choosen melting domain (marked rectangle) for the particle size distribution shown in Figure 3

[1] RWTH Aachen University – Chair for Laser Technology
[2] CFD & Multiphysics Centre of Excellence; ESI-Software GmbH

For further comparison and analysis, a particle distribution was set up manually. The built distribution is made of two particle layers arranged in a body centred cubic lattice formation made of spheres with a diameter of 30 µm (see the solid vertical line in Figure 3). This configuration was chosen because it is an acceptable trade-off between fitting in the 50 µm gap particle sizes predicted to be available for the melting process. Furthermore the packing density of this manual packing is close to the usual expected 50% packing density in reality.

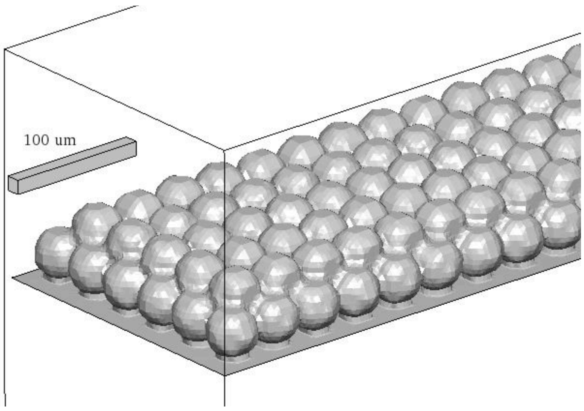

Figure 5 Manual particle packing with uniform particle diameter of 30 µm

4. SLM process simulation

Once the powder is numerically spread, the geometry is available for further analysis via the micro model, describing the energy input to the feed stock, the phase change, material consolidation and solidification. The models are based on computational fluid dynamics algorithms to solve the Navier-Stokes equations. The momentum equations are extended using source terms to account for gravitational body forces, recoil pressure and surface tension. The energy equation accounting for conduction (diffusion term) and convection is complemented with source terms accounting for the latent heat released or required during solidification/melting and evaporation/condensation as well as radiation [1, 6].

For the simulation of the SLM process, the same parameters were used as for the specimen manufacturing on a SLM 280 machine. The parameters are condensed in Table 1.

Parameter		
Scanning velocity	740	mm/s
Laser Power	175	W
Laser spot size	70	µm (Gaussian)
Platform lowering	30	µm
Material	1.2367	hot work steel

Table 1 Parameters used for the simulation and the manufacturing of the specimen

The temperature evolution at 2 locations is monitored and shown in Figure 6. The first location is chosen to be within the powder layer, where the melt pool is expected (later called melt pool) and the second is below the first point at the surface of the substrate.. The temperature gradient (from surface to substrate) is smaller in the case of spread (distribution from Figure 2) powder packing. A possible reason for this is that in the case of manual packing

[1] RWTH Aachen University – Chair for Laser Technology
[2] CFD & Multiphysics Centre of Excellence; ESI-Software GmbH

a gas pore is formed below the melt pool surface that significantly reduces the heat conductivity of the melt pool. The gas pore of the manual packed powder process is shown in Figure 7 (circled area). Gas pores significantly reduce the part quality of additive manufactured components and their origination should be avoided by choosing the process parameters carefully.

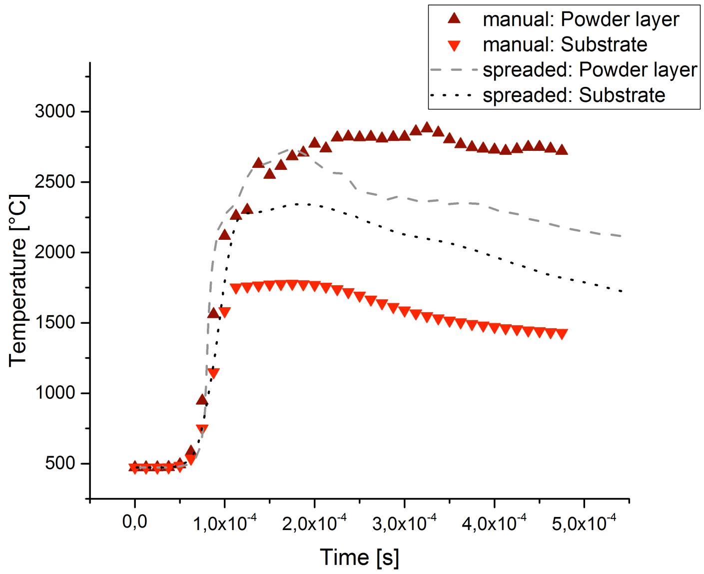

Figure 6 Time dependent simulated temperature at powder layer- and substrate surface for manual packed and simulated (spreaded) particle distributions

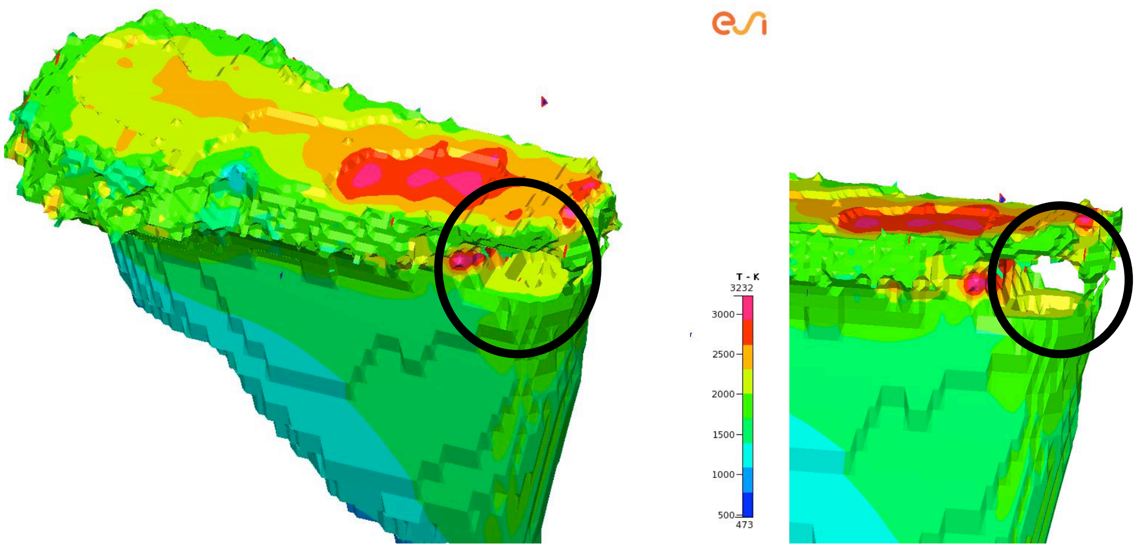

Figure 7 Simulated melt pool shape and temperature distribution of the manual packed powder bed; circled area: gas pore (scanning direction: left to right)

In the case of the simulated powder spreading (distribution: Figure 2) no gas pore is formed. The melted area along a single track is show in Figure 8.

[1] RWTH Aachen University – Chair for Laser Technology
[2] CFD & Multiphysics Centre of Excellence; ESI-Software GmbH

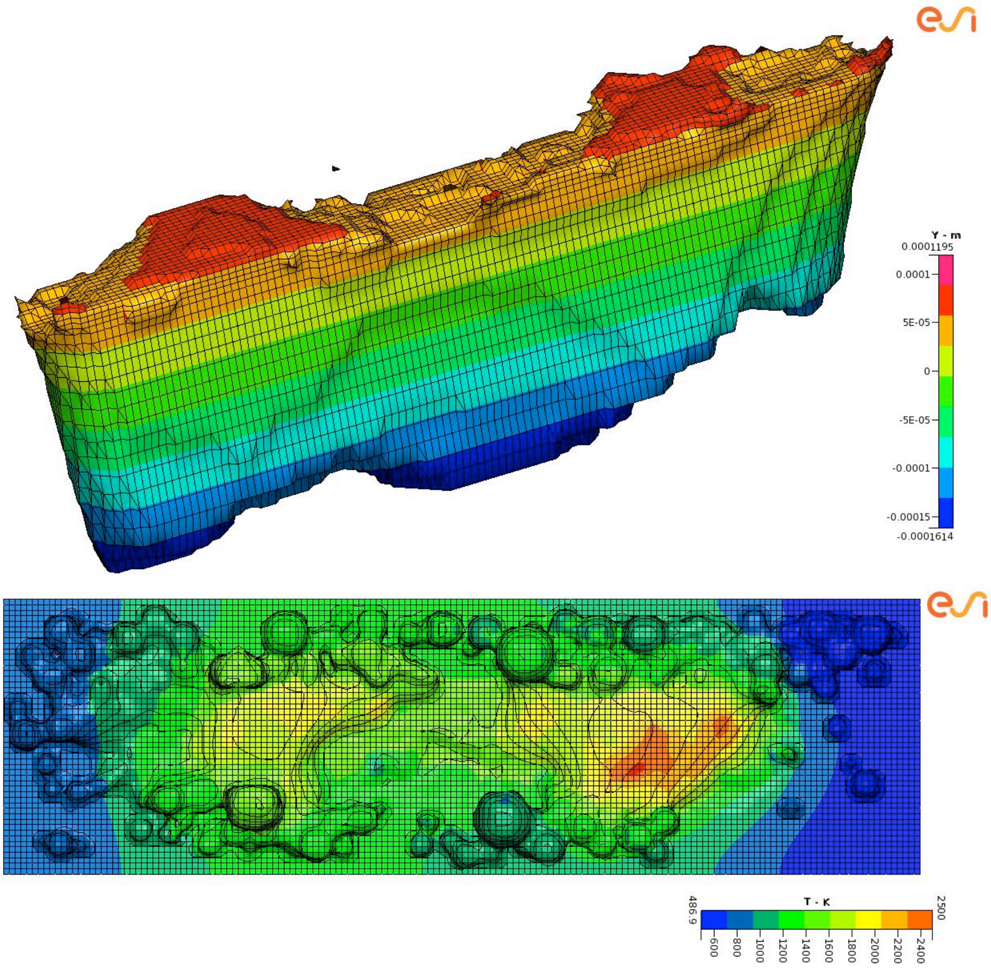

Figure 8 top: melted volumen along a single track; bottom: topview of the same track - scanning direction from left to right

A fluctuation is seen in the melt pool depth while the width is relatively constant, along the track. For verification purposes it is checked, whether or not the simulated track geometry coincides with the geometry extracted from experimental data.

The experimentally generated specimen has been cut in a way that the scanning vectors in the top (last) layer are normal to the cutting plane. After polishing and etching, the melt pool dimension (depth and width) can be seen and measured under a microscope (compare Figure 9).

The micrograph indicates a conduction like melt pool with a width to depth ration of approximately 1

[1] RWTH Aachen University – Chair for Laser Technology
[2] CFD & Multiphysics Centre of Excellence; ESI-Software GmbH

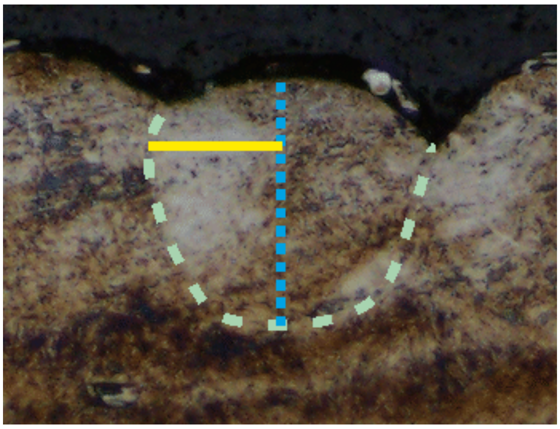

Figure 9 Generic microscopic image of a polished cross-section of the manufactured specimen for determining the meltpool dimensions; solid line: half width, dotted line: depth, dashed curve: estimated melt pool boundary

The melt pool boundary for the two simulations can be by considering the contour of material that was molten at some stage of the simulation. As can be seen from Table 2 the predictions of the manual and numerically spread powders differ significantly. For the manual powder a conduction melt pool is predicted, however the dimensions are exaggerated by a factor of 2. In the case of the numerically spread powder the melt pool aspect ratio is approx. 1.8 indicating possible keyholing.

	Experiment	**Manual Sim.**	**Spreaded (Fig. 2; 35 µm)**	**Spreaded (Fig. 3)**
Depth	111,83 ± 9,27 µm	250 µm	227 µm	Still calculating
Width	116,50 ± 18,56 µm	200 µm	122 µm	Still calculating

Table 2 Meltpool width and depth determined from light microscopic examination of a polished cross-section of a generated specimen

The difference in predicted melt pool depth is attributed to effective powder absorption coefficient. In this study optical analysis of the effective laser absorption coefficient were not performed, probably leading to an exaggerated energy input.

Regarding the quality of the manufactured workpiece, in the case of the manual particle packing the simulation shows that a huge gas pore is formed just below the melt pool surface. This does not correspond to material density measurement obtained indicating material densities in the order of 99.5%. The density of the numerically spread powder indicates high product density. We take this finding as an indication that the powder distribution is detrimental in the prediction of the material quality.

Outlook

The next step to complete and increase the reliability of this the study is to finish the calculation for the second (measured) particle distribution (shown in Figure 3) and compare them to the experimentally determined width and depth (*This will be ready for the presentation in November 2016*).

Another key aspect to look closely at in the simulation is the energy absorption and distribution mechanism, since the simulated melt pool volume is overestimated in the known two cases.

[1] RWTH Aachen University – Chair for Laser Technology
[2] CFD & Multiphysics Centre of Excellence; ESI-Software GmbH

For an advanced comparison multi track simulations should be considered because the heat transfer conditions drastically change, depending if the new track is formed purely in powder or in proximity to an already solidified track.

References

[1] M. Megahed, H.-W. Mindt, N. N'Dri, H.-Z. Duan and O. Desmaison, Metal Additive Manufacturing Process and Residual Stress Modelling, Integrating Materials and Manufacturing Innovation, 2016, 5:4. DOI: 10.1186/s40192-016-0047-2.

[2] King WE, Anderson AT, Ferencz RM, Hodge NE, Kamath C, Khairallah SA, et al. (2015) Laser powder bed fusion additive manufacturing of metals; physics, computational, and materials challenges. Applied Physics Reviews. 2(041304) doi:10.1063/1.4937809

[3] McVey RW, Melnychuk RM, Todd JA, Martukanitz RP (2007) Absorption of Laser Radiation in a Porous Powder Layer. Journal Laser Applications. 19(4):214-224.

[4] Boley CD, Khairallah SA, Rubenchik MA (2015) Calculation of Laser Absorption by Metal Powders in Addiitve Manufacturing. Applied Optics. 54(9):2477-2482. doi:10.1364/AO.54.002477.

[5] H.-W. Mindt, M. Megahed, N.P. Lavery, M.A. Holmes and S.G.R. Brown, Powder Bed Layer Characteristics – The Overseen First-Order Process Input, Metallurgical and Materials Transactions A, Vol. 47A, No. 4, 2016, DOI: 10.1007/s11661-016-3470-2.

[6] H.-W. Mindt, Brian Shula, M. Megahed, A. D. Peralta, J. Neumann, Powder Bed Models – Numerical Assessment of As-Built Quality, AIAA 2016-1657, AIAA Science and Technology Forum and Exposition 2016, 4-8 January, 2016, San Diego, CA, USA. DOI: 10.2514/6.2016-1657

[1] RWTH Aachen University – Chair for Laser Technology

[2] CFD & Multiphysics Centre of Excellence; ESI-Software GmbH

KELLERMEYER MARKUS [1], FÜHRER KAJ [2], KNAAK MICHAEL [3]

DESIGN AND ENGINEERING BY TOPOLOGY OPTIMIZATION FOR AN ADDITIVE MANUFACTURED JUMP ROBOTIC LEG

Abstract

The combination of topology optimization and additive manufacturing allows engineers to realize and assess new ideas within a significantly shorter development time. Next to reducing development time, the technology brings additive manufacturing costs closer to the costs of series manufacturing. This process is presented for the design of an additive manufactured jump robotic leg at the DLR (Deutsches Zentrum für Luft- und Raumfahrt e.V.).

Keywords

topology optimization, additive manufacturing, additive manufactured jump robotic leg

1. Introduction

Additive manufacturing technology is currently changing the possibilities for design and engineering in every industry. Complex structures, with traditional manufacturing technologies difficult or impossible to manufacture, are now feasible and provide new possibilities for lightweight engineering.

The new designs, however, are challenging to design. Their complex and organic structures require new ways of engineering them. Topology optimization, a method suggesting weight optimized designs within their working conditions, amplifies the possibilities of additive manufacturing technology allowing engineers to use the full potential of their product design.

The combination of topology optimization and additive manufacturing allows engineers to realize and assess new ideas within a significantly shorter development time. Next to reducing development time, the technology brings additive manufacturing costs closer to the costs of series manufacturing. Together with additive manufacturing, technology for topology optimization has evolved significantly in recent years. Modern topology optimization technologies provide not only design concepts but complete, ready to manufacture, designs.

2. Methods

Taking into account working conditions, loads and restrictions from manufacturing an optimal design is developed from a given design space using topology optimization.

The design, optimized for maximum stiffness and reduced weight, is ready for additive manufacturing. Unlike traditional designs, it is not the result of drawings but from calculated and optimized virtual prototyping taking into account its working conditions. To

[1] CADFEM GmbH
[2] Deutsches Zentrum für Luft- und Raumfahrt e.V. (DLR)
[3] Stratasys

complete the simulation driven development the design is analyzed within the ANSYS Workbench environment under different loading conditions before manufacturing.

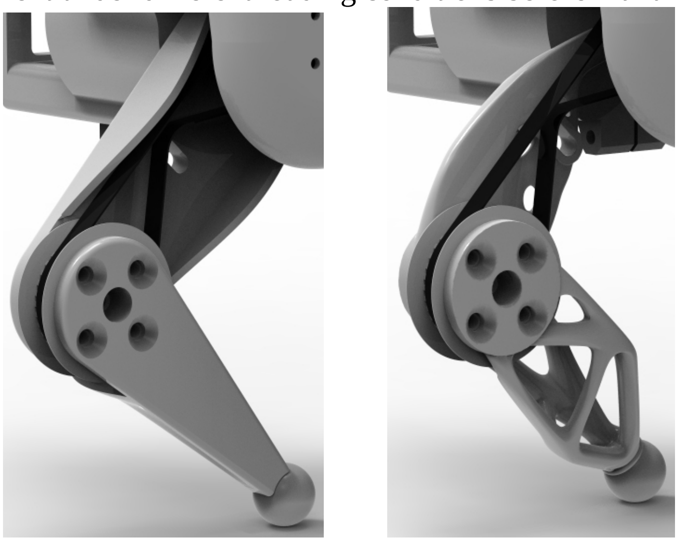

Fig. 1: Design of the jump robotic leg before and after topology optimization

3. Conclusion

The optimized jump robotic leg measures a weight of less than 40% compared with the original one but with the same level of deformation and stress. Using topology optimization this could be realized without any trial and error loop. But one has to keep in mind that the optimized leg is trimmed to the load case scenario given as input in the topology optimization algorithm only. This implies that the load acting on the leg has to be known well because there are not any reserves left to withstand loads differing to the load assumed for topology optimization.

For further investigation and optimization of the jump robotic leg including it into a controlled rigid body simulation but with keeping the robotic leg as flexible body would be possible. All this would be possible within the ANSYS Workbench environment.

References

[1] Führer, K.: „Additive Fertigung mit Hochleistungskunststoffen“, Fachkonferenz: 3D-Druck – Additive Fertigung in der Automobilindustrie, Augsburg, Oktober 2015

[2] Kellermeyer, M.: “Topologieoptimeirung für additive Fertigung”, CADFEM Journal (01|2016), S. 22-23

[1] CADFEM GmbH

[2] Deutsches Zentrum für Luft- und Raumfahrt e.V. (DLR)

[3] Stratasys

Rudolf Gradinger [1], Salar Bozorgi[1], Eric Wolfsgruber[2], Frank Palm[3]

Alloy development methodology for new Aluminium MAM powder variants

Abstract

In the cooperative, FFG funded project "GenerAl", the development of a new Aluminium alloy powder variant is in the focus of the consortium, bridging the well-known alloys AlSi10Mg and Scalmalloy® (AlMgSc) in terms of cost-to-properties ratios. The target window for e.g. ultimate tensile strength is 390-490 MPa in peak aged condition. In this context, complex alloy additions like Scandium or Lithium were excluded from the portfolio; candidates were Mg, Mn, Fe, V, Si, Cu, Ti amongst others.
A pre-evaluation was performed via desktop study assessing cost-efficient alloy additions with respect to weldability / castability (e.g. hot tearing behaviour), corrosion resistance, expected strength & elongation values, cost & availability of alloy elements, recycling issues etc.
Before prototyping the selected composition by conventional powder manufacturing processes, an experimental investigation of small amounts of molten material was done by rapid solidification methods delivering insights into grain structure after fast quenching of bulk samples (instead of powder).
These rapid solidified cones were investigated by optical light microscopy, scanning electron microscopy (SEM) equipped with energy dispersive X-ray (EDX) and differential scanning calorimetry (DSC), respectively, in order to provide an understanding of cooling rate influence on microstructures and intermetallic phases of studied alloys as well as to ensure the right choice before starting powder prototyping work as well as AM investigations using two different laser processes are applied for Aluminium powders: Laser-Powder-Cladding and Selective Laser Melting . These methodologies and the respective results are shown exemplary on two examples of alloy compositions.

1 LKR Leichtmetallkompetenzzentrum Ranshofen GmbH, Lamprechtshausenerstraße 61, 5282 Ranshofen, AT
2 Mepura Metallpulvergesellschaft m.b.H., Ranshofen, AT
3 Airbus Group Innovations, Airbus Defence and Space GmbH, Taufkirchen, DE

Chu Lun Alex Leung[1], Ricardo Tosi[2], David Wimpenny[2], Philip J. Withers[1], Peter D. Lee[1]

Three dimensional characterization on effects of preheating conditions on sintered Ti-6Al-4V powders in Electron Beam Melting (EBM) process

Abstract

Preheating is recognized as a crucial step in Electron Beam Melting (EBM) Additive Manufacturing (AM) processes. It produces a sintered structure that prevents blown powder defects, increases the effective conductivity of the powder bed and reduces final component residual stress. Although prior studies have used optical imaging of the surface or post-mortem metallography, to infer the sintered structure of Ti-6Al-4V powders after preheating, these have been limited to 2D. Furthermore, few investigations have examined the variation of thermal conditions in the build direction and across scan positions in EBM. Understanding of these effects can help predict the formation and evolution of the melting pool generated by electron beam, and their impact on the microstructure and mechanical properties of the AM components.

This study investigates the sintered structure of Ti-6Al-4V powders along build direction and across scan positions under same preheating conditions. Each sample was produced as a can that retained the partially sintered powder in the middle using an Arcam A2XX at the Manufacturing Technology Centre (MTC). This build shape of the can preserved the sintered structure as close to its original state for subsequent quantification using micro computed tomography (µ CT). Three dimensional imaging processing was used to qualitatively and quantitatively analyze both the sintered powder and pore morphology within the can for a range of sample locations and heating conditions. These results provide an improved fundamental understanding of how variations in thermal conditions along build direction during preheating stage alter sinter bed properties, enabling future process development to optimize machine parameters.

1 Manchester X-ray Imaging Facility, School of Materials, The University of Manchester, Manchester M13 9PL, UK

2 University of Birmingham / The Manufacturing Technology Centre, UK

KARL-HEINZ LEITZ [1]
PETER SINGER [1]
ARNO PLANKENSTEINER [1]
BERNHARD TABERING [1]
HEINRICH KESTLER [1]
LORENZ SIGL [1]

THERMO-FLUIDDYNAMICAL SIMULATION OF LAYER BUILDUP BY SELECTIVE LASER MELTING OF MOLYBDENUM AND STEEL

Abstract

Numerical simulations are a powerful tool to gain a fundamental process understanding of Selective Laser Melting (SLM). They allow a look into process details and to extract the influence of single process and material parameters. In this contribution a multi-physical finite element simulation model for SLM is presented. The coupled thermo-fluiddynamical model includes the absorption of laser radiation on the surface of the metal powder, conductive and convective heat transfer in the metal and the ambient atmosphere as well as melting, solidification, evaporation and condensation processes. The model is applied for an analysis of the influence of process parameters on the process and the processing result in SLM of molybdenum and steel. It shows the material specific process characteristics as well as the influence of power and energy input on surface morphology in layer buildup. The predictions of the simulation model are in good accordance with experimental metallographic data.

Keywords

Selective laser melting, multi-physical simulation, molybdenum, steel

1. Multi-Physical Simulation of Selective Laser Melting

Selective Laser Melting (SLM) is a promising approach for the additive fabrication of metallic structures from a powder base material. A laser beam is applied to build up a workpiece by melting up powder layer by layer. The technology principle is shown in figure 1 a. A blade delivers a thin powder layer with a layer thickness on the scale of the powder grain size. The powder layer is irradiated with a high power laser beam controlled by a scanner system. The powder melts up, consolidates and when the laser moves further, the material solidifies again. Subsequently, the building platform is lowered, a new powder layer is provided and the described procedure is repeated. At the end of the process the fabricated workpiece can be removed from the powder bed. Figure 1 b shows the SLM process during operation. SLM offers a high potential for future manufacturing technology. It enables unique design possibilities as well as a shortening of development times and process chains. In addition to that it is highly material efficient and profitable for small lot sizes [1].

[1] Plansee SE, Metallwerk-Plansee-Straße 71, 6600 Reutte, Austria
contact: karl-heinz.leitz@plansee.com

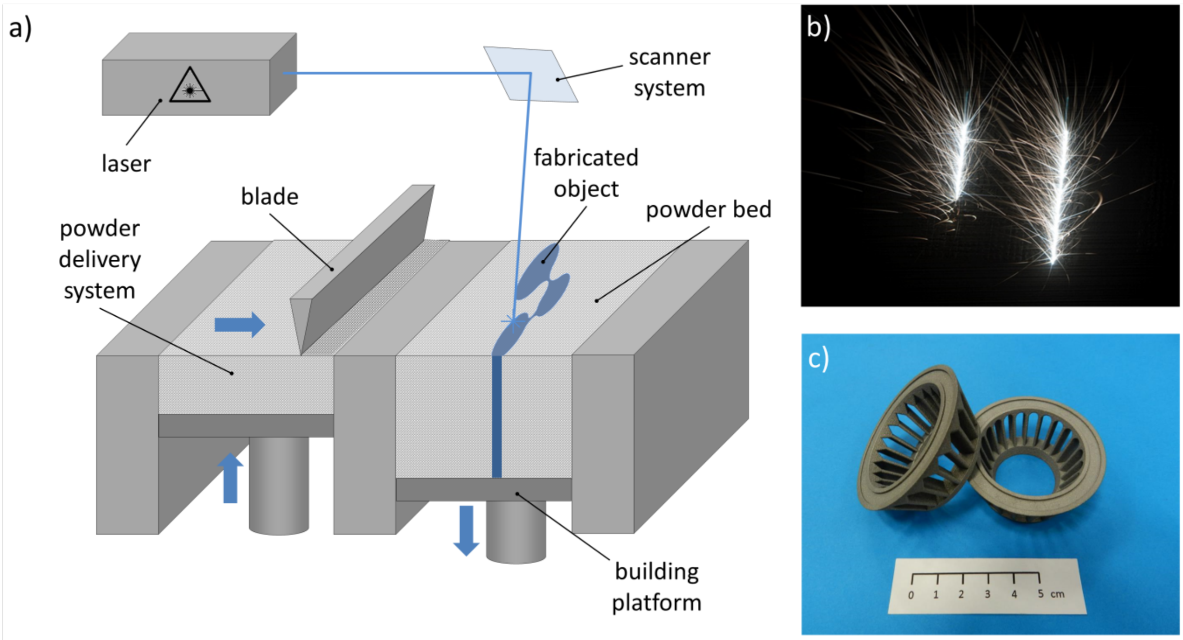

Fig. 1 Selective laser melting: a) technology principle; b) process during operation; c) molybdenum demonstrator parts fabricated at Plansee SE.

Whereas for materials like steel SLM is already well established, commercial SLM systems are available and the technology is on the transition from prototype production to industrial fabrication, SLM of molybdenum still is a big technical challenge, due to its high melting temperature and good thermal conductivity. Nevertheless, SLM of molybdenum is feasible and promising results already can be achieved. Figure 1 c shows demonstrator parts that have been fabricated by SLM of molybdenum at Plansee SE. The successful application of SLM for the processing of molybdenum requires a fundamental process understanding, as the processing result is significantly influenced by the applied powder and processing parameters. In order to understand how the characteristics of the applied material, the laser power and the feed rate influence the achievable minimum feature size, surface roughness and workpiece density, numerical simulations are a powerful tool. However, process modelling of SLM is a challenging task, as it requires a coupled thermo-fluid dynamical description of the absorption of laser radiation, conductive and convective heat transfer, phase transition and wetting processes. Approaches for such a multi-physical modelling of laser beam-matter interaction on a mesoscopic scale have been developed for a variety of laser processes [2-5] including SLM [6,7]. In [8,9] a multi-physical simulation model for SLM following this modelling approach was applied in order to analyse the influence of laser power and energy input on process dynamics and line width in SLM of molybdenum and steel. Whereas the line width directly correlates with the achievable feature size respectively resolution in SLM, the surface quality is directly connected to the surface morphology of the fabricated layers. Furthermore, the layer roughness influences the powder deposition characteristics and thereby the process dynamics as well as the achievable workpiece density. Therefore, in the following the previous work [8,9] shall be continued and the influence of laser power and energy input on surface morphology in layer buildup by SLM of molybdenum and steel shall be analysed.

2. Simulation Model

The multi-physical simulation model for SLM is based on the computational fluid dynamcis and the heat transfer module of the finite element (FE) software package Comsol Multiphysics. It includes the absorption of laser radiation on the metal surface, conductive and convective heat transfer, the fluid mechanics of melt, vapour and atmosphere as well as melting, solidification, evaporation and condensation processes. Figure 2 shows a typical simulation result of a SLM process. The model geometry consists of a powder layer on a massive base plate. The energy of the laser beam is absorbed on the surface of the metal. The metal heats up, a melt pool is formed and the melt wets the base plate as well as the neighbouring powder particles. If the energy input is high enough, evaporation occurs and the metal vapour expansion leads to a deformation of the melt pool surface. When the laser moves on, the melt pool cools down, solidifies again and a molten track is formed.

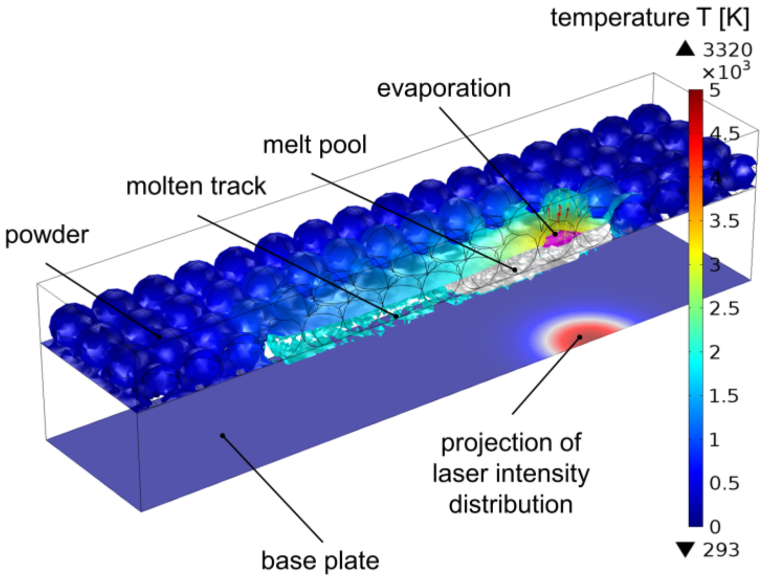

Fig. 2 Simulation model for the SLM process.

The simulation model for laser beam-matter interaction respectively SLM is based on a coupled system of four differential equations: the heat conduction equation, the continuity equation, the Navier-Stokes equation and the Cahn-Hillard equation. The heat conduction equation

$$\rho \tilde{C}_p \frac{\partial T}{\partial t} + \rho \tilde{C}_p u \cdot \nabla T = \nabla \cdot (k \nabla T) + \Gamma_{top} A Q_{Laser} - \Gamma Q_{rad} \qquad (1)$$

with the density $\rho\,[\mathrm{kg/m^3}]$, the thermal conductivity $k\,[\mathrm{W/(m \cdot K)}]$ and the interface function $\Gamma\,[1/\mathrm{m}]$ assures the conservation of energy and describes the formation of the temperature field $T\,[\mathrm{K}]$. It is assumed, that the intensity $Q_{Laser}\,[\mathrm{W/m^2}]$ of the laser is absorbed with an absorption coefficient $A\,[-]$ on the top surface $\Gamma_{top}\,[1/\mathrm{m}]$ of the metal. Angle dependency of the absorption, shadowing effects and multiple reflections are neglected, as apart from the starting phase of the process in a typical processing regime of SLM the laser energy in large part is absorbed on the smooth melt pool surface. The melt pool typically has an extent on the scale of or bigger than the laser beam and no significant keyhole formation occurs. Furthermore, thermal radiation losses on the metal surface $\Gamma\,[1/\mathrm{m}]$ according to

Stefan-Boltzmann law are considered by a heat sink Q_{rad} [W/m^2] in the heat conduction equation (1). The latent heats of melting H_m [J/kg] and evaporation H_v [J/kg] are considered by an effective heat capacity $\tilde{C}_p = C_p + \delta(T - T_m)H_m + \delta(T - T_v)H_v$ [J/(kg · K)].

The incompressible continuity equation

$$\boldsymbol{\nabla} \cdot \boldsymbol{u} = Q_v \tag{2}$$

with the velocity $\boldsymbol{u}$ [m/s] assures the conservation of mass. It includes a source term

$$Q_v = \dot{m} \cdot \Gamma \cdot \left(\frac{1}{\rho_{vap}} - \frac{1}{\rho_{met}}\right) \ [1/\mathrm{s}] \tag{3}$$

with the evaporation rate $\dot{m}$ [kg/(m^2 · s)], the vapour density ρ_{vap} [kg/m^3] calculated on the base of the ideal gas law and the metal density ρ_{met} [kg/m^3] accounting for the density change during evaporation.

The incompressible Navier-Stokes Equation

$$\rho \frac{\partial \boldsymbol{u}}{\partial t} + \rho(\boldsymbol{u} \cdot \boldsymbol{\nabla})\boldsymbol{u} = -\boldsymbol{\nabla} p + \mu \boldsymbol{\nabla}^2 u + \rho \boldsymbol{g} + \boldsymbol{F}_\sigma \tag{4}$$

with the velocity u [m/s], the pressure p [N/m^2], the viscosity μ [Pa · s], the gravity constant g [m/s^2] and the surface tension force F_σ [N/m^3] assures the conservation of impulse.

The Cahn-Hillard equation for the phase function Φ [−]

$$\frac{\partial \Phi}{\partial t} + \boldsymbol{u} \cdot \boldsymbol{\nabla}\Phi = \boldsymbol{\nabla} \cdot \frac{\gamma\lambda}{\varepsilon^2}\psi + Q_v' \tag{5}$$

$$\psi = -\boldsymbol{\nabla} \cdot \varepsilon^2 \boldsymbol{\nabla}\Phi + (\Phi^2 - 1)\Phi \tag{6}$$

with the mobility γ [(m · s)/kg], the mixing energy density λ [N], the surface tension coefficient σ [N/m] and the capillary width $\varepsilon = 2\sqrt{2} \cdot \lambda/(3 \cdot \sigma)$ [m] is the base of the multi-phase description. The source term

$$Q_v' = \dot{m} \cdot \Gamma \cdot \left(\frac{1 - \phi}{\rho_{vap}} + \frac{\Phi}{\rho_{met}}\right) [1/\mathrm{s}] \tag{7}$$

accounts for the evaporation process. Based on the phase function Φ [−] it is distinguished between metal and atmosphere. Additionally, within the metal phase based on the temperature a distinction is made between solid, liquid and vapour phase. In the solid phase the viscosity μ [Pa · s] is strongly increased and the surface tension force F_σ [N/m^3] is restricted to the surface of the liquid metal.

The described implementation of evaporation follows an approach described by Sun and Beckermann in [10]. The evaporation rate $\dot{m}$ [kg/(m^2 · s)] is calculated on the base of the Hertz-Knudsen formula [11]:

$$\dot{m} = \varphi_{vap} \cdot (p_{vap} - p_0) \cdot \sqrt{\frac{M}{2\pi RT}} \tag{8}$$

$$p_{vap} = p_0 \cdot exp\left(\frac{H_v M}{R} \cdot \left(\frac{1}{T_v} - \frac{1}{T}\right)\right) \tag{9}$$

with the vapour phase fraction φ_{vap} $[-]$, the vapour pressure p_{vap} $[\mathrm{N/m^2}]$, the molar mass M $[\mathrm{kg/mol}]$ and the ideal gas constant R $[\mathrm{J/(mol \cdot K)}]$. For the calculation an ambient pressure of $p_0 = 1$ bar is assumed.

3. Simulation Results

The simulation model for SLM was applied in order to analyse the influence of laser power $P[\mathrm{W}]$ and energy input ρ_E $[\mathrm{J/m}]$ on surface morphology. Both SLM from molybdenum and steel (1.4404) powder in air atmosphere were regarded. The computational domain has a size of $360\ \mu m \times 400\ \mu m \times 200\ \mu m$. It consists of a simple cubic arranged monomodal powder layer of 9×10 particles (particle size $d_{part} = 40\ \mu\mathrm{m}$) positioned on a base plate with a thickness of $d_{plate} = 80\ \mu\mathrm{m}$. To model the building platform for the outer plate boundaries a temperature of $T_0 = 293$ K was prescribed. The powder was scanned by three lines of $s = 160\ \mu\mathrm{m}$ at a hatch distance of $d_{hatch} = 100\ \mu\mathrm{m}$. The focus size of the Gaussian laser beam applied for irradiation was $d_{focus} = 130\ \mu\mathrm{m}$. The FE-mesh applied for the simulation consists of 116002 tetrahedral elements with a characteristic size of 5 μm in the particle layer and 20 μm in the boundary regions, respectively. Typical computation times for a layer were found to be in the range of 16 – 72 h on 4 cores of a dual CPU Intel Xeon E5-2630 v2 Dell Precision T5610 workstation. For the simulation temperature dependent material properties were applied. Those are listed in Tab. 1. Outside the temperature range available in literature material properties were assumed to be constant.

	steel	molybdenum	air
density $\rho[\mathrm{kg/m^3}]$	$8.0 \cdot 10^3 \ldots 7.7 \cdot 10^3$	$10.2 \cdot 10^3 \ldots 9.7 \cdot 10^3$	1.2…0.12
heat capacity $C_p[\mathrm{J/(kg \cdot K)}]$	485…746	244…562	1015…1306
thermal conductivity $k[\mathrm{W/(m \cdot K)}]$	13…25	139…84	$2.6 \cdot 10^{-2} \ldots 6.6 \cdot 10^{-2}$
viscosity $\mu[\mathrm{Pa \cdot s}]$	$5.4 \cdot 10^{-3} \ldots 2.3 \cdot 10^{-3}$	$7.5 \cdot 10^{-3} \ldots 5.0 \cdot 10^{-3}$	$1.8 \cdot 10^{-5} \ldots 7.0 \cdot 10^{-5}$
surface tension $\sigma[\mathrm{N/m}]$	1.80…1.72	2.34…2.27	
absorption coefficient $A[-]$	0.31…0.27	0.27…0.34	
melting temperature $T_m[\mathrm{K}]$	1810	2873	
evaporation temperature $T_v[\mathrm{K}]$	3133	5833	
melting enthalpy $H_m[\mathrm{J/kg}]$	$2.8 \cdot 10^5$	$2.9 \cdot 10^5$	
evaporation enthalpy $H_v[\mathrm{J/kg}]$	$6.1 \cdot 10^6$	$5.6 \cdot 10^6$	

Tab. 1 Temperature dependent material data (blue: low temperature regime, red: high temperature regime) [12 - 19].

Figure 3 shows simulation results for layer buildup by SLM from molybdenum and steel powder at standard parameters for volume buildup (standard power P_0 [W], standard energy input ρ_{E0} $[\mathrm{J/m}]$) applied at Plansee SE. It becomes obvious that SLM of molybdenum and steel operate in different process regimes. Whereas for molybdenum the melt pool size is restricted to the focal spot area and no evaporation occurs, for steel the melt pool is significantly longer and strong evaporation is found. These differences can be deduced to the higher thermal conductivity and evaporation temperature of molybdenum (compare Tab. 1).

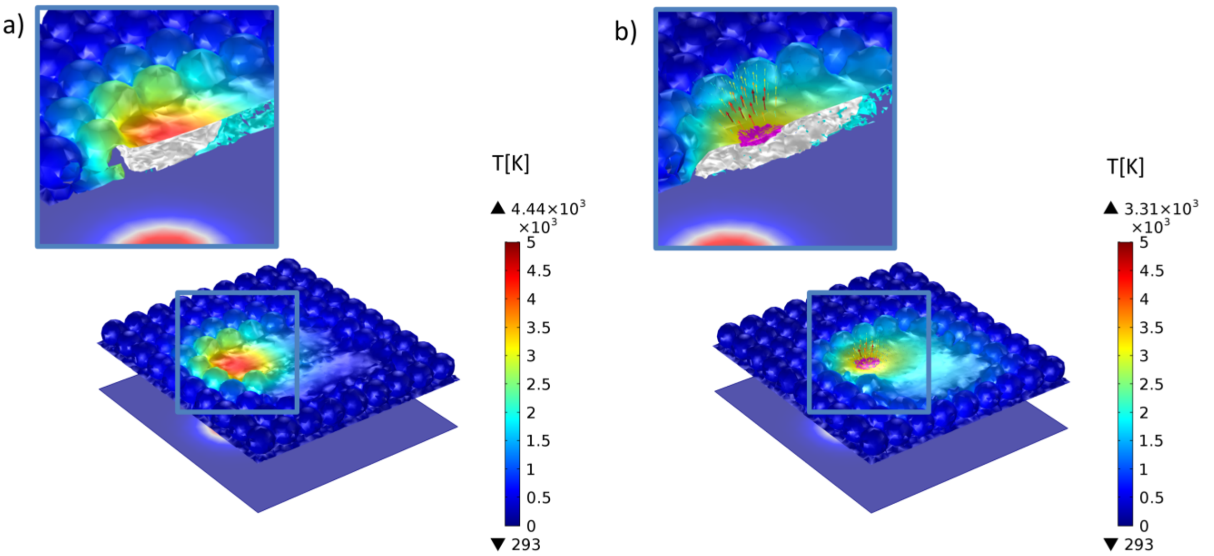

Fig. 3 Simulation of layer buildup from 40 µm powder by SLM at standard parameters for volume buildup (standard power P_0 [W], standard energy input ρ_{E0} [J/m]): a) molybdenum, b) steel.

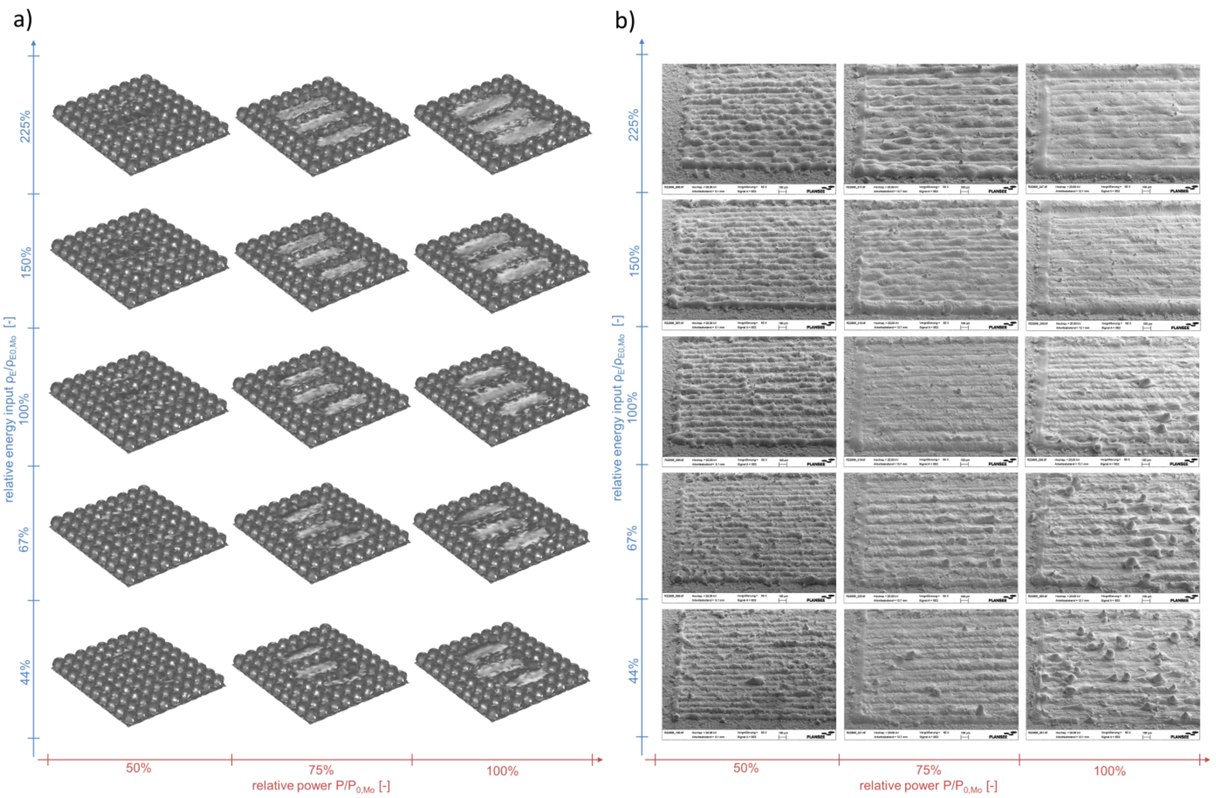

Fig. 4 Layer buildup by SLM of molybdenum ($P_{0,Mo}$ [W] and $\rho_{E0,Mo}$ [J/m] are standard power and energy input for volume buildup from molybdenum): a) simulation results (360 μm ×400 μm), b) experimental results (magnification scalebar for electron micrographs 100 μm).

Emanating from those results results laser power P [W] and energy input ρ_E [J/m] were varied in a range from $50\,\% - 100\,\%$ respectively $44\% - 225\,\%$ with respect to standard parameters for volume buildup (standard power P_0 [W], standard energy input ρ_{E0} [J/m]) from the respective material. The simulation results for molybdenum and steel are shown in figures 4 a and 5 a. For both materials a decreasing surface roughness can be observed with increasing laser power and energy input. From those results average surface roughnesses $R_a = \frac{1}{N}\sum_i |z_i - \bar{z}|$ were determined in the irradiated rectangle of $160\ \mu m \times 200\ \mu m$. The obtained surface roughnesses depending on power respectively energy input are plotted in figures 6 and 7. The roughness level of the simulated steel layers is lower in a wide parameter range. This can be ascribed to the larger melt pool. At high energy inputs disturbances of the molten surface connected with a slight increase of surface roughness can be observed (compare figure 5). This can be attributed to melt pool disturbances due to evaporation. A look at the influence of laser power and energy input shows that, whereas for molybdenum a pronounced power dependency of the surface roughness is found, for steel the energy input is the dominant process parameter. For molybdenum both energy input dependency and power dependency slightly increase with increasing power respectively energy input, whereas for steel these slightly decrease (compare figures 6 and 7). This demonstrates that the process window for SLM of molybdenum is narrower compared to steel. Those results are in accordance with formerly presented results concerning the influence of energy input and laser power on line width in SLM of molybdenum and steel presented in [8,9].

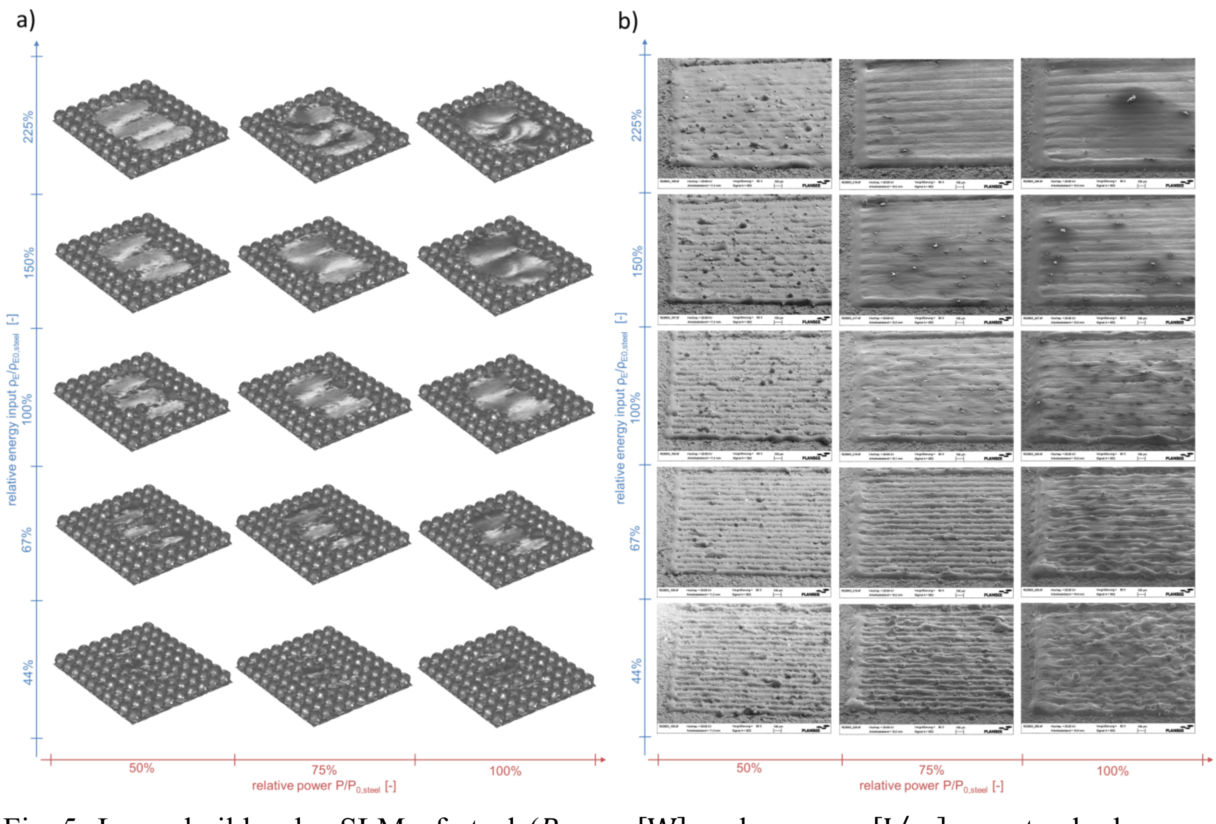

Fig. 5 Layer buildup by SLM of steel ($P_{0,steel}$ [W] and $\rho_{E0,steel}$ [J/m] are standard power and energy input for volume buildup from steel): a) simulation results ($360\ \mu m \times 400\ \mu m$), b) experimental results (magnification scalebar for electron micrographs $100\ \mu m$).

4. Experimental Validation

For a validation of the simulation model a comparison of the simulation results to experimental data was performed. Figures 4 b and 5 b show scanning electron microscope (SEM) images of layers produced from single layers of molybdenum and steel powder at parameters corresponding to those applied for the simulation. The general appearance of the surface morphology shows good qualitative correspondence to the simulation results. The narrower process window derived from the simulation data is confirmed by the experimental results. In order to make a quantitative comparison of obtainable surface roughness, the surface topology of the samples was measured with a chromatic white light sensor (FRT CWL) and the surface roughness R_a was determined from the height data in an area of $500\ \mu m \times 500\ \mu m$ from 100×100 equidistant measurement points. The surface roughnesses R_a obtained from $n = 3$ independent experiments for each parameter set are plotted in figures 6 and 7.

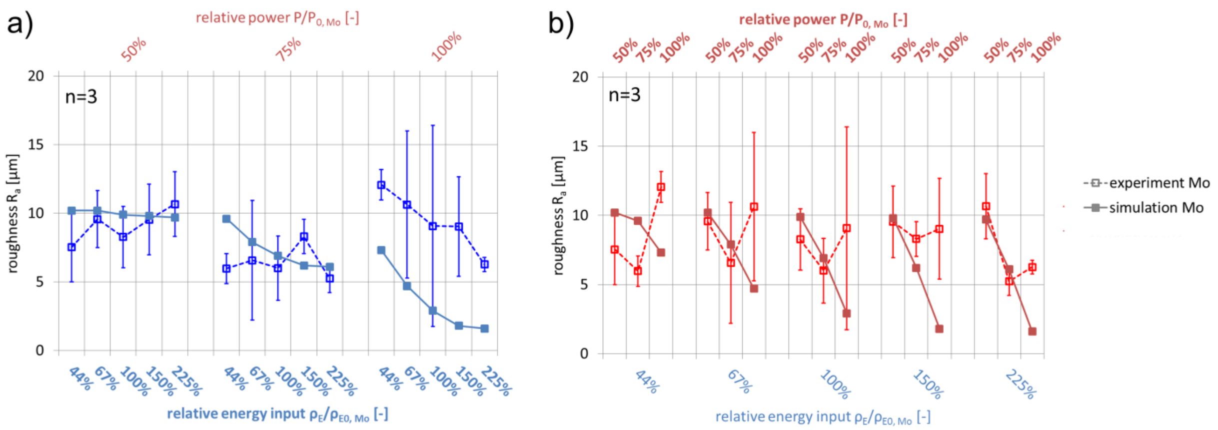

Fig. 6 Surface roughness in layer buildup by SLM of molybdenum ($P_{0,Mo}$ [W] and $\rho_{E0,Mo}$ [J/m] are standard power and energy input for volume buildup from molybdenum) - simulation vs. experiment: a) energy input dependency; b) power dependency.

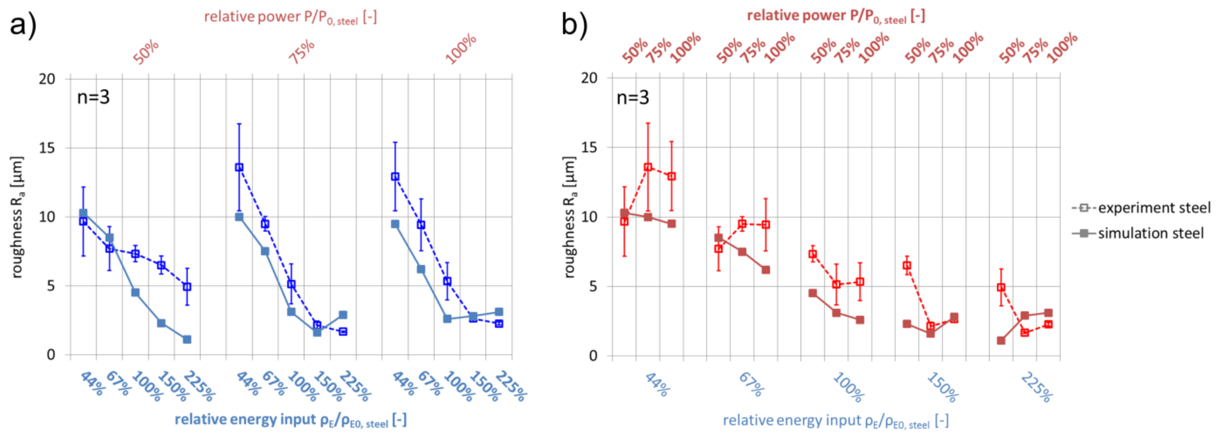

Fig. 7 Surface roughness in layer buildup by SLM of steel ($P_{0,steel}$ [W] and $\rho_{E0,steel}$ [J/m] are standard power and energy input for volume buildup from molybdenum) - simulation vs. experiment: a) energy input dependency; b) power dependency.

Both order of magnitude and overall trend show good correlation to the data obtained from the simulations. For molybdenum at high laser power and low energy input slightly higher surface roughnesses are observed experimentally. This can be attributed to the generally known balling effect at high feed rates in SLM [20,21]. The simulation results do not show this effect. It is assumed that this has its origin in the relatively coarse discretisation with an element size of $d_{part}/8$ and in the idealized simple cubic monomodal particle arrangement, both leading to a smoothed and more stable melt pool. Nevertheless, the results demonstrate that, even if the processing window for SLM of molybdenum is narrower at sufficient energy input, surface qualities are achievable comparable to those of steel.

5. Conclusions

Multi-physical process simulations are a versatile tool to develop a fundamental process understanding of SLM. The presented thermo-fluid dynamical simulation model is able to describe the material specific characteristics and the influence of process parameters on obtainable surface morphology in SLM of molybdenum and steel. For molybdenum, due to the high thermal conductivity and evaporation temperature, there is only a small melt pool and the influence of the laser power on the surface roughness is severely pronounced. For steel the melt pool is significantly longer and evaporation plays an important role. The energy input is the dominant process parameter.

The presented results demonstrate that SLM is a promising approach for the processing of molybdenum. At sufficient energy input surface roughnesses comparable to steel are achievable. However, due to the narrower process window, a fundamental process understanding and an experienced operator are essential to assure a stable, repeatable high-quality processing result.

References

[1] R. Schiffler, Additive Schichtarbeit zwischen gestern und morgen, VDI Nachrichten (2015, Volume 15), p.22

[2] M. Geiger, K.-H. Leitz, H. Koch, A. Otto, A 3D transient model of keyhole and melt pool dynamics in laser beam welding applied to the joining of zinc coated sheets, Production Engineering (2009, Volume 3), p.127

[3] A. Otto, H. Koch, K.-H. Leitz, M. Schmidt, Numerical Simulations – A Versatile Approach for Better Understanding Dynamics in Laser Material Processing, Physics Procedia (2011, Volume 12), p.11

[4] K.-H. Leitz, H. Koch, A. Otto, M. Schmidt, Numerical simulation of process dynamics during laser beam drilling with short pulses, Applied Physics A (2012, Volume 106), p.885

[5] K.-H. Leitz, Mikro- und Nanostrukturierung mit kurz und ultrakurz gepulster Laserstrahlung, Meisenbach Verlag (2013) – ISBN 978-3-87525-355-9

[6] F.-J. Gürtler, M. Karg, K.-H. Leitz, M. Schmidt: Simulation of laser beam melting of steel powders using the three-dimensional volume of fluid method. In: Physics Procedia (2013, Volume 41), 874-879.

[7] S. A. Khairallah, A.T. Anderson, A. Rubenchik, W.E. King, Laser powder-bed fusion additive manufacturing: Physics of complex melt flow and formation mechanisms of pores, spatter and denudation zones, Acta Materialia (2016, Volume 108), p.36

[8] K.-H. Leitz, P. Singer, A. Plankensteiner, B. Tabernig, H. Kestler, L.S. Sigl, Multi-Physical Simulation of Selective Laser Melting of Molybdenum, Proceedings of the Euro PM2015, Reims (2015)
[9] K.-H. Leitz, P. Singer, A. Plankensteiner, B. Tabernig, H. Kestler, L.S. Sigl, Multi-Physical Simulation of Selective Laser Melting, Metal Powder Report (2016) – in press
[10] Y. Sun, C. Beckermann, Diffuse interface modeling of two-phase flows based on averaging: mass and momentum equations, Physica D (2004, Volume 198), p.281
[11] H. Hügel, F. Dausinger, Fundamentals of laser-induced processes, Landolt-Börnstein (2004, Volume VIII/1C), p.3
[12] Comsol Multiphysics Material Library Version 5.0, © 1998-2014 COMSOL AB
[13] C.J. Smithells, Metals Reference Book, Butterwoth (1967)
[14] H. Stöcker, Taschenbuch der Physik, Harri Deutsch Verlag (2000)
[15] P.-F. Paradis, T. Ishikawa, N. Koike, Non-contact measurements of the surface tension and viscosity of molybdenum using an electrostatic levitation furnace, International Journal of Refractory Metals & Hard Materials (2007, Volume 25), p.95
[16] Landolt-Börnstein – Zahlenwerte und Funktionen, Springer Verlag (1963)
[17] W.D. Wood, H.W. Deem, C.F. Lucks, Handbook of High-Temperature Materials – Thermal Radiative Properties, Plenum Press (1964)
[18] M.J. Assael, K. Kakosimos, R.M. Banish, J. Brillo, I. Egry, R. Brooks, P.N.Quested, K.C. Mills, A. Nagashima, Y. Sato, W.A. Wakeham, Reference Data for the Density and Viscosity of Liquid Aluminum and Liquid Iron, J. Phys. Chem. Ref. Data, (2006, Volume 35, No.1), p.285
[19] R.F. Brooks, I. Egry, S. Seetharaman, D. Grant, Reliable data for high-temperature viscosity and surface tension: results from a European project, ECTP Proceedings (2001), p.631
[20] I. Yadroitsev, Selective laser melting, Lambert Academic Publishing (2009)
[21] J.-P. Kruth, G. Levy, F. Klocke, T.H.C. Childs, Consolidation phenomena in laser powder-bed based layered manufacturing, Annals of the CIRP (2007, Volume 56), p.730

RUDOLF PICHLER

FULL JOB QUALITY ASSURANCE IN LASER MELTING PROCESSES FOR PARTS WITH HIGH RELIABLE REQUIREMENTS

Abstract

High Level Industries are the most prominent enablers for Additive Manufacturing (AM) Technologies and they want to speed up the transformation from its use of single prototyping to the professional use in series production. An inevitable must for AM-products is a high reliable quality assurance (QA) process which frankly spoken is not yet satisfying. This all of course has also got highest relevance for the Selective Laser Melting (SLM) processes.

In situ-monitoring is the latest promising approach for doing such a real time feedback instrument in QA of SLM processing. Its development and step into maturity is at the very beginning, it is expectedly rather expensive and it still needs human expertise for doing quality interpretation or corrective measures. Current state is that in spite of first successful applications it cannot fully replace X-Raying, CT and Destructive Testing of representative specimen because the risks remaining for high reliable parts still must come down. But in-situ monitoring is the right step into the right direction and so far there is nothing better available by now for getting more knowledge about the melting process and its results. Its measurement principles, its capabilities and its progress requirements for further development is presented in this article.

Keywords

Selective laser melting, in-situ-monitoring, melt pool monitoring, optical tomography, quality assurance for high reliable parts, high level industry, quality assurance in powder bed fusion processes, future research in QA for selective laser melting.

1. Introduction

Among all disruptive technologies Additive Manufacturing (AM) - and as one of its specialities the Selective Laser Melting (SLM-) Technology definitely is revolutionizing the world of construction and manufacturing. It provides a rich bunch of advantages and new opportunities into the seemingly squeezed world of even already with CNC-technology and automization penetrated world of manufacturing. It appears as if nearly all barriers and restrictions in manufacturing have gone and the construction engineers no longer must take care of maybe too poor feasibilities in manufacturing. One can build parts half weight, one doesn't need special tools, one can do part count reduction, the lead times to launch manufacturing has become as short as never before, one can save efforts for assembly and the finest thing at all, you can build parts you were not capable at all before. For taking advantage all these benefits many a company is ready to spend a handful money more to buy this new fascinating technology and hope to step into the new manufacturing wonderland.

Is a matter of fact that the SLM technology is a complex one, needs a lot of attention and devotion and in the end is a too expensive one if not used in a very goal oriented way. Aside the cost issue and a still nonprofessional and effort taking pre- and post-processing it is especially the aerospace, the automotive and the healthcare industry which have highest interest to gain its attractive and cutting edge benefit out of using the SLM technology and that is why it is them who primarily are driving the progress in its usability.

But exactly these willing users are well known as providers of high reliable products, means products that fulfil much higher requirements than usual products/commodities of everyday or industrial life. Exactly these industries cannot concede any inconsistencies to the outcome of this new way of manufacturing.

In this context QA again has turned out to be a very important facilitator for giving confidence that this promising new technology with its so own characteristics has really got the power to generate products without any weaknesses in repeatability, proven density, tensile strength, ductility, geometric accuracy, surface roughness and much more. Bringing these new types of products into conditions of a series production the more QA has to turn out to be practical, robust and reliable. But where is the SLM-technology standing in this concern?

2. Quality Assurance (QA) in Selective Laser Melting (SLM) processes

2.1. Scopes of the SLM Process out of the view of QA

For realizing a robust SLM process QA has to master a rich bundle of influences and parameters that finally decide about to fail or not to fail. A systematic approach has to consider all of these. Fig. 1 should give not more than an idea how manifold the influences are.

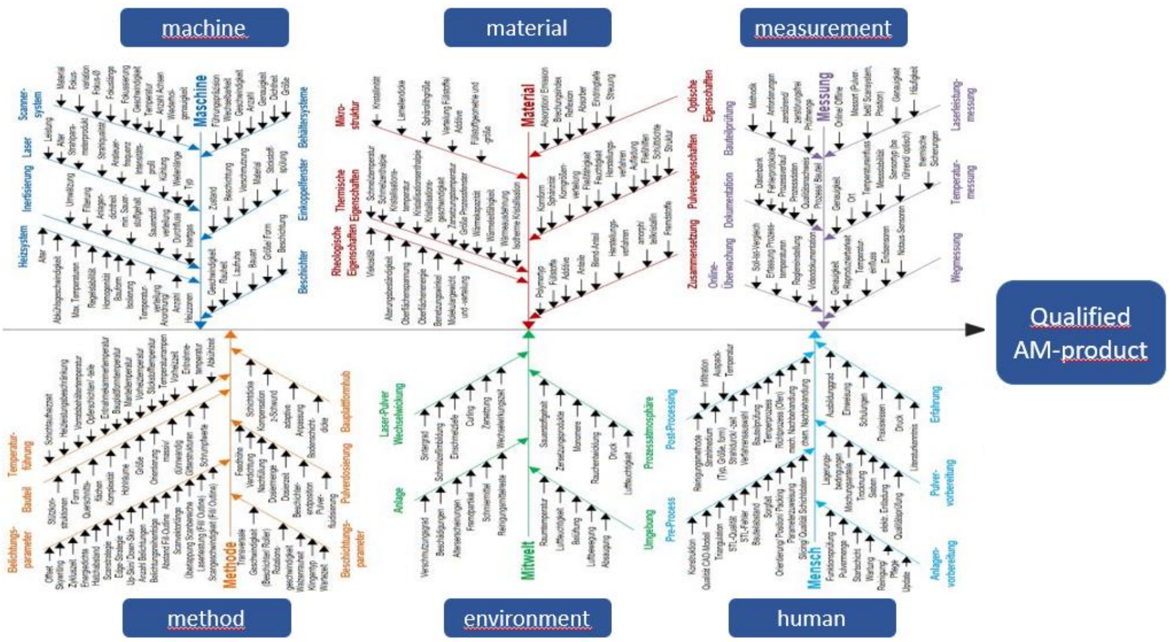

Fig.1: Ishikawa Diagram for building a part with Additive Technology, source: A. Wegner, Dissertation, Duisburg 2015

Another systematic approach is following the sequence of operations in the SLM process. This results in 4 main sectors:

1. The Powder (distribution of size, humidity, purity)
2. The Manufacturing Environment (operator, room temperature and room humidity)
3. The Machine (processing and process control)
4. The Post Processing (way of separation from building plate, heat treatment, surface treatment, machining, etc.)

A sound QA takes care of all of these so many impacts and no single item out of these 4 clusters can be disregarded. Nevertheless the following presentation concentrates on the core process of the melting process in the build chamber. Herein there are 2 major types of mechanisms to be monitored if not already controlled.

First there is everything that the machine and its periphery has to provide as <u>**inputs for the process**</u> like powder, laser energy, protection gas, cooling and much more. Thanks to the machine suppliers there are a lot of defaults and already given parameter-sets for certain jobs to have a high chance – sometimes a guarantee - to start a successful print job. Quite many of these inputs - e.g. the temperatures of the platform and the building space, the percentage of oxygen in the protection gas atmosphere, etc. - are not only monitored but controlled like we are used to have it as a standard in modern industrial machinery.

Second there is the <u>**melting process itself**</u> that significantly and finally decides if the system is heading for quality or not. Out of approx. 200 parameters to be set for doing a print job there remain at least more than 50 parameters that directly influence the melting process [1]. Normally an implemented industrial process (with defined parameters) ideally is led by using in-process control what finally and automatically will end up in a product of quality. SLM-processing has not yet reached this stage of development.

It is evident that SLM-processes still are inclined to fail though machine and powder suppliers provide parameter settings and well developped procedures. The multiple set of influences that are still not sufficiently known or are not yet able to be controlled still lead to typical defects such as cavities, shrink holes, gas pores, solid inclusions, slags, incomplete fusions, porosity, cracking, thermal issues, delamination, pores, cracking and density variations. And this simply does not lead to an approval of the SLM technology not at all for series production purposes. If we talk about the needs of the High Level Industries requirements even rise dramatically.

2.2. Special Requirements of the High Level Industry

Industries like aerospace, automotive and healthcare have to provide products which have to be highly reliable because people’s life and safety depend on them. That is why they have to meet very strict rules when introducing their products on their markets.

Providing reliable products under series conditions means to achieve reproducibility and make process risks to come down to an acceptable level. QA is forced to provide a system that is able to cover following imperatives:

a) Detect all defects being out of tolerance
b) Detect these defects as soon as possible
c) Do this all with means of NDT
d) Do this all automatized
e) Provide a sound Q-documentation and -protocol

In detail ad a) There is no tolerance in accepting defects of any certain kind. Especially the optimization in weight must make sure that each zone of the material provides the theoretical material properties for the load when in operation. The probability of detection (POD) of defects of a certain and defined kind must be 100 %.

In detail ad b) The process itself is expensive because of the powder materials, the long lasting process and the costly equipment. If a defect occurs that is impossible to be repaired each minute longer in the build chamber would be pure waste, means the sooner the detection the better it is. At certain materials unequal heat input or too fast heat dissipation can lead to distortion or to cracks. There is no way to have it repaired by HIP-processing or heat treatment!

In detail ad c) Destructive Testing means the loss of the very part and would make the testing procedure to not more than a comparison. Such forms of testing cannot be accepted by the High Level industry. The more they cannot afford loosing expensively built parts. Therefore using NDT methods is a must! Besides this it is far off interest and costs to apply a high time-consumption for doing post-process analysis.

In detail ad d) For reasons of speed, accuracy, lead time and statement efficiency there is no other way than to have the correction loops done automatically. Any manual procedure would turn out to be costly and also endanger a final serious quality statement.

In detail ad e) For further use - especially in the mentioned high level industry - SLM parts must give evidence that the produced parts meet quality (or not). The proof of their quality is inevitable and there remains the only question how efficiently this can be done. With intention to avoid costly testings after the completed building job there is left one motto “Certify as you build” which means that all quality data needed for a sound documentation are generated while the building job is done.

2.3. The QA-Contribution of Standardisation Organisations

All renowned Standardisation Organisations (ISO, ASTM, BS, DIN, …) are busy to provide a common language and offer early and sufficient orientation in the new world of Additive Manufacturing by a maximum of cooperation [2]. First editions and drafts regarding the powder topic the test environments and special materials are available. Exemplified for the aerospace industry as representative of this article there are to mention:

- ISO 17296-3: (Draft Standard): Additive manufacturing - General principles - Part 3: Main characteristics and corresponding test methods, Edition 2014-09
- ASTM F 3049: Characterizing Properties of Metal Powders Used for Additive Manufacturing Processes
- DIN 35224: (Pre order for Edition 2016-09) Welding for aerospace applications - Acceptance inspection of powder bed based laser beam machines for additive manufacturing
- DIN 65122: (Draft Standard) Aerospace series - Powder for additive manufacturing with powder bed process - Technical delivery specification, Edition 2016-06

Common use in industrial life is that the suppliers simply refer to the requirements of their customers. And these requirements always are correlating to the level of trust they have in a certain technology, e.g. aviation industries and similar have their own specifications. It depends on them if they refer to standards or not. The standardisation organisations the more have to struggle to get all relevant and suitable informations from an industry that especially in this case not always is interested to bring their innovative concepts into public.

2.4. State of the Art of Detection of SLM Defects

According to the layer-wise build up the typical defects in SLM-processes are very tiny and flat, means there is only little spatial extension what makes X-Ray and Ultrasonic Tests commonly fail [3]. Changing over to X-ray computer tomography (CT) of e.g. a cylindrical part with diameter 10 mm and length 70 mm pores with a length of 50 µm and bigger can be detected. Tests with parts knowing that they have pores of a size of 10 µm could not be verified via CT.

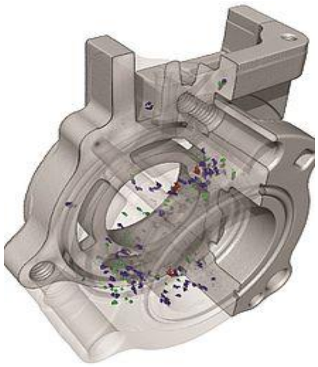

Fig. 2: industrial CT scan of an aluminum casting, source: https://en. wikipedia.org

CT diagnostics definitely can provide higher resolutions but then you are limited to the part size. An empirical formula says that the desired resolution times 2000 gives the maximum length of the part to be checked. (eg. a part with dimension of 200 mm leads to an approx. maximum achievable resolution of 100 µm what for some application is not sufficiently satisfying.

CT diagnostics is limited by the density of the material and this can cause the well-known poor POD of CT. The experience of a Tier 2 supplier for aircraft engines tells that the POD for “lack of fusion” via CT is not higher than approx. 50 % what for high reliability parts of course is not acceptable.

However, an even high resolution CT does not give profound evidence if a part meets quality requirements or not. It does not come by chance that people out of the aircraft business clearly state that they do not see a future in CT for their demands. But even in best case for industrial use in series production such a quality statement would come much too late. The more such a QA process does not provide any further insights why and how some defect occurred.

That is why there has always been a big need for an in-situ and real-time process monitoring if not process control. First products are available some are in development.

3. In-situ Monitoring as the better Approach for NDT in SLM

The obviously better approach for getting quality referred feedback from the SLM manufactured product is to get the relevant data straight from the melting process itself. “In-situ” is a Latin phrase that means "on site" or "in position" or "locally". In this context it says that the intended measurement takes place right where the material is additively generated, means right in the build chamber and straight away when the local melting happens. In-situ monitoring implicitly also says that we are also talking about a real-time-capture of data.

3.1. Working Principle of In-situ Monitoring

The entire quality information for the SLM-product is generated via scanning relevant layer informations (pixels) while processing and finally piling them up to a 3D -“as built” model (see Fig. 3) showing voxels. Such models give valuable indications to the quality of the whole product, of the full job. The results come close to the resolution of a CT but does not have its disadvantages with its extra efforts after the print job. The 3D -“as built” model is available more or less right after the last layer melted.

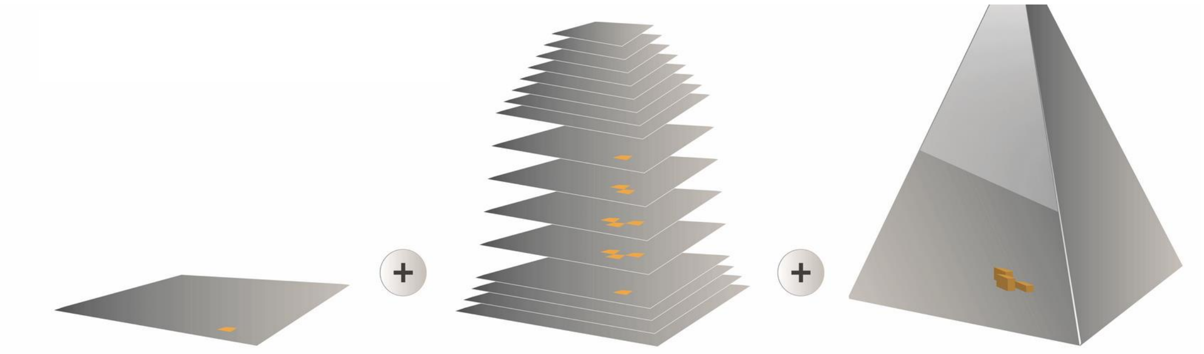

Fig. 3: From 2D pixels to 3D voxels via piling up the layer informations; source: EOS GmbH

The physical principles for getting these layer informations are based on the measurement of the local electromagnetic radiation emitted by the plasma or metal vapor plume during laser melting that correlates with the process quality in laser welding and melt pool behaviour [4].

3.2. Actual available in-situ monitoring systems

In principal there are four sensor systems that could be applied for getting direct information form the building/melting process. Either ultrasonic, acoustic, thermographic or optical methods are possible. The actual survey tells that research is done in all four sensor categories but watching the activities of machine manufacturers shows that mainly thermographic and optical ways are really pursued. Some characteristics are given in Fig. 4

System	Used Sensors	Advantages	Disadvantages
Optical Monitoring	Photodiodes or Photo arrays	High measurement frequencies possible	Small zone of surveillance Little until no observation of the surroundings.
Thermographic Monitoring	High resolution digital cameras or Pyrometers	Surveillance of the whole platform. Capture of temperatures and cooling rates possible	Low geometrical resolution of cameras lead to bad “mapping”

Fig. 4: Pros and Cons of optical and thermographic monitoring systems, acc. [3]

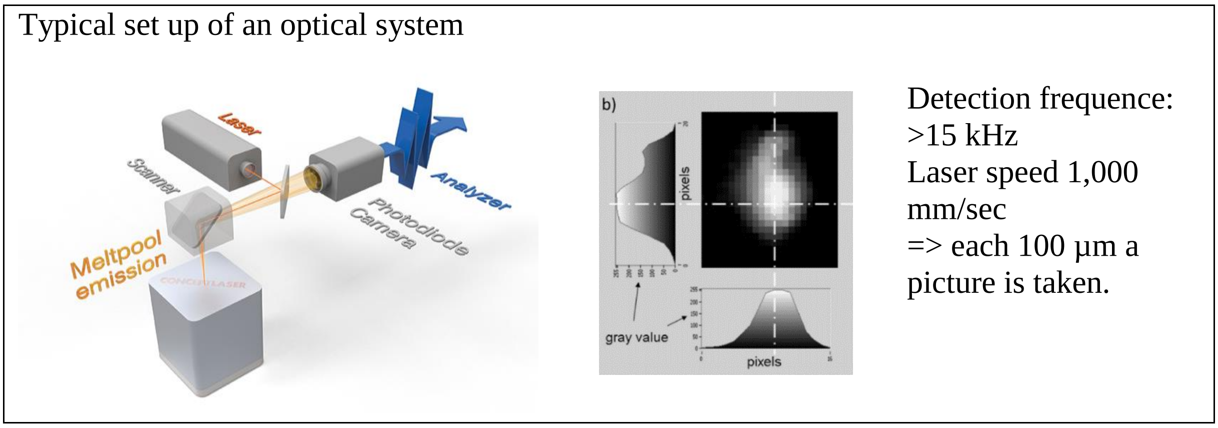

Fig. 5: Set up of such an optical in-situ-monitoring system, source: Concept Laser Inc.

The art of getting really useful informations for a quality statement is located in the analyser. It is the very gadget (made of HW and SW) that contains the specific know how of the developers of such monitoring systems. It consists of sensors and filters (HW) and interpretation rules (SW) that finally make dumb manifold captured signals to valueable informations about effective deviations and inconsistencies. The analyser also is the place where comparisons with target values or simulated results are done.

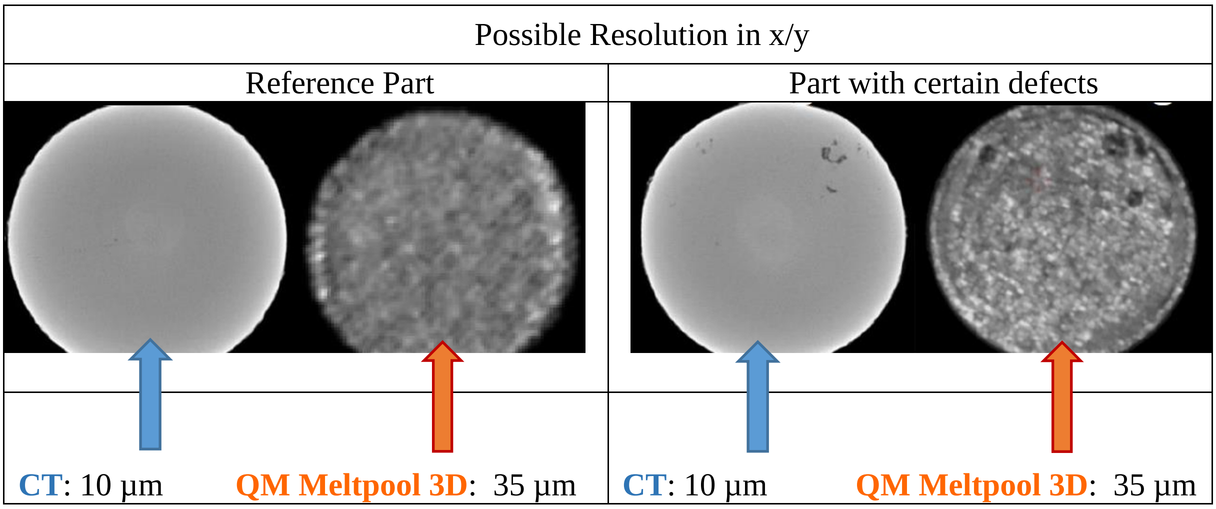

Fig. 6: Comparison of Resolutions: CT vs QM Meltpool 3D; Source: Concept Laser Inc.

Though there is an immediate offer of well-prepared informations it remains to the experts to interpret these results to come to a sound quality statement. There always is the question if all inconsistencies could be even detected and if the interpretation goes right. As soon as we arrive at very tiny maximum sizes of pores, fusion defects or similar the decision about the quality status becomes really hard.

The high requirements of the aerospace industry and the needs for a series production made a consortium consisting of MTU Aero Engines AG, EOS GmbH and Carl Messtechnik develop a completely new system for getting more satisfying and instant feedback from the building process with brand name “Optical Tomography (OT)”

3.3. Optical Tomography (OT) as latest highlight in SLM in-situ-monitoring

Instead of infrared detectors or optical sensors the setup of OT is done with a high resolution s-CMOS camera (approx. 5.5 MP) which continuously measures the light emission while selective melting. The major difference to the so far shown systems is that the measurement of the OT-Application does not capture only the actual welding zone but always the entire build platform. Under certain rules the image data of each single layer is selected and integrated to one more densified and compacted data file per layer. The compilation of all these single compacted layer informations finally lead to a 3D picture of the part based on a much shorter data volume.

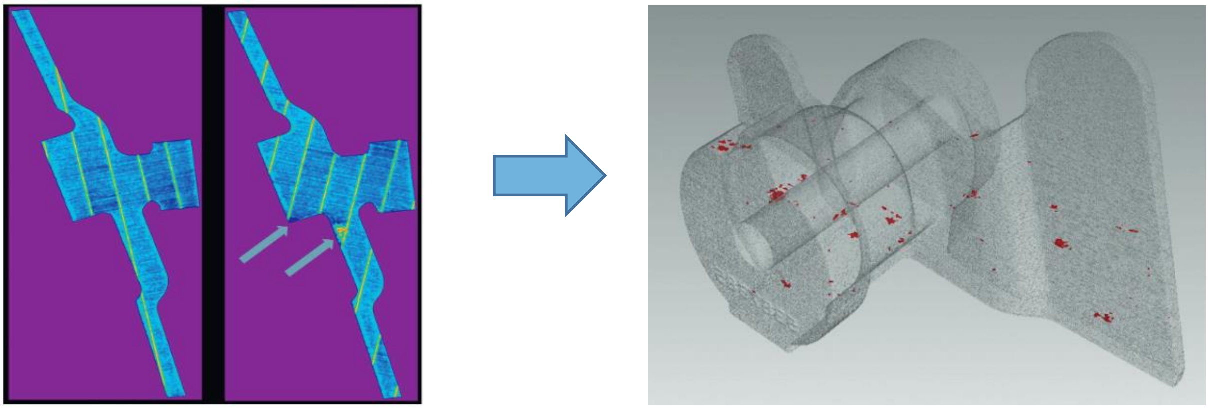

Fig. 7: left picture: 2 different layers out of OT-measurement, one without defect (left), one with defect (right), right picture: compilation of all layer informations lead to the 3D model [3]

The geometric resolution is quite high, e.g. scanning a 250 mm x 250 mm layer will lead to a resolution of 0.1 mm per pixel. This holistic procedure also enables to extract statements about the cool down behaviour of each single welding spot.

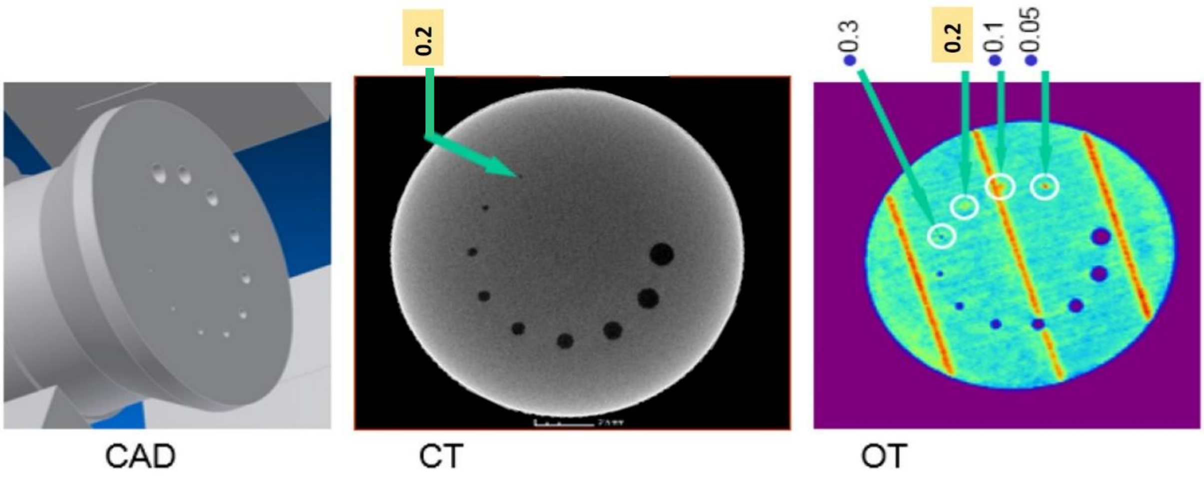

Fig. 8: High spatial resolution of OT for detection of even small deviations in geometry and radiation, source: V. Karl, monitoring system for the quality assessment in additive manufacturing [8]

3.4. Actual Status of providers of in-situ monitoring systems

Machine Supplier	Product	Measurement	Availability
Concept Laser GmbH	QM Meltpool 3D	Thermographic	Available
Eos GmbH	EOSTATE MeltPool	Optical	Available
SLM Solutions GmbH	Melt Pool Monitoring	Thermographic	In ß-Test, expected in 2017
Eos GmbH	Optical Tomography	Optical Coherence Measurement	in development earliest end of 2017
Renishaw plc	---	---	In development
Trumpf GmbH+Co. KG	---	---	In planning
Additive Technologies	---	---	In planning

Fig. 9: SLM machine manufacturers and their in-situ monitoring products, status July 2016

3.5. In-situ monitoring - as it is actually practiced

There is to state that the marketing departments of the few in-situ monitoring providers again have been doing a good job. Their announcements and promises quite often are ahead of reality and they are talking of product features which are not really ready for market.

As for these systems still are monitoring systems – though resolutions close to a CT – there remains the need of an experienced interpretation of these data. For supporting these quality interpretations it still is usual that on the same platform in parallel a print job with building several specimen is done. These are used for later destructive tests like tensile yield testing, fatigue tests or even chemical analytics.

CT and even x-raying are still companions of a modern in-situ monitoring system. The importance of getting undoubted facts for evaluating the quality status of parts with high reliability requirements is too high as getting loose of established and more or less confidential tools too early.

4. Conclusions and Outlook

The use of SLM-technologies in industrial series production and/or for the production of high reliable AM parts requires a trustworthy QA-system to find its broad acceptance. Destructive evaluation methods, representative methods and postponed testings are not deemed as appropriate means for enabling SLM-technologies for these purposes. First available in-situ monitoring systems are enlightening this big challenge though these products still need augmented usability and significance. All available systems – as its name clearly tells - are feedback or monitoring systems. Its provided informations still need the expertise of well experienced people in order to interpret this gained data and evaluate the actual quality status.

So far there is no automatized control mechanism available that that is ready to deduct control measures directly out of the captured monitoring data. Not sooner than this one can talk about a “Melt Pool *Control*“ system or meanwhile often heard “Closed-Loop-*Control“* system. Possible outputs for control could be dynamically adjusted laser power, selectively corrective melting cycles, dynamical adaption of in-process cooling procedures or similar. Asking the experts they say that there is no solution expected within the next 3-5 years. Developping such control systems is exactly the inevitable direction where industry, machine manufacturers and research are heading for. So the agenda for future activities consists of following topics:

- Persecution of a still better understanding of the details in the SLM processes. Use of existing monitoring systems to learn. Steady awareness that any result is always bound to a certain material and to a certain machine if not to a certain holistic process.

- Improvement of detection resolutions and the probability of detection (POD), creation of undoubted interpretations of captured inconsistencies for providing the fundament for later automatized control loops and measures.

- Integration of Image Data Processing and Big Data Analysis for getting even higher reliable quality statements. Excessive utilization of DoE based research.

5. References

[1] M. Malesh, B. Lane, et.al, Measurement Science Needs for Real-time Control of Additive Manufacturing Powder Bed Fusion Processes, NISTIR 8036, 2015

[2] S.K. Everton, M. Hirsch, P. Stravroulakis, R.K. Leach, A.T. Clare, Review of in-situ process monitoring and in-situ metrology for metal additive manufacturing, Materials and Design 95 (2016)

[3] G. Zenzinger, J. Bamberg, B. Henkel, T. Hess and A. Ladewig, Online Prozesskontrolle bei der additiven Fertigung mittels Laserstrahlschmelzen, ZfP Zeitung 140, Juni 2014

[4] T. Purtonen, A. Kalliosaari, A. Salminen, Monitoring and adaptive control of laser processes, Physics Procedia 56 (2014) 1218 – 1231

[5] S. Clijsters, T. Craeghs, S. Buls, K. Kempen, J.-P. Kruth, In situ quality control of the selected laser melting process using a high speed, real-time melt pool monitoring system, Springer, August 2014

[6] T.G. Spears, S.A. Gold, In-process sensing in selective laser melting (SLM) additive manufacturing, Integrating Materials and Manufacturing Innovation, (2016) 5:2, Springer Open Journal

[7] H. Krauss, C. Eschey, M.F. Zäh, Thermography for Monitoring the Selective Laser Process, Institute for Machine Tools and Industrial Management, TU München, 2012

[8] V. Karl, Monitoring system for the assessment in Additive Manufacturing,
AIP Conf. Proc. 1650, 171 (2015)

MICHAEL KITZMANTEL [1,*], LILLA VÁLY [1], DAVID GRECH [1], ERICH NEUBAUER [1], ĽUBOŠ BAČA [2], NILS STELZER [2], GRAŻYNA MOŻDŻEŃ [2]

CHALLENGES FOR XXL COMPONENTS BY POWDER AND WIRE METAL DEPOSITION – 4M SYSTEM

ABSTRACT: Whenever thinking about additive manufacturing for metals, it is very often a powder bed combined with a laser or electron beam system, that comes into ones mind. A very promising system for large parts (>1m) is based on shape welding. This study focuses on the use of a plasma transferred arc system combined with powder or/and wire feed for MAM. The technology is quite well known for a range of materials including steels. We investigate in this study the potential for XXL space and aircraft components built up from oxygen sensitive aluminium and titanium alloys, looking into the metallurgy of phase formations, microstructures, inclusions, processing atmospheres and its influences on the material properties of the final 3D part. All of this gains in importance with the in-house build-up of a stable machine for repeatable results which is also discussed in this study.

Keywords: Titanium, powder blown process, space components

1. Introduction

Large additively built-up metallic parts with structure size of several meters redefine the technology of 3D printing [1-4]. Logistics need to be rediscussed when large components can be directly manufactured in the location where they will be used. Instead the machine or the printer is transferred to the building site. For large parts also the saving of raw materials gains more and more in significance [5]. Based on a very simple and modular concept we were constructing a 5-axis system using a plasma transferred arc welding torch as energy and temperature source. This makes the machine very much affordable. The precision we reduced to tolerances of one millimetre, as we believe, that large structures will anyway need to be post-machined in at least some areas, where tight tolerances need to be hold by the construction and technical needs.

One very exciting topic of the 4M System is the use of multiple powder feeders to be able to create graded structures and reinforced areas (in x-y plane and also in z direction!). For example you need in one location higher stiffness and in another area softer but light material is requested. Powder technology allows exactly this to play with material properties all around the produced parts. Of course challenges need to be overcome and tricky problems need to be solved. In the following study we have investigated these topics using the material systems of pure Titanium and Titanium 6wt%Aluminium 4wt%Vanadium alloy (grade5).

[1] RHP, RHP-Technology GmbH, Seibersdorf, Austria
[2] AAC, Aerospace & Advanced Composites GmbH, Wiener Neustadt, Austria
* corresponding author: michael.kitzmantel@rhp-technology.com

2. The 4M System

The machine used for this study was built using modular components and consists mainly of the motion system (X-Y-Z + B-C axes) and the welding unit (power supply + powder feeder). The machine is able to provide a printing volume of 1.500 × 850 × 200 mm with the linear axes whilst the C-axis can be tilted from 0° to 90° with reference to the X-Y (horizontal) plane. A Siemens Sinumerik 840d sl governs the motion control and deposition parameters using CNC commands. This allows for a high degree of freedom in machine utilisation and customisation since peripherals can be added or removed according to the job's need.

The plasma torch works by generating a pilot flame of ionised Ar gas which then ignites to a transferred arc on command, delivering up to 250 Amps in continuous Direct Current. (this is the PTA system). The current experiments are being carried out using a negative electrode – positive substrate configuration.

The installed torch-powder feeder system can deliver up to 2 kg per hour of Ti powder; spherical powders with diameter range 70-150 μm are generally used with these powder feeder systems since their flowability is optimal for such applications. Figure 1 shows a photographic image of the 4M machine, including the torch and powder feeder.

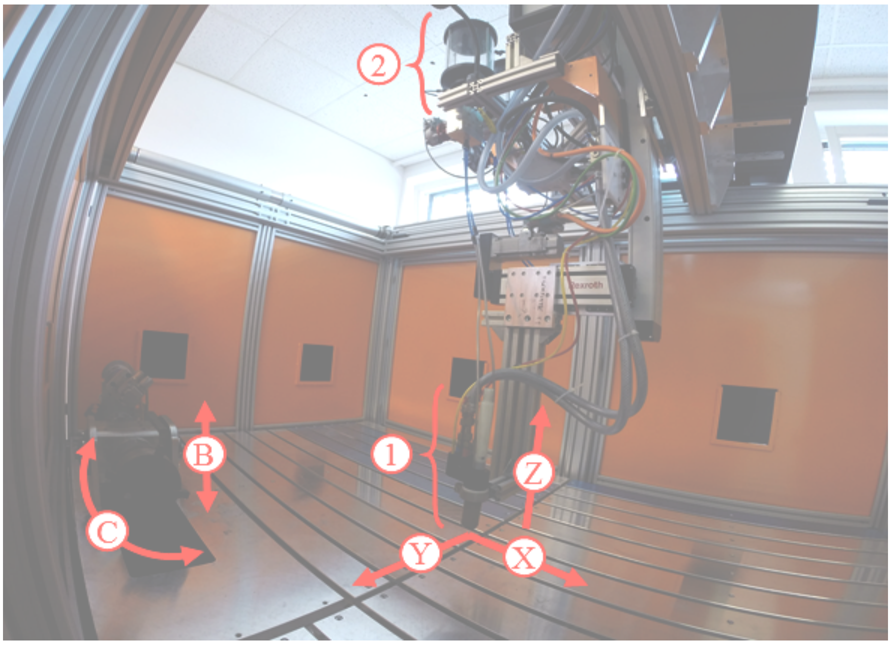

Fig. 1: 4M System: PTA based AM machine used for the fabrication of XXL 3D metallic parts. Axes of motion are labelled accordingly (X, Y, Z, B, C) whilst component 1 indicates the torch and component 2 indicates the powder feeder.

Figure 2 shows how a pool of molten material is produced during the deposition process. Several variables need to be taken into consideration to obtain a seam, and ultimately the bulk material, with the desirable properties. Some of such variables are portrayed in said image. The dominant variables for the PTA process are (i) the strength of the transferred arc, (ii) the travelling speed and (iii) the powder feed rate; these determine the geometry and temperature of the weld pool.

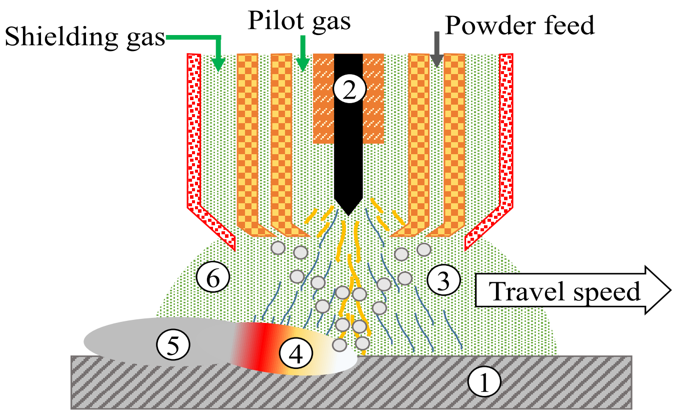

Fig. 2: Schematic representation of some variables which are encountered in the PTA process. (1) Choice of substrate and its initial temperature (2) Tungsten electrode is responsible for generating both the pilot and transferred arc (3) Powder is injected into the transferred arc (4) Transferred creates a molten pool which swells up on with added material (5) Powder fuses in the pool and solidifies into a seam (6) Inert gases, eg Ar or He/Ar mixture, are used to prevent oxidation during seam deposition

3. Materials and methods

Several studies showed promising results for the use of Titanium and Titanium alloys for additive manufacturing [6]. In this study we prepared samples with the plasma transferred arc system combined with powder feed. For our experiments we used commercial pure titanium and titanium alloy. We produced test walls with Titanium Grade1 powder [7] on Titanium Grade2 substrate and with Titanium Grade5 powder [8] on Titanium Grade5 substrate without shielding atmosphere. Table 1 shows the data of the powders and the substrates.

.

Table 1. Data of the powders and substrates

Powder/Substrate	Grainsize/Geometry
Titanium Grade1 powder	75-180 μm
Titanium Grade5 powder	106-180 μm
Titanium Grade2 substrate	Plate, 5×200×200 mm
Titanium Grade5 substrate	Plate, 5×200×20 mm

Before the deposition process the surface of the substrates was cleaned by sandblasting and by isopropyl alcohol. Table 2 shows the welding parameters of the test walls. We used the same built up strategy, powder feed (6,3 g/min) and travel speed (50mm/min) during welding both test parts. The currents were changed due to the welding properties of the different titanium. The machine built up 20 layers on each other producing test walls with 140 mm length. Both test walls were produced from one side, the plasma torch carried out the first layer and the subsequent layers were started from the starting point of the first layer as well.

Table 2. Welding parameters

Seam Nr.	Powder material	Substrate material	Layer Nr.	Pilot arc	Welding arc	Powder feed	Travel speed
S89	Ti Grade1	Ti Grade2	20	35A	130A	6,3g/min	50mm/min
S150	Ti Grade5	Ti Grade5	20	40A	120A	6,3g/min	50mm/min

Fig.3 shows the deposited parts numbered S89 and S150. Specimen were cut out of these test walls for tensile testing, for microstructure analysis and for oxygen and nitrogen analysis.

Fig. 3 Deposited parts numbered S89 and S150

4. Experimental results

We prepared tensile test samples out of the test walls. The titanium specimens were sliced by Fanuc Robocut α-OB wire cutting machine based on ASTM E 8M-04 standard. Fig.4 shows the cut specimens and the tensile test results of commercially pure titanium (test part numbered with S89).

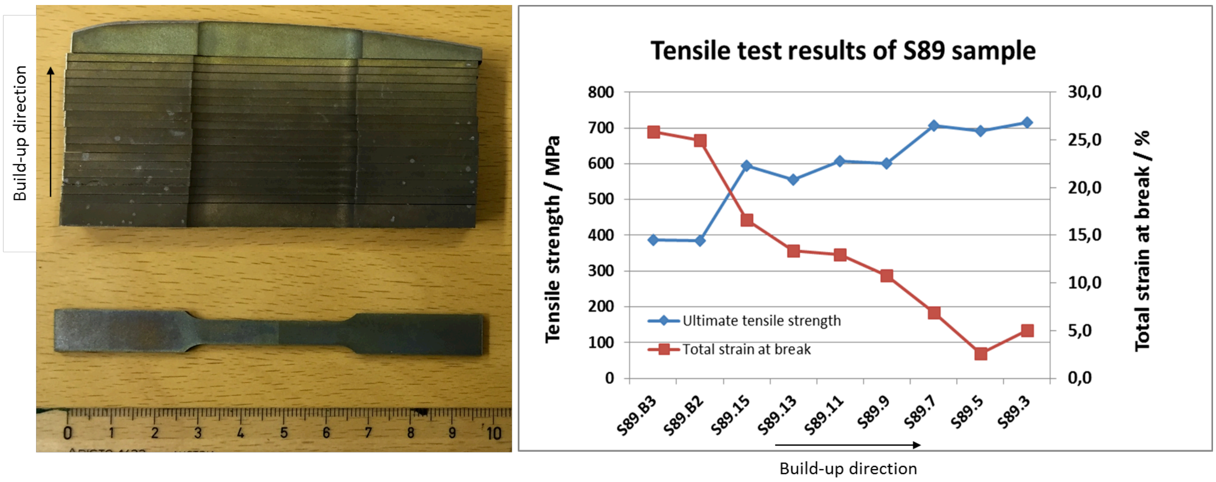

Fig. 4 Tensile test specimens and results of S89 test walls

The samples labelled with B (S89.B3, S89.B2, S89.B1) are from the Titanium Grade2 substrate and the subsequent specimens are from the deposited layers using Titanium Grade1 powder. The blue graph represents the ultimate tensile strength and the red graph the total strains at break. We can observe on the chart that the tensile strength of samples is proportionally increasing along the build-up direction in contrast to the total strain at break.

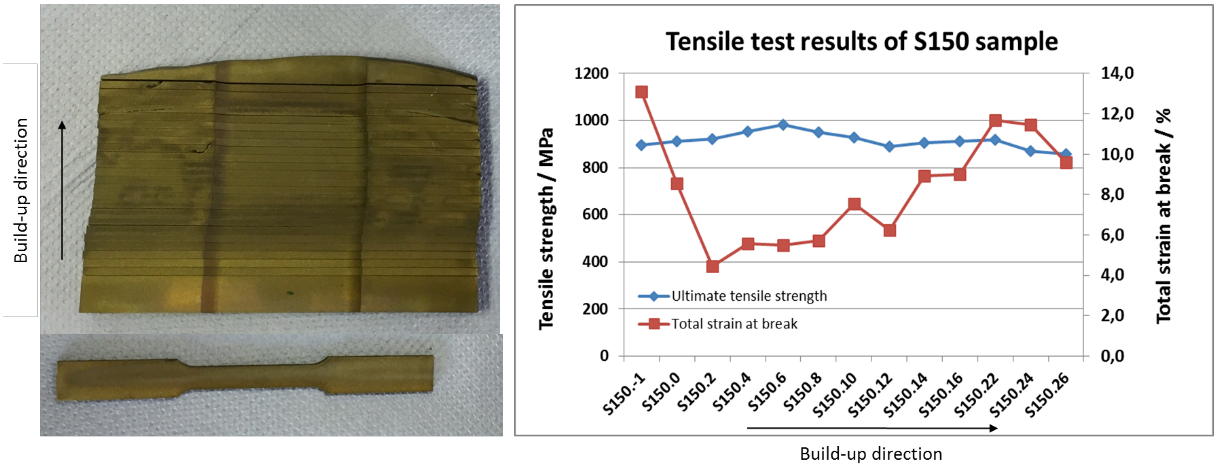

Fig. 5: Tensile test specimens and results of S150 test walls

Fig. 5 shows that the Titanium Grade5 specimens have not so significant changes in the ultimate tensile strength by increasing the number of the deposition layers like at the commercial pure titanium samples. The strength is decreasing minimally in the build-up direction in contrast to the elongation. We can conclude that the elongation is increasing. The S150.-1, S150.0, S150.2 samples were cut out of the Titanium Grade 5 basis plate and the other specimens (S150.4 - S150.26) out of the deposition produced by the PTA machine.

For collecting more information about the relationship between the deposition process and the material properties we have prepared cross section samples for microstructure analysis as well. Fig. 6 shows the microstructure images of the commercial pure titanium sample (S89) and the Titanium Grade5 sample (S150).

On both optical microscopy pictures it is clearly visible that the grains have grown a lot in the build-up direction during the solidification after the deposition process. The alfa-beta phases of Titanium Grade 5 sample (S150) make easily distinguishable the big grains in contrast to the alpha phases of commercial pure titanium.

We can observe that the big grains seem to have a significant effect to the changing of the ultimate tensile strength and of the total strain at break.

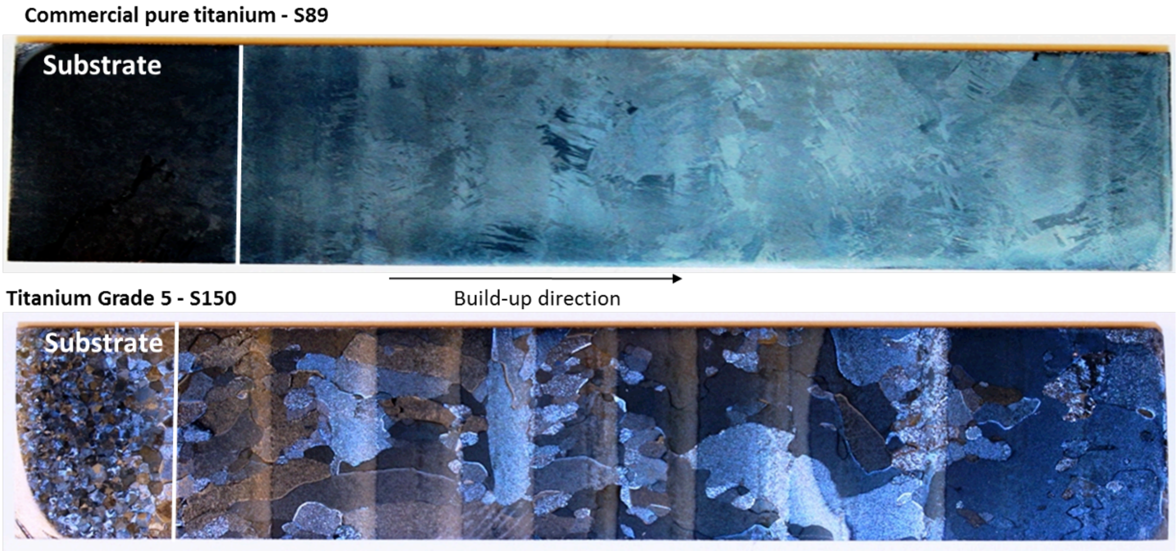

Fig. 6 Microstructure of the S89 (commercially pure titanium) and S150 (Titanium Grade5)

Other cross section samples were cut out of the test walls and they were prepared for oxygen and nitrogen analysis by carrier gas hot extraction. The commercial pure titanium sample (S89) contained 0,20% oxygen and 0,056% nitrogen. The oxygen content is 0,02% lower than the limit value for the Titanium Grade 1 powder based on the material certificate but the nitrogen content was exceeding the limit with 0,026%.

In the case of the Titanium Grade 5 sample as well the oxygen content and the nitrogen content were lower compared to the maximum allowed content for the Titanium Grade 5 powder. The oxygen and nitrogen values of test parts show negligibly small deviation from the tolerated values. In our further work we will focus on the microstructure and the effects on grain growth.

Table 3 Oxygen and nitrogen content of samples [1][7]

Material	Comments	O	N
Ti Grade1 powder Material Cerificate	*allowed*	*Max. 0,18%*	*Max. 0,03%*
S89 - Ti	Test part	0,20%	0,056%
Ti Grade5 powder Material Cerificate	*allowed*	*Max. 0,20%*	*Max. 0,05%*
S150 – Ti64	Test part	0,18%	0,040%

5. Challenges for XXL parts

We have identified several fields of interest as challenges for XXL part manufacturing. Several effects, like stresses and deformation, are well known from welding and also powder bed laser sintering technologies. With scaling-up the process and the parts produced, these effects become much more significant and have to be solved for a reliable production.

5.1 Deformation and internal stresses

PTA deposition involves the use of a high temperature plasma torch – ca. 20.000 K – to create a melt-pool. This also brings about a large temperature gradient between the surface and the underlying material or the deposited material and the substrate. Due to this large temperature difference, these materials will shrink/contract in a different amount, which results in what is called internal stress and which manifests itself as warpage/deformation and cracking. Such occurrences can be seen in Figure 7a and b. Internal stresses can never be completely eliminated, only reduced to a level where they can be compensated for, with for example machining or deposition optimisation.

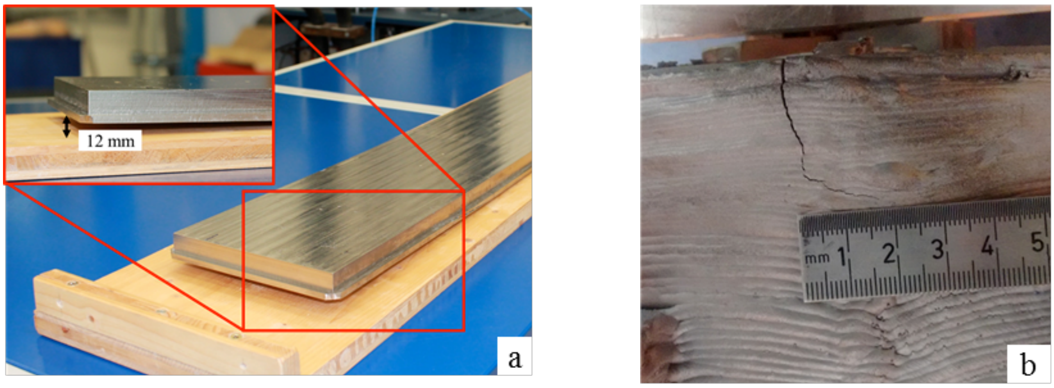

Fig. 7 (a) Internal stresses causing upward deflection of a 1,2 m part (b) crack formation during deposition of Ti6Al4V alloy

Applying a stress-relief heat treatment specific to the deposited material is one of the easiest ways to reduce deformation. This was shown to work for the part in Fig 7 (a) where most of the warpage was eliminated following such process.

On the other hand, cracks prove to be more difficult to overcome since this is an issue relating to the material rather than the structure, hence process optimisation needs to be material specific.

5.2 Atmosphere contamination

Susceptibility of a material to oxidise in air upon heating ranges from none (platinum group metals) to medium (eg stainless steels) to heavy (eg Titanium and even more so aluminium). Due to their low density and yet high mechanical strength, both titanium and aluminium (and their alloys) are the best candidate materials for exploitation of the PTA AM process. Special care need to be taken to avoid excess intake of oxygen during processing of these materials since otherwise their mechanical properties are lost due to the formation of oxides.

For one of our prototypes a shielding tent, as shown in Figure 8, was erected to fabricate it in an Ar atmosphere so that oxides formations would be kept to a minimum. By evacuating then filling up the tent with Ar, an atmosphere containing about 700 ppm oxygen was achieved.

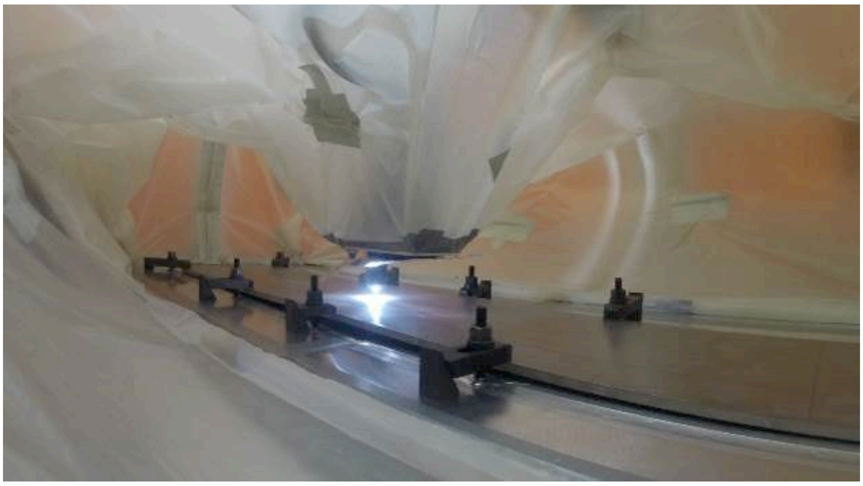

Fig. 8 Image showing a 1,2×0,5 m Ti-CP substrate inside the shielding tent

Construction of shielding tents is no easy task, especially when big parts are to be enveloped. One has to compensate for the distance to be travelled in all directions, choose a material able to withstand high temperature and U.V. radiation, be impermeable, flexible but yet strong enough to not tear when the torch is moving. It was also possible to easily access inside so perform maintenance cleaning on the torch since a long deposition time was required. Several improvements need yet to be applied to improve the long-term performance of such shielding tent, especially since conservation of Ar gas reduces the production costs and hence increases the profit return.

5.3 Complex shape build-up

As per most processes, pre-planning helps in reducing errors and problems during and after fabrication. The PTA AM is no less of such case, if not more so. Planning includes:

1. Choice and preparation of appropriate powder/s
    a. Powders need to have good flowability to avoid inconsistent powder feed rate
    b. Since most build-ups can take hours if not days to complete, powders mixtures must not naturally segregate through time
2. Deposition of test seams
    a. No model can precisely relate a given set of deposition parameters to the dimensions of a seam or more practically a wall. Therefore such parameters need to be found empirically prior to each job in order to obtain a seam which would result in a wall having the required thickness, height, fluidity and surface roughness.
    b. Mechanical and microstructural characterisation can also be carried out on such test seams/walls to obtain information on the sturdiness of the printed part. This also reduces the need for destructive testing on the finished part.

3. Build-up strategy

    a. Generation of an appropriate tool-path will lessen the burden on any required post-processing, for example machining and testing. Some factors are taken into account to (1) avoid severe deformation (2) compensate for post-machining limitations (3) PTA deposition limitations (4) failures during deposition and more. These factors include seam dimensions, pre-heating, cooling time, one continuous seam vs multi-paths, contour definition and so much more.

    b. Another drawback of ALM is that small errors in a single layer will accumulate and lead to a large discrepancy after several layers. Figures 9 a and b show two of the most recurring once where the walls end up having different heights. This occurred principally due to powder deposition efficiency and overlapping seams. The latter was later compensated for in the tool path whilst the former is yet to be addressed.

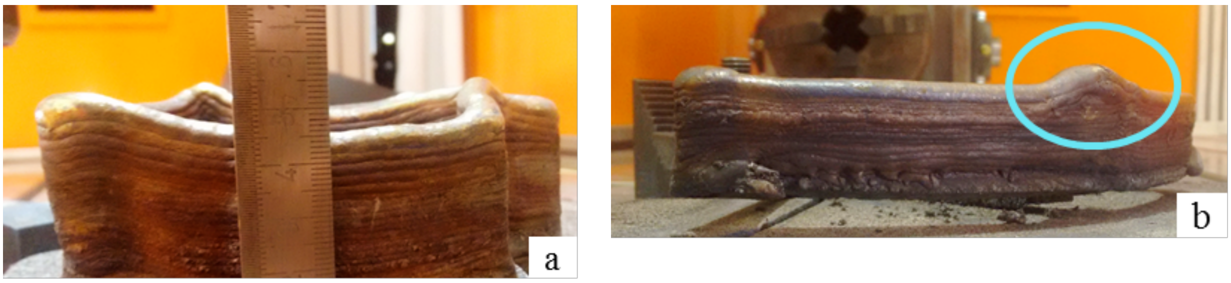

Fig. 9 (a) Part having unequal wall height (b) Bulging due to overlapping seams

Having finished with preparation, production can start. The PTA process is still under development and hence dedicated observation need to be given so that the process and machine performance are familiarised with. In due time and experience, the process must be consolidated into full automation so that robust, repeatable and reliable products can be realised. Software, machine and human aspects have to be integrated for a holistic and yet specialised process for the production of high performance and functionality parts.

6. Conclusion and Outlook

High expectations are set for XXL 3D printing of metal parts. We have set-up a complete 5-axis system to investigate material and process behaviour in a systematic way for oxygen sensitive materials like titanium, aluminium and their alloys. Initial results presented in this study show the feasibility for using the 4M system for these material combinations and address the risks and challenges to be solved for future investigations and applications.

We were able to show the significant difference in mechanical behaviour between Ti and Ti64 alloy (grade5) when building up the bulk material by a PTA system. Nitrogen and Oxygen content were measured for the starting powders and the final parts, resulting in a fairly good behaviour. We are looking forward to further improvements in the near future also for manufacturing “real-sized” parts and test them in realistic applications.

7. References

[1] E. C. Santos, M. Shiomi, K. Osakada, and T. Laoui, “Rapid manufacturing of metal components by laser forming,” Int J Mach Tool Manu, vol. 46, pp. 1459–1468, 2006.
[2] Sears, J.W., “Direct Laser Powder Deposition – State of the Art,” Powder Materials: Current Research and Industrial Practices, Proceedings of the 1999 Fall TMS Meeting, Ed. By F.D.S. Marquis, 213-226, (1999).
[3] Roger S. Storm, Vladimir Shapovalov, James C. Withers, and Raouf O. Loutfy, Plasma Transferred Arc Rapid Additive Manufacturing, TITANIUM ADVANCES AT AEROMAT 200
[4] J. Mazumder, J. Koch, J. Nagarthnam, and J. Choi, “Rapid manufacturing by laser aided direct deposition of metals,” Adv Powder Metall Part Mater, vol. 4, no. 15, pp. 107–118, 1996.
[5] H. Zhang, J. Xu, and G. Wang, “Fundamental study on plasma deposition manufacturing,” Surf Coat Technol, vol. 171, no. 1-3, pp. 112 – 118, 2002.
[6] B. Baufeld, O. V. der Biest, and R. Gault, “Additive manufacturing of Ti6Al4V components by shaped metal deposition: Microstructure and mechanical properties,” Materials and Design, vol. 31, no. Supplement 1, pp. S106 – S111, 2010.
[7] AP&C Advanced Powders & Coatings: Material Certificate No: MC-16-028 (2016)
[8] AP&C Advanced Powders & Coatings: Material Certificate No: MC-15-083 (2015)

HADI MOZTARZADEH [1], DARREN J HUGHES [1], SAMPAN SETH [1], GREGORY J GIBBONS [1], HODA AMEL [1], RICHARD J DASHWOOD[1]

THE EFFECT OF PROCESS PARAMETERS ON RESIDUAL STRESS EVOLUTION IN PLASMA TRANSFERRED ARC CLADDING (PTA) OF Ti-6Al-4V

Abstract

Plasma Transferred Arc Cladding (PTA) is currently used as a metal-based Additive Manufacturing (AM) technique to make parts in a layer-by-layer fashion. In this study the effects of three process parameters on the evolution of residual stresses in parts made out of Ti-6Al-4V is investigated. Two different deposition strategies are used in a wire-feed process to make geometries on a substrate of the same material. To measure residual stresses on the test specimen, two methods are used: curvature measurement and neutron diffraction. A comparison of the data from the two techniques is performed, which provides a baseline for mapping residual stresses in metal-based Additive Manufacturing.

Furthermore, by studying the microstructure of the initial wire and final parts a picture of the evolution of microstructure is given. To study the microstructure of the final parts, different heights of the specimen are considered to investigate the effect of dwell time between layers. This will help to customize the process parameters towards required and/or favourable final material properties.

Keywords

Plasma Transferred Arc Cladding (PTA), Additive Manufacturing (AM), Titanium alloy, Residual Stress, Neutron Diffraction

1. Introduction

Titanium and its alloys have over the years proven themselves to be technically superior and cost effective materials for a wide range of applications for the demanding performance and reliability requirements of the medical, aerospace, automotive, petrochemical, and nuclear and power generation industries. This is because of their good combination of mechanical properties to include low density, excellent high temperature mechanical properties, good corrosion resistance and excellent specific strength [1], [2].

Additive Manufacturing (AM) is a technology that enables the fabrication of complex, near net shape components by depositing consecutive layers of a specific material. This technique offers a high geometrical flexibility and great potential for time and cost savings in comparison to conventional manufacturing technologies [3]. The AM of small and medium-sized Ti–6Al–4V parts represents an interesting case for a number of industrial applications.

Plasma Transferred Arc Cladding (PTA) coupled with 3-axis CNC platform has recently been used as a metal-based AM technique. Linear beads of material are deposited by using PTA to manufacture parts in a layer-by-layer fashion. A range of metallic materials have been used in this technique, such as titanium alloys, Inconel and high chromium steel. Understanding the effects of the manufacturing process on the performance of the final part is the key when highly reliable functional product is required [1-3].

[1] WMG, University of Warwick, Coventry, CV4 7AL, UK

Residual stresses are important in additive manufactured beads as they induce high, tensile/compressive stress combined with unfavourable microstructure changes and flaws [4]. Diffraction techniques and in particular neutron diffraction is a viable option to measure residual stresses in weld depositions [5]. Another technique to measure residual stresses within coatings and layers is the curvature measurement [6]. By using the Euler-Bernoulli theorem, the resulting changes in curvature due to deposition could be interpreted as bending stress which is an indication of residual stresses. Curvature can be measured using contact methods such as profilometry or without direct contact such as using laser scanning [6].

2. Methodology; manufacturing of the parts

Process parameters for a PTA welding are described in the literature [7]. These are summarised in Table 1 for the wire-based PTA used in this study.

Table 1 – Process parameters for PTA as an AM process

Parameter	Value Range	Unit
Plasma Gas Flow Rate (PGFR)	0.5	l/min
Wire Feed Rate (WFR)	1	m/min
Traverse Speed/Weld Speed	50	mm/min
Energy Density	~135	MJ/m^2
Deposition Strategy	Linear/Zig-Zag	-
Dwell Time	60 or 180	sec

The energy density in Table 1 was calculated from both the traverse speed (weld speed) and current. Since the PTA cladding has been used as an AM technique, the phenomena between layers should be counted as a process parameter. This is considered to be the 'dwell time' between layers to give an indication of the temperature of a layer. Two different dwell time is considered for this study. As shown in Table 1, sample 1 has a dwell time of 60 sec and sample 2 has a dwell time of 180 sec. The cooling temperature of each layer was captured by using a pyrometer to take the effect of dwell time into account. The rest of process parameters are the same for both samples. The fixture of the substrate and the direction of deposition are shown in Fig 1. A one-way linear deposition path was chosen due to the position of wire-feeder, electrode and torch on the PTA [8, 9]. However, further work is under way looking at the effect of path type (e.g. zig-zag). The deposition was continued until the height reached 50 mm for each sample. This has resulted in 27 layers for each sample and a wall width of 12 mm.

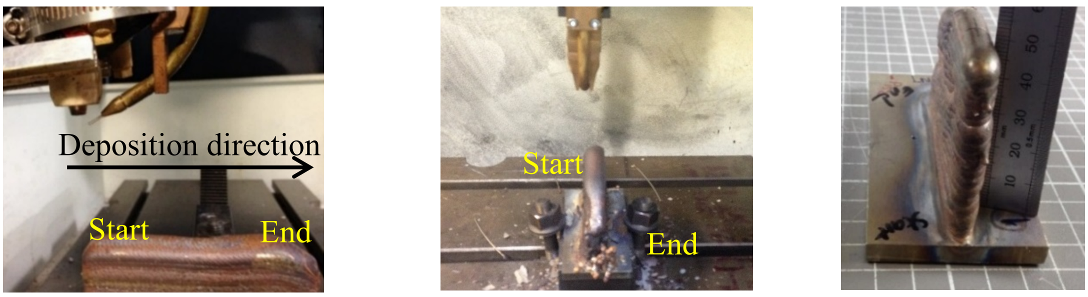

(a) One-way deposition; torch and wire Feeder

(b) Deposition direction and clamping of the substrate

(c) Sample No. 1

Fig. 1 – Building / deposition strategy and sample No. 1

[1] WMG, University of Warwick, Coventry, CV4 7AL, UK

3. Material model and microstructural analysis

Chemical composition of the Ti-6Al-4V wire is given in Table 2 and nominal material properties of the wire and substrate are given in Table 3. An optical microscope was used to study the microstructure of the cross section of the deposited beads to facilitate an understanding of the phases. For the purpose of microstructural analysis, a two layer sample was built using the same 'linear' deposition strategy. The process parameters and the direction of cladding were the same as the actual parts for residual stress measurement. Micrographs were obtained by an optical microscope using polarised light to analyse the microstructure.

Table 2 – Chemical composition of the Ti-6Al-4V wire

Element	Ti	Al	V	Fe	O	C	N	H	Y	Others
%Weight	Balance	6.75	4.5	0.3	0.2	0.08	0.05	0.0125	0.005	0.5

Table 3 – Nominal material/mechanical properties of the Ti-6Al-4V wire/substrate

Property	**Value**	**Unit**
Tensile Strength, Ultimate	950	MPa
Tensile Strength, Yield	880	MPa
Modulus of Elasticity	113.8	GPa
Poisson's Ratio	0.342	-

4. Residual stress measurement

Curvature measurement and neutron diffraction were used to measure the residual stresses. According to the curvature measurement technique, the resulting change in the curvature of the substrate due to deposition makes it possible to calculate the corresponding variations in stress as a function of the geometry of the part and material property. The basis for this technique is the Euler-Bernoulli theorem to measure the deformation (bending) of the part and calculate the internal bending moment and then determine the longitudinal bending stress [6].

The results for the deflection of the substrates are shown in Fig 2 (measured by CMM). A polynomial curve fitting was conducted to derive the curvature equation.

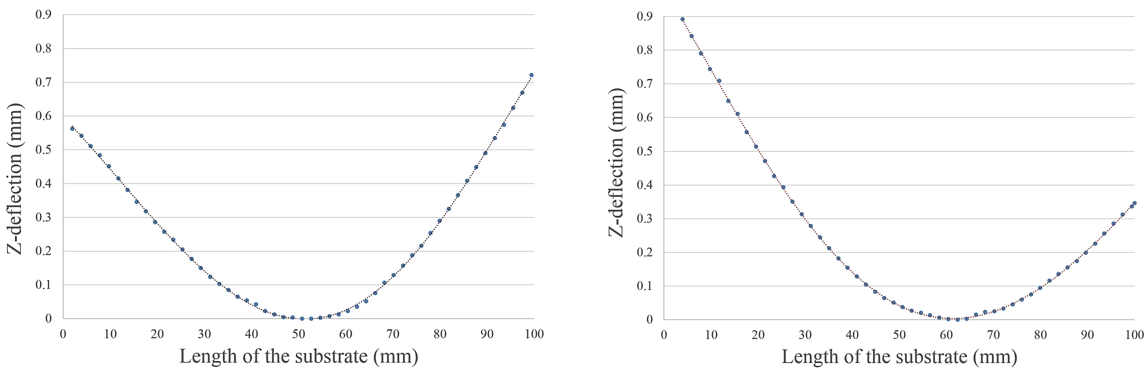

(a) Sample 1 (60 sec dwell time) (b) Sample 2 (180 sec dwell time)

Fig. 2 – Z-deflection of the substrate from CMM measurements

1 WMG, University of Warwick, Coventry, CV4 7AL, UK

Residual strains were also determined using non-destructive neutron diffraction technique, at the SALSA beamline at the Institut Laue-Langevin (ILL) [10]. A neutron wavelength of 1.69 Å was used and the titanium alpha-phase (101) peak at ≈42.2° $2\theta_0$ was selected for the scans. The gauge volume was defined by vertical and horizontal collimators giving an effective gauge volume of ≈2 mm^3. Two scan lines were chosen to conduct the measurement along them as shown in Fig. 3. Seven points were chosen along the horizontal scan-line (1) which is 20 mm below the reference point. The scanned points started from the lateral surface towards the middle of the sample with a distance of 5 mm between each point. Thus, the scanned points started from 0 mm and ended at 30 mm with respect to the lateral surface on the start-side of the beads. On the vertical scan-line (2), nine points were scanned; starting from 10 mm below the reference point until the last point which is at the intersection of the wall and the substrate.

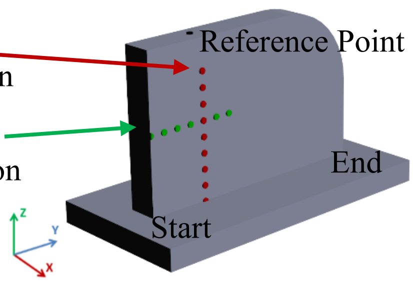

Fig. 3 – Schematic of the part and neutron diffraction measurement points

Neutron diffraction provides information on the average lattice spacing 'd' within the gauge volume under stress, the atomic lattice deforms, consequently the lattice acts as a strain gauge [5]. The d spacing can be obtained by using Bragg's law (Eq. 1) [5].

$$n\lambda = 2d\sin\theta \qquad \text{Eq. 1}$$

Where λ is the wavelength, n is an integer, d is the spacing between the planes of the atomic lattice and 2θ is the angle between the incident and scattering beams. To calculate the principal strains a fixed wavelength and known θ_0 (stress-free condition) is assumed. Typically the d spacing is scanned in all three principal directions (Y: longitudinal, Z: Transverse and X: out of plane) and the principal strains are calculated using Eq. 2 [5].

$$\varepsilon = \frac{d-d_0}{d_0} = -\cot\theta.(\theta-\theta_0) \qquad \text{Eq. 2}$$

In the PTA samples, it is likely that there will be local variations in microstructure leading to corresponding variations in θ_0. According to the geometry and dimensions of the samples (12 mm in thickness); a plane stress condition was assumed. To implement this assumption, the out-of-plane stress was forced to zero, allowing calculation of both in-plane stress components and any variation in θ_0. It was shown that the variation of θ_0 along both scan-lines is negligible and therefore the plane stress assumption was implemented by adjusting the θ_0 to obtain zero stress on the normal direction to the walls (X-axis in Fig 3).

5. Results and discussion

The micrograph images shown in Fig. 4 obtained from different regions of the two layer sample, to study the differences between bottom, middle and top of the deposited layers.

[1] WMG, University of Warwick, Coventry, CV4 7AL, UK

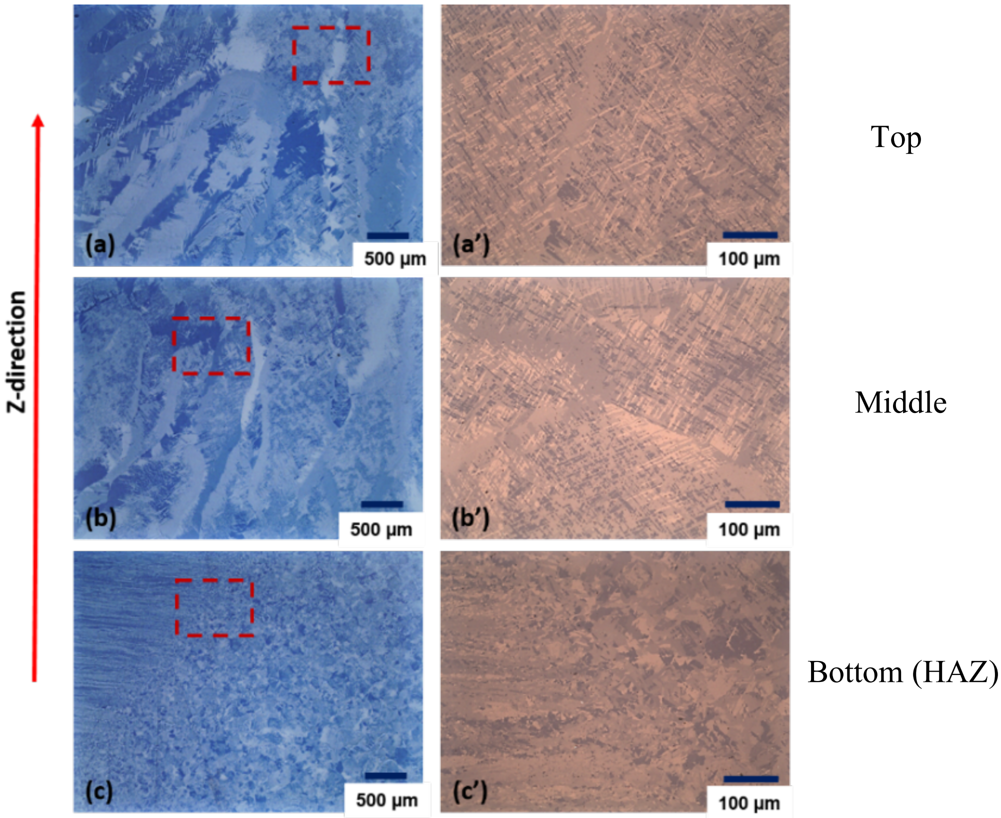

Fig 4 – optical micrographs of the cross section of two layers of Ti-6Al-4V weld sample showing (a and a') top, (b and b') middle and (c and c') bottom of the layers (HAZ)

From Fig. 4(a) to (c), increase in columnar β grain size from bottom to top was observed. This was attributed to the rate of solidification during the process, where precipitation of directionally oriented Body Centred Cubic (BCC) β grains was observed, in the direction of the plasma source (Z-direction). Due to rapid cooling rates, when the temperature of the weld falls below the β transus temperature, precipitation of hexagonal close packed (HCP) α phase was seen, as in Fig. 4 (a)-(c).

Fig. 4 (a') and (b') show a higher magnification optical micrographs of the selected regions from the top and middle which illustrate a finer lamella microstructure. This widmanstatten or Basket weave type microstructure has been reported by previous researchers as a results of precipitation of α phase within the β grains due to rapid cooling cycles during the process [11]. A coarser microstructure was seen towards the bottom of the weld which can be seen in Fig. 4 (c'). Previous studies have shown that due to repeated thermal cycles in a multi-layer PTA cladded Ti-6Al-4V deposits (which causes re-heating of the previous layer), coarsening of α phase can occur as the temperature of the layers away from the heat source remains below the β transus temperature [12].

To account for the dwell time between layers, Fig. 5 plotted the temperature history of the first 10 layers for the samples 1 and 2, captured by a pyrometer. The temperature of the new layer increases as more layers are deposited. The cooling rate however, shows a consistent trend for both samples 1 and 2. Considering sample 1 with a shorter dwell time, after depositing 10 layers, the temperature of the previous layer before depositing a new one is well above 500 °C. However, for sample 2 with a longer dwell time, this temperature is kept under 500 °C before depositing the next layer.

[1] WMG, University of Warwick, Coventry, CV4 7AL, UK

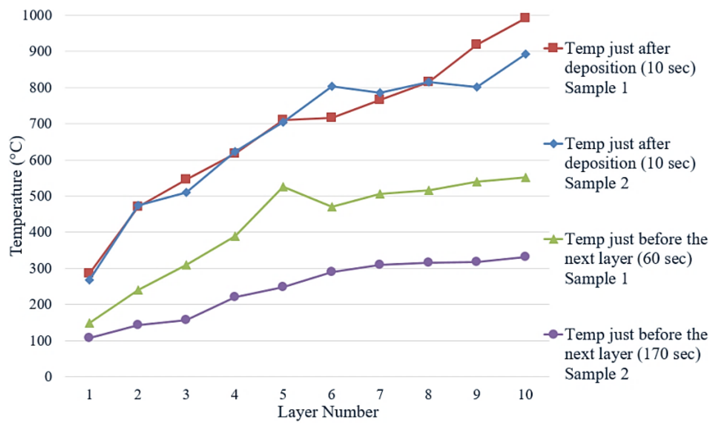

Fig 5 – Temperature history of the first 10 layers for samples 1 and 2; 10 sec after depositing the layer and 10 sec before depositing the next layer

Residual stresses calculated by curvature measurement and neutron diffraction along scan-line 1 are plotted in Fig. 6 and neutron diffraction results along scan-line 2 are plotted in Fig. 7 for both samples.

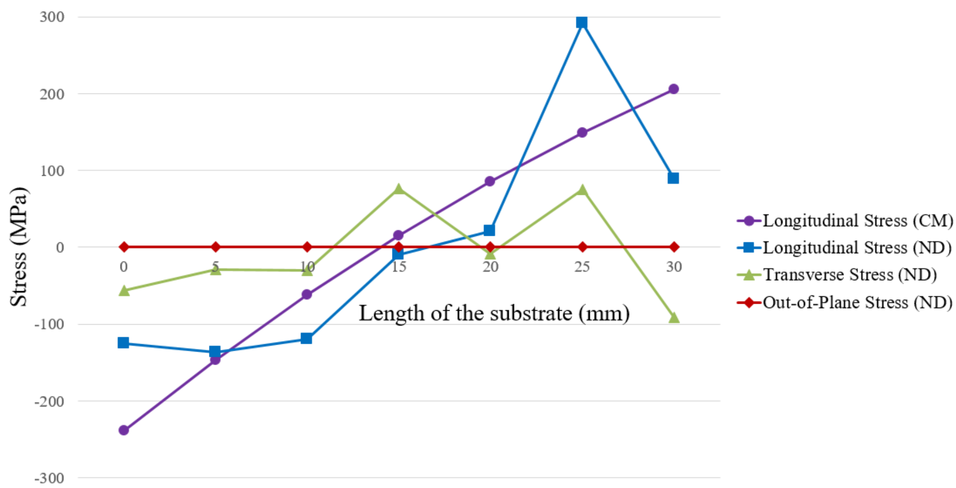

(a) Sample 1 (shorter dwell time: 60 sec)

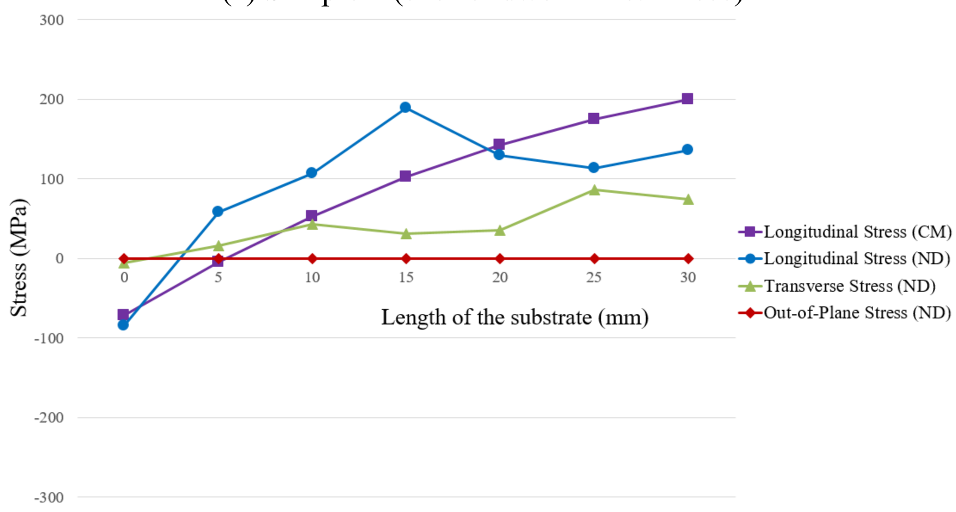

(b) Sample 2 (longer dwell time: 180 sec)

Fig 6 – Residual stress measurement along scan-line 1: longitudinal stress (Y) by Curvature Measurement (CM) and Neutron Diffraction (ND), transverse stress (Z) is also included

[1] WMG, University of Warwick, Coventry, CV4 7AL, UK

For both of the scan lines 1 and 2, the results from neutron diffraction include the residual stress on both longitudinal (Y) and transverse (Z) directions, calculated via the plane stress assumption which means stress on the out-of-plane (X) direction is zero. As shown in Fig. 6 for the scan line 1, the bending stress due to curvature was also included. This is calculated by using a 5th order differential equation to account for the variation of bending moment as a function of the length along the longitudinal direction (Y). The bending calculation was performed for the same length as the scan-line 1 for the neutron diffraction results (see Fig 3).

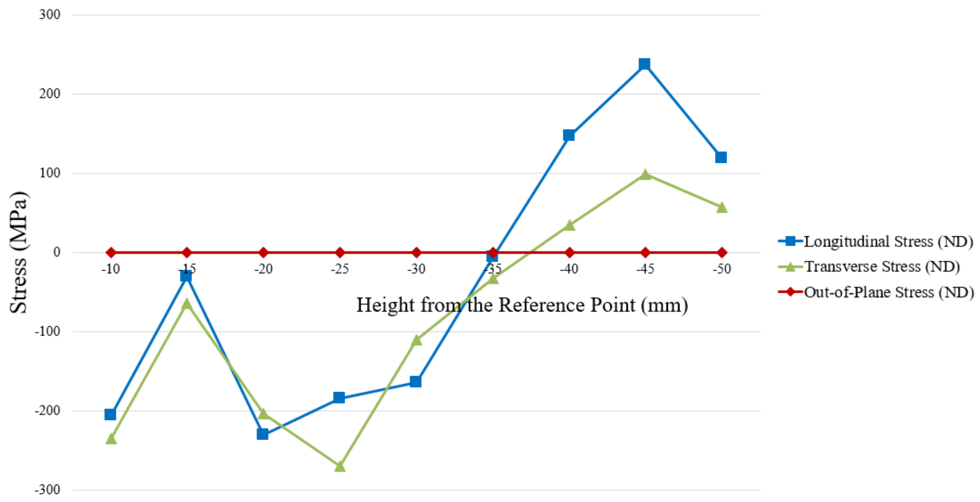

(a) Sample 1 (shorter dwell time: 60 sec)

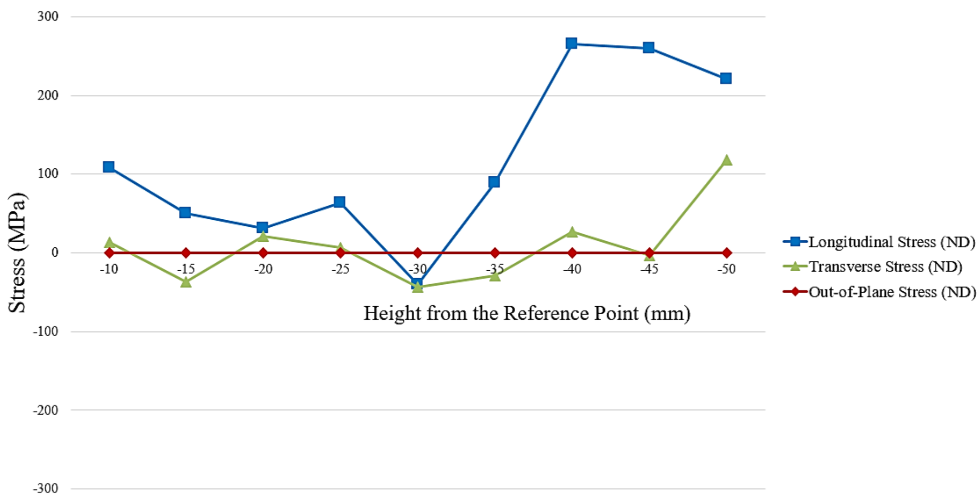

(b) Sample 2 (longer dwell time: 180 sec)

Fig 7 – Residual stress measurement along scan-line 2: longitudinal (Y) and transverse (Z) stresses by Neutron Diffraction (ND)

According to the distribution of the stress along scan-line 1 (Fig. 6), the longitudinal stress starts with a compressive stress at the lateral surface and then increases towards the centre of the part. Almost at the middle of the part a tensile stress can be observed by both bending measurement and neutron diffraction.

Neutron diffraction results give a full image of the stress state at each point while the bending stress only represents the longitudinal stress (Y). However, comparing the results from neutron diffraction and curvature measurement, the majority of the stress magnitude can

[1] WMG, University of Warwick, Coventry, CV4 7AL, UK

be assumed to be on the longitudinal direction. This can be understood by the clamping strategy as well as the geometrical condition of the deposition as shown in Fig 1.

Comparing the results obtained for both samples in Fig. 6, shows that by increasing the dwell time between layers, the magnitude of stress is decreased. In the sample 1 (short dwell time), the maximum stress is seen at approximately 250 MPa in both compression and tension. For the longer dwell time specimen (sample 2), the peak values drop to approximately $\pm$100 MPa. This can be attributed by the effect of dwell time and the cooling phenomena between layers as illustrated in Fig. 5. With increased dwell time, cooling occurs more effectively and therefore, stress relief is believed to be occurring between layers which results in reduced residual stress.

To obtain for a comprehensive overview of the variation of stress within the samples, a vertical scan-line (2) was also considered. Fig. 7 shows the residual stresses along scan-line 2 (along Z-axis) determined by neutron diffraction. As described in Fig. 3, nine points were scanned on the scan-line 2, starting from 10 mm below the reference point until the intersection of the wall and the substrate. The same plane stress assumption was applied in calculating the stresses in Fig 7. Stresses on both in-plane principal directions (Y and Z) are plotted along scan-line 2 to give a thorough overview of the stress state. As shown in Fig. 7 the variation of stresses on scan-line 2 is more than the variation of the stresses on scan-line 1 for both longitudinal (Y) and transverse (Z) components. This is an indication of the effect of layer by layer deposition process on the evolution of residual stresses which indicates that as the number of deposited layers increases the evolution of residual stresses rises.

According to Fig. 7, the magnitude of the longitudinal stress at the bottom layers for both samples are at the same range roughly 200 MPa and both samples show a tensile stress, while the difference between stress within the two samples disperses when moving towards the top layers. So, it can be concluded that the dwell time has a negligible effect on the stress state at bottom layers as the thermal gradient is not very high at that stage. However, when the number of layers increases the effect of dwell time becomes more considerable. This can be understood by referring to the temperature history of the layers for both short and long dwell time scenarios, as plotted in Fig. 5.

An interrogative point in sample 2 (Fig. 7) is the presence of mainly tensile stress within the sample while the other sample (1) showed tensile-compressive stress within the layers. This could be related to the fact that scanned points were chosen from 10 mm below the top layer and ended at the intersection of the wall and the substrate. Therefore, the stress state at the top of the wall as well as at the substrate is still unknown. It can be presumed that the balancing compressive stresses are likely to occur in the regions where not scanned. However, this can be validated by other stress measurement techniques which are under investigation and will be reported elsewhere.

As shown in Fig. 7, as we move towards the top layers, the variation of the longitudinal stress in sample 1 (short dwell time) is much larger than the variation of the same component of stress in sample 2 (longer dwell time). This again confirms that by increasing dwell time more stress relieving phenomena is allowed between layers and the final residual stress state becomes more homogenous across the sample. While, by increasing the speed of deposition and shortening the dwell time, there is not enough time for the stress relief to occur.

On the scan-line 2, the variation of the longitudinal (Y) component of the stress is dominant which conforms to the trend observed on the horizontal scan-line 1. This recommends the importance of considering the longitudinal stress as the main contributor to the residual stress evolution, as it follows the directional deposition of the layers. This trend is under further investigation and will be discussed elsewhere.

[1] WMG, University of Warwick, Coventry, CV4 7AL, UK

6. Conclusion

The wire-based PTA coupled with a 3-axis CNC was used as an AM technique to build parts. This fabrication method offers exciting potential for net shape manufacturing of metal-based components. To investigate the evolution of residual stresses associated with the process parameters and dwell time, two samples with two different dwell times (short and long) were built out of Ti-6Al-4V on the substrates of the same material. A two layer sample was also made with the same process parameters for the purpose of microstructural analysis. Micrographs were obtained to study the effect of heating and cooling process on the final microstructure of the part. Reheating of the underneath layer while depositing a new one was shown to have impact on the final microstructure.

On the multi-layered samples, for the residual stress analysis, thermal gradient between layers was measured to capture the temperature history of the layers and account for the effect of cooling-time between layers on the evolution of residual stresses. To have a full picture of the residual stress state, neutron diffraction scans were performed across both horizontal and vertical directions on the deposited walls. Curvature measurements was also used to study the residual stresses along the horizontal direction.

It was shown that increasing the dwell time could reduce the peak levels of residual stresses within the part. On the horizontal scan-line, residual stresses were seen to be compressive at the lateral surface of the part tending towards tension away from the deposition start point. A correlation between the results from neutron diffraction and curvature measurement on the horizontal scan-line confirms that the majority of the residual stress could be interpreted as longitudinal (bending) stress. This was also observed on the magnitude of longitudinal stress on the vertical scan-line. Therefore, it could be concluded that the longitudinal stress along the height of the walls should be considered as the main contributor into evolution of the residual stresses. This could be associated with the nature of layer-by-layer deposition during the additive manufacturing process and the significance of the direction of deposition in metal-based additive manufacturing.

By increasing the dwell time between depositions, the magnitude of stress decreased. This indicates that allowing the layers to cool down before depositing the next layer could help relieving stresses which raises due to deposition and fast heating and cooling process. In fact, by allowing more cooling, the effect of fast heating is compensated.

The effect of dwell time on initial deposited layers is less than the top layers. By increasing the number of layers, the effect of dwell time becomes more considerable as the higher thermal gradient occurs between depositions.

Acknowledgement

The authors would like to thank the Institut Laue-Langevin (ILL) for the allocation of experimental beam time and Dr Thilo Pirling for all technical inputs and support during this study.

References

[1] M. Roggensack, M. H. Walter, and K. W. Bsning, "Studies on laser- and plasma-welded titanium," vol. 6507, no. 1983, pp. 104–107, 1993.

[2] E. Akman, a. Demir, T. Canel, and T. Sinmazçelik, "Laser welding of Ti6Al4V titanium alloys," *J. Mater. Process. Technol.*, vol. 209, no. 8, pp. 3705–3713, 2009.

[1] WMG, University of Warwick, Coventry, CV4 7AL, UK

[3] B. Baufeld, E. Brandl, and O. Van Der Biest, “Wire based additive layer manufacturing: Comparison of microstructure and mechanical properties of Ti-6Al-4V components fabricated by laser-beam deposition and shaped metal deposition,” *J. Mater. Process. Technol.*, vol. 211, no. 6, pp. 1146–1158, 2011.
[4] D. W. Brown, T. M. Holden, B. Clausen, M. B. Prime, T. a. Sisneros, H. Swenson, and J. Vaja, “Critical comparison of two independent measurements of residual stress in an electron-beam welded uranium cylinder: Neutron diffraction and the contour method,” *Acta Mater.*, vol. 59, no. 3, pp. 864–873, 2011.
[5] C. Acevedo, A. Evans, and A. Nussbaumer, “Neutron diffraction investigations on residual stresses contributing to the fatigue crack growth in ferritic steel tubular bridges,” *Int. J. Press. Vessel. Pip.*, vol. 95, pp. 31–38, 2012.
[6] P. J. J. Withers and H. K. D. H. K. D. H. Bhadeshia, “Residual stress Part 1 – Measurement techniques,” *Mater. Sci. Technol.*, vol. 17, no. 4, pp. 355–365, 2001.
[7] J. Wilden, J. P. Bergmann, and H. Frank, “Plasma Transferred Arc Welding—Modeling and Experimental Optimization,” *J. Therm. Spray Technol.*, vol. 15, no. 4, pp. 779–784, 2006.
[8] F. Martina, M. J. Roy, B. A. Szost, S. Terzi, P. A. Colegrove, S. W. Williams, P. J. Withers, J. Meyer, and M. Hofmann, “Residual stress of as-deposited and rolled wire+arc additive manufacturing Ti–6Al–4V components,” *Mater. Sci. Technol.*, vol. 0836, no. March, p. 160224043911007, 2016.
[9] L. L. Parimi, R. G. A., D. Clark, and M. M. Attallah, “Microstructural and texture development in direct laser fabricated IN718,” *Mater. Charact.*, vol. 89, pp. 102–111, 2014.
[10] W. P. J. Hughes D J, Bruno G, Pirling T, “First impressions of salsa: The new engineering instrument at ill,” *Neutron News*, vol. 17, no. 3, pp. 28–32, 2006.
[11] N. Poondla, T. S. Srivatsan, A. Patnaik, and M. Petraroli, “A study of the microstructure and hardness of two titanium alloys: Commercially pure and Ti-6Al-4V,” *J. Alloys Compd.*, vol. 486, no. 1–2, pp. 162–167, 2009.
[12] A. Addison, J. Ding, F. Martina, H. Lockett, and S. Williams, “Manufacture of Complex Titanium Parts using Wire + Arc Additive Manufacture 2 . As Deposited Mechanical Properties,” *Titan. Eur. 2015*, 2015.

[1] WMG, University of Warwick, Coventry, CV4 7AL, UK

J. STOCKINGER[1], C. WIEDNIG[1], N. ENZINGER[1], C. SOMMITSCH[1],
D. HUBER[2], M. STOCKINGER[2]

ADDITIVE MANUFACTURING VIA COLD METAL TRANSFER

Abstract

The goal of this study was to find suitable welding parameters for a quick and economic repair of forging tools. Therefore geometries made of hot working tool steel were generated using wire based Cold Metal Transfer (CMT) procedure. Welding and geometric parameters were varied and their influence on the mechanical characteristics of the welded structure was investigated.

The microstructure of the manufactured geometries was examined by light optical microscopy (LOM). The mechanical properties were determined by hardness testing and tensile testing.

The automated process combines low heat input and a precise metal deposition with low dilution. This promises a near net shape manufacturing with reduced subsequent machining time, which reduces total costs of the produced or repaired part.

Keywords

Cold Metal Transfer; Wire Arc Additive Manufacturing; X40CrMoV5; Large Part Additive Manufacturing;

Introduction

In addition to the classic cladding process, additive manufacturing (AM) methods are developed for additive manufacturing of medium and large size components with limited requirements on accuracy and surface quality due to subsequent subtractive finishing. In cooperation with *BÖHLER Schmiedetechnik GmbH & Co KG*, a study was carried out to investigate the possibility to complement the current manual repair processes of the big forging tools with an automated process. The scope was to investigate the feasibility of the CMT - process of *Fronius International GmbH* to repair outworn tools in terms of geometry, mechanical and metallurgical properties.

1. Literature

Due to the size of the tools, the process of repair, the nature of the material and the associated preheating temperature, direct energy deposition (DED) methods are favourable. DED describes processes which channel energy generated by laser, electron beam, plasma or arc into a narrow region, which heat a filler on the substrate that is deposited into the melt pool. The substrate gets melted at the moment it gets deposited [1].

[1] Graz University of Technology, Institute of Materials Science and Welding, AT
[2] Böhler Schmiedetechnik GmbH & Co KG, AT

DED processes can utilize metal and non-metal in wire and powder form, both with advantages and drawbacks [1].

DED with metal, direct metal deposition (DMD), using wire or powder enables the production of near net shape geometries. Forging tools are post-processed by CNC machining to achieve required manufacturing tolerances [2][3].

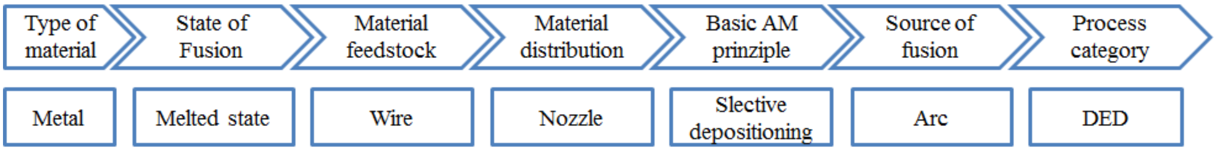

Fig. 1 Classification of process according to [4]

1.1 Additive Manufacturing with Wire & Arc

Powder feed AM processes are leading technologies performing complex geometries and surface qualities [5]. For industrial purposes wire feed processes has received considerable attention [6], [7]. They are an accumulation of the simplicity and robustness of approved processes with the opportunities of modern technologies like laser, electron beam, robotics or digital power supplies. Wire based cladding processes have deposition rates up to 100% [1]. The constant dimension and feed of the wire enlarge the reproducibility of performed welds [8]. Due to the small surface area of wire compared to powder, reaction with the atmosphere is low. Furthermore wire is much easier and safer to handle than powder. Handling powder should be dealt with care regarding dehumidification, dust generation, fire and explosions [3], [9]. High application rates make wire methods environmental and user-friendly. Powder techniques have a limited number of processable materials and alloys, whereas wire based processes can count a huge number of qualified filler materials for welding applications, which in research can be even increased using flux-cored wires [10], [11]

1.2 Cold Metal Transfer (CMT)

CMT was chosen as promising arc based additive manufacturing method [12]–[14], predestined through its low heat input and dilution characteristics [12].

The lower heat input and dilution ensures continuous deposition and to prevent already deposited material from “burn through” [12].

In the CMT-standard procedure the welding wire is moved toward the base material until the short circuit occurs. After the adjusted current flow, the digital controlled power supply interrupts the energy flow and starts the retraction of the welding wire [15]. In addition to the pinch effect as main responsible factor, the retraction of the wire and the mass inertia leads to a droplet detachment at lower current levels compared to standard GMAW methods [13]. The dip-transfer at lower energy level is responsible for the spatter reduction, the lower welding temperature and lower dilution with the base material and the preceding layers [12], [16].

The described CMT-standard process can be expanded by combining CMT with pulse welding cycles (CMT-pulse) for higher welding energy, or by negative electrode polarity

[1] Graz University of Technology, Institute of Materials Science and Welding, AT
[2] Böhler Schmiedetechnik GmbH & Co KG, AT

alternating with positive polarity pulsing phases(CMT-advanced) for higher deposition rates [15].

1.3 Materials

The used base material (BM) is the hot work tool steel EN/DIN X40CrMoV5-1 (1.2344) or Böhler specific W302. This steel has excellent high hot wear resistance, hot tensile properties, adequate toughness and heat checking resistance [17]. The plate size for the experiments was approximate 120x300mm with a thickness of 20mm.

The used filler material (UTP A 73 G 3) is particularly suitable because of its high strength, toughness and heat resistance at increased temperatures. It is used for wearing layers in forging tools and hot work dies [18]. According to the data sheet, the converted hardness of the weld material is 412-459 HV10 [18]. Based on DIN EN180 18265 (2004-02) the hardness equates a tensile strength of 1327 N/mm² to 1481 N/mm².

Table 1 : Nominal composition of used materials (wt%)

	C	Si	Mn	Cr	Mo	V	Ti
Base	0,39	1,1	0,4	5,2	1,4	0,95	-
Wire	0,25	0,5	0,7	5,0	4,0	-	0,6

2 Experiments

All welds were performed with the CMT- standard process using the welding source TPS4000-CMT. CORGON 12s2 was used as active shielding gas. According to [18] the welding torch was positioned in neutral position. For all experiments, the base material was preheated to at least 400°C [17]. The preheating required an electric heating in combination with a temperature measurements of the base plate and the generated geometry. To observe the temperature of both, several thermocouples (TC) type K were used. TC were placed on the base plate and after every third manufactured layer. With this setup the temperature during welding was measured.

The automation of multi-layer weld operations with CMT, in contrast to AM processes with defined layer thicknesses (e.q. powerdebed), requires a knowledge of the expected layer dimensions. With the first tests, height and width for different parameter sets (Table 2) in multiple geometric configurations (Table 3), were determined.

The layer build-up shown in Fig. 2 were separated in single-track - multilayer (e.g. 1x10) and multi-track - multilayer (e.g. 4x10) welds. The single-track test were examined to determine the parameters that yield the maximum total height of the compound layers. For mechanical testing and practical relevance multilayer welds were generated.

[1] Graz University of Technology, Institute of Materials Science and Welding, AT
[2] Böhler Schmiedetechnik GmbH & Co KG, AT

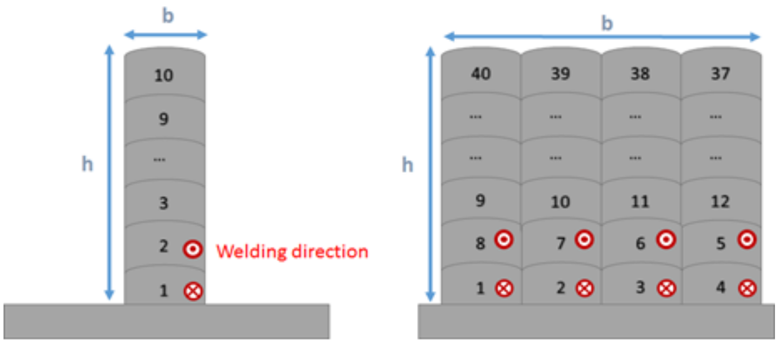

welding direction (alternating each layer)
h total height (mm)
b total width (mm)

Fig. 2 Geometries 1x10 (left) and 4x10(right) with weld direction

In order to reduce the number of influencing parameters and establish a comparison, all tests were performed with a constant welding speed of 10 mm/s. To mitigate the effects of acceleration and deceleration the layers were welded with alternating directions. To avoid overheating of the BM and to prevent deposited material from excessively melt, the cool-down time between the layers was 60s. There was no cooling time between welds within a layer.

The chosen sets of parameters covers the power range of the available digital inverter power source. The wire feed was adopted from inverter settings.

Table 2: Welding parameter sets

Welding set	Current (A)	Voltage (V)	Wire feed (m/min)	Heat input (kJ/cm)	Theoretical deposition (mm^3/s)	(kg/h)
A	100	11.2	2.2	1.1	41.47	1.16
B	160	13.6	4.8	2.1	90.48	2.53
C	223	14.7	7.2	3.2	133.83	3.75
D	250	20.0	8.3	5.0	156.45	4.38

All generated samples were stress relief heat treated with maximal temperature of 550°C, a holding time of 5h and subsequent cooling with 50°C/h. The heat treatment was performed according to Böhler specifications.

Table 3: Configurations of generated welds

	Single-track (set-tracks x layers)	Multi-track (set-tracks x layers)
(a)	A-1x10	A-3x10
(b)	B-1x10	B-4x35
(c)	C-1x10	C-3x35
(d)	D-1x10	

Two DIN 50125 – B6x30 tensile specimen were generated of each of the two regular multi-track probes (B, C). All specimen were oriented in h-direction. The tests were performed at room temperature.

3 Results

[1] Graz University of Technology, Institute of Materials Science and Welding, AT
[2] Böhler Schmiedetechnik GmbH & Co KG, AT

Four singletrack welds with 10 layers were generated (Fig. 3), each with different welding parameters (Table 3). As represented in Fig. 4 the achieved height and width are increasing to the maximum at set C. With set D the growth of the width rises in combination with a decreasing height. With the performed LOM investigation no lack of fusion could be determined.

[1] Graz University of Technology, Institute of Materials Science and Welding, AT
[2] Böhler Schmiedetechnik GmbH & Co KG, AT

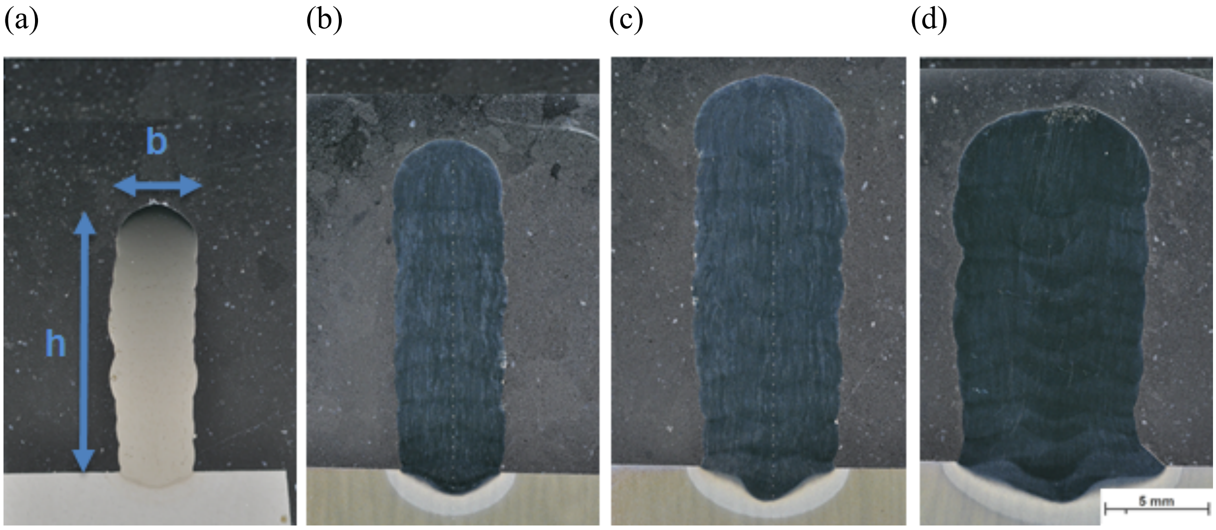

Fig. 3 Macrostructure of single track welds

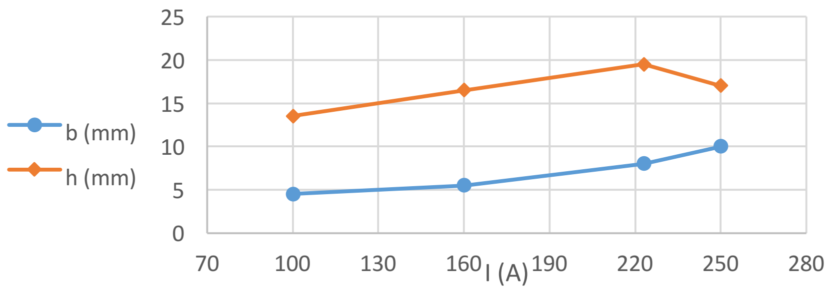

Fig. 4 Geometries of single track welds; Height (h), Width (b)

Three multi-track welds (Fig. 5) were generated. For set A (100A) no comparable declaration of the dimensions could be made (Fig. 5(a)). Tracks got either no connection to the previous track or no connection to the previous layer. With parameter set B (160A) a sample with 73mm height and 15 mm width was established (Fig. 5(b)). With parameter set C (223A) a sample with 93 mm height and 15 mm width was established (Fig. 5(c)), but one track less was needed to obtain the same width as with set B.

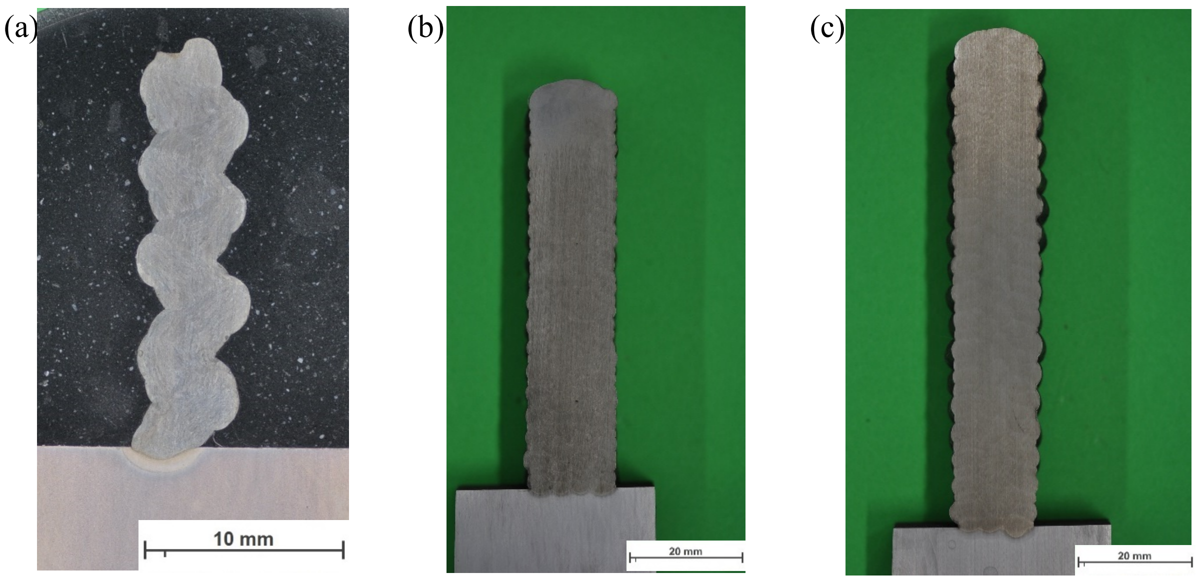

Fig. 5 Macrostructure of multitrack welds

[1] Graz University of Technology, Institute of Materials Science and Welding, AT
[2] Böhler Schmiedetechnik GmbH & Co KG, AT

The outer contours established with set B (Fig. 5(b)) was finer than with set C (Fig. 5(c)). Lack of fusion was found in all multitrack welds, but pronounced with parameter set B. More defects were found at lower layers of the welds. The amount and size of pores in the base material and in the welded geometries were compared.

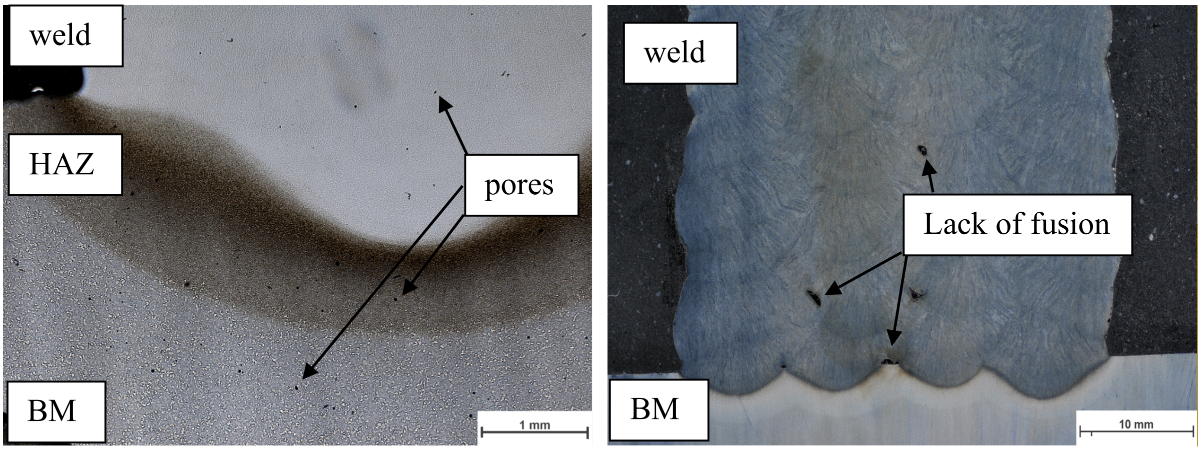

Fig. 6 Pores in weld and BM (left), lack of fusion BM - weld, weld - weld (right)

The hardness (HV1) measurements were taken using an automated test equipment with multiple testing points per test.

Table 4: Average hardness and standard deviation of welds

	Single-track		Multi-track	
	Hardness (HV1)	Deviation (HV1)	Hardness (HV1)	Deviation (HV1)
Set B/160A	517	56	542	24
Set C/223A	516	39	532	37

The tensile test result for the B - parameter (160A) specimen showed an average R_m of 1441 MPa and an elongation at rupture of 1.7 %. The C – parameter (223A) specimen achieves R_m of 1591 MPa with an elongation at rupture of 13 %. While reduction in area contraction was evident at C – samples, attended with a higher elongation after fracture, there was no visible contraction at B – samples. All cracked surfaces indicated brittle fracture.

4 Discussion

As shown in Fig. 4, the total height increases with heat input and wire feed at singletrack welds. The maximum growth was gained with set C (223A). Despite the higher material feed the total height decreases due to excessive heat input and width growth when using higher current.

With the lowest current parameter set A (100A), it was not possible to produce a multitrack multilayer weld. Multiple attempts generated structures where the preceding layer or aside track are not joined. Fig. 5(a) shows a profile where the aside tracks but not the preceding layer could be connected, leading to a step shaped build-up. This occurs with small track off-set. Enlarging the distance between the tracks resulted in separate structures.

[1] Graz University of Technology, Institute of Materials Science and Welding, AT
[2] Böhler Schmiedetechnik GmbH & Co KG, AT

The amount and size of the pores in the welds of remaining sets, are comparable to those in the base material.

Lower temperatures at the beginning of the experiment (close to substrate) could be responsible for the higher number of lack of fusion in lower layers. Furthermore the number of defects is decreasing with a higher welding current and therefore higher temperatures. The cooling time between each layer is necessary to prevent the BM from overheating and to ensure a temperature of the previous layer where its melt is minimal.

The hardness of the weld material is higher than specified, especially at multitrack welds regardless of the parametric set.

The tensile strength of all specimen was higher than the calculated minimum, the C – probes reached higher values than the B – probes.

5 Conclusions

- Parameters for additive purposes have been determined.
- Layer geometries for different parameter sets were ascertained.
- For all welds with same configuration reproducible results were achieved.
- Single-track welds with low energy were proven to be possible. For gaining multitrack welds a minimal energy input is needed to ensure fusion of the tracks among each other.
- Porosity found in the weld is equal to that of the base material.
- Lack of fusion is predominant in probes. By removing the oxide film after every track and optimizing the distance between the tracks better results are expected.
- Higher deposition rates could be achieved by reducing the height gain per track.
- Hardness of multi-track probes is higher than singletrack probes.
- The tensile strength of all samples, even extracted in build-up direction (h – direction), achieved adequate values.

6 Outlook

- A closed rectangular contour will be manufactured with multiple tracks and layers to analyse the process behaviour during direction changing.
- Tensile and Charpy test will be carried out with varying specimen orientations within the welded probe, to determine the isotropic behaviour of the mechanical properties of the layer by layer manufactured structure.
- Charpy tests will be performed for several temperatures to find out the brittle ductile transition temperature of the filler material.

[1] Graz University of Technology, Institute of Materials Science and Welding, AT
[2] Böhler Schmiedetechnik GmbH & Co KG, AT

[1] I. Gibson, D. Rosen, and B. Stucker, *Additive Manufacturing Technologies*. New York, NY: Springer New York, 2015.
[2] K. P. Karunakaran, S. Suryakumar, V. Pushpa, and S. Akula, "Low cost integration of additive and subtractive processes for hybrid layered manufacturing," *Robot. Comput. Integr. Manuf.*, vol. 26, no. 5, pp. 490–499, 2010.
[3] B. Baufeld, E. Brandl, and O. Van Der Biest, "Wire based additive layer manufacturing: Comparison of microstructure and mechanical properties of Ti-6Al-4V components fabricated by laser-beam deposition and shaped metal deposition," *J. Mater. Process. Technol.*, vol. 211, no. 6, pp. 1146–1158, 2011.
[4] ASTM 52900:2015-12, "Standard Terminology for Additive Manufacturing – General Principles – Terminology," *ASTM Int.*, p. 19.
[5] P. Wanjara, M. Brochu, and M. Jahazi, "Electron beam freeforming of stainless steel using solid wire feed," *Mater. Des.*, vol. 28, no. 8, pp. 2278–2286, 2007.
[6] E. Brandl, B. Baufeld, C. Leyens, and R. Gault, "Additive manufactured Ti-6A1-4V using welding wire: Comparison of laser and arc beam deposition and evaluation with respect to aerospace material specifications," *Phys. Procedia*, vol. 5, no. PART 2, pp. 595–606, 2010.
[7] L. E. Murr, "Metallurgy of additive manufacturing: Examples from electron beam melting," *Addit. Manuf.*, vol. 5, pp. 40–53, 2015.
[8] J. Gockel, J. Beuth, and K. Taminger, "Integrated control of solidification microstructure and melt pool dimensions in electron beam wire feed additive manufacturing of Ti-6Al-4V," *Addit. Manuf.*, vol. 1–4, pp. 119–126, 2014.
[9] E. Brandl, F. Palm, V. Michailov, B. Viehweger, and C. Leyens, "Mechanical properties of additive manufactured titanium (Ti-6Al-4V) blocks deposited by a solid-state laser and wire," *Mater. Des.*, vol. 32, no. 10, pp. 4665–4675, 2011.
[10] "Direkter Metallauftrag durch Laserauftragschweißen mit Draht," *stahl und eisen*, vol. 135, no. 3, p. 1, 2015.
[11] D. S. Nowotny, "Generatives Laser-Draht-Auftragschweißen," *Fraunhofer Inst. für Werkstoff- und Strahltechnik - Jahresbericht 2012*, vol. 1, p. 143, 2012.
[12] P. Gerhard, K. Ferdinand, and C. Harald, "Manufacturing of turbine blades by shape giving CMT Welding," in *Metal Additive Manufacturing Conference*, 2014, p. 10.
[13] P. Almeida and S. Williams, "Innovative process model of Ti–6Al–4V additive layer manufacturing using cold metal transfer (CMT)," in *Proccedings of the 21st Annual International Solid Freeform Fabrication Symposium*, 2010, p. 11.
[14] J. Gu, J. Ding, S. W. Williams, H. Gu, J. Bai, Y. Zhai, and P. Ma, "The strengthening effect of inter-layer cold working and post-deposition heat treatment on the additively manufactured Al–6.3Cu alloy," *Mater. Sci. Eng. A*, vol. 651, pp. 18–26, 2016.
[15] J. Bruckner and S. Egerland, *Schweißpraxis aktuell: CMT-Technologie*. WEKA MEDIA GmbH & Co. KG, 2013.
[16] J. Feng, H. Zhang, and P. He, "The CMT short-circuiting metal transfer process and its use in thin aluminium sheets welding," *Mater. Des.*, vol. 30, no. 5, pp. 1850–1852, 2009.
[17] Boehler, "Boehler W302 - Hot work tool steel." BÖHLER Edelstahl GmbH, p. 12, 2011.
[18] Böhler Welding Voestalpine, "UTP A73 G3," vol. 03, no. 0, pp. 382–385, 2014.

[1] Graz University of Technology, Institute of Materials Science and Welding, AT
[2] Böhler Schmiedetechnik GmbH & Co KG, AT

Nutal Nicolas. [1], Collette Jean-Paul. [2], Crahay Jean.[1], Jochem Hélène.[3], Larnicol Maïwenn.[1], Magnien Julien.[4], Masse Christian.[3], Rigo Olivier.[4], Vanhumbeeck Jean-François.[1] and Pambaguian Laurent[5].

SURFACE PROCESSING FOR METAL PARTS MADE BY ADDITIVE MANUFACTURING

Abstract

In the frame of ESA's General Support Technology Programme (GSTP 6 E. 1 Clean Space Initiative), focus was set on the surface processing of metal parts made by additive manufacturing (AM). Recently, AM raised a significant interest. Indeed, lightweight and complex shapes can be designed and manufactured with customizable material compositions, which are of prime importance for space and industry applications. However, as AM technologies lead to quite rough surface finish, a better understanding of the impact of surface characteristics on the material behaviour is needed to expand the use of AM for high performance parts. This study aims at proposing and testing various surface finishing techniques for metal (Ti6Al4V) parts made by AM, in order to check their compatibility, evaluate their properties and derive guidelines for future applications.

This paper is devoted to the first steps of surface preparation, namely material removal. Focus is set on chemical mechanical methods (tribofinishing), chemical and electrochemical methods. The selected methods were tested on prototype parts to check their capabilities. Surface parameters were analyzed like achieved roughness, loose particles, material removal rate, etc., as well as limitations in terms of geometry, homogeneity and applicability.

Keywords

Surface finishing, additive manufacturing, tribofinishing, chemical polishing, electro-chemical polishing, roughness, loose particles.

1. Introduction

Through the Clean Space Initiative [1], ESA showed its interest on manufacturing techniques having low environmental impact. Within this framework, AM offers significant reduction of waste material compared to classical subtractive manufacturing. Besides, the flexibility of the AM process allows the introduction of more efficient manufacturing practices, by reducing the production and inspection steps and thus simplifying the production chain. Finally, the dramatic decrease in the amount of raw materials combined with the design optimisation and possible reduction of life-cycle steps, enables energy consumption decreasing and CO_2 footprint reduction.

Nowadays, AM technologies applied on metals are able to produce functional, complex and optimized parts, which make them attractive for the industry. The achievable

[1] CRM Group, Liège, Belgium
[2] Walopt, Liège Belgium
[3] Thales Alenia Space, Toulouse, France
[4] Sirris, Liège, Belgium
[5] ESA-ESTEC, Noordwijk, The Netherlands

geometrical complexity allows developing more efficient parts (lighter, with internal cavities or channels…). Today, the most relevant metallic materials for AM application are titanium (Ti6Al4V) and aluminium alloys (A357, A356) [2].

A key issue of AM is the high surface roughness, up to 20 microns Ra, and limited size accuracy of the produced parts. Moreover, the AM process leads to non-melted powders sticking to the surface that are prone to be leached latter in the process, which is an important issue for industrial processes. Besides, the surface texture of the different faces of the parts varies according to their orientations, in the hollow bodies and the structures. It is known that such a finish is likely to impact the performance of the parts. These issues could be overcome by a combination of, on the one hand, optimization of raw material, AM facilities and processing parameters, and, on the other hand, by an appropriate selection of post-treatment steps for surface improvement, for instance abrasion, etching or deposition processes.

Previous results showed the interest of the chemical mechanical methods (tribofinishing) to reach low roughness but with several drawbacks (angle rounding, poor accessibility and poor dimensional accuracy) [3]. Chemical and electrochemical methods are now under evaluation. The selected methods were tested on prototype Ti6Al4V SLM and EBM parts to check their capabilities. Surface parameters were analyzed like achieved roughness, material removal rate, etc., as well as limitations in terms of geometry and applicability.

2. Additive manufacturing process parameters and samples

250HL SLM machine from SLM Solutions was used to process titanium (SLMT samples). EBMT titanium samples were processed using A2 EBM machine from ARCAM. Powder layer thickness was 30 microns for SLM and 50 microns for EBM. The laser power was 350W. Concerning EBM, the maximum power was 4000W.

Titanium powders for SLM were acquired from TLS and from ARCAM for EBM. The powders are spherical and within expected size range.

As depicted on the top of Fig.1, the samples treated in this study were designed so as to integrate various types of structures that can be met in AM parts:

- Surfaces parallel/perpendicular to the support plate;
- Tilted surfaces (45°);
- Lattice, with different sizes;
- Heat ducts;
- Round surface;
- Hollow structure.

The sample dimensions are 35*15*30 mm.

The as-produced parts are illustrated on the bottom of Fig.1. On the first sight, the samples produced by EBM are rougher than those produced by SLM.

Fig.1: Proposed design (left), part produced in titanium by SLM (centre) and titanium by EBM (right).

Moreover, due to the process itself, EBMT samples have non-fully sintered powder, hard to remove, trapped inside the part ("the cake"). This is an issue for potential applications.

3. Characterization methods

2-D roughness measurements were performed using Mitutoyo SJ210 system. The roughness was measured in the vertical direction regarding to the support. Ten measurements were realized each time to have an average value.

The weight of the samples was measured using Mettler Toledo XS205 DU weighing equipment. The weight loss was estimated as the sum of the weight loss after three successive 15 min ultrasonic cleaning in ethanol.

The removal rate was determined as the weight difference before and after the processing, taking into account the treated surface.

The samples underwent surface observation using electron microscope (JEOL 7001).

4. Surface treatment methods

Tribofinishing (TF) FBA 24 turbo system from Rösler, shown on the left on the Fig.2, was used to perform the surface treatment of the samples (named -T). This is a mechanical-chemical polishing process using "chips" to abrade the samples. Ceramic RXX 10/15S chips were selected to treat the titanium samples. During the process, the "chips" were automatically cleaned by a mix of a soap and water.

Fig.2: Rösler FBA 24 turbo tribofinishing system (left) and electropolishing cell.

The treatments were performed at maximum frequency up to 25 hours for titanium. After treatment, the parts were cleaned in an ultrasonic bath filled with ethanol to remove dust and cleaning water.

The chemical polishing (CP) was performed using HF/HNO3/H2O solution (1/1/2). The samples, named –CP, were immersed in the solution with thorough mixing up to 2 min. Then, the samples are cleaned in ethanol and rinsed with deionized water.

The laboratory set-up illustrated on the right part of the Fig.2 was used to perform the electropolishing (ECP) on the samples (named –ECP). It is constituted of a cylindrical counter electrode, a cooling system and a specimen handling jig. Commercial solution from poligrat was used as chemical polishing electrolyte. The tension used for the tests ranged from 5 up to 30V.

5. Reference samples

The surface of the as-produced Ti AM parts was characterised. Weight loss measurements were performed to determine the amount of loose particles resulting from AM processing. Besides, the roughness of the samples was characterized after ultrasound cleaning. The results of these measurements are shown in Table 1.

Table 1: Roughness properties, loose particles and removal rate of the selected samples.

Sample ID	Ra (µm)	Rz (µm)	Rsk (µm)	Loose particles (g)	Removal rate (g/(cm².min))
SLMT Ref	10.5+/-0.4	56.9+/-2.3	0.06+/-0.26	0.014	/
EBMT Ref	24.7+/-2.2	121.1+/-11.9	-0.30+/-0.09	0.023	/
SLMT-T	0.3+/-0.1	1.1+/-0.2	/	0.006	0.002
EBMT-T	2.9+/-0.8	25.9+/-5.8	-1.84+/-0.7	0.030	0.005
SLMT-CP	7.1+/-0.4	33.7+/-1.6	0.29+/-0.14	0.007	0.544
EBMT-CP	16.4+/-1.1	84.2+/-2.3	-0.30+/-0.15	0.029	0.29
SLMT-ECP	4.1+/-0.2	23.9+/-2.0	/	0.018	0.022
EBMT-ECP	11.9+/-1.2	63.9+/-3.8	/	0.025	0.056

As can be seen, the reference samples undergo weight losses due to loose particles. These particles are incompletely melted during the AM process and are therefore weakly adherent. The EBM processed samples undergo almost twice weight loss compared to SLM samples.

Roughness of the parts depends on the process too. EBMT parts are rougher than SLMT titanium parts. The SEM surface analysis of the samples is shown on Fig.3.

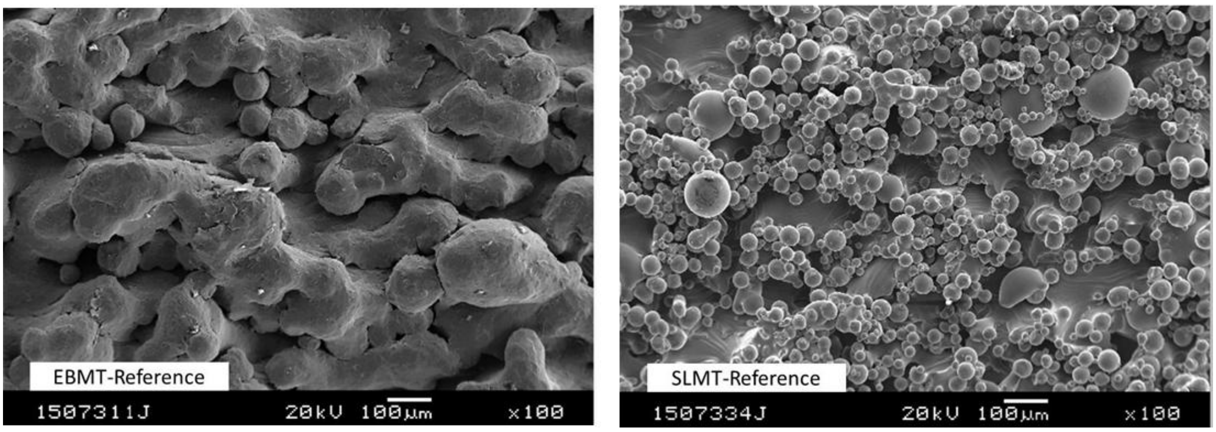

Fig.3: SEM pictures showing the surface structure of the as-produced samples.

The surface morphologies of the two samples are very different. These pictures confirm that the titanium powders used for the SLM are smaller than those used for the EBM. The microstructure of the SLMT reference sample indicates that the smallest titanium beads do not seem to be bonded tightly to the surface.

6. Effect of the tribo-finishing on the surface properties

The samples processed with the TF system were analysed. After 25 hours treatment, this equipment allows reaching roughness below 1µm Ra for the SLMT samples and around 3µm Ra for EBMT samples. The Rz of the SLMT samples is very low. That indicates that the dense area of the SLM part was reached, which is not the case for the EBMT samples that shows high Rz value. Due to the removal of the peaks of the surface of the samples EBMT, the Rsk value of the samples decreases. This is confirmed by the SEM analyses of the samples shown here below:

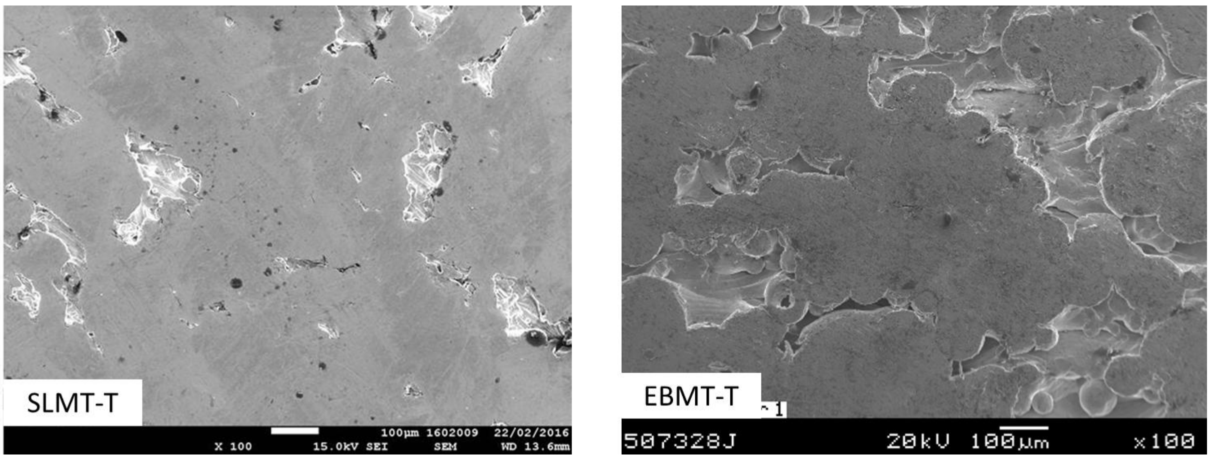

Fig.4: SEM pictures of the SLMT-T and EBMT-T samples.

The levelling effect of the TF is demonstrated on those two pictures. It can be seen that some original powder remains within the porosities after 25 hours treatment for the EBMT-T sample. However, after such a treatment, a rather dense structure is obtained.

The TF allows removing some loose particles due to the vibratory effect. As a consequence, the weight loss after cleaning decreases. Nevertheless, this effect is limited to the areas accessible by the abrading chips. Therefore, the inner areas of the part are not cleaned. As a consequence some non-fully sintered loose particle remains.

In both cases, the removal rate is very low, below 0.01 g/(cm².min). This removal rate is more important at the beginning of the process due to low adherence particles. It decreases as the dense area of the part is reached.

Concerning the homogeneity of the process it can be stated that TF abrasion is more important on the edge of the parts. Besides, TF had almost no effect on heat ducts or tilted areas as the size of the chips used to abrade the structure are larger than the free space.

7. Effect of the chemical polishing on the surface properties

The CP performed on the samples allows decreasing the Ra roughness from 10.5 down to 7.1µm for SLMT-CP samples and from 24.7 down to 16.4µm for EBMT-CP samples. A decrease is also observed for the Rz values. On the contrary, the Rsk value of the SLMT-CP sample increases, compared to the reference whilst it remains constant for the EBMT-CP sample. These measurements indicate that the CP removes matter and particles on the surface of the part, both on the peaks and the valleys. As a consequence, the Ra value decrease, as well as Rz values but the Rsk values do not vary significantly due to this "homogeneous" removal. This phenomenon is observed for the SLMT-CP sample, shown on the Fig.5

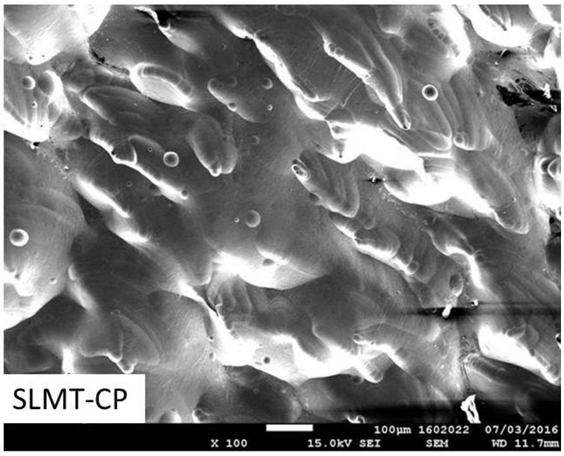

Fig.5: SEM pictures of the SLMT-CP sample.

This picture illustrates the effect of the chemical polishing. Indeed, the material removal being "homogeneous" on the part, the achieved roughness, starting from the as-built state, is quite high. Besides, the chemical polishing allows reaching the dense area of the part, as illustrated on this picture.

The loose particles are removed using the CP. Indeed, the weight loss observed on the Table 1 almost comes only from the first cleaning. Indeed, after two cleaning the weight loss is almost zero, for the SLMT-CP sample. This is the main advantage of this technique. Indeed, the loose particles, showing important specific surface, are preferentially treated by the solution. Such an effect is also observed for the cake observed on the EBMT-CP samples.

The removal rate ranges from ~0.3 (EBMT-CP sample) up to ~0.5 (SLMT-CP sample) g/(cm².min). This removal rate is important and is kept almost constant till the concentration of the solution is modified. However, the reactivity can decrease as the high specific surfaces are treated.

The homogeneity of the CP process is quite poor. Indeed areas with high overall specific surface, i.e. lattices structure, are more affected than flat areas due to overheating. Besides, if the solution is not circulated, local overheating can appear which will increase the reactivity of the solution and therefore increase the removal rate. Finally, the “cake” inside EBMT parts may induce also overheating as it is constituted by aggregated particles.

8. Effect of the electro-chemical polishing on the surface properties

ECP allows reducing significantly the roughness of the samples, down to 4.1µm and 11.9µm for SLMT-ECP and SBMT-ECP samples respectively. This modification is accompanied with a significant decrease of the Rz values. These measurements confirm the capacities of the method to smooth the surface.

This phenomenon is observed for the SLMT-ECP sample, shown on the Fig.6.

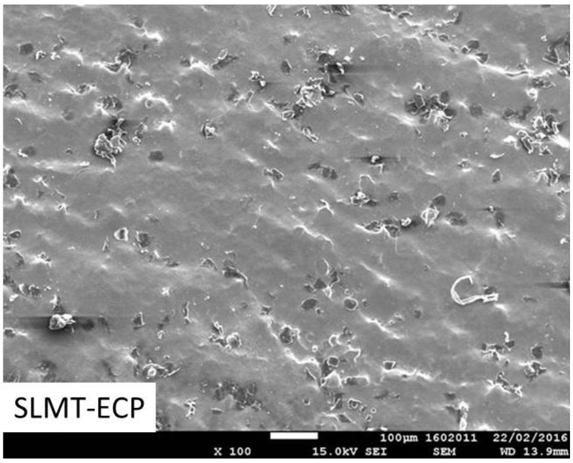

Fig.6: SEM pictures of the SLMT-CP sample.

As can be seen, the ECP allows reducing the roughness. The material removal is fairly located at the peaks of the surface that concentrate the current. As a consequence, the roughness decrease is more important than for chemical polishing. Here too, the dense area of the part is reached for the SLMT-ECP sample.

Some loose particles are removed from the part using the ECP. However, the loose particle removal is limited to areas facing the counter-electrode. Inner areas and lattices are not easily cleaned. The “cake” is therefore not treated. As a consequence, the amount of loose particles is not significantly modified.

The removal rate ranges from ~0.02 (SLMT-ECP sample) up to ~0.06 (EBMT-ECP sample) g/(cm².min). This removal rate is significant compared to samples processed by TF but lower than those reached for the chemical polishing. Here, the removal rate is influenced by the concentration of the electrolyte in the solution, which decreases as the treatment proceeds.

The homogeneity of the CP process is quite good for areas facing the counter-electrode. However, peaks are smoothened. On the contrary, surfaces that do not face the counted-electrode are not treated. Even if smaller counter-electrode could be imagined to polish inner areas, the treatment of lattices seems very hard.

9. Evaluation of the methods

From the previous observation and tests, different remarks can be drawn about the potentialities and drawbacks of the selected methods, regarding the main AM issues.

9.1. Loose particles removal

Loose particles are a key issue of the AM process. In the industry it can lead to defects in the product or be the cause of process damage. Therefore, it is important to assess if the methods could help loose particles removal:

- The TF leads to loose particle removal due to the vibration and abrasion. However, particles entrapped in hollow or complex structures are not influenced by the TF as the chips are too large to access these areas. As a consequence some non-fully sintered loose particle remains.
- CP allows loose particles and “cake” removal. Indeed, due to the principle of this method, the loose particles, showing important specific surface, are preferentially treated by the solution. The effect is observed on flat or round surfaces, as well as on inner areas or lattices.
- Loose particle removal is observed for the samples treated using the ECP. However this effect is limited to areas facing the counter-electrode. Therefore, the amount of loose particles is not significantly modified after the processing.

9.2. Surface roughness

Surface roughness has to be decreased. Indeed, roughness acts as a trap for dust which can contaminate industrial processes and products. Besides, the mechanical properties of the parts, especially the fatigue properties, are influenced by the surface finish. Here is a summary of the selected methods potentialities and drawback:

- Using TF, roughness down to a few µm Ra can be achieved on accessible surfaces, preferentially flat, or edges and corners. However, acute angles, lattice, hollow structures are not properly treated.
- CP leads to a kind of homogeneous matter removal on both peaks and valleys. This homogeneous treatment has therefore a limited effect on the roughness parameters. Besides, it is expected that due to local over reaction, different roughness could be reached on different areas of the part, depending on the local environment.
- Acceptable roughness is reached using the ECP process. Here too, the effect is limited to areas facing the counter-electrode.

9.3. Removal rate and process homogeneity

Material removal rate and process homogeneity are essential parameters to be taken into account for the evaluation of the methods. Indeed, removal rate will influence the price of the part processing and process homogeneity will drive the possible applications of the part. Here is a summary of the selected methods potentialities and drawback:

- TF reduces roughness of flat surfaces but rounds the edges and corners. This rounding could be taken into account with proper design considering homogeneous angle rounding thanks to parts rotation. Nevertheless, the limited accessibility of the TF confines the methods to parts with limited complexity. This method has very low removal rate which could impede its use.
- The CP removal rate is very important. Parts are treated in a few minutes. However, the homogeneity of the CP process is quite poor. Local overheating, due to limited solution circulation or local high overall specific surface, leads to increased solution reactivity and therefore increased local inhomogeneous removal rate.
- The removal rate of the ECP is medium. The ECP treatment is quite homogeneous for the areas facing the counter-electrode even if sharp edges will be rounded a bit.

9. Conclusions

This paper proposed an approach to the surface treatment of parts produced by AM using tribofinishing, chemical polishing and electrochemical polishing. The effect of those methods on the surface properties (roughness, loose particles) and volume properties (removal rate) were evaluated. Besides, the limitations in terms of geometry and applicability were discussed. These observations were performed on titanium Ti6Al4V alloys made by SLM and EBM.

The preliminary observations led to the conclusion that used alone, none of the methods could solve roughness and loose particles issue. Besides except chemical polishing, the accessibility of the methods will be an issue for the surface treatment of complex parts with lattices or hollow bodies. On the contrary flat surfaces or high radius curvatures could be treated homogeneously down to a few µm Ra. Another potential issue to solve is the homogeneity of the treatment. Indeed none of the methods could reach homogeneous treatment on each surface in a single step. These issues have to be taken into account during the design of the parts. A potential solution could be to use the complementarities of the selected methods to reach desired properties.

10. Acknowledgements

This work has been founded by the European Space Agency ESA-ESTEC under contract number 4000113253/15/NL/SW. The authors wish to thank their colleagues who have made this work possible.

11. List of abbreviations

Table 2: List of abbreviations.

AM	Additive Manufacturing
EBM	Electron Beam Melting
SLM	Selective Laser Melting

TF	Tribo-Finishing
EP	Electro-Polishing
ECP	Electro-Chemical Polishing
SLMT	Selective Laser Melting of Titanium
EBMT	Electron Beam Melting of Titanium

12. References

1. Barbier, X. Compendium of Potential Activities for 2013 & 2014 GSTP-6 Element 1 (ref TEC-SGT/2013-006/XB). (2013).
2. Flake, J. & Campbell, C. *Manufacturing Technology for Aerospace Structural Materials*. (Elsevier, 2011).
3. Nutal, N. *et al.* Surface engineering for parts made by additive manufacturing. in *IAC 2015* (2015).

L. Wu[1,2], S. Leuders[1], T. Niendorf[2]

The impact of processing parameters for LBM – multi-target optimization for different length scales

Abstract

Laser beam melting (LBM) of metals as a 3D-printing technique allows for a tool-free production of complex tools and components directly from CAD-data. Nevertheless, LBM-processed materials often suffer from process-induced defects, whereby the mechanical properties can be inferior to those of conventionally processed materials. Based on recent investigations of different LBM-processed alloys focusing on powder characteristics, process parameters and post-treatment conditions, it can be revealed that these factors strongly influence the material characteristics at all length scales, i.e. macro-, meso-, micro- and nano-scale. In addition, these influence factors are highly interrelated so that a comprehensive consideration is crucial for both material- and process-developers. In order to address the increasing demand for LBM-produced parts, linked with an increasing number of available LBM-systems and alloys, a time and cost efficient methodology for determination of LBM process parameters needs to be developed. This methodology shall be based on the interactions between material and laser and the repeated post-solidification heat dissipation, which are described by the results of experimental investigations and process simulations.

[1] voestalpine Additive Manufacturing Center GmbH, 40549 Düsseldorf, Germany
[2] University of Kassel, Institut für Werkstofftechnik, 34125 Kassel, Germany

Ralph Mayer[1], Risshu Bergmann[2]

Additive Manufacturing with Maraging Steel

Abstract

The introduction of additive manufacturing with 1.2709 maraging steel enables new potential for highly efficient temperature controls of mould and die insets. This technology is increasingly used for high-performance milling tools.

While conventional manufacturing methods only allow straight drilling, the additive manufacturing method allows greater freedom for the design of the cooling channels. The creation of conformal cooling channels can be realised today by layered laser melting methods. It is also possible to use these methods to build on top of already conventionally manufactured parts, i.e. manufacturing methods can be combined in one part. With these methods, the so-called 'hotspots' in the mould and die insets, which can cause increased cycle times or quality issues, can be eliminated efficiently. The cycle time can be reduced up to 60%.

In relation to milling tools, additive manufacturing can help to optimise the flow of coolant inside the tools. Curved cooling channels reduce coolant pressure loss and can be positioned close to the cutting blades to enable an optimal supply of coolant. In Addition, the design of the clamping slots can be optimized to allow a higher number of blades with the same diameter of the tool. This leads to 50% faster feed speed.

The advances in laser technology, optics, mirror control and software have improved the density and surface roughness of the additively manufactured parts, which makes the additive manufacturing process an interesting prospect for the creation of many industrial metal parts.

[1] LBC Engineering
[2] Renishaw GmbH, Karl Benz Str. 12, 72124 Pliezhausen

David Schäfer[1]

Additive Design & Manufacturing – Products of Tomorrow

Subitem

- Challenges for industrial additive manufacturing
- New applications due to advanced additive design knowledge
- Successful outsourcing with FIT Additive Manufacturing Group

Abstract

Additive Manufacturing (AM) is a disruptive manufacturing technology for complex parts in plastics and metals such as aluminum, titanium, tool steel, stainless steel, and Inconel. Overcoming existing limitations of conventional production techniques, AM objects can have almost any shape or geometry. Additive Manufacturing is used efficiently for single parts as well as volume manufacturing. In order to exploit the full potential of AM, its application as well as specific challenges regarding design and technology require deep understanding. With twenty years of experience in this field, the FIT Group is a world leading specialist for Additive Design and Manufacturing (ADM), with the biggest capacities in Europe. We support you in launching Additive Design and Manufacturing as a major manufacturing technology. In order to leverage the technological and economic benefits. After evaluating your range of products and components to find the most suitable ones for ADM application, we will together develop new or redesigned versions. We will also assist in implementing the manufacturing process while simultaneously developing quality and performance targets and measurement methodologies, with the ultimate aim of a cost effective and reliable manufacturing and Q.C. process.

[1] FIT AG, Eichenbühl 10, 92331 Lupburg, DE

ISTVÁN HATOS, HAJNALKA HARGITAI[1]

ADVANCED CONFORMAL COOLING BY HEAT-CONDUCTING PINS

Abstract

With the development of layer manufacturing technologies injection mould inserts with conformal cooling channels can be manufactured. If the cooling channels can be placed along the geometry, the heat removal is uniform and effective. In tight mould regions, formation of cooling channel is not possible or not efficient. The combination of conformal cooling and heat conductive insert can be an ideal solution for the effective cooling.

Keywords

DMLS, laser sintering, conformal cooling, hybrid mould, heat-conducting copper pins.

1. Introduction

Injection moulding is one of the most important polymer processing technologies. The most significant phase of the injection moulding cycle is the cooling time of the part, which can amount to more than half the whole cycle. One of the best ways to achieve a reduction in cooling time is to use mould inserts with conformal cooling [1-6].

With layer manufacturing technologies, parts with complex internal structures can be built, which can be a major advantages for injection moulds. The cooling channels can have complex form, which cannot be manufactured with conventional methods, such as drilling or milling. Tooling companies are increasingly employing additive manufacturing (AM) technologies to fabricate tools with integrated conformal cooling channels. Selective Laser Sintering (SLS) is one of the AM techniques which able to manufacture 3D parts from powder materials. The powder material is selectively scanned and sintered according to the two-dimensional cross-section of the sliced model of the CAD geometry. At the beginning these systems were limited to work with polymer powders. Direct Metal Laser Sintering (DMLS) and Selective Laser Melting (SLM) are at present the most widespread techniques and both technology use metal powders without coatings [7-10].

In case of injection moulds from steal alloys, the tool with conformal cooling channels can extract more heat than with conventional cooling, but in many cases a tool from good thermal conductive copper based alloy can extract more heat with conventional cooling compared to steel tool with conformal cooling [11].

In some cases formation of conformal cooling channel is not possible for geometric reason, mainly in tight mould regions. These hot spots have high impact on the part quality and cycle time. Tool steels have low heat conductive capacity compared to poor aluminium, copper or silver. Thermal conductivity value for 1.2709 maraging tool steel (generally used for additive tools) is 15-20 [W/mK at 20°C] depending from heat treatment. The combination of conformal cooling channels and fitted heat conductive inserts can serve an ideal cooling solution for tools with tight mould regions [12-13].

[1] Szechenyi Istvan University, Gyor, Hungary – hatos@sze.hu, hargitai@sze.hu

2. Object

In our research work an injection moulding tool insert with conformal cooling channels was designed by modifying that of having conventional cooling system (finger). As reference the model of the original tool was used **(Fig.1.)** and to compare the efficiency of cooling, thermal simulations were carried out. Fitting of the new tool insert to the existing cooling circuit and the linear design of the cooling channels were important aspects of the design.

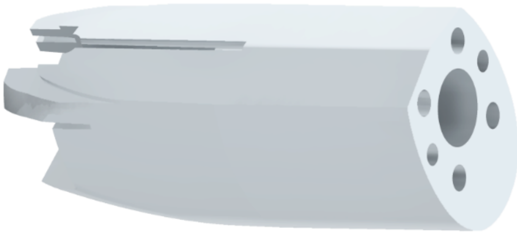

Fig.1. 3D model of the original insert.

3. Simulation

For the injection moulding simulations Autodesk Moldflow (2014) software was used. The parameters used for the simulation derived from the production. The results of the simulation in case of original tool were checked by thermal imaging. The thermographic image of heat distribution confirmed the accuracy of the simulation model. Based on the results of both simulation and thermographic test in terms of cooling the protruding surfaces were identified as the critical areas of the original tool **(Fig. 2.).**

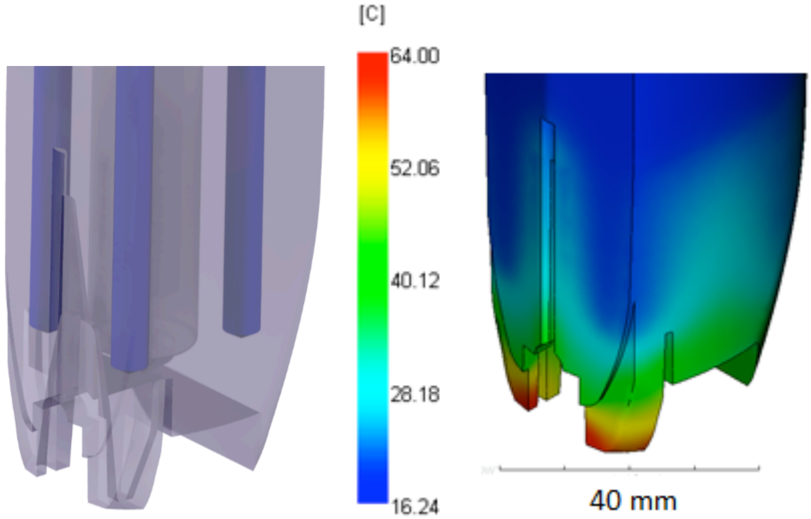

Fig. 2. The 3D modell and the temperature distribution of the original mould.

Using the original model, a version with conformal cooling was designed, fitted to the previous system with Ø4 mm holes. As the minimum allowable distance between the cooling circuit and tool wall, 3 mm was determined. Direct cooling of the protrusions was discarded, even using small (Ø1.5 mm) cooling hole can serve only a partially solution, but this application can cause the clogging of the thin channel. The own designed mould with the conformal cooling channels and the result of the thermal simulation can be seen on **Fig.3**.

[1] Szechenyi Istvan University, Gyor, Hungary – hatos@sze.hu, hargitai@sze.hu

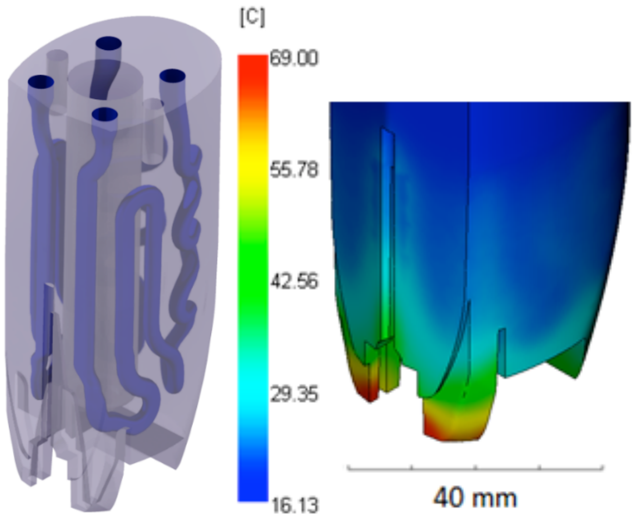

Fig.3. The mould with conformal cooling and the temperature distribution.

Comparing the simulation results of the original and conformal cooling systems it can be concluded, that by following the same initial conditions better cooling efficiency cannot be achieved by conformal cooling.

4. Hybrid tooling

Since we could not achieve a positive result with the conformal cooling itself, a special solution was designed, where the heat from the critical areas by using a good thermally conductive material was lead to the cold parts. Thermal conductivity of tool steels and other metals with high coefficient can be seen in **Table 1**.

Material	Thermal conductivity at 20 °C [W/mK]
MaragingSteel MS1 (age hardened)	20
1.2343	25,3
Copper	398
Silver	418

Table 1. Thermal conductivity of mould steels and high conducting materials [14-16]

Based on the temperature distribution image of the tool insert the formation of conformal cooling is not necessary along the full length of the insert and therefore the tool was divided into a conventional produced part and a built part. From those parts, which cannot cool by the cooling channels, the heat was removed by thermocouples. For this purpose two pieces of Ø2 mm pin and a 2 mm thick sheet were used (**Fig. 4**). In terms of thermal conductivity pure copper or silver inserts are most efficient. The application of pure silver was rejected, because of its softness and thus the low strength the tight fitting of inserts is difficult to implement.

[1] Szechenyi Istvan University, Gyor, Hungary – hatos@sze.hu, hargitai@sze.hu

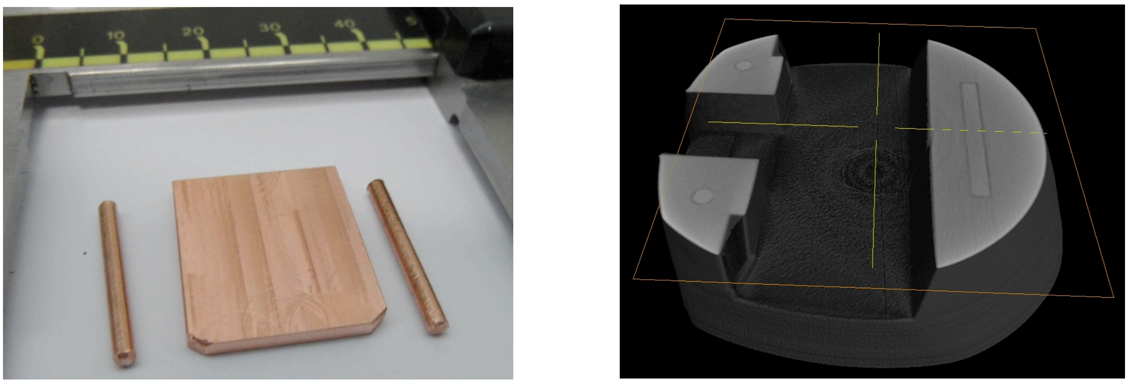

a) b)

Fig. 4. Copper inserts (a) and the computed tomography image of the built tool with the inserts (b).

Thermal distribution of the tool containing copper inserts is shown in **Fig. 5.** It is important to note that in the simulation there was no air gap between the inserts and the mould. To achieve the simulation results in practise a production process solution is needed to apply in that the copper inserts are continuously connected to the wall of the tool and contact with the coolant.

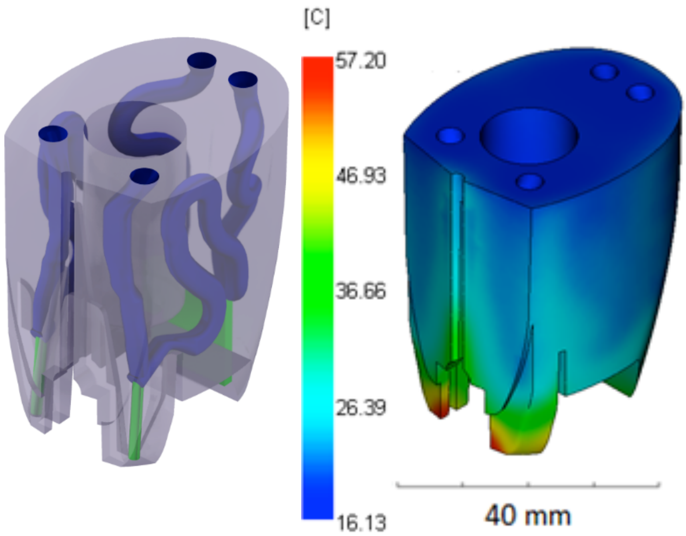

Fig.5. The mould with conformal cooling and the temperature distribution.

The cooling efficiency of the mould with the copper inserts was examined during the complete injection moulding process. It can be seen in **Fig. 6** that by the end of the cooling time (19 s) ~9 °C lower temperature of the critical section could have been achieved with the new design than that of the original cooling system in the same section. Moreover, due to the conformal cooling the temperature distribution of the mould became much smoother.

[1] Szechenyi Istvan University, Gyor, Hungary – hatos@sze.hu, hargitai@sze.hu

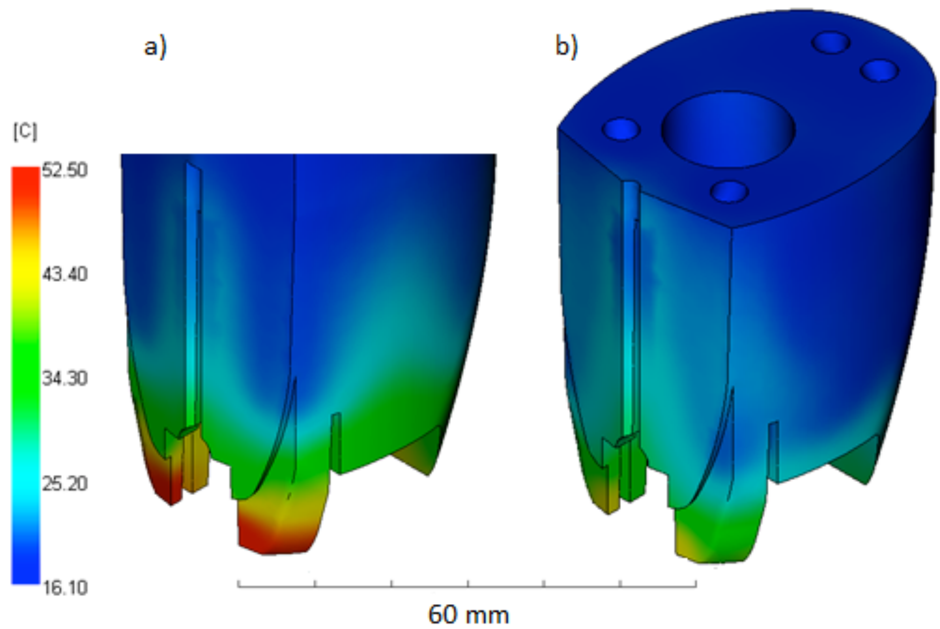

Fig. 6. The temperature distribution of the original (conventionally produced) (a) and the DMLS produced (b) tool inserts (t=19 s).

5. Manufacturing

The production of the tool insert with the new design was carried out by Direct Metal Laser Sintering, which is a multi-step process. As a first step, the tool is printed with the insert height and then stopped the process (**Fig. 7 a**.). Then metal powder is removed from the hole and the insert is placed into that (**Fig. 7 b**). It is important that the top of the insert must be in the same plane with the last layer of the built part (**Fig. 7 c**) and then continue to build (**Fig. 7 d**). To ensure the best filling with the insert, after reversing the tool it can be melted in the hole with a brazing process (**Fig. 7 e**).

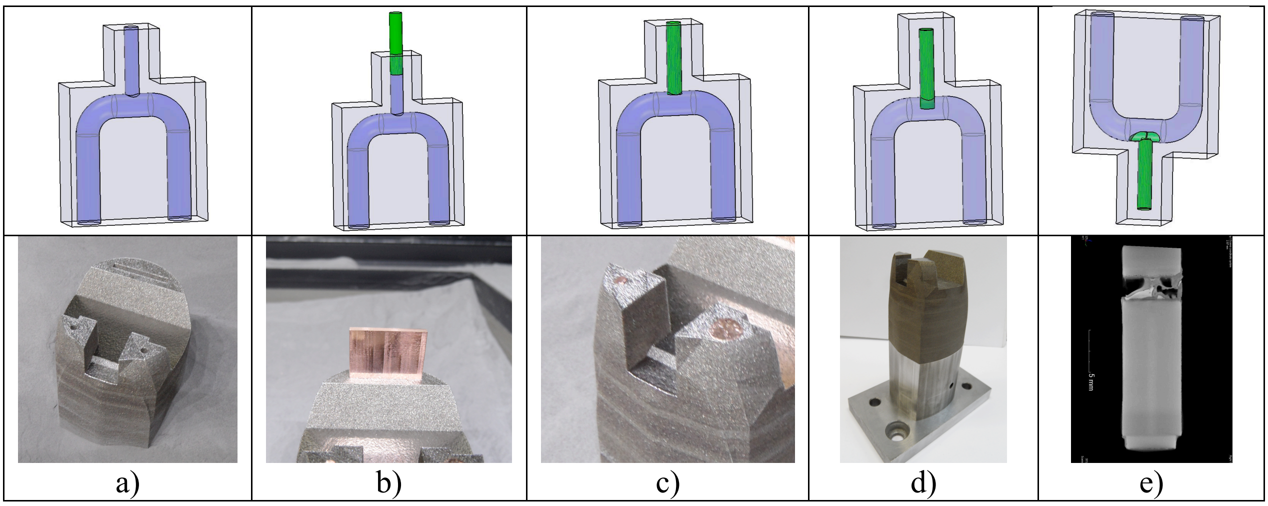

Fig. 7. Manufacturing process (a-d) and a computed tomography image in one section (e).

The connection of the tool and the copper insert were examined by computed tomography and cross sectional optical microscopic images. After the powder deposition the upper part of the copper insert is scanned by laser beam, so interesting to observe the interface

[1] Szechenyi Istvan University, Gyor, Hungary – hatos@sze.hu, hargitai@sze.hu

of the two materials. In our experiments EOS M270 DMLS equipment was used with parameters applied for MS1 type maraging steel sintering. No porosity was detected in the region of steel-copper connection (interface area) by CT investigation **(Fig. 8)** and the same results were found by optical microscopic observation in the cross section **(Fig. 9).** Despite the tight fit air gap remained between the copper insert and the wall of the tool without heat treatment **(Fig.8).**

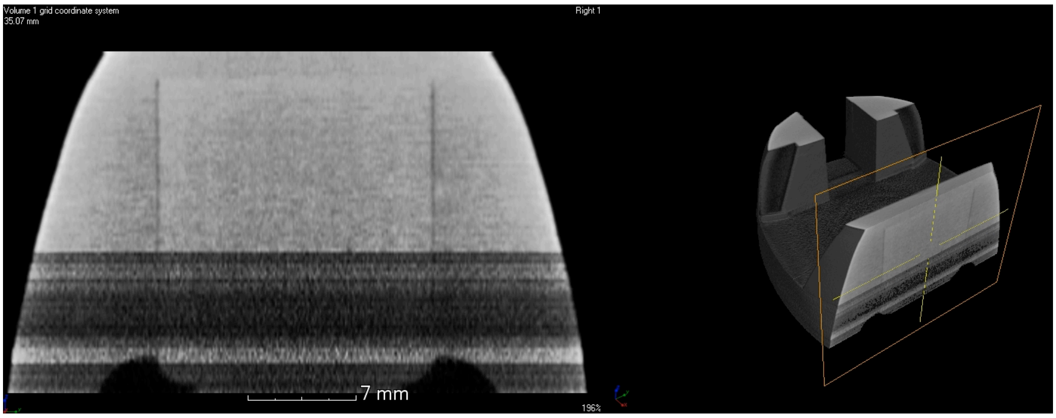

Fig. 8. CT image about the contact.

By heat treatment above the melting point of the copper of the inverted parts the coherent surface air gap decreased. Based on the cross sectional optical micrographs it can be stated that there is a good wetting between the copper and the MS1 sintering steel. The molten copper is filling in the pieces of the surface roughness and micro-cavities formed in a continuous connection between the two metals **(Fig.9).**

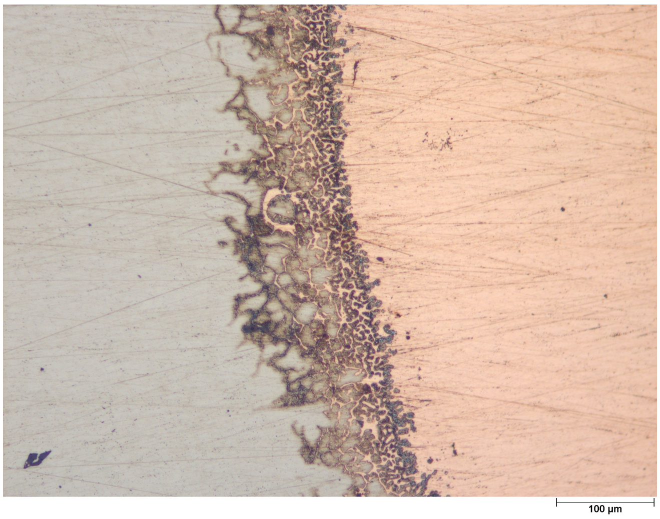

Fig. 9. Contact on the side walls.

References

[1] W. Michaeli, M Schönfeld: Komplexe Formteile kühlen, Kunststoffe, Vol. 08, 2006, p. 37-41
[2] S. Mayer: Optimized mold temperature control procedure using DMLS, EOS Whitepaper
[3] I. Ilyas, C. Taylor, K. Dalgaro, J. Gosden: Design and manufacture of injection mould tool inserts produced using indirect SLS and machining processes, Rapid Prototyping Journal 16 (2010), 429-440

[1] Szechenyi Istvan University, Gyor, Hungary – hatos@sze.hu, hargitai@sze.hu

[4] H. Hassan, N. Regnier, C. Pujos, E. Arquis, G. Defaye: Modeling the effect of cooling system on the shrinkage and temperature of the polymer by injection molding, Applied Thermal Engineering 30 (2010), 1547-1557
[5] A. Agazzi, V. Sobotka, R. LeGoff, Y. Jarny: Optimal cooling design in injection moulding process – A new approach based on morphological surfaces, Applied Thermal Enginnering 52 (2013), 170-178
[6] H. Hassan, Nicolas Regnier, C. Le Bot, G. Defaye: 3D study of cooling system effect on the heat transfer during polymer injection molding, International Journal of Thermal Science 49 (2010), 161-169
[7] E. C. Santos, M. Shiomi, K. Osakada, T. Laoui: Rapid manufacturing of metal components by laser forming, Internal Journal of Machine Tools & Manufacture 46 (2006), 1459-1468
[8] M. Shellabear, O. Nyrhilä: DMLS – Development history and state of the art, LANE 2004 Conference, Erlangen, Germany, Sept. 21-24, 2004
[9] A. J. Pinkerton: Lasers in additive manufacturing, Optics & Laser Technology 78 (2016), 25-32
[10] S. Siddique, M. Imran, M. Rauer, M. Kaloudis, E. Wycisk, C. Emmelmann, F. Walther: Computed tomography for characterization of fatigue performance of selective laser melted parts, Materials & Design 83 (2015), 661-669
[11] B. Zink, F. Szabó, I. Hatos, H. Hargitai, J. G. Kovács: Simulation study of DMLS mold inserts (in Hungarian), Műanyag- és Gumiipari Évkönyv 12 (2014), 80-87
[12] R. Westhoff: Konturfolgende Temperierung auf dem Vormarsch, Kunststoffe International 08 (2016), 24-26
[13] Info leaflet about Hermle MPA technology (V10/2015), http://www.hermle-generative-manufacturing.com/cms/en/download/ (28 July 2016)
[14] Material data sheet: EOS MaragingSteel MS1, http://www.eos.info/ (28 July 2016)
[15] Dörrenberg: 1.2343, http://www.doerrenberg.de/ (28 July 2016)
[16] http://www.morganbrazealloys.com/downloads-3/mechanical-physical-properties (28 July 2016)

[1] Szechenyi Istvan University, Gyor, Hungary – hatos@sze.hu, hargitai@sze.hu

D.J. Hughes [1], H. Moztarzadeh[1], G. Gibbons[1], R. Dashwood[1]

The potential of central facilities to improve understanding of metal additive processes

Abstract

Central facilities offer access to unique tools that can provide an insight into the internal processes that control part quality in metal additive manufacturing. On one hand, synchrotron X-ray sources can give very intense beams that may be used to study these processes in-situ. On the other hand, neutron (reactor or spallation) sources provide extremely penetrating beams that can be used to probe the internal characteristics of metal components. In this presentation we will discuss the key characteristics of each type of facility and give examples of their use to study the complex processes that occur during additive manufacturing.

It will be shown that high intensity synchrotron X-ray beams can be used to perform a physical simulation of the actual additive process. Using advanced sample heating stages, it is possible to perform a simulation of the heating and cooling experienced during the manufacturing stage. In this way, phase transformations and residual stress development can be tracked in-situ which allows accurate input to finite element simulations of the process.

Furthermore, it will be discussed how neutrons enable non-destructive and internal analysis of the residual stress state of a manufactured component. The neutron beam is effectively employed as an atomic strain gauge, allowing mapping of internal stresses.

[1] WMG, The University of Warwick, Coventry, CV4 7AL, UK

CHRISTOPHER WALLIS [1], BRUNO BUCHMAYR [1], MICHAEL KITZMANTEL [2], ELMAR BRANDSTÄTTER [3]

ADDITIVE MANUFACTURING OF MARAGING STEEL ON A COPPER SUBSTRATE USING SELECTIVE LASER MELTING

Abstract

Additive manufacturing (AM) such as Selective Laser Melting (SLM) became a promising manufacturing process for the industry in the last years. Among its numerous research topics the fabrication of hybrid materials with the AM technology gained a special interest. The topic of this work deals with the additive processing of maraging steel on a copper substrate via SLM. The objective is to present our recent results in research of the hybrid system maraging steel/copper which presents a promising metal combination for diverse applications, e.g. in heat exchangers. To accomplish this, different process parameters have been used for building samples. Within these samples the binding zone of maraging steel and copper has been studied to evaluate a stable process window for producing a dense and strong metal compound. Using light optical microscopy the interface was examined for pore and crack appearance, furthermore the dilution was examined. The chemical composition in this region was measured by using EDX attached to a scanning electron microscope. The mechanical properties of the samples, in particular the binding strength between both metals, were assessed using a tensile testing machine. Within this presentation, the relations between SLM process parameters and microstructure, and properties are presented and discussed.

Keywords

Selective laser melting, hybrid, maraging steel, copper, microstructure

1. Introduction

Selective laser melting (SLM) represents one of various additive manufacturing technologies for processing metals [1]. SLM is a layer upon layer laser-welding process in which numerous achievements of processing a large variety of metals have been made [1,2]. On the other hand, welding of dissimilar materials is a different field of research. In general, welding to form hybrid structures of dissimilar materials represents a major scientific and technical challenge. Successful investigations on joining steel with copper (Cu) have been made using high-power density heating sources such as laser beam welding [3]. They are able to control the mixing of liquid steel and Cu to restrict metastable liquid phase separation which my lead to segregations of high- or low-melting-point phases inside the seam [3]. Since laser welding has been regarded as a major joining process [3], SLM is considered to be a promising technology to fabricate complex geometry and metal-hybrids, respectively. Especially steel/Cu is a promising and in many cases studied hybrid system because of its physical and mechanical properties [2-4]. Steel/Cu parts are applied in fusion reactors [5], conformal cooling channels [6-8], automotive, rail and aviation industries [9]. Maraging steel, basically, features high strength and fracture toughness with low dimensional changes under load, which makes it promising for aircraft, aerospace industries or for tooling applications [10]. Combining

1 Montanuniversitaet Leoben, Austria – Chair of Metal Forming
2 RHP-Technology GmbH, Seibersdorf, Austria
3 Joanneum Research Materials, Niklasdorf, Austria – Laser Processing

these properties with the high thermal conductivity of Cu may provide interesting applications for heat-exchangers or tools used in plastic injection moulds and metal casting dies in the future.

The current work has the objective to study the fabrication of additive manufactured maraging steel on a Cu-substrate, focusing on the relations between SLM process parameters and microstructure, and discussing its mechanical properties. The materials used in this work feature large differences in physical properties, namely high strength by maraging steel and high conductivity by Cu. An intact and rigid bonding of both materials shall be achieved. While previous studies concentrate on producing steel/Cu dissimilar joints by laser welding [3] or steel/Cu parts by multi-material processing [2], this study concentrates on SLM-parts of maraging steel produced on a Cu-substrate.

2. Experiments

2.1 Material

Spherical maraging steel powder (1.2709) with a particle size distribution of 16-48 µm and a D50 of 29 µm was used (analysis performed by Boehler Edelstahl). The spherical shape is important for the flowability of the powder, which guarantees a good powder layer deposition [2,11]. A Cu-plate (2.0090) with a dimension of 60x70x3 mm³ was used as substrate.

2.2 Selective Laser Melting

An EOSint M280 machine was used to fabricate the selective laser melted samples. It is equipped with an Ytterbium-fibre laser with a wavelength of 1064 nm and a maximum laser power of 400W. The process chamber is filled with N_2-gas, which is why the oxygen level during building is below 1 %. To evaluate adequate processing parameters for fabricating maraging steel on Cu a parameter study was performed. The most relevant parameters for the SLM-process in this work are laser power P_L, laser scan speed v_L, distance between laser tracks Δ_{xy} and layer thickness h. The correlation between these parameters and the energy input on the powder bed can be described by equation (1) and (2). E_L is the energy input per length and E_V the energy input per volume.

$$E_L = \frac{P_L}{v_L} \qquad (1)$$

$$E_V = \frac{P_L}{v_L \cdot \Delta_{xy} \cdot h} \qquad (2)$$

Due to the high thermal conductivity of the Cu-substrate, it is assumed that heat dissipates faster than on a steel-substrate. Consequently, to ensure a fully melted scan track and dense specimens, a high energy input was applied. Tab.1 shows the parameters in use. The energy input was altered by changing the laser scan speed v_L while the other parameters were fixed.

Tab.1: SLM-process parameter sets 1 to 6 for maraging steel on Cu.

Parameter	**1**	**2**	**3**	**4**	**5**	**6**
v_L [mm/s]	480	565	640	738	800	960
P_L [W]	285					
Δ_{xy} [mm]	0,11					
h [µm]	40					
E_L [J/mm]	0,6	0,5	0,45	0,4	0,35	0,3
E_V [J/mm³]	135	115	101	88	81	68

2.3 Metallographic Characterisation

Cuboids of 10x10x5 mm^3 were produced for the metallographic characterisation (Fig.1a). The vertical cross-section of the samples has been polished and etched to examine the steel/Cu interface and the microstructure of maraging steel, using light optical microscopy. For further examinations the samples were ion milled and examined by scanning electron microscopy (SEM) on a Leo1525 and EVO MA15, by energy dispersive spectroscopy (EDS) on an EVO50, and by electron back scattered diffraction (EBSD) from EDAX-TSL.

2.4 Mechanical Characterisation

Pull-off cylinder specimens of 10mm in diameter (Fig.1b) were built on Cu-plates, which were pulled off on a tensile testing machine (Roell Z250 from Zwick). Furthermore a tensile shear test was performed on steel/Cu-parts with a geometry shown in Fig.1c. The overlap of the tensile shear specimens is 2 mm. It was chosen to be small enough to enable the material separation occurring at the interface. To compare the results with the mechanical properties of maraging steel, tensile shear specimens of maraging steel were produced (Fig.1d). Additionally, an elastic finite element analysis on Abaqus FEA from Simulia was performed to estimate the stress distribution under load. Concluding, the microhardness was tested along the interface on a M1C010 from EMCO-test to obtain additional information about the dilution. Using the Vickers hardness test, a test load of 100g was applied (HV 0.1).

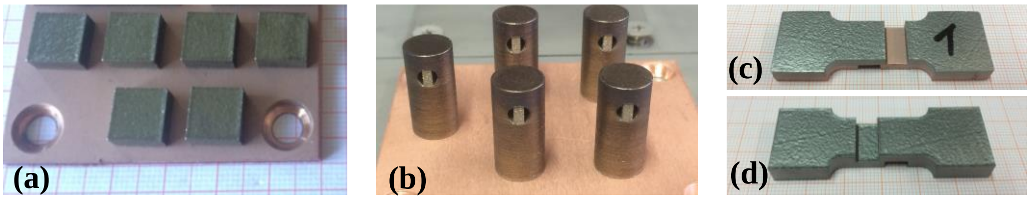

Fig.1: a) Steel/Cu cuboids, b) pull-off specimens, c) tensile shear specimens of maraging steel/Cu and d) maraging steel.

3. Results

3.1 Metallographic Characteristics

Successfully a steel/Cu hybrid-system with an intact interface was fabricated. Metallographic analysis presents an influence of different process parameters on the microstructural characteristics of the interface.

Light Optical Microscopy

The optical images of the as-polished steel/Cu interface in Fig.2 illustrate different characteristics at different parameter settings. Microcracks near the interface on the steel side can be seen, which become less with decreasing energy input (set 1 to set 6) and indicate a relation between energy input and the appearance of microcracks.
Comparing the Cu-surface at the edge of the images with the position of the interface, it is obvious, that higher energy input causes a deeper penetration of steel, leading to a lower situated interface in the Cu-plate (Fig.2a versus 2f). The interface has a wavy appearance with an observed dilution of approximately 70 µm.

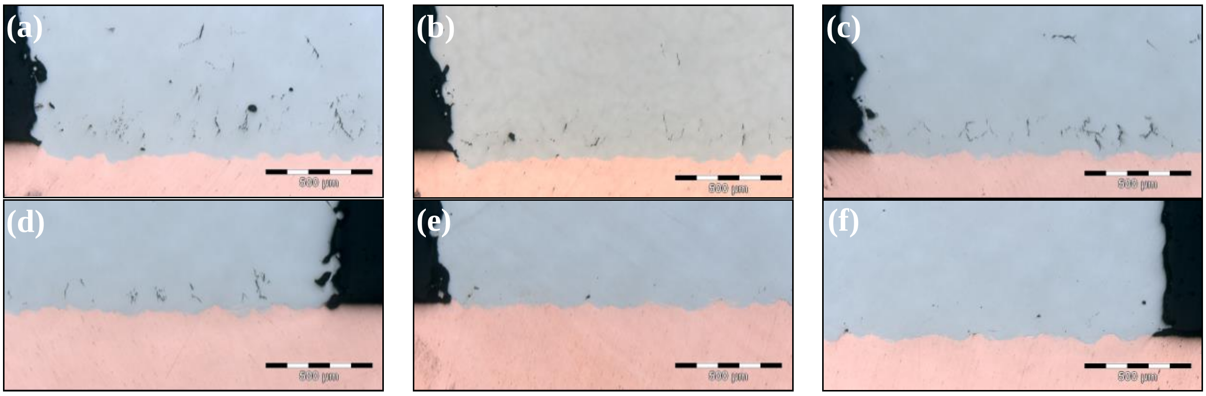

Fig.2: As-polished cross-sectional optical images of steel/Cu samples built with parameter a) set 1, b) set 2, c) set 3, d) set 4, e) set 5 and f) set 6.

To investigate the crack formation, Fig.3a presents an etched cross-section of the sample built with parameter set 1, where welding tracks with melt pool boundaries can be observed. The microcracks, presenting a "jagged" morphology, run through the melt tracks and boundaries and have a rough crack surface (Fig.3b-c).

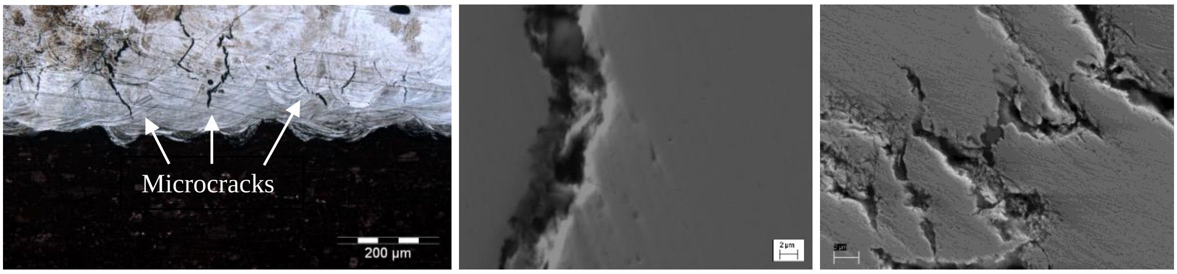

Fig.3: a) Optical image of sample built with parameter set 1 after etching; b-c) high magnification SEM images of microcracks with a rough crack surface.

According to the observations in Fig.2, parameter set 6 was rated to be the most promising parameter set for further investigations on a defect-free steel/Cu joint. For further investigations, the sample, which has been produced with parameter set 6, was analysed by scanning electron microscopy.

Scanning Electron Microscopy

The cross-sectional SEM images of the steel/Cu specimen is shown in Fig.4a and 4b. Here the wavy appearance in the intermixed region can be seen, forming microstructural bands of maraging steel and Cu. No further phases could be observed at the interface, suggesting a phase formation without intermetallic phases, corresponding to the binary phase-system Fe-Cu with a low solubility in the solid state between both metals [3,12]. An EDS-analysis was performed for an exact identification of the elements in the intermixed region and the extent of diffusion during the SLM-process.

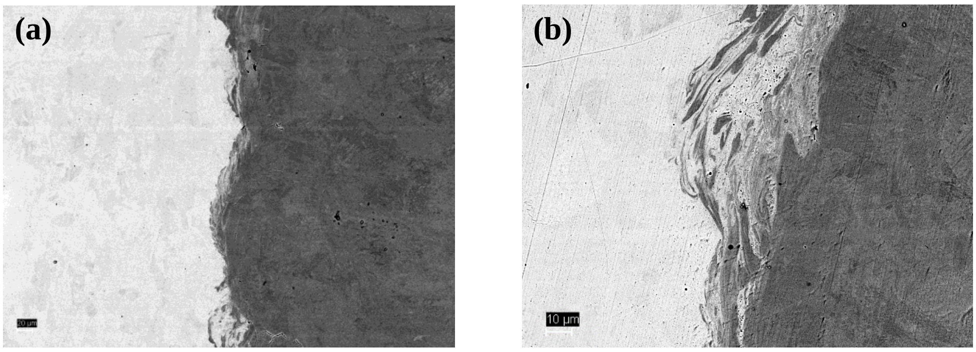

Fig.4: a) SEM image of the intermixed region steel/Cu, b) with higher magnification.

Energy Dispersive Spectroscopy

In the intermixed region an EDS-mapping and line scan was performed to obtain information about the chemical composition and the extent of diffusion, respectively. Fig.5 shows the elemental mapping and the composition distribution across the interface. Cu migrates up to 150 µm into steel, while little diffusion of Fe and its alloy elements (Ni, Mo, i.a.) in Cu occurs. Besides, a homogeneous distribution of steel alloys can be noted, indicating the absence of further phases or segregations.

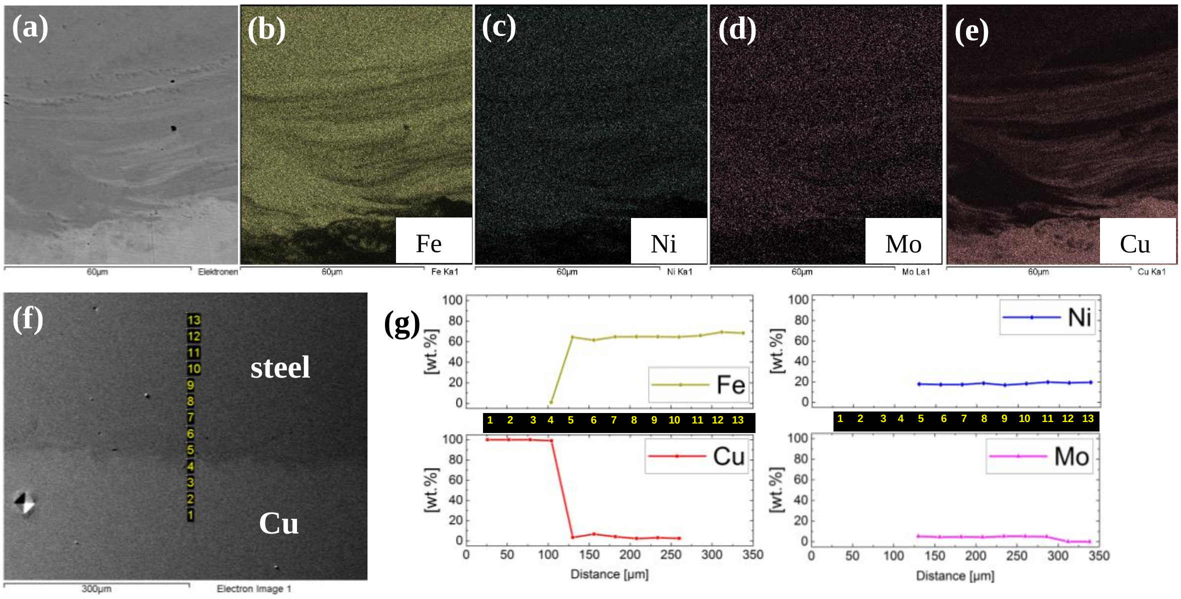

Fig.5: a) SEM image; b-e) EDS-mapping of the interface steel/Cu; f) EDS scan-line and g) the composition distribution of Fe, Cu, Ni and Mo.

Electron Back Scattering

The EBSD-analysis of the maraging steel/Cu system was carried out, detecting copper and ferrite and martensite, respectively. The inverse pole figure (IPF)-orientation maps in Fig.6a-b illustrate the orientations of the steel- and Cu-grains by different colours, which are enlisted in the IPF-colour key (Fig.6c, left). Blue coloured grains indicate a (111)-crystal orientation parallel to the scanning surface, (101) are indexed with green and (001) with red. The colour-information is summarized in a pole figure in Fig.6c (right). According to the pole figure, in steel no preferred orientation exists. In Fig. 6a an ultrafine, non-oriented microstructure with grains of a few µm size can be observed, which is attributed to the fast cooling rates of the

SLM-process [13], while the copper phase features bigger grains. As already seen in Fig.5, the interface is characterized by microstructural bands, caused by dilution.

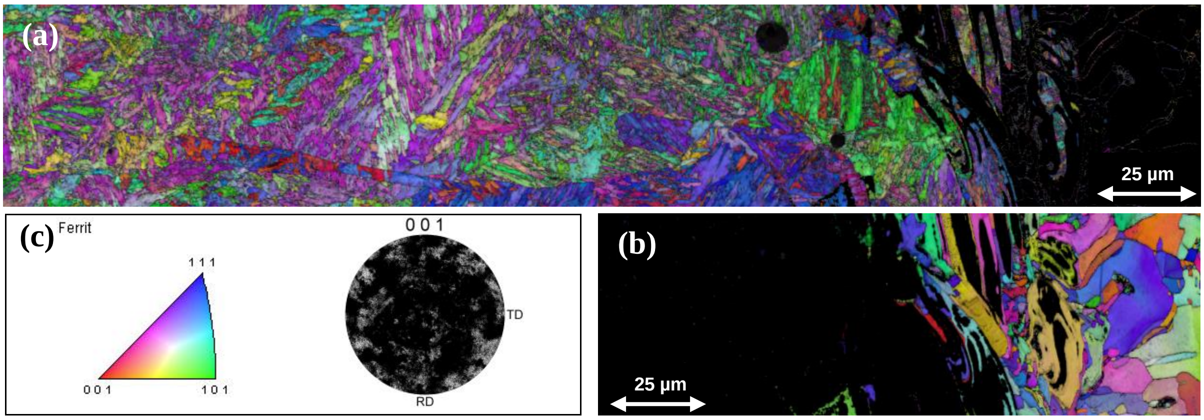

Fig.6: EBSD-scan results of the phase a) martensite and b) Cu in an orientation map. c) IPF-colour key and pole figure of maraging steel.

3.2 Mechanical Properties

Pull-off test

After accomplishing the production of a dense and defect-free interface between Cu and maraging steel, the mechanical properties were tested. At first the pull-off test was performed. Applying a tensile force on the cylinder the Cu-substrate began to deform plastically until material failure in Cu occurred. The fracture pattern exhibits characteristics of a ductile overload fracture, for example the pulled-out Cu-mass with fracture at 45° to the main load direction (Fig.7). The steel/Cu interface remained undamaged. Consequently the binding strength of the interface was higher than the tensile strength of Cu. A maximum tensile force of 17 kN was measured before the steel cylinder was pulled off. To obtain quantitative values for the binding strength, a tensile shear test was performed.

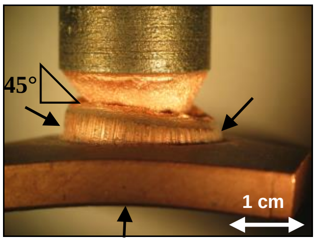

Fig.7: Pull-off test sample after tensile pull-off test. Arrows mark plastic deformation of Cu.

Tensile shear test

A finite-element-method (FEM) simulation on Abaqus identified the zones of highest stress, which are located at the edges of the overlap (Fig.8). The stress distribution in the test sample is symmetric to the interface plane. Because Cu has a lower strength compared to maraging steel the beginning of the material failure will be expected on the copper side at the end of the overlap region (marked in Fig.8)

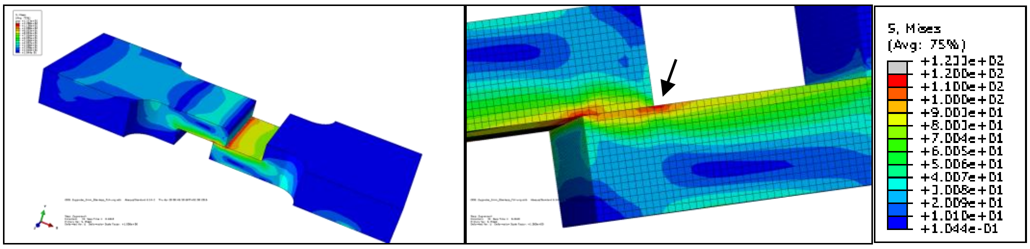

Fig.8: FEM-simulation on the tensile shear specimens with regions of highest stress (red zone, marked by arrow).

The tensile shear test showed that the binding strength of the SLM-produced steel/Cu hybrid was that strong, that the fracture occurred in Cu. In Fig.9a-c the fracture surface presents a fracture angle of 45° to main load direction and characteristics of a ductile fracture surface, corresponding to a ductile overload fracture. The SEM images show the beginning of fracture at the edge of the overlap region in Cu, as expected from FEM-simulations. After the fracture initiation comes the fracture plane with tear ridges and microvoids, indicating ductile fracture due to shearing (Fig.9c). Furthermore a contraction on the side of the Cu-branch can be observed (marked in Fig.9a), revealing a multi-axial stress state.

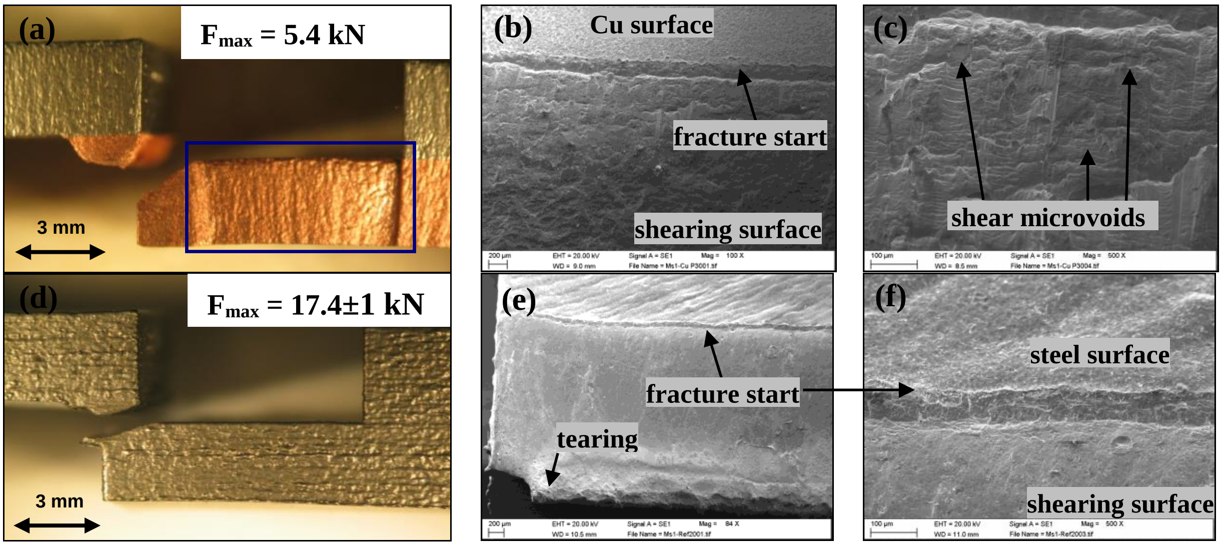

Fig.9: Specimens after tensile shear test. Steel/Cu-hybrid (a) with SEM images of fracture surface (b,c). Steel-reference specimen (d) with SEM images of fracture surface (e,f).

The fracture surface of the maraging steel reference sample in Fig.9d-f exhibits a similar failure pattern with characteristics of ductile fracture like steel/Cu. Here the fracture happened near the interface, so the adhesive shear strength τ_{shear} was calculated by using equation (3).

$$\tau_{shear} = \frac{F_{\max}}{A} \qquad (3)$$

$F_{\max}$ is the maximum force and A the overlap-area. Maraging steel has an adhesive shear strength of τ_{shear} = 672±35 MPa. Because the fracture of the steel/Cu sample did not take place at the interface, τ_{shear} cannot be derived. The maximum force the specimens can withstand is listed in Fig.9a and d and amounts 5.4 kN for the steel/Cu joint and 17.5±1 kN for maraging steel.

Microhardness

The trend of the microhardness through the intermixed region demonstrates a sharp transition from 94 HV in Cu to 480 HV in maraging steel. According to the results in Fig.10 the transition area is about 100-200 µm in length scale, which corresponds to the extent of diffusion assessed from the EDS-line scan.

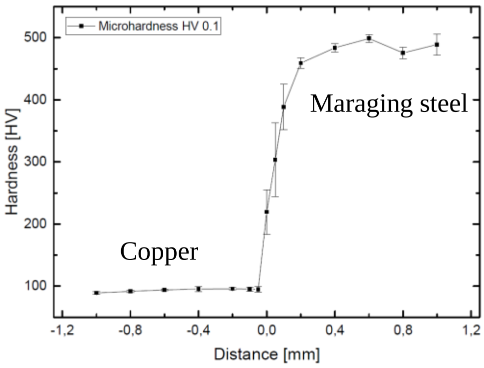

Fig.10: Microhardness trendline through the intermixed region of maraging steel/Cu.

4. Discussion

Producing a maraging steel/Cu hybrid by SLM requires appropriate process parameters. Regarding the specimens in Fig.2 the influence of process parameters on the microstructure can be observed. Near the interface microcracks with a jagged morphology appear, having rough flanks. Mercelis and Kruth [14] described the formation of high residual stresses in SLM-parts, causing microcracks. Those stresses arise from two mechanisms, temperature gradient mechanism (TGM) and the cool-down phase of molten top layers [14]. In TGM a temperature gradient between the upper and lower layers emerges due to rapid heating of the top surface and a low thermal conductivity of the underlying material, causing thermal residual stress. In the second mechanism stress is induced during the cooling of the molten top layer. When thermal contraction is restricted by the cooler underlying material, inner stresses develop. The microcracks in this work appear less frequently with decreasing energy input, confirming a relation between energy input and crack formation. Yuan and Gu [15] described an influence of process parameters on the temperature field, leading to different temperature gradients. The crack formation near the steel/Cu interface suggests also an influence of Cu, causing an inner stress field. This stress field tends to vary with increasing building height in which crack formation finally ceases. Describing the stresses by simulations of the temperature field for selective laser melted hybrid-parts presents an interesting field for future investigations.

The SEM images in Fig.4a show the intermixed region of steel/Cu with microstructural bands which are aligned parallel to the weld/substrate interface. They derive from convective mixing of the melt, which has been noted in previous studies concerning laser melting [4].

The overall EDS-mapping in Fig.5 exhibits the distribution of alloy components in the intermixed region, which confirms the presence of microstructural bands of different composition. These fluctuations of composition are attributed to convection in the molten pool due to the laser induced Marangoni effect, which were also identified by Phanikumar et al. in [4]. Moreover, Fig.5 shows a homogeneous distribution of the alloy elements. Consequently no segregation occurred, which would be unlikely due to high solidification rates in SLM.

The aforementioned characteristic high cooling rates of SLM lead to a fine-grained microstructure in maraging steel, as the EBSD-scan in Fig.6 illustrates. The orientation map in Fig.6a exhibits typical microstructural features of martensite with ultrafine grains, while Cu has a grain size of larger scale except for the Cu-rich bands in the fusion zone, caused by remelting. The different grainsize of Cu demonstrates the extent of fusion in the substrate. The intermixed region of about 100 µm width appears relatively small in comparison to conventional Cu/Fe-fusion techniques [3,4], owing to the localized energy input with a laser beam of 100 µm in diameter.

The pull-off test on steel/Cu samples identifies Cu to be the weakest component among the 3 structural regions (maraging steel, Cu and the interface). Severe plastic deformation of the Cu-plate occurred while the interface was intact, affirming the high binding strength of the steel/Cu interface. A maximum tensile load of nearly 17 kN was necessary to pull out the steel cylinder from the Cu-substrate. The tensile shear test verified that the binding strength of the SLM-produced steel/Cu hybrid was high, so the fracture occurred in Cu. The FEM-simulation in Fig.8 illustrates that the highest stress levels are located at the interface, where material failure started. The fracture propagates through Cu at an angle of approximately 45° to the load direction. The fracture plane in Fig.9b-c and displays microvoids with tear ridges like the reference specimen in Fig.9d-e, confirming ductile failure by shearing stress.
The results of the microhardness test exhibit a sharp transition from Cu to maraging steel, corresponding to an intermixed region of 100-200 µm width. In this region the hardness values reveal a large deviation, which can be attributed to the existence of microstructural bands forming a rough interface. When the indenter strikes a Cu- or steel-rich region the hardness values scatter. Furthermore, Fig.10 reveals that the transition area starts at the interface, indicating that mostly Cu has migrated into steel. This outcome is in accordance with the observations from the EDS analysis and verifies a low level of dilution.

5. Conclusion

Investigations of the SLM-produced maraging steel/Cu system have been made, focusing on the process parameter-related microstructure of the interface and on the binding strength. The following observations have been made:

1. The process parameters influence the outcome of the microstructural interface. The lower the energy input by increasing the laser scan speed, the less microcracks occurred in steel near the interface.
2. SLM-parts of maraging steel and Cu with a crack-free interface were successfully fabricated by adjusting the process parameters to higher laser scan speeds.
3. The interface consists of an intermixed region which features microstructural bands of Cu and steel, forming because of convection in the molten pool.
4. EDS-line scan demonstrates that migration of Cu into steel occurred to an extent of 150 µm while no significant concentration of steel in Cu was detected, corresponding to a strongly localized energy input of SLM.
5. The EBSD-analysis exhibits a fine-grained microstructure in maraging steel, attributed to the high cooling rates and subsequently rapid solidification in SLM.
6. Pull-off and tensile shear tests exhibited a higher binding strength than the strength of the Cu-substrate.
7. The abrupt rise in microhardness at the interface indicates a small intermixed region of about 100-200 µm width and are in accordance with the results of the EDS-line scan.

References

[1] Wohlers Report 2014 - 3D Printing and Additive Manufacturing State of the Industry, Wohlers Associates, Inc. (2014)

[2] Z.H. Liu, D.Q. Zhang, S.L. Sing, C.K. Chua, L.E. Loh, Interfacial characterization of SLM parts in multi-material processing: Metallurgical diffusion between 316L stainless steel and C18400 copper alloy, Materials Characterization (2014, vol.94), p.116

[3] S. Chen, J. Huang, H. Zhang, X. Zhao, Microstructural Characteristics of a Stainless Steel/Copper Dissimilar Joint Made by Laser Welding, Metallurgical and Materials Transactions A (2013, vol.44), p.3690

[4] G. Phanikumar, S. Manjini, P. Dutta, K. Chattopadhyay, J. Mazumder, Characterization of a continuous CO2 laser-welded Fe-Cu dissimilar couple, Metallurgical and Materials Transactions A (2005, vol.36), p.2137

[5] K.D. Leedy, J.F. Stubbins, Copper alloy-stainless steel bonded laminates for fusion reactor applications: Crack growth and fatigue, Materials Science and Engineering A (2001, vol.297), p.19

[6] L. Wang, Q.S. Wei, P.J. Xue, Y.S. Shi, Fabricate Mould Insert with Conformal Cooling Channel Using Selective Laser Melting, Advanced Materials Research (2012, vol.502), p.67, 2012

[7] A.B. Spierings, G. Levy, L. Labhart, K. Wegener, Production of functional parts using SLM – Opportunities and limitations, Innovative Developments in Virtual and Physical Prototyping, Leiria (2011), p.785

[8] D. Dimitrov, A. Moammer, T. Harms, Cooling channel configuration in injection moulds, Innovative Developments in Virtual and Physical Prototyping (2012), p.355

[9] O. Yilmaz, H. Celik, Electrical and thermal properties of the interface at diffusion-bonded and soldered 304 stainless steel and copper bimetal, Journal of Materials Processing Technology (2003, vol.141), p.67

[10] E. Yasa, K. Kempen, J.P. Kruth, L. Thijs, H.J. Van, Microstructure and mechanical properties of maraging steel 300 after selective laser melting, 21st Annual International Solid Freeform Fabrication Symposium, Austin (2010), p. 383

[11] M. Averyanova, Ph. Bertrand, B. Verquin, Studying the influence of initial powder characteristics on the properties of final parts manufactured by the selective laser melting technology, Virtual and Physical Prototyping (2011, vol.6), p.215

[12] I. Magnabosco, P. Ferro, F. Bonollo, L. Arnberg, An investigation of fusion zone microstructures in electron beam welding of copper-stainless steel, Materials Science and Engineering A (2006, vol.424), p.163

[13] Z.H. Liu, D.Q. Zhang, K.F. Leong, C.K. Chua, Crystal Structure Analysis of M2 High Speed Steel Parts Produced by Selective Laser Melting, Materials Characterization (2013, vol.84), p.72

[14] P. Mercelis, J.P. Kruth, Residual stresses in selective laser sintering and selective laser melting, Rapid Prototyping Journal (2006, vol.12), p.254

[15] P. Yuan, D. Gu, Molten pool behaviour and its physical mechanism during selective laser melting of TiC/AlSi10Mg nanocomposites: Simulation and experiments, Journal of Physics D: Applied Physics (2015, vol.48)

Markus Brillinger[1], Franz Haas[1], Norbert Enzinger[2], Stefan Pfanner[3]

BASIC CHARACTERISATION OF 17-4PH STRUCTURE BY SELECTIVE LASER MELTING

Abstract.

In this work selective laser melting (SLM) was used to produce different structures made out of stainless steel 17-4PH for basic characterization. Therefore 17-4PH as manufactured by SLM without post heat treatment and after a heat treatment (650°C for 1 h) were compared with a wrought material with heat treatment. Properties which are studied in this work are the stress-strain diagram, hardness, notch impact energy and surface quality as a function of the part orientation with respect to the building direction. Considering mechanical properties, a clear anisotropy is observed in the as manufactured state, which is not so distinctive in the heat treated condition. The strength of the wrought material is about twice as large as that of the selective laser molten components. The Charpy impact test shows lower values of the SLM part after heat treatment compared to the as manufactured condition. Due to the manufacturing process the differences in roughness between differently orientated surfaces is very large. These differences can be reduced by post-processing methods, such as glass bead blasting.

Keywords

Selective Laser Melting, 17-4PH, heat treatment, part orientation, building direction

1. Introduction

The implementation of additive manufacturing in the production processes of various parts advances very quickly. A promising technology of additive manufacturing is the Selective Laser Melting (SLM) process. Many applications of this technology are emerging: For instance, biological compatible materials can be used for dental implants and prosthesis [1-5]. The aerospace industries try to apply this technology to increase the properties of the turbine blades [6]. The basic properties of the SLM parts are of prime importance for all applications. In a consequence to this the properties of SLM 17-4PH (with and without heat treatment) must be compared with a wrought material (with heat treatment). The nominal chemical composition of the 17-4PH is shown in table 1. The heat treatment of the SLM material and the wrought material are shown in figure 1.

Table 1. Chemical analysis of the 17-4PH (>1wt%) according EN10088.

C	Si	Mn	Cr	Ni	Cu	Nb
0.04	0.25	0.40	15.40	4.40	3.30	0.30

[1] Institute of Production Engineering (IFT), Graz University of Technology, Graz
[2] Institute of Materials Science and Welding (IWS), Graz University of Technology, Graz
[3] Anton Paar GmbH, Graz

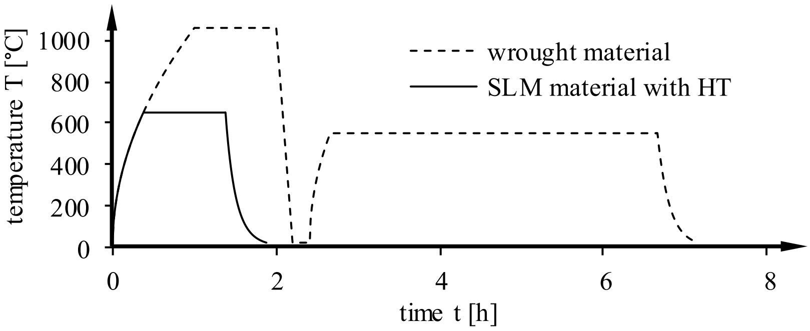

Figure 1. Heat treatment (HT) of the wrought material and the SLM material.

The SLM-process can be described as follows: The basic material, metallic powder with a given chemical composition, is positioned layer by layer. A laser fuses every new powder layer with the already fused component below. To use the best settings for the selective laser melting process much experience and good skills of the machine operator are needed [7]. Due to manufacturing layer by layer in one direction – the so-called build direction – the parts contain certain porosity [8] and the behavior of the component is more or less anisotropic [9-14]. In this paper, special attention is paid to this anisotropy. The best way to detect the roughness of SLM surfaces is a confocal microscopy. Using a computerized analysis program with a Gaussian low pass filter of 0.8mm grants the best results [15].

2. Experimentals and Results

To investigate this anisotropy the test samples must be placed in different positions and sample orientations inside the building volume of the SLM machine. For the basic characterization of the anisotropy following tests were performed: tensile test, charpy V-notch test, Vickers hardness test and roughness test of the surface. Figure 2 shows the building volume inside the used SLM (EOS M280) machine with the test samples placed in different orientations.

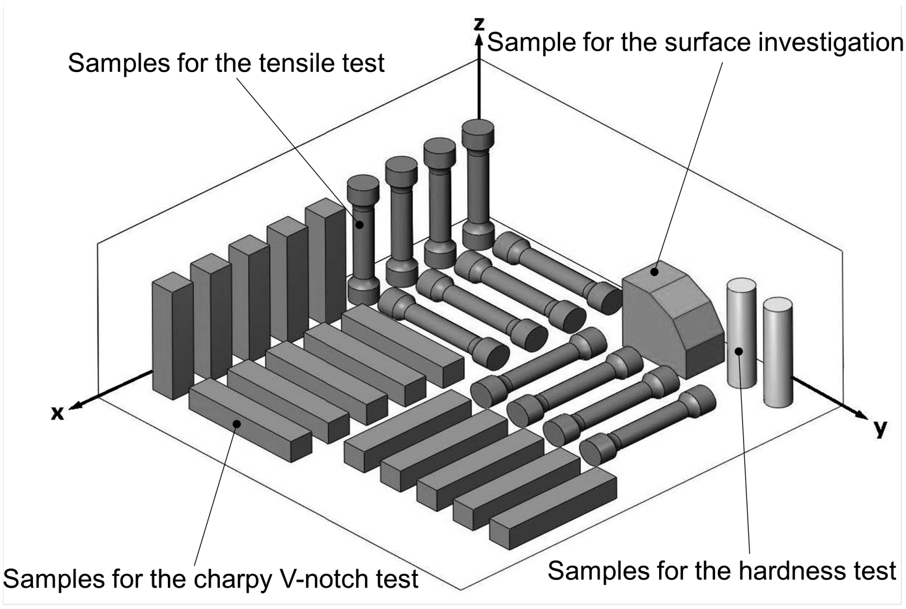

Figure 2. Building volume filled with samples in different part orientations.

Due to the fact, that selective laser molten 17-4PH parts are commonly used in heat treatment condition [16], for every main orientation a specimen with and without heat treatment was investigated. The samples for the tensile test and the Charpy V-notch test are manufactured with oversize and afterwards they are machined into standardized dimensions.

- *Tensile test*

Figure 3 shows the stress-strain chart of the tensile tests. There are a big difference between wrought material and SLM material (with and without heat treatment).

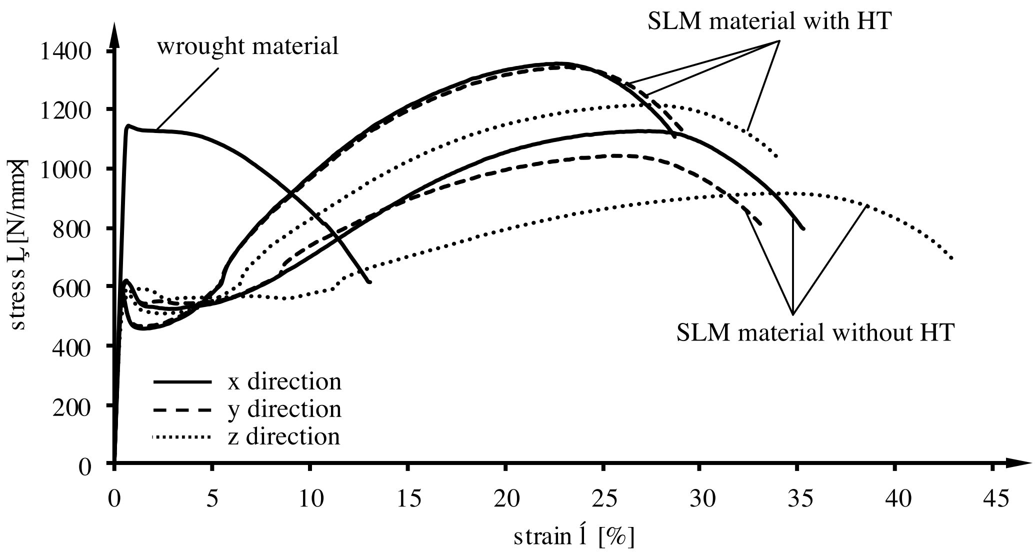

Figure 3. Influence of heat treatment (HT) of the wrought material and laser melted material (SLM) on the stress strain curve.

Table 2. Results of the tensile test.

	SLM material without heat treatment			**SLM material with heat treatment**			**wrought material**
sample orientation	x	y	z	x	y	z	-
E [GPa]	172	178	176	187±2	195±5	188±5	198±2
Re [MPa]	615	620	592	588±2	590±1	586±1	1142±1
Rm [MPa]	1126	1043	916	1359±4	1342±2	1213±3	-
A [%]	29	29	36	20±1	19±1	26±1	13±1

In Table 2 the analysis of the stress-strain charts is presented. The anisotropy of the SLM material without heat treatment is higher than that of the SLM material with heat treatment. If heat treatment is used the anisotropy of the samples oriented in x and y orientations are significantly lower. Nevertheless, samples with heat treatment which are orientated in build direction (z) are very different from x and y orientation. This difference does not change significantly due to heat treatment. The tensile strengths (Rm) increases by applying the defined heat treatment, but the yield strengths (Re) remains steady.

Wrought material has a considerable higher yield strength and lower fracture elongation compared with SLM material. Depending on heat treatment condition and orientation UTS of SLM parts is lower or higher compared to wrought material.

- *Hardness test*

The hardness was determined by Vickers-microhardness test. The results are summarized in table 3 and show higher values for the laser molten material with heat treatment compared to SLM material without HT. Due to the heat treatment the hardness can be improved, but the hardness of the wrought material can't be achieved.

Table 3. Results of the hardness test.

	SLM material without heat treatment	**SLM material with heat treatment**	**wrought material**
HV1	234±17	264±30	364±27

- *Charpy V-notch test*

In table 4 the Charpy V-notch energy is given. The SLM material without heat treatment shows the highest anisotropy, which can be reduced by the heat treatment. However, the heat treatment reduces the toughness. Of all tested Charpy V-notch test specimen the wrought material has the lowest values.

Table 4. Results of the Charpy V-notch test.

	SLM material without heat treatment			**SLM material with heat treatment**			**wrought material**
notch plane	yz	xz	xy	yz	xz	xy	-
Av [J]	142±2	140±2	161±5	80±2	82±4	89±2	72±2

- *Surface investigation*

Figure 4 shows the surface quality of the SLM sample with heat treatment with respect to the surface orientation. The typical surface structures of the SLM process show welding beads at horizontal orientated surfaces. This surfaces have the lowest roughness. Vertical orientated surfaces presents the highest roughness. This is based on the pre-sintering of metal powder along the exterior contour. In gerneral can be said, that the roughness is more pronounced by higher angles between build direction (z) and surface.

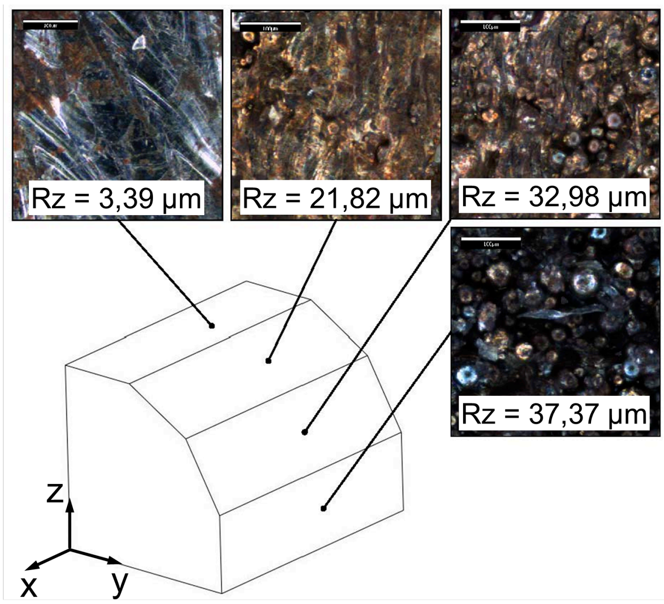

Figure 4. Surface quality of the laser melted material with heat treatment (HT).

3. Conclusion

All investigated properties show significant differences between SLM and wrought material. The heat treatment has a significant influence on properties. The SLM material presents a significant anistropy which depends on the sample orientation. The following aspects must be considered to manufacture parts by using SLM technology:

- Due to the manufacturing process the manufactured parts show a high anistropy.

- The differences of the properties between the x- and y- sample orientation are lower than the differences between the x- and y- sample orientation and the z-orientation.

- The Anisotropy can be reduced by using a heat treatment but it cannot be removed.

- The heat treatment modifies the propoerties of the investigated material: strength and hardness increase, the Charpy-V notch toughness, fracture elongation and the surface roughness decrease.

- The surface quality of the part depends on the surface orientation. Due to the manufacturing process horizontal orientated surfaces present the lowest and vertical orientated surfaces the highest roughness. This means that all selective laser molten parts present areas with a higher and lower roughness.

References

[1] Trainia T, Manganob C, Sammonsc R L, Manganod F, Macchib A and Piattelli A 2008 Direct laser metal sintering as a new approach to fabrication of an isoelastic functionally graded material for manufacture of porous titanium dental implants *Dental Materials 24* ed A Piattelli (London: Elsevier) pp 1525–1533

[2] Williams J M, Adewunmi A, Schek R M, Flanagan C L, Krebsbach P H, Feinberg S E, Hollister S J and Das S 2005 Bone tissue engineering using polycaprolactone scaffolds

fabricated via selective laser sintering *Biomaterials 26* ed S Dasi (London: Elsevier) pp 4817–4827
[3] Ryan G, Pandit A and Apatsidis D P 2006 Fabrication methods of porous metals for use in orthopaedic applications *Biomaterials 27* ed D P Apatsidis (London: Elsevier) pp 2651–2670
[4] Wu G, Zhou B, Bi Y, and Zhao Y 2008 Selective laser sintering technology for customized fabrication of facial prostheses *The Journal of Prosthetic Dentistry 100/1* ed Y Zhao pp 57–60
[5] Vandenbroucke B and Kruth J P 2007 Selective laser melting of biocompatible metals for rapid manufacturing of medical parts *Rapid Prototyping Journal 13/4* (Emerald Group Publishing) ed B Vanderbroucke pp 196–203
[6] Das S, Fuesting T P, Danyo G, Brown L E, Beaman J J and Bourell D L 2000 Direct laser fabrication of superalloy cermet abrasive turbine blade tips *Materials and Design 21* ed S Das (London: Elsevier) pp 63-73
[7] Khaing M W, Fuh J Y H and Lu L 2001 Direct metal laser sintering for rapid tooling: processing and characterisation of EOS parts *Journals of Materials Processing Technology 113* ed J Y H Fuh (London: Elsevier) pp 269-272
[8] Simchi A, Petzoldt F and Pohl H 2003 On the development of direct metal laser sintering for rapid tooling *Journals of Materials Processing Technology 141* ed A Simchi (London: Elsevier) pp 319-328
[9] Murr L E, Martinez E, Hernandez J, Collins S, Amato K N, Gaytan S M and Shindo P W 2012 Microstructures and Properties of 17-4 PH Stainless Steel Fabricated by Selective Laser Melting *Journal of Materials Research and Technology 1 (3)* ed L E Murr (London: Elsevier) pp 167-177
[10] Chen Z, Zhou G and Chen Z 2012 Microstructure and hardness investigation of 17-4PH stainless steel by laser Quenching *Materials Science and Engineering A 534* ed Z Chen (London: Elsevier) pp 536–541
[11] Gratton A 2012 Comparison of Mechanical, Metallurgical Properties of 17-4PH Stainless Steel between Direct Metal Laser Sintering (DMLS) and Traditional Manufacturing Methods *Proceedings of The National Conference On Undergraduate Research (NCUR)* ed A Gratton pp 423–431
[12] Lin X, Cao Y, Wu X, Yang H, Chen J and Huang W 2012 Microstructure and mechanical properties of laser forming repaired 17-4PH stainless steel *Materials Science and Engineering A 553* ed X Lin (London: Elsevier) pp 80–88
[13] Wang J, Zou H, Li C, Qiu S and Shen B 2006 The effect of microstructural evolution on hardening behavior of type 17-4PH stainless steel in long-term aging at 350° *Materials Characterization 57* ed J Wang (London: Elsevier) pp 274–280
[14] Wang J, Zou H, Li C, Qiu S and Shen B 2008 The spinodal decomposition in 17-4PH stainless steel subjected to long-term aging at 350°C *Materials Characterization 59* ed J Wang (London: Elsevier) pp 587–591
[15] Grimm T, Wiora G and Witt G 2015 Characterization of typical surface effects in additive manufacturing *Surface Topography: Metrology and Properties 3* ed T Grimm (IOP Publishing)
[16] Yan M F, Liu R L and Wu D L 2010 Improving the mechanical properties of 17-4PH stainless steel by low temperature plasma surface treatment *Materials and Design 31* ed M F Yan (London: Elsevier) pp 2270–2273

Reynier I. Revilla[1], Jingwen Liang[1], Stéphane Godet[2], Iris De Graeve[1]

Understanding the local corrosion mechanism of additive manufactured AlSi10Mg specimens

ABSTRACT

During the additive manufacturing (AM) of metal alloys the melting occurs in layers of pre–alloyed metal powders forming small melt volumes or melt pools which rapidly solidify, as a result the final microstructure of the solid piece can achieve unique, directional growth features [1]. As is well known, the microstructure and material composition strongly influence the corrosion behavior of metals. A great number of studies characterizing the microstructure of additive manufactured specimens have been carried out in the past years; among the materials studied AlSi10Mg alloys have also been the focus of attention [2–4]. In AM AlSi10Mg parts silicon crystallizes in a diamond–like phase that decorates the primary face–centered cubic (α–Al) aluminium cellular grains [3]. The cell size varies over the melt pool due to the thermal gradient created by the moving heat source; resulting in finer cells towards the middle of the melt pools, and larger cells in the melt pool borders. However, little has been done to analyze the influence of the microstructures on the corrosion behavior of these components. Cabrini et al. [5–7] studied the effect of surface finishing processes, surface orientation, and post–heat treatment on the corrosion behavior of AlSi10Mg parts. The researchers concluded that the resistance to corrosion decreases with the surface roughness, possibly associated with a less defective aluminium oxide film in smoother samples. Additionally, a selective corrosion of α–Al in the border of the melting tracks was detected; which the authors associated with an increased content of silicon and the interruption of the silicon network in heat affected zones.

In order to gain a better understanding of the corrosion mechanism exhibited by additive manufactured AlSi10Mg specimens and the influence of microstructures on the corrosion behavior, a thorough microstructural analysis combined with local electrochemical techniques is necessary. For this we have employed scanning electron microscopy (SEM) and scanning Kelvin probe force microscopy (SKPFM). A morphological characterization of corroded areas was executed, revealing that crystallographic pitting develops in the aluminium grains inside the melt pool borders, from where corrosion spreads to adjacent zones. Additionally, the local Volta

[1] Vrije Universiteit Brussel (VUB), Electrochemical and Surface Engineering (SURF), Pleinlaan 2, 1050 Brussels, BE
[2] 4MAT, Université Libre de Bruxelles (ULB), 50 av. F.D. Roosevelt (CP 165/63), 1050 Brussels, BE

potential analysis showed that there is a close relation between the cellular grains' size and the potential difference between the silicon and the aluminium phase. In regions with larger and coarser microstructures greater potential difference between the phases was found, which represents a higher driving force for galvanic corrosion. This could explain the selective corrosion attacks observed in the melt pool borders of AM AlSi10Mg pieces. During the investigation a conventional cast aluminium alloy of approximately the same chemical composition was used as a reference. Even though there are great differences between the microstructures of the cast Al alloy and the AM specimens, the value of the corrosion potential was comparable for all the samples analyzed. This could be because all the materials studied have approximately the same chemical composition, and the electrochemical test conducted represents a macroscopic behaviour of the surface rather than a localized effect.

References

[1] L.E. Murr, S.M. Gaytan, D.A. Ramirez, E. Martinez, J. Hernandez, K.N. Amato, P.W. Shindo, F.R. Medina, R.B. Wicker, Metal fabrication by additive manufacturing using laser and electron beam melting technologies, J. Mater. Sci. Technol. 28 (2012) 1-14.

[2] E. Brandl, U. Heckenberger, V. Holzinger, D. Buchbinder, Additive manufactured AlSi10Mg samples using Selective Laser Melting (SLM): Microstructure, high cycle fatigue, and fracture behavior, Mater. Des. 34 (2012) 159-169.

[3] L. Thijs, K. Kempen, J.P. Kruth, J. Van Humbeeck, Fine-structured aluminium products with controllable texture by selective laser melting of pre-alloyed AlSi10Mg powder, Acta Mater. 61 (2013) 1809-1819.

[4] D. Manfredi, F. Calignano, M. Krishnan, R. Canali, E.P. Ambrosio, E. Atzeni, From powders to dense metal parts: characterization of a commercial AlSiMg alloy processed through Direct Metal Laser Sintering, Materials 6 (2013) 856-869.

[5] M. Cabrini, S. Lorenzi, T. Pastore, S. Pellegrini, D. Manfredi, P. Fino, S. Biamino, C. Badini, Evaluation of corrosion resistance of Al–10Si–Mg alloy obtained by means of Direct Metal Laser Sintering, J. Mater. Process. Tech. 231 (2016) 326-335.

[6] M. Cabrini, S. Lorenzi, T. Pastore, S. Pellegrini, E.P. Ambrosio, F. Calignano, D. Manfredi, M. Pavese, P. Fino, Effect of heat treatment on corrosion resistance of DMLS AlSi10Mg alloy, Electrochimica Acta 206 (2016) 346-355.

[1] Vrije Universiteit Brussel (VUB), Electrochemical and Surface Engineering (SURF), Pleinlaan 2, 1050 Brussels, BE

[2] 4MAT, Université Libre de Bruxelles (ULB), 50 av. F.D. Roosevelt (CP 165/63), 1050 Brussels, BE

[7] M. Cabrini, S. Lorenzi, T. Pastore, S. Pellegrini, M. Pavese, P. Fino, E.P. Ambrosio, F. Calignano, D. Manfredi, Corrosion resistance of direct metal laser sintering AlSiMg alloy 48 (2016) 818-826.

[1] Vrije Universiteit Brussel (VUB), Electrochemical and Surface Engineering (SURF), Pleinlaan 2, 1050 Brussels, BE
[2] 4MAT, Université Libre de Bruxelles (ULB), 50 av. F.D. Roosevelt (CP 165/63), 1050 Brussels, BE

YAZHENG LIU*, BO JIANG, DAN ZHANG, CHAO HUANG, CHAOLEI ZHANG

EFFECT OF RETAINED AUSTENITE ON MECHANICAL PROPERTIES OF BEARING ROLLER STEEL FOR LARGE SIZE SHIELD TUNNELLING MACHINE

Abstract

In this paper, the effect of retained austenite on mechanical properties of bearing roller steel for large size shield tunnelling machine was studied by orthogonal heat treatment experiment. The results show that the quenching temperature is the main factor affecting the retained austenite volume fraction ($f_{\gamma R}$). When the quenching temperature is in the range of 815~830 ^{o}C, the best mechanical properties are obtained. In this condition, the $f_{\gamma R}$ is in the range of 12.8%~17.7%, the retained austenite is filmy form and the thickness is about 20nm. When the quenching temperature is raised to 845 ^{o}C, the mechanical properties get worse, the $f_{\gamma R}$ is in the range of 20.3%~23.2%, the retained austenite is blocky form and the thickness is about 80~180nm.

Keywords: bearing steel; heat treatment; retained austenite; mechanical property

1. Introduction

The large size shield tunnelling machine has been widely used as the main excavation tool on the constructions of traffic tunnel, underground railway, cross-ocean tunnel and river-crossing tunnel. Under the work condition, the shield tunnelling machine can only forward when excavating. The main bearing is the main part of shield tunnelling machine. The replacement of the failure bearing is very complex during excavating and may bring immeasurable financial losses. Thus, the safety of the bearing can often directly determine the service life of shield tunnelling machine. The strength and toughness of the bearing roller steel for large size shield tunnelling machine should be both improved in order to get a good combination of abrasive resistance, fatigue performance and impact energy. High carbon chromium bearing steel has been always used on the bearing roller. Undoubtedly, there will exist some retained austenite in the steel after quenching and tempering. The retained austenite is one of the key factors affecting the strength and toughness of bearing. The effect of the volume fraction and the form distribution of retained austenite on the strength and toughness of different size high carbon chromium bearing steel have been focused by researchers from all over the world.

Moderate retained austenite is beneficial to the improvement of the toughness and contact fatigue life of bearing. Too much retained austenite can result in decrease in hardness, contact fatigue life and wear resistance. However, when the amount of retained austenite is too small, it may also lead to insufficient of toughness because it is easy to crack formation and reduce the contact fatigue life. For high carbon chromium bearing steel, retained austenite is usually between 6% to 15% [1]. In Qian’s study about steel GCr15 [2], the fatigue life of bearing is the highest when the amount of retained austenite is 19.3%. The magnetic method, metallographic analysis and X-ray diffraction method was used by Sun [3] to measure the amount of retained austenite of steel GCr15. The amount of retained austenite was 17.5%、20.8% and 19.0%, respectively. Although the amount of retained austenite in bearing steel is slightly affected by measurements, it is mainly depends on the material and heat treatment process.

[1] School of Materials Science and Engineering, University of science and technology Beijing, Beijing 100083
*Corresponding author: lyzh@ustb.edu.cn

In this study, the heat treatment orthogonal experiment was carried out. The amount of retained austenite was determined by X-ray diffraction method [4]. The morphology of retained austenite was observed by TEM. The influence of the number and morphology of retained austenite on mechanical properties of bearing steel was discussed.

2. Experimental materials and methods

The experimental material was spheroidizing annealed bearing steel GCr15SiMn with the diameter of 150 mm. The chemical composition is 1.02%C, 0.55%Si, 1.07%Mn, 0.006%P, 0.001%S, 1.49%Cr, 0.02%Cu and the balance Fe.

To improve the effectiveness of the heat treatment experiment, heat treatment experiment was carried out by four factors and three levels orthogonal experiment. To reduce the influence factors and improve the accuracy of experiment, the quenching soaking time was all set to 1 hour. The experiments were arranged according to the four factors and three levels orthogonal table L9 (34). Heat treatment experimental scheme is shown in Table 1. Numbers inside the parentheses represent the level, K.

Table 1 Scheme of Heat treatment experimental

Factor / Test Number	Quenching temperature $T_1/^oC$	Quenching soaking time t_2/h	Tempering temperature $T_2/\,^oC$	Tempering soaking time t_2/h
1#	815(1)	1	150(1)	2(1)
2#	815(1)	1	165(2)	4(2)
3#	815(1)	1	180(3)	6(3)
4#	830(2)	1	150(1)	4(2)
5#	830(2)	1	165(2)	6(3)
6#	830(2)	1	180(3)	2(1)
7#	845(3)	1	150(1)	6(3)
8#	845(3)	1	165(2)	2(1)
9#	845(3)	1	180(3)	4(2)

Mechanical properties of experimental steels were measured after heat treatment. A Zeiss EVO18 scanning electron microscope and F-20 transmission electron microscope were used to observe the microstructure morphology. The retained austenite phase was measured by DMAX-RB 12KW rotating anode diffractometer. Macro hardness of the experimental steel was determined by TH320 full Rockwell hardness.

3. Results and discussion

3.1. Heat treatment and microstructures

The microstructures of 1#~9# test steels were granular carbide and martensite in the matrix, as shown in Fig. 1. With the quenching temperature increasing from 815 ^oC to 845 ^oC, the number and size of undissolved carbide decrease. Through quantitative statistic by Image tool software, the average size of granular carbides of all the steels is less than 1μm, and the

[1] School of Materials Science and Engineering, University of science and technology Beijing, Beijing 100083
*Corresponding author: lyzh@ustb.edu.cn

network carbide level is less than level 1. When the quenching temperature is 845 ^{o}C, the impact toughness decreases in the bearing steel. At this temperature, more content of carbon dissolves in austenite and finally results in the formation of high carbon martensite, which will worsen the ductility. When the quenching temperature is between 815 ^{o}C and 845 ^{o}C, carbides are reasonable in quantity and uniform in size.

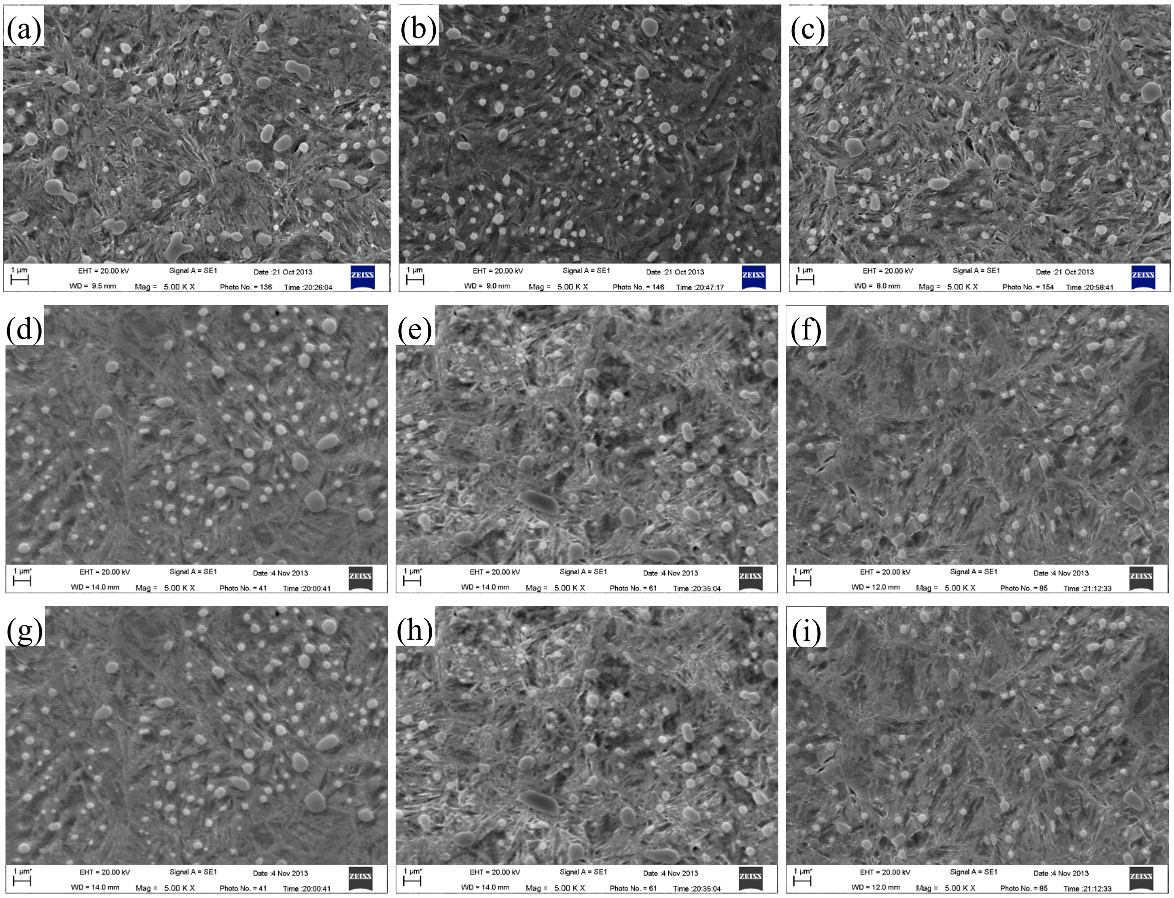

Fig. 1 Microstructures of the tested steel. (a) 1#; (b)2#; (c) 3#; (d) 4#; (e) 5#; (f) 6# ; (g) 7#; (h) 8#; (i) 9#

3.2 Heat treatment and mechanical properties

Three tensile values, three impact values and six hardness values were measured for each tested steel. The data of tensile strength(R_m), yield strength($R_{p0.2}$), unnotched impact toughness(A_k) and hardness were taken as arithmetic mean value. The mechanical properties of 1#~9# steels were shown in Table 2. According to the results of mechanical properties, the influences of heat treatment parameters on the strength, micro hardness and impact properties were analysed. The results of the analysis were shown in Table 3. Among them, K_1, K_2, K_3 and R denote the average values and difference between maximum and minimum values, respectively.

Table 2 Mechanical properties of 1#~9# steels

Test Number	Mechanical properties			
	R_m/MPa	$R_{p0.2}$/MPa	A_k/J	HRC

[1] School of Materials Science and Engineering, University of science and technology Beijing, Beijing 100083
*Corresponding author: lyzh@ustb.edu.cn

1#	2064	1182	78	62.8
2#	2307	1477	50	61.5
3#	2246	1537	96	61.3
4#	2104	1254	48	62.5
5#	2075	1543	105	61.7
6#	1962	1387	73	62.6
7#	1775	1028	53	62.0
8#	2043	1093	19	63.5
9#	2183	1158	79	63.0

Table 3 The analysis of orthogonal test

Mechanical property	Experimental parameter	Influence factors		
		Quenching temperature/T_1	Tempering temperature/T_2	Tempering soaking time/t_2
R_m /MPa	K_1	2206	1981	2023
	K_2	2047	2142	2198
	K_3	2000	2130	2032
	R	206	161	175
	Optimum level	815 ^{o}C	165 ^{o}C/180 ^{o}C	4h
$R_{p0.2}$ /MPa	K_1	1399	1155	1221
	K_2	1395	1361	1286
	K_3	1093	1361	1396
	R	306	206	175
	Optimum level	815 ^{o}C/830 ^{o}C	165 ^{o}C/180 ^{o}C	6h
A_k/J	K_1	75	60	57
	K_2	75	58	59
	K_3	50	83	85
	R	25	25	28
	Optimum level	815 ^{o}C/830 ^{o}C	180 ^{o}C	6h
HRC	K_1	61.9	62.4	63.0
	K_2	62.3	62.2	62.3
	K_3	62.8	62.3	61.7
	R	0.9	0.2	1.3
	Optimum level	830 ^{o}C/845 ^{o}C	150 ^{o}C	2h

[1] School of Materials Science and Engineering, University of science and technology Beijing, Beijing 100083
*Corresponding author: lyzh@ustb.edu.cn

Based the analysis of range method, the effects of quenching temperature(T_1), tempering temperature(T_2) and tempering time (t_2) on tensile strength are of 206 MPa, 161 MPa and 175 MPa respectively. The optimal process is: T_1=815 °C, T_2=165/180 °C, t_2=4h. The effects on yield strength are of 306 MPa, 206 MPa and 175 MPa respectively. The optimal process is: T_1=815/830 °C, T_2=165/180 °C, t_2=6h. The effects on unnotched impact toughness are of 25 J, 25 J and 28J respectively. The optimal process is: T_1=815/830 °C, T_2=180 °C, t_2=6h. The effects on hardness are of 0.9, 0.2 and 1.3 respectively. The optimal process is: T_1=830/845 °C, T_2=150 °C, t_2=2h.

Therefore, the effect of experimental parameters on R_m, $R_{p0.2}$, A_k and hardness can be ordered as follows respectively: $T_1>t_2>T_2$; $T_1>T_2>t_2$; $t_2>T_2=T_1$; $t_2>T_1>T_2$. The results show that quenching temperature is the main influence factor on tensile strength, yield strength, impact toughness, and hardness. The second influence factor is tempering soaking time.

3.3 Retained austenite and mechanical properties

In Jatczak's[5] study of retained austenite on steel 52100 (GCr15), the volume fraction of retained austenite was determined from the integrated intensities of austenite and ferrite peaks using the method described in [5] with:

$$f_{\gamma R} = \frac{(1/n_\gamma)\sum_1^n (I_\gamma^{hkl}/R_\gamma^{hkl})}{(1/n_\alpha)\sum_1^n (I_\alpha^{hkl}/R_\alpha^{hkl}) + (1/n_\gamma)\sum_1^n (I_\gamma^{hkl}/R_\gamma^{hkl}) + f_\theta} \qquad (1)$$

Where f_θ is the volume fraction of all carbides in the material, I_γ^{hkl} and I_α^{hkl} the integrated intensities of austenite and ferrite peaks, respectively, n_γ and n_α the numbers of {*hkl*} lines for which the integrated intensities have been measured, and R_γ^{hkl} and R_α^{hkl} are theoretical intensities presented in Table 4[5]. The austenite lattice parameter was calculated from three austenite diffraction peaks $\{200\}_\gamma$, $\{220\}_\gamma$ and $\{311\}_\gamma$ using Cohen's method [6].

Table 4 Theoretical line intensities (R-values) for the ferrite and austenite phases in steel for Co radiation (λ=1.79021 Å)[5]

{*hkl*}phase	{200}γ	{220}γ	{311}γ	{200}α	{211}α
R	37.0	20.4	30.1	14.8	32.4

Fig.2 shows the X-ray diffraction spectra of 1#~9# steels. According to equation (1), Table 4 and Fig. 2, the volume fraction of retained austenite ($f_{\gamma R}$) has been determined, as Fig. 3(a) shows. When the quenching temperature is 815 °C, $f_{\gamma R}$ of 1#~3# steels is between 12.8% and 13.5%. When the quenching temperature is 830 °C, $f_{\gamma R}$ of 4#~6# steels is between 16.0% and 17.7%. When the quenching temperature is 845 °C, $f_{\gamma R}$ of 7#~9# steels is between 20.3% and 23.2%.

Hence, the quenching temperature is the main factor on $f_{\gamma R}$. When quenching temperature is in the range of 815~845 °C, $f_{\gamma R}$ increases about 1% with the quenching temperature increasing about 3 °C, as shown in Fig. 3(b). On the other hand, tempering temperature and tempering soaking time has smaller influence on $f_{\gamma R}$. Compared with quenching temperature, when tempering temperature is in the range of 150~180 °C and tempering soaking time is in the range of 2~6h, the amount of change of $f_{\gamma R}$ is only between 2% and 4%.

[1] School of Materials Science and Engineering, University of science and technology Beijing, Beijing 100083
*Corresponding author: lyzh@ustb.edu.cn

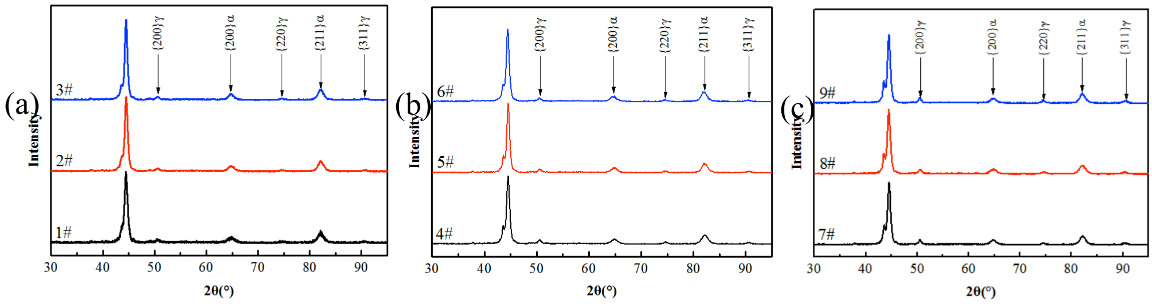

Fig. 2 Diffraction spectra of GCr15 steel.

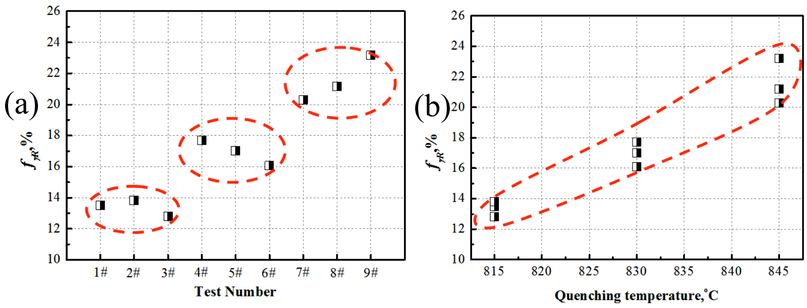

Fig. 3 Relationship between quenching temperature and $f_{\gamma R}$.

Typical TEM micrographs of retained austenite are shown in Fig. 4. Fig. 4(c) is dark field photographs of Fig. 4(b). Fig. 4(d) is the diffraction pattern of point A in Fig. 4(b). TEM observation reveals that the higher the quenching temperature is, the more the retained austenite is. When the quenching temperature is 815 °C(3#) and 830 °C(6#), there are more film type retained austenite than block type, the thickness of retained austenite is about 20nm. When the quenching temperature is 845 °C(8#), more block type retained austenite exists in steel, the thickness of retained austenite is 80~180nm.

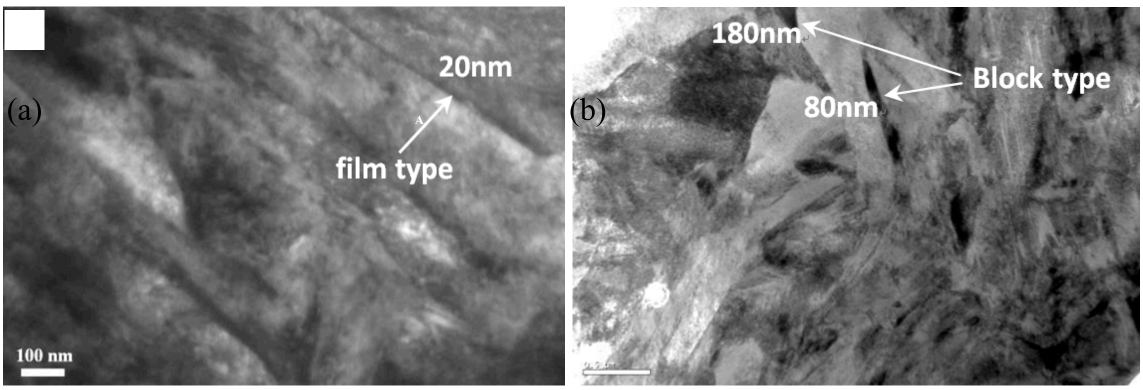

[1] School of Materials Science and Engineering, University of science and technology Beijing, Beijing 100083
*Corresponding author: lyzh@ustb.edu.cn

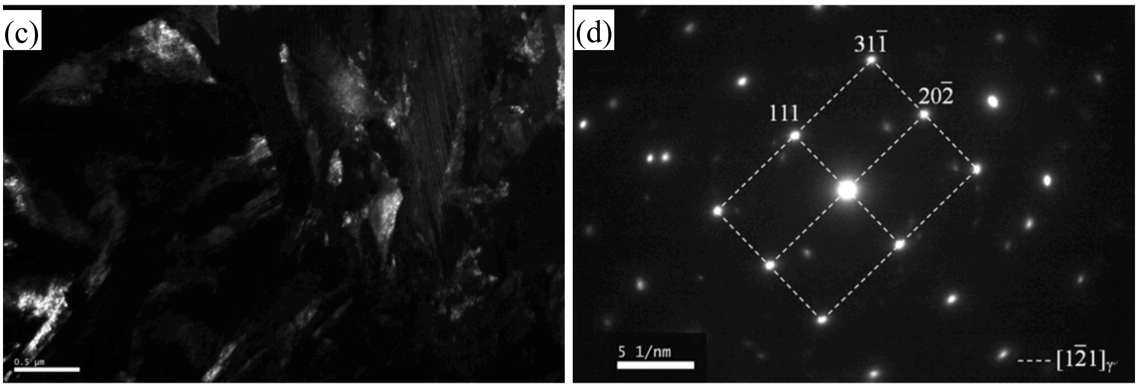

Fig. 4 TEM micrographs of test steels.(a) 3#；(b) 8#；(c) Dark field photographs in (b)；(d) The diffraction pattern of point A in (b)

Fig. 5 shows the effect of $f_{\gamma R}$ on mechanical properties of steel GCr15SiMn. It reveals that $f_{\gamma R}$ has significant influence on R_m, A_k and HRC. The ordinate parameters are the average value. According to Table 2 and Fig. 5, when quenching temperature is between 815~830 °C, $f_{\gamma R}$ is 12.8%~17.7%, HRC is 61.3~62.8, A_k is 48~105 J; when quenching temperature is 845 °C, $f_{\gamma R}$ is 20.3%~23.2%, HRC is 62.3~63.8, A_k is 19~79 J. With the increase of $f_{\gamma R}$, hardness increases, while impact toughness and tensile strength decrease. When the quenching temperature is 845 °C, more carbon dissolves in austenite which makes martensite harder. The decrease of impact toughness and tensile strength is due to the large austenite grain size and too much retained austenite volume.

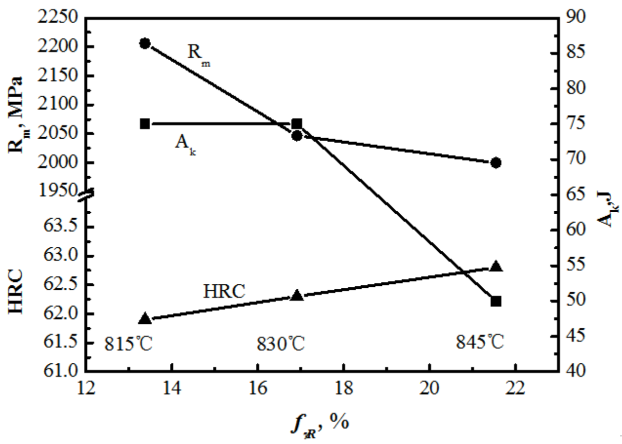

Fig. 5 Effect of $f_{\gamma R}$ on mechanical properties.

Thus, the large volume fraction from 20.3% to 23.2% and the block type of retained austenite are bad for mechanical properties, especially for the impact toughness. When $f_{\gamma R}$ is 12.8%~17.7% and retained austenite is film type, impact toughness was greatly improved with small change of hardness and tensile strength. The optimum heat treatment process for steel GCr15SiMn is as followings: The quenching temperature is 815~830 °C, quenching soaking time is 1h, Tempering temperature is 165~180 °C, and tempering soaking time is 4~6h.

There are both advantages and disadvantages of retained austenite that in high carbon chromium bearing steel. Usually, retained austenite are block or film type[7, 8]. The film shaped retained austenite contains higher carbon content, which will be more stable at room temperature. Besides, retained austenite will act as the obstacle to prevent the crack

[1] School of Materials Science and Engineering, University of science and technology Beijing, Beijing 100083
*Corresponding author: lyzh@ustb.edu.cn

propagation. The impact toughness and tensile strength will decrease and the dimensional stability will get worse when retained austenite is too much. As a result, in order to ensure the comprehensive mechanical properties of GCr15SiMn bearing steel, $f_{\gamma R}$ should be controlled in 12.8%~17.7%. In this condition, retained austenite is mainly film type. There will be a better combination of the hardness, tensile strength and impact toughness of GCr15SiMn bearing steel.

4. Conclusions

(1) Quenching temperature is the main factor on tensile strength, yield strength, impact toughness and hardness. Tempering temperature and tempering soaking time has smaller influence mechanical properties.

(2) Quenching temperature is the main factor on $f_{\gamma R}$. When the quenching temperature is 815~830 ^{o}C, there are more film type retained austenite with the thickness is about 20nm. When the quenching temperature is 845 ^{o}C, there are more block type retained austenite with the thickness is 80~180nm.

(3) The comprehensive mechanical properties of GCr15SiMn bearing steel is the best when $f_{\gamma R}$ is 12.8%~17.7%. The optimum heat treatment process for steel GCr15SiMn is as followings: The quenching temperature is 815~830 ^{o}C, the quenching soaking time is 1h, the tempering temperature is 165~180 ^{o}C, and the tempering soaking time is 4~6h.

References

[1] F Hengerer, Dimensional stability of high carbon bearing steels, Ball Bearing Journal (1988, Volume 231), p.26
[2] K Qian, J.H. Li and X.B. Wu, Study on retained austenite and fatigue life test of GCr15 bearings, Machinery (2009, Volume 47), p.78 (in chinese)
[3] J Sun, H Yang and X.X Zhao, Content determination of retained austenite in rolling bearing steel, Journal of Netshape Forming Engineering (2011, Volume 3), p.6
[4] R.L. Bannerjee, X-ray determination of retained austenite, Journal of Heat Treatment (1981, Volume 5), p.147
[5] C.F. Jatczak, J.A. Larson and S.W. Shin, Retained austenite and its measurements by x-ray diffraction, society of automotive engineers, Inc. Warrendale, PA (1980)
[6] B.D. Cullity and S.R. Stock, Elements of x-ray diffraction (3rd Edition), Addison-Wesley, Massachusetts (2001)
[7] H.K.D.H. Bhadeshia and D.V. Edmonds, Bainite in silicon steels: a new composition property approach I, Metal Science (1983, Volume 17), p.411
[8] H.K.D.H. Bhadeshia, High Performance Bainitic Steels, Materials Science Forum (2005, Volume 500), p.63

[1] School of Materials Science and Engineering, University of science and technology Beijing, Beijing 100083
*Corresponding author: lyzh@ustb.edu.cn

PRASHANTH KONDA GOKULDOSS [1], JÜRGEN ECKERT [1,2]

TUNING OF TENSILE PROPERTIES IN NANO-STRUCTURED ALLOYS PROCESSED BY SELECTIVE LASER MELTING

Abstract

Selective laser melting (SLM) is a powder-based additive manufacturing technique used to produce 3-D metal parts by selective melting of the metal powders dictated by CAD data. Because of the high degree of freedom offered by this process, it is possible to build parts with extremely complex geometries that would otherwise be difficult or impossible to produce using conventional manufacturing processes. The SLM samples generally have superior mechanical properties than their cast counterparts due to the high cooling rates leading to a fine-grained microstructure. Moreover, the tensile properties of the nano-structured alloys processed by SLM can be tailored either by in-situ or ex-situ treatments. The present work focuses on the various in-situ treatments that can be used to tune the tensile properties of the SLM processed materials. The results demonstrate that SLM not only can be used for producing parts with complex shape and size but also gives an additional degree of freedom to manipulate and design their properties.

Selective Laser Melting, Rapid Quenching, Mechanical Properties, Tensile Properties

1. Introduction

Selective Laser Melting (SLM) is one of the additive manufacturing processes that is used to produce three dimensional near-net-shaped metal parts layer by layer using a 3D Computer Aided Design (CAD) or a Computer Tomography (CT) scan data [1-3]. Since the components are build layer by layer, it offers a high degree of freedom, which makes it possible to produce parts with extremely complex geometries. The SLM process is theoretically capable of building parts with extremely complex shapes and any geometries that are otherwise difficult or impossible to produce using the available conventional manufacturing processes. It also offers the advantage of producing parts with complex structures in it (like the lattice structures) [2].

Another major advantage of the SLM process compared to the available conventional manufacturing processes is the extremely fast cooling rate observed during the processing stage due to the small volume of the melt pool, restricted mainly by the diameter of the laser beam [4]. It has been reported that a cooling rate of $\sim 1 \times 10^5$ K/s is observed during the SLM process and it offers the possibility to produce materials with fine microstructures with improved mechanical properties [4,5]. Some of the application of the SLM components include aerospace industry, where complex parts overcoming the limitations of conventional manufacturing can be produced and also it may result in the reduction of parts needed, thereby reducing the dead weight of the final component. It also finds it applications in the medical field allowing the model to be customised to the patient's anatomy in the form of prosthetics. Automobile, dental and jewellery industries find the SLM process useful, not only to reap its benefits but also to improve the functionality and applicability of the parts for a wide range of applications [6].

[1] Erich Schmid Institute of Materials Science, Austrian Academy of Sciences, Jahnstrasse 12, A-8700 Leoben, Austria

[2] Department Materials Physics, Montanunivertät Leoben, Jahnstrasse 12, A-8700 Leoben, Austria

There are several reports that are published in the field of Selective Laser Melting. Most of the reports deal with the new composition development and parameter optimization, topological optimization, design optimization and microstructure-property correlation [7-11]. However, not much importance is given on the influence of parameters on the microstructure and mechanical properties of the parts produced by SLM. Accordingly, the present work focuses on the ways the mechanical properties can be tuned for the SLM processed Al-12Si alloy.

2. Material and Methods

Al-12Si (Wt.% - nominal composition) is chosen for the present study, because it's a conventional casting composition and has good fluidity and weldability. The Al-12Si gas-atomized powder with an average particle size of 50 µm is used to prepare bulk specimens by SLM using an SLM 250 HL device from SLM solutions (previously MTT Solutions). Since Al-based alloy are prone to oxidation (very reactive), the fabrication process was carried out under Ar atmosphere to avoid the parts from getting contaminated by oxygen. The following standard parameter was used: hatch spacing 110 µm and a hatch style rotation of 73° with a power of 320 W for both contour and volume and laser scan speed of 1455 mm/s for the volume and 1939 mm/s for the contour. The laser power and laser scan speed were varied for some samples and the values are mentioned wherever necessary.

Phase analysis of the samples were performed by X-ray diffraction (XRD) using a D3290 PANalytical X'pert PRO with Co-Kα radiation (λ = 0.17889 nm) in Bragg-Brentano configuration. The microstructure of the SLM samples as well as the fracture surface was characterized by optical microscopy (OM) using a Zeiss Axioskope 40 microscope and by scanning electron microscopy (SEM) using a Gemini 1530 microscope. The tensile tests were carried out at ambient temperature using an ISTRON 8562 testing facility under a quasistatic loading with a strain rate of ~ 1×10^{-4} s^{-1}. The strain accumulated in the sample was measured using a Fiedler laser-extensometer.

3. Results and Discussion

A detailed characterization of the Al-12Si sample fabricated by SLM has been reported elsewhere [1] and only the relevant information necessary for the present manuscript will be discussed here. Al-12Si SLM sample shows an extremely fine cellular type microstructure with core of the cells rich in Al (500 – 1000 nm) and the boundaries are segregated with Si phase (thickness: 200 nm) [1]. The Si phase along the boundaries is present as a continuous skeleton network (Fig. 1). This is on the contrary to the Al-12Si SLM sample produced by the conventional casting process, where a near eutectic microstructure with pro-eutectic Al and eutectic Al-Si is observed (Fig. 1). In addition, the microstructure of the Al-12Si SLM sample is anisotropic in nature, where a relatively coarse cells are observed along the hatch overlaps and a finer morphology is observed along the core of the tracks [1]. Moreover, the hatch overlaps are the preferential sites for the segregation of the Si phase and the concentration of the Si phase along the hatch overlaps is two time higher than that of the core of the hatch (Fig. 1). In addition, the Al-12Si SLM samples show texture along the <200> Al plane and a supersaturated solid solution of Si phase in Al is also observed. The Al-12Si SLM samples show a yield strength of 260 MPa and an ultimate strength of 385 MPa, which is four and three times higher than the yield and ultimate strengths of Al-12Si produced by conventional casting process respectively (Fig. 2) [1]. However, this improved tensile strength comes at an

[1] Erich Schmid Institute of Materials Science, Austrian Academy of Sciences, Jahnstrasse 12, A-8700 Leoben, Austria

[2] Department Materials Physics, Montanunivertät Leoben, Jahnstrasse 12, A-8700 Leoben, Austria

expense of ductility, where the fracture strain of the Al-12Si SLM sample has been found to be only ~ 3% (Fig. 2). The cracks initiate at the hatch overlaps, where a coarse morphology is observed along with segregation of more Si phase. The fractured sample shows a step like fracture morphology (Fig. 1) [1].

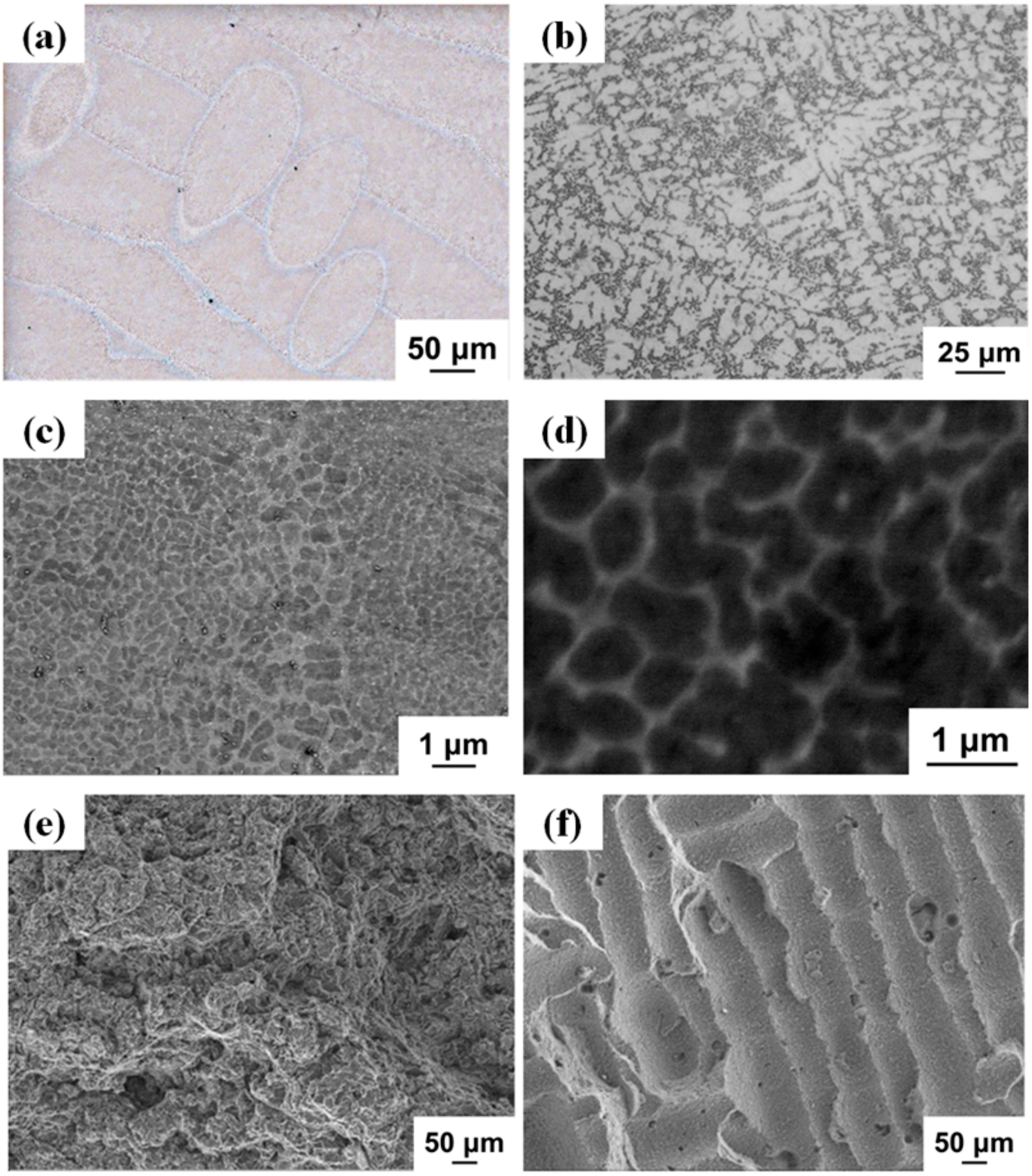

Fig. 1. Microstructure of the Al–12Si samples (a) Optical Microstructure of the sample prepared by SLM (b) Optical microstructure of the sample prepared by Casting, (c and d) SEM micrographs of the sample prepared by SLM and (e and f) fracture surface of the samples prepared by casting and SLM respectively [1]. Copyright 2013. Adapted with permission from Elsevier Science Ltd.

[1] Erich Schmid Institute of Materials Science, Austrian Academy of Sciences, Jahnstrasse 12, A-8700 Leoben, Austria

[2] Department Materials Physics, Montanunivertät Leoben, Jahnstrasse 12, A-8700 Leoben, Austria

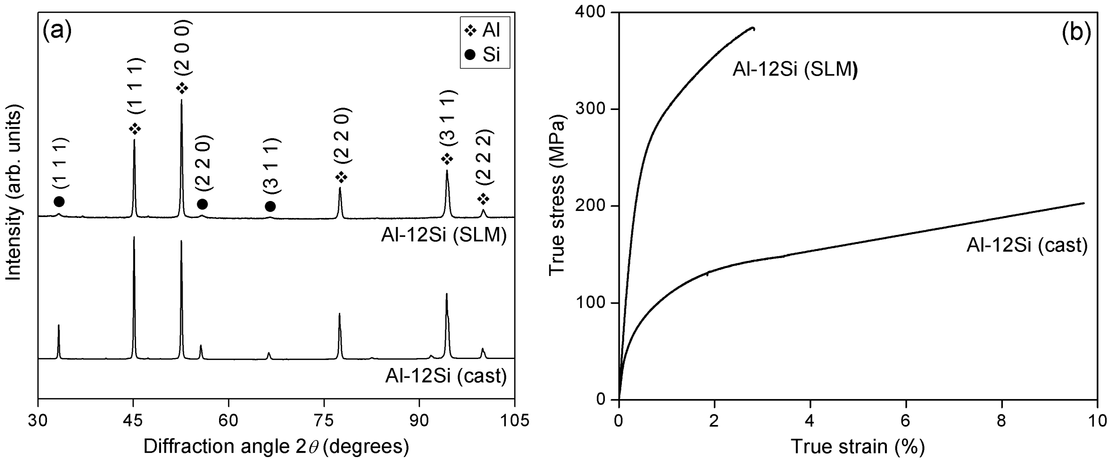

Fig. 2. (a) XRD patterns (λ=0.17889nm) and (b) room temperature tensile tests of the cast and as-prepared SLM Al–12Si samples [1]. Copyright 2013. Adapted with permission from Elsevier Science Ltd.

The SLM processing parameters were varied in order to evaluate the variation in the mechanical properties Al-12Si SLM samples. It has been observed that by changing the power and keeping the other parameters constant, both the strength and the ductility of the Al-12Si SLM samples decrease (Fig. 3(a)). This decrease in the mechanical properties of the Al-12Si SLM samples are due to the significant changes in the microstructure. It has been observed (not shown here) that the porosity levels in the SLM processed samples increases with the decrease in the laser power there by severely hampering the mechanical properties of the samples.

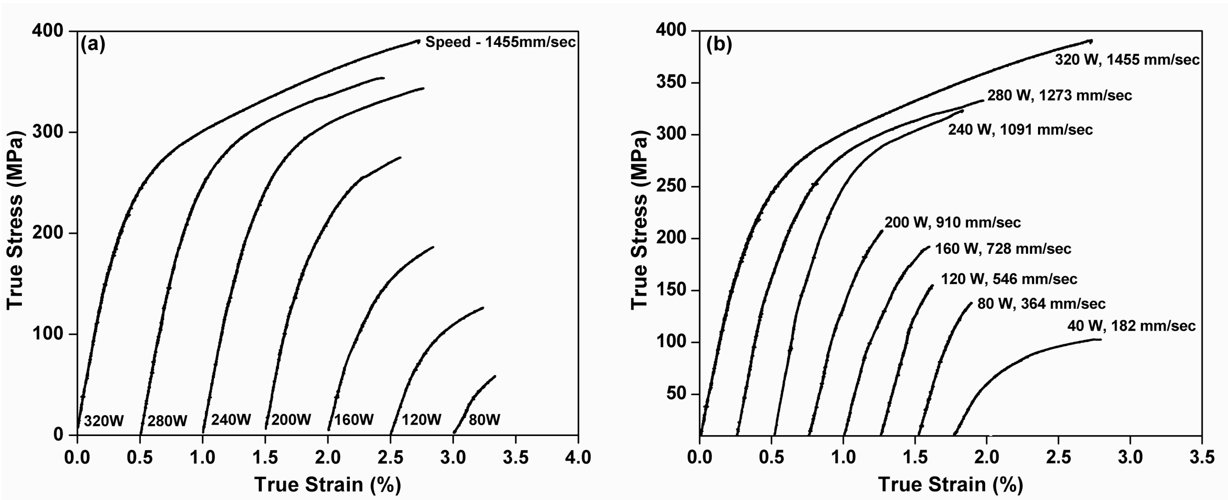

Fig. 3. Room temperature tensile tests of the Al-12Si samples (a) as a function of decreasing laser power and (b) as a function of changing laser power and laser scan speed combination, however maintaining a constant energy density.

One of the important equations that govern the amount of energy supplied to the SLM powder bed is defined as the:

Energy Input = (Laser Power) / (Scan Speed × Layer Thickness × Laser Spot Size) ..... (1)

[1] Erich Schmid Institute of Materials Science, Austrian Academy of Sciences, Jahnstrasse 12, A-8700 Leoben, Austria
[2] Department Materials Physics, Montanunivertät Leoben, Jahnstrasse 12, A-8700 Leoben, Austria

The above equation suggests that the energy supplied to the powder bed strongly depends on the laser powder, laser scan speed, layer thickness of the process and the spot size of the laser used []. The other attempt used in the present manuscript is to evaluate the variation of mechanical properties at a constant energy input, however changing the laser power and laser scan speed. To maintain a constant energy input, whenever the laser powder in increased, the laser scan speed has to be decreased accordingly and vice versa. The Al-12Si SLM samples produced by maintaining a constant energy input, thereby varying the laser powder and laser scan speed combination, show the hampering of the tensile properties at lower laser power / lower laser scan speed combination (Fig. 3(b)). This suggests that even though the energy density or the energy input is maintained a specific combination of laser powder and laser scan speed is required to maintain the soundness of the sample, thereby achieving improved mechanical properties. Similarly, other factors like the hatch distance (80 – 125 µm) and the hatch style (single melt strip hatch, checker board hatch style and meander hatch style) were effectively varied and a significant differences in the mechanical properties were observed. In addition, external annealing treatments were carried out for the Al-12Si samples. With increase in the annealing time / annealing temperature, the microstructure eases out from a cellular morphology to a composite like microstructure. The mechanical properties can be varied in a controlled way, where the ductility of the Al-12Si SLM samples increases at the expense of its strength. The above results suggests that there are several in situ and ex situ ways the mechanical properties of the Al-12Si samples fabricated by SLM can be varied.

4. Conclusion

Al-12Si alloys processing by SLM show that improved mechanical properties can be achieved compared with the same alloys processed by conventional casting process. In addition, the SLM process offers the advantage of working with the mechanical properties of the alloys either in situ during the fabrication process or ex situ after the fabrication process. The change in parameter of the production process like the laser power / laser scan speed / layer thickness / hatch distance / hatch style will have a significant influence on the microstructure and in turn the mechanical properties. Also, external annealing treatment can be carried out to change the mechanical properties. The results suggest that the SLM process offers the possibility to produce parts with desirable mechanical properties that can be optimized either during the production process (in situ) or after the fabrication of the parts (ex situ).

References

[1] R.A. Wilmans, C.S. and A.R. Dresler, title of article, Steel Research (2004, Volume x), p.243

[1] K.G. Prashanth, S. Scudino, H. J. Klauss, K. B. Surreddi, L. Löber, Z. Wang, A. K. Chaubey, U. Kühn and J. Eckert, Microstructure and mechanical properties of Al-12Si produced by selective laser melting: Effect of heat treatment, Materials Science and Engineering A (2014, 590) p.153

[2] H. Attar, L. Löber, A. Funk, M. Calin, L.C. Zhang, K.G. Prashanth, S. Scudino, Y.S. Zhang and J. Eckert, Mechanical behavior of porous commercially pure Ti and Ti-TiB composite materials manufactured by selective laser melting, Materials Science and Engineering A (2015, 625) p.350

[1] Erich Schmid Institute of Materials Science, Austrian Academy of Sciences, Jahnstrasse 12, A-8700 Leoben, Austria

[2] Department Materials Physics, Montanunivertät Leoben, Jahnstrasse 12, A-8700 Leoben, Austria

[3] K.G. Prashanth, H. Shakur Shahabi, H. Attar, V.C. Srivastava, N. Ellendt, V. Uhlenwinkel, J. Eckert and S. Scudino, Production of high strength $Al_{85}Nd_8Ni_5Co$ alloy by selective laser melting, Additive Manufacturing (2015, 6) p.1
[4] H.Y. Jung, S.J. Choi, K.G. Prashanth, M. Stoica, S. Scudino, S. Yi, U. Kühn, D.H. Kim, K.B. Kim and J. Eckert, Fabrication of Fe-based bulk metallic glass by selective laser melting: A parameter study, Materials and Design (2015, 86) p.703
[5] S. Pauly, L. Löber, R. Petters, M. Stoica, S. Scudino, U. Kühn and J. Eckert, Processing metallic glasses by selective laser melting, Materials Today (2013, 16) p.37
[6] C.Y. Yap, C.K. Chua, Z.L. Dong, Z.H. Liu, D.Q. Zhang, L.E. Loh and S.L. Sing, Review of selective laser melting: Materials and applications, Applied Physics Reviews (2015, 2) p.041101-1
[7] K.G. Prashanth, S. Scudino, A.K. Chaubey, L. Löber, P. Wang, H. Attar, F. P. Schimansky, F. Pyczak and J. Eckert, Processing of Al-12Si-TNM composites by selective laser melting and evaluation of compressive and wear properties, Journal of Materials Research (2016, 31) p.55
[8] K.G. Prashanth, B. Debalina, Z. Wang, P.F. Gostin, A. Gebert, M. Calin, U.Kühn, M. Kamaraj, S. Scudino and J. Eckert, Tribological and corrosion properties of Al-12Si produced by selective laser melting, Journal of Materials Research (2014, 29) p.2044
[9] P. Ma, K.G. Prashanth, S. Scudino, Y.D. Jia, H.W. Wang, C.M. Zou, Z.J. Wei and J. Eckert, Influence of annealing on mechanical properties of Al-20Si processed by selective laser melting, Metals (2014, 4) p.28.
[10] K.G. Prashanth, R. Damodaram, S. Scudino, Z. Wang, K. Prasad Rao and J. Eckert, Friction welding of Al-12Si parts produced by selective laser melting, Materials and Design (2014, 57) p.632
[11] P. Ma, Y. Jia, K.G. Prashanth, S. Scudino, Z. Yu and J. Eckert, Microstructure and phase formation in Al-20Si-5Fe-3Cu-1Mg synthesized by selective laser melting, Journal of Alloys and Compounds (2016, 657) p.430

[1] Erich Schmid Institute of Materials Science, Austrian Academy of Sciences, Jahnstrasse 12, A-8700 Leoben, Austria
[2] Department Materials Physics, Montanunivertät Leoben, Jahnstrasse 12, A-8700 Leoben, Austria

Pavel Krakhmalev[1]

Solidification microstructure and texture in SLM of metallic material

Abstract

Selective laser melting is a manufacturing method involving complete remelting of a thin powder layer at the substrate, thus building layer by layer 3D final objects of required shape. Processes occurring during manufacturing are complex, involve melting, overheating of the molten metal, conventional processes in a molten pool, rapid solidification and, due to the layer by layer manufacturing manner, thermal cycling of solidified layers.

To understand the final microstructure, one should take into consideration many processes involved in the formation of final microstructure. Firstly, processes happening at the solidification of molten pool and formation of a high-temperature phase (austenite) from the liquid. Then, take into consideration changes in microstructure occurring at rapid cooling of the high-temperature phase. Finally, thermal cycling of already solidified inner regions, taking place due to the layer by layer manufacturing manner. This investigation is dedicated to advanced characterization of stainless steels and Ti alloys manufactured by SLM, using SEM, EDS, TEM, EBSD, APT and XRD methods to gain fundamental understanding of the development of microstructures in ferrous and titanium materials.

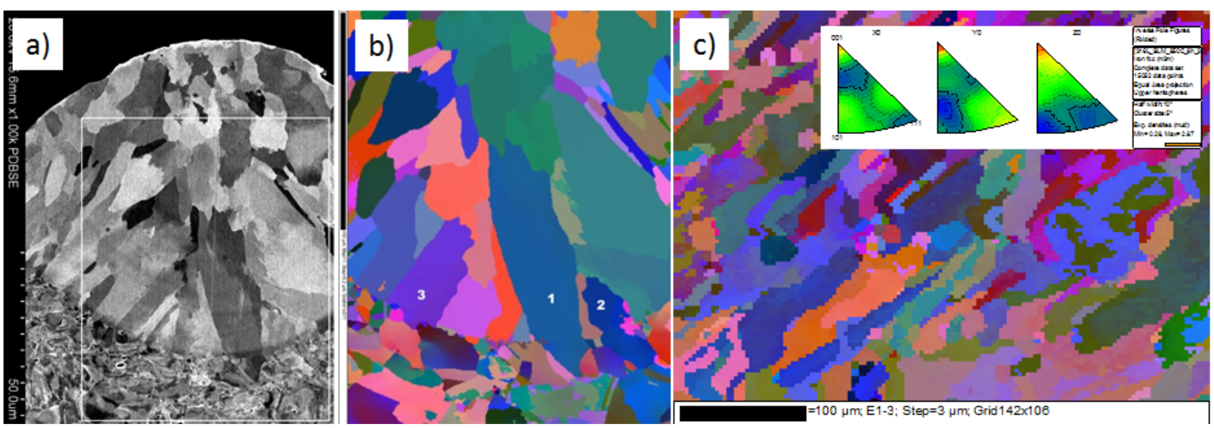

Microstructure of SLM316L, (a) - colonies in the a single track, (b) – EBSD map of fusion boundary, grains 1, 2 and 3 inherited crystallographic orientation from substrate, (c) – EBSD map and inversed pole figures, a transverse cross-section of 3D specimen.

Solidification of materials in SLM manufacturing is relatively similar to processes observed in welding. The solidification is controlled by the solidification rate and thermal gradients. It is shown, with an example of austenitic stainless 316L steel, that cellular crystallization is a typical solidification mode, observed in ferrous, and also in Ni alloys. The microstructure then consists of colonies of cells all of which grow in one crystallographic direction, for cubic crystals in <100> direction. The colonies epitaxially re-nucleate at the solidification front, thus inheriting crystallographic orientations from previous layers. In the competitive crystallization, the preferable crystallization direction is controlled by crystallographic orientations of a colony and the laser movement direction. Therefore, crystallization texture of an austenitic phase could be controlled by a manufacturing strategy, thus providing quasi-isotropic or anisotropic microstructure and mechanical behavior. For Ti alloys a columnar structure is commonly observed in prior beta phase grains, possibly due to the other thermophysical characteristics of the molten pool.

[1] Department of Engineering and Physics, Karlstad University, SE-651 88 Karlstad, Sweden

In materials with solid phase transformations, rapid cooling from the austenitic phase resulted in a formation of martensite as observed for various ferrous alloys and for Ti alloy. In Ti alloys, it usually leads to disappearance of crystallization texture. Then, due to the layer by layer nature of SLM manufacturing, in-situ thermal cycling takes place in situ. It resulted in thermal activation of diffusional processes in the material, which lead to changes in the final microstructure and properties. Due to short time of every cycle these processes are not the same as for instance conventional tempering. In a 420 martensitic stainless steel, thermal cycling resulted in carbon partitioning and formation of a high content of reversed austenite observed by XRD and EBSD methods. Carbon partitioning preferable takes place at cell boundaries, inherited by the martensitic phase from the parental austenite. In Ti alloys thermal cycling resulted in the formation of beta phase and partial transformation of alpha prime martensite to the equilibrium alpha phase.

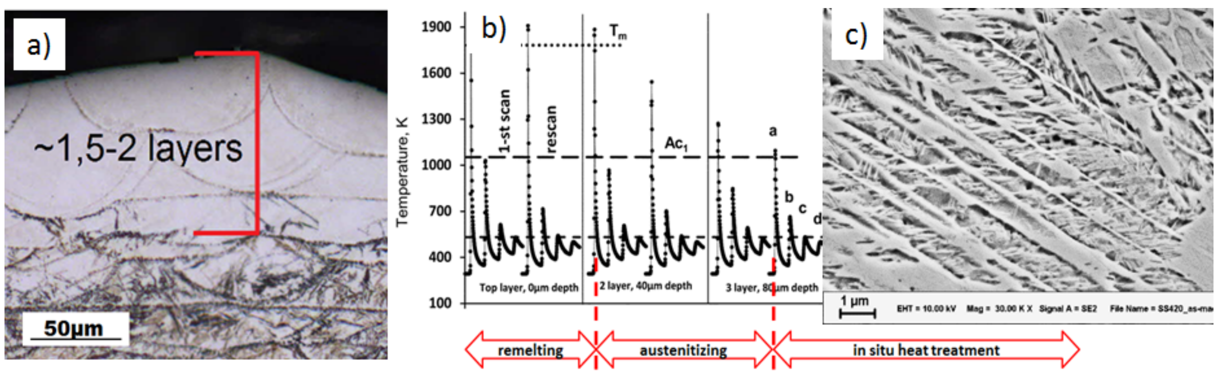

Microstructure of SLM 420, (a) – fresh martensite in the near surface region, (b) – simulated thermal cycling for top 5 layers, (c) – inner region martensitic structure, reversed austenite decorated inherited from austenite phase cell boundaries.

Thermal cycling has a regular effect in the inner regions of manufactured object, but it is different in near surface regions. Due to limited amount of cycles, top layers of martensitic stainless and some tool steels have a fresh martensitic structure. This effect has been reported for many ferrous materials and was observed not only in SLM but also in LMD manufactured tool steels. Simulation of thermal cycles could be used to predict depth of the top martensitic layer, while heat treatment is necessary to obtain regular microstructure in the near-surface regions.

P. Krakhmalev, G. Fredriksson, I. Yadroitsava, N. Kazantseva, A. du Plessis, I. Yadroitsev, Deformation Behavior and Microstructure of Ti6Al4V Manufactured by SLM, Physics Procedia, 83, 2016, 778-788.

P. Krakhmalev, I. Yadroitsava, G. Fredriksson, I. Yadroitsev, In situ heat treatment in selective laser melted martensitic AISI 420 stainless steels, Materials & Design, 87, 2015, 380-385.

Yadroitsev, P. Krakhmalev, I. Yadroitsava, Hierarchical design principles of selective laser melting for high quality metallic objects, Additive Manufacturing, 7, 2015, 45-56.

Yadroitsev, P. Krakhmalev, I. Yadroitsava, Selective laser melting of Ti6Al4V alloy for biomedical applications: Temperature monitoring and microstructural evolution, Journal of Alloys and Compounds, 583, 2014, 404-409.

Yadroitsev, P. Krakhmalev, I. Yadroitsava, S. Johansson, I. Smurov, Energy input effect on morphology and microstructure of selective laser melting single track from metallic powder, Journal of Materials Processing Technology, 213, 2013, 606-613.

15th, 16th and, 17th RAPDASA Annual International Conference, South Africa, 2014, 2015 and 2016;

POWDERMET 2015 section AMPM, 17-20 May, 2015 San-Diego, USA;

26th Annual International Solid Freeform Fabrication Symposium,10-12 August 2015, Austin, Texas, USA;

SFF Symposium 2015 - 26th Annual International Solid Freeform Fabrication Symposium, Austin, Texas USA on 10-12 August 2015;

MS&T2015-Materials Science & Technology 2015, 04 October 2015 – 08 October 2015, Columbus, USA;

[1] Department of Engineering and Physics, Karlstad University, SE-651 88 Karlstad, Sweden

25th International SAOT Workshop on Laser Based Additive Manufacturing, November, 23 – 24, 2015;

9th International Conference on Photonic Technologies, September, 19-22, 2016;

[1] Department of Engineering and Physics, Karlstad University, SE-651 88 Karlstad, Sweden

Stephan Ziegler[1], Jan Bültmann[2], Dr.-Ing. Simon Merk[3]

Lightweight construction by lattice structures made of steel – mechanical properties and freedom of design

Abstract

The qualification of lattice structures for custom part properties is performed on two different types of structures: type f2cc,z, and hollow-sphere structures. Different laser exposure strategies and their influence on the microstructure and mechanical properties of the lattice structures are examined experimentally. The development of scaling laws is based on a large number of different types and configurations of lattice structures (e.g., the specific energy absorption in dependence of the cell width of the structures). Based on these results, a design methodology is proposed that systemizes the process of designing function components with custom part functions by integrating lattice structures to functional components.

Keywords

Selective Laser Melting (SLM), lattice structures, stainless steel, mechanical properties, fatigue behaviour, design freedom.

1. Introduction

The integration of lattice structures in functional components is one of the most promising approaches to exploit the full technology potential of the SLM process. The main advantages of cellular materials are a great stiffness to weight ratio and great energy absorption and damping capabilities. Beside these advantages process time can be reduced by substituting solid material by lattice structures in areas of lower stress. Moreover SLM allows to modify the part functions e.g. stiffness locally by an adjustment of the geometric parameters of the lattice structures.
Depending on the stress or on particular functions of part areas, lattice structures are substituting solid material. This combination of lattice structures and solid material results in extreme lightweight parts with customized part functions, which cannot be built by conventional manufacturing technologies such as casting or cutting. The main challenges in designing these type of customized parts are the intricate modelling of the macroscopic behaviour, the mostly unknown mechanical properties and the absence of a design methodology for components with customized part functions. Therefore, especially the compression and fatigue behaviour provides a great potential of functional integration for components.

2. State of the Art

1 RWTH Aachen University, Chair for Laser Technology LLT
2 RWTH Aachen University, Department of Ferrous Metallurgy
3 Trumpf Laser- und Systemtechnik GmbH

Several researchers are investigating the unique capability of manufacturing lattice structures with SLM [3] [4] [5] [6] [7] [8]. The overall goal to effectively make use of the unique properties of lattice structures in real parts is illustrated in Fig. 1.

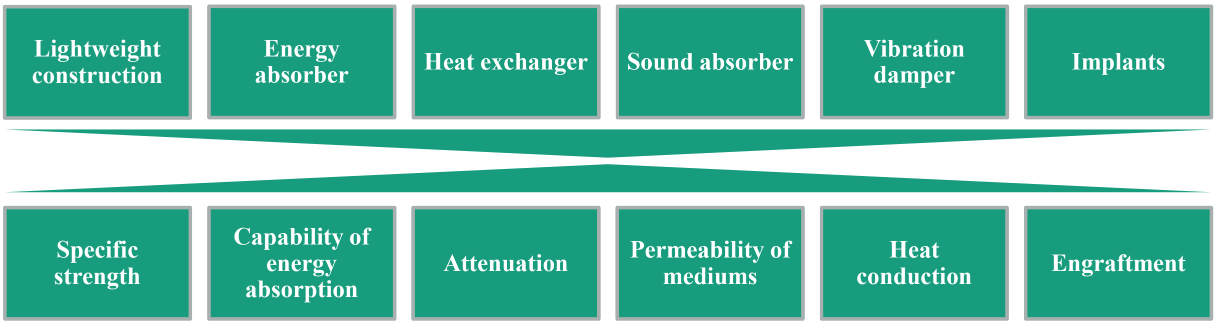

Figure 1: Applications and derived part functions of cellular material

Depending on the stress or on particular functions of part areas, lattice structures are substituting solid material. This combination of lattice structures and solid material results in extreme lightweight parts with customized part functions which cannot be built by conventional manufacturing technologies such as casting or cutting. The main challenges in designing these type of customized parts are the intricate modelling of the macroscopic behaviour, the mostly unknown mechanical properties and the absence of a design methodology for components with customized part functions.
Rehme [3] investigated the properties of cubic lattice structures into detail and suggests a classification in analogy to crystallography (see Fig. 2). To manufacture these types of structures Rehme introduces the so called point-like exposure, a special scanning strategy. Structure types with horizontal struts are not considered by Rehme due to the overhang restriction of SLM process. In his research various lattice structure blocks with a constant strut diameter of approx. 500 µm are manufactured in different relative densities. The relative density of the cell types is varied by different cell widths from 1.5 to 6 mm. The mechanical properties of the lattice structures are determined in tensile, compression and shear tests. If one considers the specific mechanical properties (MPa per kg), structure type f2cc,z shows the overall best performance of all structure types. [3]

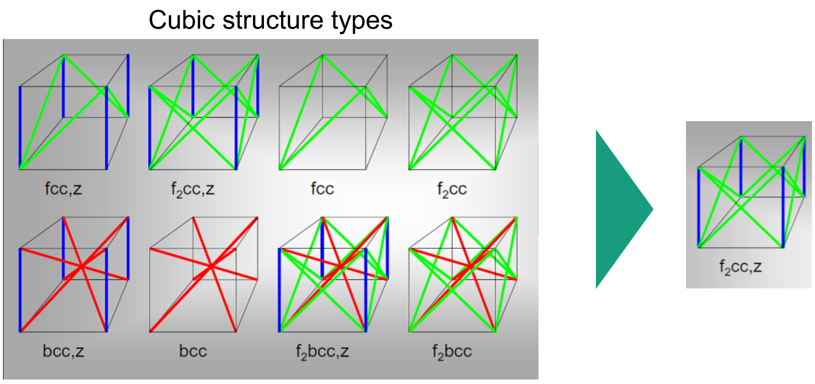

Figure 2: Classification of cubic lattice structures according to Rehme [3]

One need to consider that this structure type shows a highly anisotropic behaviour and may not be built in any build-up direction. Nevertheless cubic lattice structures are the most investigated type of lattice structures and first scaling laws to describe the mechanical properties of these structure in dependence of geometric parameters are developed by Rehme

1 RWTH Aachen University, Chair for Laser Technology LLT
2 RWTH Aachen University, Department of Ferrous Metallurgy
3 Trumpf Laser- und Systemtechnik GmbH

et al. The functional behaviour of lattice structure can usually be described in good accordance to the following exponential equation [3]:

$$\frac{K^*}{K_{solid}} = C * \left(\frac{\rho^*}{\rho_{solid}}\right)^n; \quad (2.1)$$

K^*: *Property of cellular material;*
K_{solid}: *Property of solid material;*
C: *Constant of proportionality;*
ρ^*: *Density of cellular material;*
ρ_{solid}: *Density of solid material.*

The lack of scaling laws to describe the mechanical properties of lattice structures, the absence of isotropic structure types and the limited understanding of the influence of different scanning strategies on the mechanical properties currently hinder the further distribution of lattice structure designs.

3. Qualification of Lattice Structures Manufactured by Selective Laser Melting (SLM)

The qualification of lattice structures for custom part properties is performed on two different types of structures. To continue and extend the research on structure type f2cc,z, research on the influence of different scanning strategies on the mechanical properties of this type of anisotropic structure are carried out. To complement the research with a more isotropic structure, a hollow-sphere structure is developed considering the main restrictions of the SLM process. The hollow-sphere structure is composed of a hollow-sphere with a predefined wall thickness and diameter. To remove the un-molten powder, every sphere contains four little holes. The spheres have a defined overlap of usually 5% of the diameter. This guarantees the stable connectivity of the spheres. The holes of the inner spheres form little channels to enable a smooth removal of the powder through the outer spheres. The examined structure types and their main geometric parameters are illustrated in Figure 3. The aggregated parameter relative density is the most common parameter to allow a comparison of the mechanical properties of different structure types and the most common input parameter for the scaling laws.

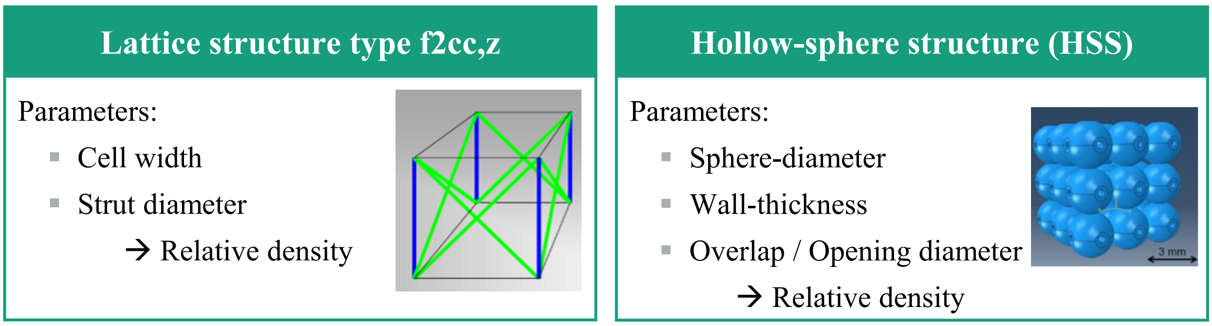

Figure 3: Examined structure types and main geometric parameters [10]

There are two ways to manufacture cubic lattice structures by SLM: Point-like exposure and contour-hatch exposure. At the point-like exposure single points are exposed with laser radiation. Layer by layer only single points are exposed until the final lattice structure is build.

[1] RWTH Aachen University, Chair for Laser Technology LLT
[2] RWTH Aachen University, Department of Ferrous Metallurgy
[3] Trumpf Laser- und Systemtechnik GmbH

The size of the strut diameter is determined by exposure time at the single points and the melt pool propagation, which is determined by the material properties. Very small structures can be built by this exposure style. The main advantages of this scanning strategy are the reduction of process time and reduced amount of machine data. The complex geometry of lattice structures is fractionized into a set of points that causes only little amount of machine data. Currently the PL exposure is not a machine standard in most of the industrial systems, which restrain the further distribution of this type of scanning strategy.
The second scanning strategy, which is used to manufacture lattice structures by SLM, is the conventional Contour-Hatch exposure. In contrast to the Pointlike exposure, the contour of the single struts is scanned with a little offset to consider the melt pool propagation. The inner volume of a strut is filled by so called hatch vectors. The main advantages of the Contour-Hatch scanning strategy are the freedom of geometries, which can be manufactured by this machine standard scanning strategy. In opposition to the Pointlike exposure, contour-hatch exposure is not limited to lattice structures and can be used for more volumetric geometries. The contour scan usually leads to better surface quality of the manufactured specimens. A disadvantage of this scanning strategy is the relatively high process time which is caused by the high number of scanning vectors and scanner delays that appear during the scanning of e.g. round contours. The investigated scanning strategies are illustrated in Fig. 4 with their main advantages and disadvantages.

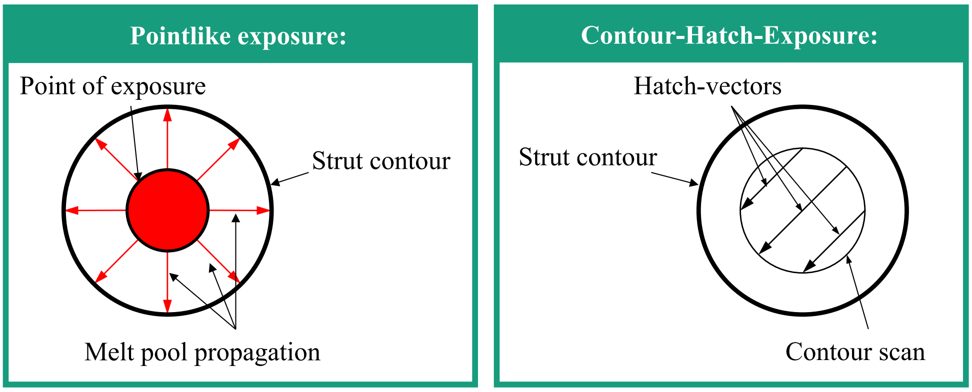

Figure 4: Investigated scan strategies for the manufacture of lattice structures [10]

To investigate the influence of different scanning strategies on the mechanical properties of lattice structures, blocks of lattice structures (10 x 10 x 15 unit cells, type f2cc,z) are built with both Pointlike exposure and Contour-Hatch exposure. Before the mechanical tests, the process parameters of both scanning strategies are optimized regarding material density and geometric deviation from the CAD model. Three Contour-Hatch parameters (CH1-3) are choosen which result in a material density higher than 99,90 % and geometric deviations smaller than 5%. For the Pointlike exposure one parameter set is choosen (PL). Quasi-static compression tests are carried out according to DIN EN ISO 50134 [9] to compare the mechanical response of lattice structures manufactured by different scanning strategies. The results of the compression tests can be found in Fig. 5. If one compares the stress-strain curves of the specimens manufactured with different scanning strategies, it is clearly visible that the specimens manufactured by Pointlike exposure are less resistant against compressive loads.

1 RWTH Aachen University, Chair for Laser Technology LLT
2 RWTH Aachen University, Department of Ferrous Metallurgy
3 Trumpf Laser- und Systemtechnik GmbH

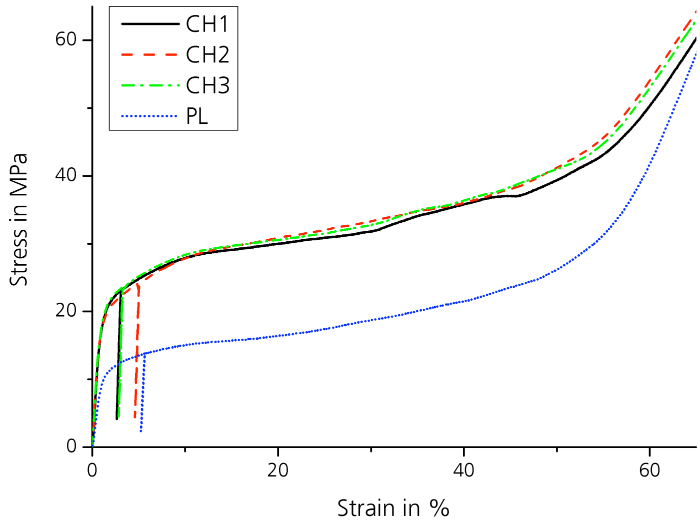

Figure 5: Comparison of stress-strain curves for specimens manufactured by different scan strategies [10]

The specimens manufactured by Contour-Hatch exposure outperform the Pointlike exposed specimens in terms of stiffness, yield stress R_{p1} and specific energy absorption E50 (see Table 1).

Table 1: Comparison of the main properties of lattice structure under compressive load [10]

Property	CH1	PL
Stiffness m [MPa]	4318	2695
Yield stress Rp1 [MPa]	20,07	10,05
Specific energy absorption E50 [mJ/mm³]	16,01	10,04

The stiffness of the Contour-Hatch specimens is about 37%, the Yield stress R_{p1} about 50% and the Specific energy absorption E50 about 37% higher than the Pointlike exposure specimens.
The reason for these differences can be found by investigating the microstructure of the lattice structures. Therefore EBSD-analysis are carried out that allow a detailed look on the crystalline structure and the size and orientation of the grains. The EBSD results show that both specimens exhibit the same gamma phase austenite. Differences can be found in the grain size and orientation. The Pointlike exposure specimens are composed of columnar grains and larger diameters, which are orientated towards the build-up direction. The Contour-hatch exposure specimens exhibit a random and stochastic distribution of grains with smaller diameters. No clear orientation of the grains is visible. (see Fig. 6)
The reason for the different microstructures can be found in the way how laser energy is deposited into the powder bed. The cooling-down rate for the Pointlike exposure specimens is much lower than for the Contour-Hatch exposure specimens, giving the material more time to form larger grains with a specific orientation. Another reason is the repeating remelting of

[1] RWTH Aachen University, Chair for Laser Technology LLT
[2] RWTH Aachen University, Department of Ferrous Metallurgy
[3] Trumpf Laser- und Systemtechnik GmbH

already exposed layers due to a quite long exposure time at single spots at the Pointlike exposure.

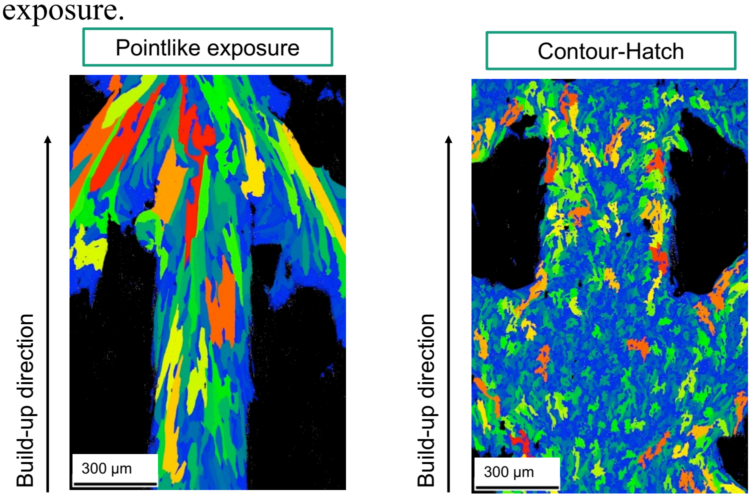

Figure 6: Investigation of grain size and orientation of lattice structures manufactured by different scanning strategies [10]

In general smaller grains lead to better mechanical properties than larger grains. This correlation can be transferred to the lattice structures and explain why Contour-Hatch specimens show better results than Pointlike exposed specimens regarding the mechanical response under compressive load. These results lead to the conclusion that Contour-Hatch scanning strategy is more suitable for the manufacturing of lattice structures with SLM.
To manufacture the hollow sphere structure, the Contour-Hatch scanning strategy needs to be applied due to the more volumetric design of hollow-spheres. Again, specimens are manufactured to carry out quasi-static compression tests according to DIN EN ISO 50134. Fig. 7 shows stress-strain curves of three samples from the same test series. All samples exhibit a wall thickness of 250 µm and a constant diameter of 3 mm. The reproducibility of the stress-strain curves within the test series is given. (see Fig. 7)

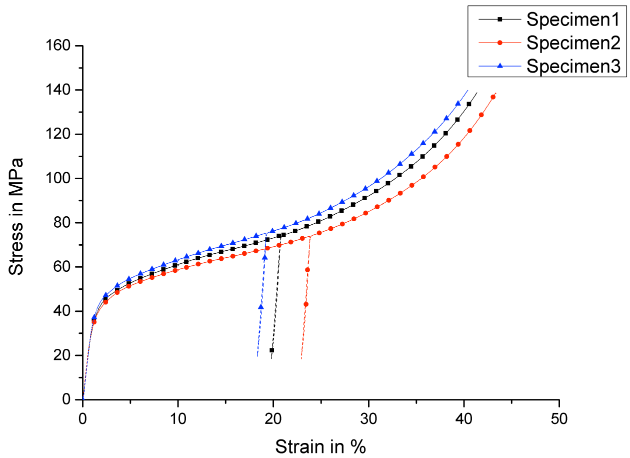

Figure 7: Exemplary stress-strain diagram for hollow-sphere structures with a wall thickness of 250 µm [10]

One of the main advantages of cellular materials is the adjustment of mechanical properties through the modification of geometric parameters of the structures. Fig 8 shows the influence of different wall thicknesses from 250 – 350 µm on the stress-strain curve of hollow-sphere

1 RWTH Aachen University, Chair for Laser Technology LLT
2 RWTH Aachen University, Department of Ferrous Metallurgy
3 Trumpf Laser- und Systemtechnik GmbH

structures. The stiffness, yield strength and specific energy absorption can be adjusted by the wall thickness of the hollow-sphere structures.

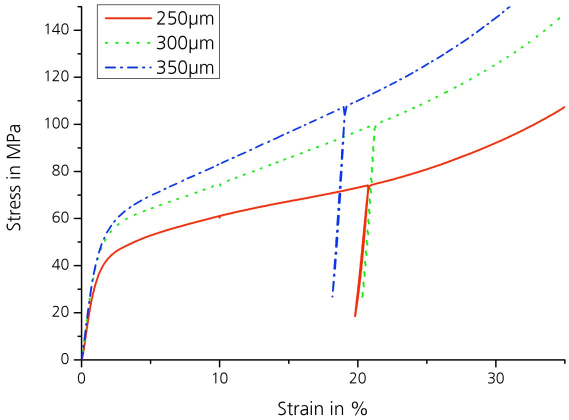

Figure 8: Stress-strain diagram of hollow-sphere structures with different wall thicknesses [10]

Another test series was built to investigate the influence of the build-up direction on the mechanical properties of the hollow-sphere structure. Therefore hollow-sphere specimens were built in a lying and standing position on the substrate plate.

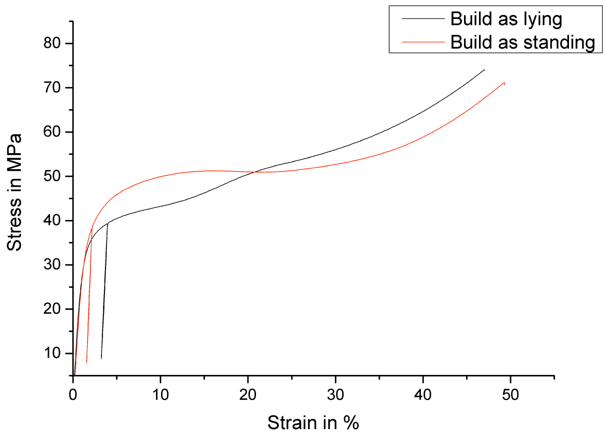

Figure 9 Stress-strain diagram of hollow-sphere structures build in different directions [10]

To validate the isotropy of the hollow-sphere structures, specimens in two build-up direction are built and tested under compressive load. In Fig. 9 the stress-strain curve of these specimens are illustrated. The stress-strain curves do not exactly follow the same route. Compared to the anisotropic cubic lattice structures, the hollow-sphere structure can be seen as quasi-isotropic in the two investigated directions. The reason for the deviations of the course of the lying and standing specimens can be found in the orientation of metallurgical faces inside the specimen's microstructure. For the lying samples the compression direction is aligned to the metallurgical faces which supports shearing along these faces. This results in a lower resistance against compressive loads and an earlier yielding and a lower stiffness of lying specimens (see Fig. 9). For the standing samples the metallurgical faces are orientated perpendicular to the compression direction. This results in a higher resistance to the compressive loads.

[1] RWTH Aachen University, Chair for Laser Technology LLT
[2] RWTH Aachen University, Department of Ferrous Metallurgy
[3] Trumpf Laser- und Systemtechnik GmbH

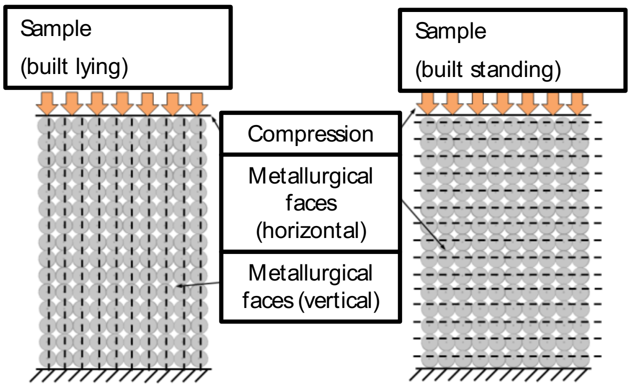

Figure 10 Orientation of metallurgical faces for lying and standing samples [10]

The next step to qualify lattice structures for custom part properties is the development of scaling laws based on a large number of different types and configurations of lattice structures. Therefore a large amount of lattice structures of type f2cc,z and hollow-sphere structures are built. Fig. 11 shows an exemplary scaling law of a lattice structure of type f2cc,z for the Specific energy absorption E50 in dependence of the cell width of the structures. Lattice structures with cell widths from 1,5 to 5 mm were built. To achieve a greater stiffness and energy absorption the lattice structures are covered with skins of a thickness of 250 µm. Two groups of structures exist: one with only vertical skins (V) and one with vertical and horizontal skins (VH). The course of the stress-strain diagram of VH structures is given in Fig. 11. As one can see the Specific energy absorption is decreasing with increasing cell widths. The strut diameter is fixed in this experiment and as a consequence the relative density is decreasing with increasing cell widths resulting in a lower energy absorption. Moreover Fig. 11 shows that the specific energy absorption is scalable over a broad range from 180 mJ / mm³ to below 10 mJ/mm³. Depending on the application the specific energy absorption can be customized through a variation of the cell width, respectively relative density. The red line in Fig. 11 shows the Fit for scaling law with power laws. The quality of the Fit for scaling law is very high with a Cor.R2 of larger than 99%. The scaling law can be used to determine the suitable structure configuration for specific applications, also between the experimental determined values.

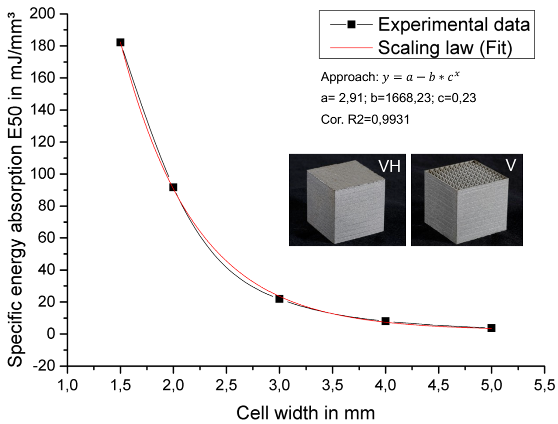

Figure 11 Exemplary scaling law for specific energy absorption in dependence of cell width of lattice structures (type f2cc,z with skins)

1 RWTH Aachen University, Chair for Laser Technology LLT
2 RWTH Aachen University, Department of Ferrous Metallurgy
3 Trumpf Laser- und Systemtechnik GmbH

The benefit of scaling laws to find an appropriate set of structures will be discussed in the following for a crash box example. In formula student competitions there are clear guidelines for the designing of a crash box. The energy that needs to be absorbed is 7350 J. The deceleration must be lower than 20 g to avoid serious damages to the driver. To determine a structure configuration that enables the absorption of exactly 7350 J, the scaling law "Absorbable Energy" can be used. For different strain rates this scaling law is illustrated in Fig. 12 for a lattice structure of type f2cc,z. Depending on the strain rate, three different cell widths are capable to absorb the necessary amount of energy of 7350 J. The strain defines the deceleration distance which is important to fulfil the requirement of a deceleration lower than 20 g. For 50 % strain a cell widths of 4,1 mm is capable to absorb the necessary energy. The length of the structure, respectively the number of unit cells in impact direction, must be chosen to guarantee a deceleration lower than 20 g. A structure with a length of approx. 200 mm could fulfill this requirement.

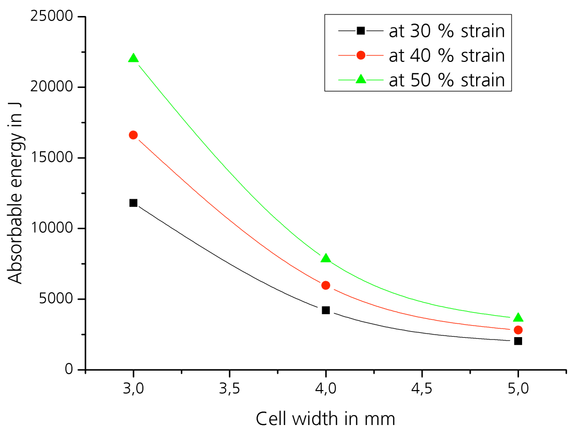

Figure 12 Scaling law "Absorbable Energy" of structure type f2cc,z for different strains

Finally, based on these results a design methodology (see Fig. 13) is proposed that systemizes the process of designing function components with custom part functions by integrating lattice structures to functional components.

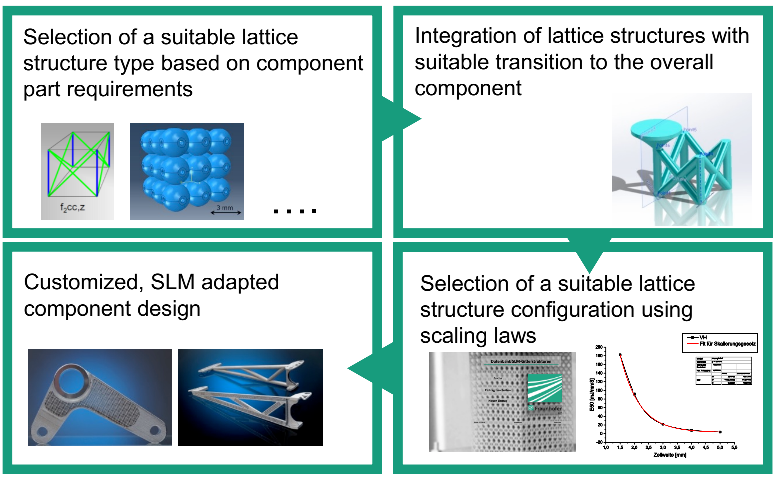

Figure 13 Methodology for component design with customized component functions

The design methodology consists of four steps. The first step is the selection of a suitable lattice structure type depending on the application. For some applications, like the above

[1] RWTH Aachen University, Chair for Laser Technology LLT
[2] RWTH Aachen University, Department of Ferrous Metallurgy
[3] Trumpf Laser- und Systemtechnik GmbH

discussed crash box, a more anisotropic structure is needed. For other light-weight applications a more isotropic structure like the hollow-sphere structure might be useful. The second step is the integration of the lattice structures with a suitable transition to the overall component design. The third step is the selection of a suitable lattice structure configuration using scaling laws. The structure database supports the design engineer during this process. Last is the assembly of the lattice structure to a customized, SLM adapted component design.

References

[1] Ashby MF. The properties of foams and lattices. Philosophical Transactions of the Royal Society A: Mathematical, Physical and Engineering Sciences 2006;364(1838):15-30.

[2] Gibson LJ, Ashby MF. Cellular Solids, Structure and properties. 2nd ed.: Cambridge University Press; 1997. ISBN: 0 521 49911 9.

[3] Rehme O. Cellular Design for Laser Freeform Fabrication [Dissertation]. Hamburg: Technische Universität Hamburg-Harburg; 2009. 302 // XXII, 273 S.

[4] Rehme O; Emmelmann C, editors. Cellular Design for Laser Freeform Fabrication; iLAS; 2007. 6 p.

[5] Rehme O. Additive Manufacturing zellularer metallischer Strukturen. Deutsche Gesellschaft für Materialkunde e.V.; 11.05.2011. 29 p.

[6] Gümrük R, Mines R. Compressive behaviour of stainless steel micro-lattice structures. International Journal of Mechanical Sciences 2013;68:125-39.

[7] Shen Y, Cantwell WJ, Mines RA, Ushijima K. The Properties of Lattice Structures Manufactured Using Selective Laser Melting. AMR 2012;445:386-91.

[8] Hao L, Raymont D, Yan C, Hussein A, Young P. Design and Additive Manufacturing of Cellular Lattice Structures 2011.

[9] DIN. Prüfung von metallischen Werkstoffen – Druckversuch an metallischen zellularen Werkstoffen; 2008(50134).

[10] Merkt, S. Qualifizierung von generativ gefertigten Gitterstrukturen für maßgeschneiderte Bauteilfunktionen. Dissertation RWTH Aachen. 2015

1 RWTH Aachen University, Chair for Laser Technology LLT
2 RWTH Aachen University, Department of Ferrous Metallurgy
3 Trumpf Laser- und Systemtechnik GmbH

ALEXANDER WALZL[1], BRUNO BUCHMAYR[1]

TOPOLOGY OPTIMISATION – DESIGN TOOL FOR FUTURE MANUFACTURING METHODS

Abstract

The current paper investigates the advantages and disadvantages of the commonly used optimisation methods (topology, topography, size and shape). Further the importance of lattice structures is analysed and highlighted. Referring to the screening of the optimisation methods the benefit of them, regarding additive manufacturing, is emphasised. Additive manufacturing means not only design freedom, there is also a paradigm shift from manufacturing-driven design to design-driven manufacturing.

Keywords

Additive manufacturing, DMLS, SLM, topology optimisation, shape optimisation, size optimisation, lattice structures, bionic structures, powder bed fusion, relative density, Hyper Works

1. Introduction

Light weight design using topology optimisation is a very smart way to develop new parts with a high value of economy. The most commonly used optimisation target is mass reduction. The weight influences the costs of operation of the part. Accelerated mass needs a lot of kinetic energy. This topic is very important for the automotive industry, trucks, subways and for aerospace components. This paper summarises the advantages of the classical optimisation method for the additive manufacturing technology with respect to the production of light and stiff parts. The additive manufacturing method supports very complex geometries, which is therefore best suited for topology optimised structures. By combining material, topology optimisation and additive manufacturing energy resources can be saved, which leads to financial benefits in all phases of lifetime.

2. Optimisation methods

The field of optimisation ranges from a sparse shape change to a total reconstruction of a part. Commonly used optimisation technologies can be divided into four significant groups, like topography, topology, shape and size optimisation.

[1] Chair of metalforming, Montanuniversity of Leoben, 8700 Leoben, Austria

2.1 Topography optimisation

The basic intention of topography optimisation is the reformation of the surface area of sheet metal parts. The basic strategy of the algorithm is the enlargement of the cross-sectional moment of inertia by adding several kinds of beads that increase the stiffness of the whole construction [1, 2]. With this technology it is possible to build very stiff structures just by using sheets of the desired material. To show the enlargement of stiffness of plane sheet metals, a simple topography optimisation using the commercial software HyperWorks from Altair is demonstrated.

A simple plane sheet metal (20x20mm) is loaded by one concentrated force (10N) in one corner. Others are restricted by non-movement and non-rotational conditions. The plane bending result shows a maximum displacement of about 0.98mm. Next step was the preparation of the model for topography optimisation. Optimisation problems always need response parameters, design constraints and several kinds of objective functions. Only with these parameters the optimisation can be finished successfully. In the case of topography optimisation we need at least two design responses (total static displacement and compliance), one design constraint (displacement < 0,05mm) and one objective (minimize the compliance to maximize the stiffness). In addition to those parameters two diagonal symmetry conditions are added to the model. The resulting topography is shown in Fig. 1.

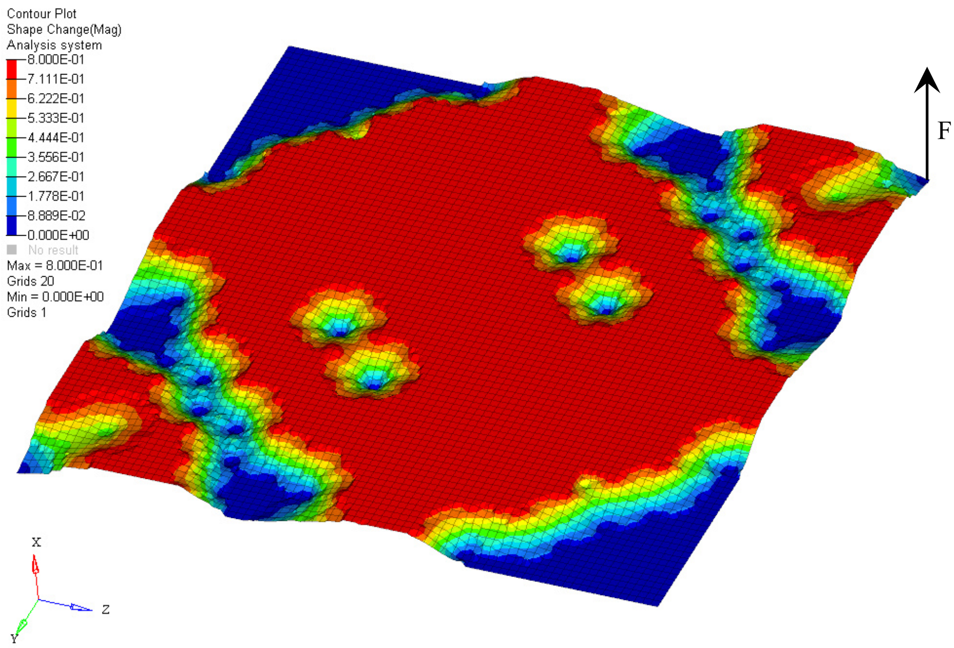

Fig. 1: Optimised sheet metal by topography optimisation regarding bending by a concentrated force (other corners fixed) with two planes of symmetry.

The geometrical adaption results in a reduction of the maximum displacement of approximately 56% (from 0.98mm to 0.43mm).

2.2 Topology optimisation

After the topography optimisation the topology optimisation is the most important technology to implement lightweight aspects during the development of parts. Compared to topography optimisation the topology optimisation generates light and stiff bulky parts. One of the best known topology optimisation algorithms is the soft kill option (SKO) by C. Mattheck [3, 4].

$$E_{n+1} = E_n + k\left(\sigma_n - \sigma_{ref}\right) \quad \textbf{Eq. 1}$$

This method provides a solution of a stiff geometry based on a bulk material. After each iteration step the difference of local Young's modulus will be increased by the algorithm (Eq. 1). By this, the difference became larger and larger. At the end of the optimisation a strict divided structure (Fig. 2) is generated [4].

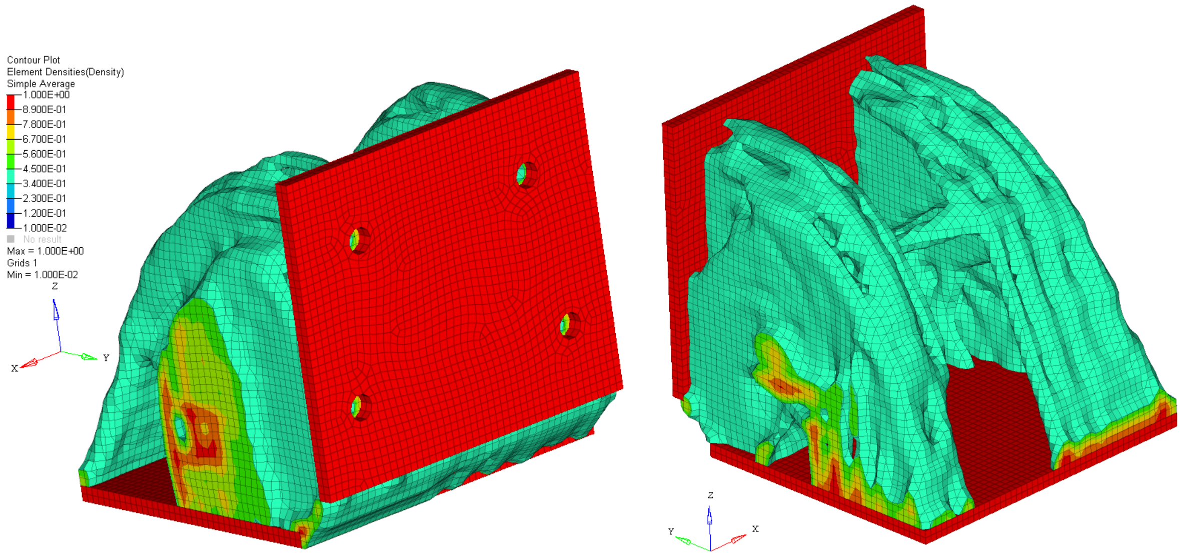

Fig. 2: Topology optimised bracket with strut diameter and stress constraint (different forces applied on the mounting plate with a fixed-constraint on the whole bottom plate lower surface) – Young's modulus of the empty space is zero.

The resultant structure is very close to the shape of branches or roots of trees. The basic functionality of topology optimisation is the determination of the stressed areas and generation of strut structures around them. The minimum and maximum strut size depends on the initial parameter of optimisation. It is possible to specify the resultant geometry and the desired material by adding some stress restrictions to the optimisation task.

2.3 Size and shape optimisation

The next optimisation technology is called size or free-size optimisation. With this method it is possible to adjust a given structure by thickening of struts, walls or body-sections. This optimisation generates the major benefit, if it is performed after the topology optimisation. Further it is a useful tool to generate stress dependent lattice structures. Additionally, algorithms to smooth sectional changes or edges are necessary. In this way, notch factors can be reduced tremendously (Fig. 3) [4, 5].

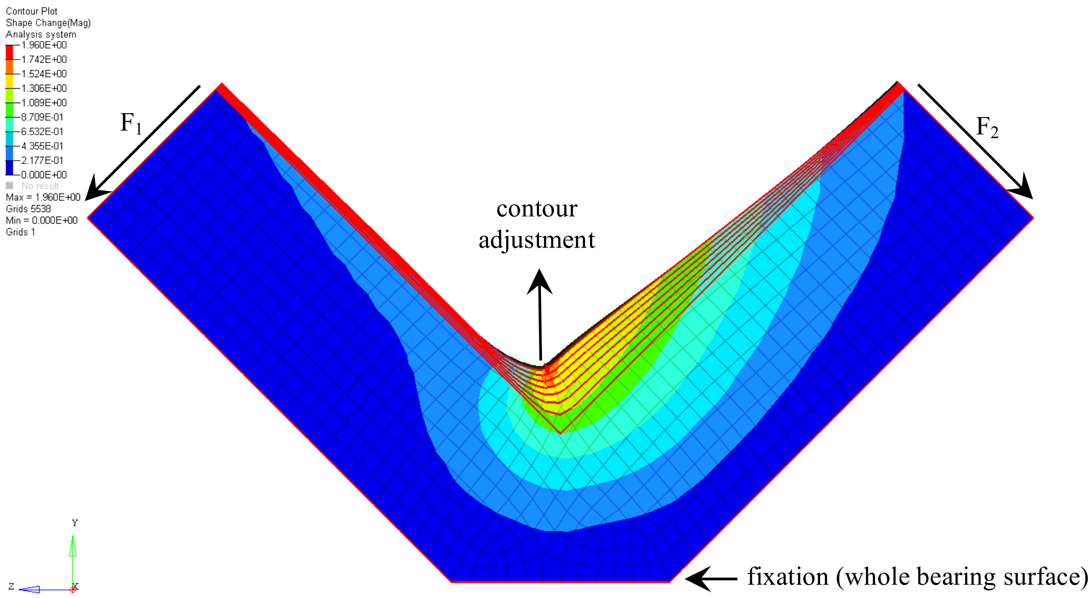

Fig. 3: Shape optimisation – ease of a critical edge. Red highlighted lines represent several iteration steps to minimise the maximum stress in the edge (F_1<F_2).

By the help of shape optimisation it is possible to ease this critical area [6]. The same method of reducing notch stress, can be seen in the nature. Some bionic design concepts are based upon the minimising of stress (energy). A further example is the chance of growth rate of bones under loads. The cross sectional density of human trabecular bones shows an irregular open cell structure with different strut thicknesses. Areas with high stresses tend to thicker struts while areas with low stresses show thinner struts. This natural design method allows the bone to be light and stiff enough. This biological principle is also self-adjusting, which provides optimal safety conditions.

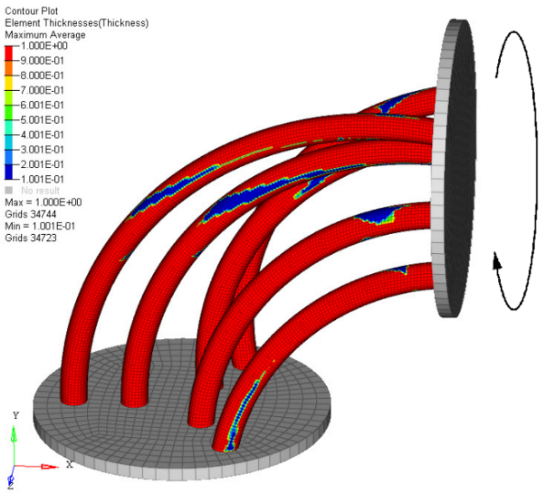

Fig. 4: Size optimisation of pipes with a torsion load. The thickness of the pipes (initial thickness 1mm) are adjusted by the existing stress.

A 3D pipe-construction (Fig. 4) loaded by a moment generates a complex derivation of stress in the part. During the size optimisation the right diameter of the pipes is determined. The result is a design proposal with a distribution of the pipe wall-thickness. These four optimisation methods (topology, topography, size and shape optimisation) are the basic tools to develop new products for light weight requirements as well as for minimizing the waste of expensive natural resources.

2.4 Lattice optimisation

The automated lattice optimisation is a quite novel technology to implement lightweight design. The basic function of this technology is the substitution of the previously generated mesh by many bars. Altair's HyperWorks [7] provides different types of lattice structures for example tetrahedral, cubic, pyramidal and pentahedral element cell type. Since HyperWorks 13 the rough Young's modulus of these cells is calculated by equation Eq. 2.

$$E = E_0 * \rho^P \qquad \textbf{Eq. 2}$$

The parameter "P" represents the density sensitivity of the lattice structure and controls the generation of the relative density distribution. The calculation of the mechanical properties of arbitrary cell structures are developed by L. Gibson and M. Ashby [8, 9].With the relative Young's modulus it is possible to feed the algorithm and press the optimisation iteration ahead. In addition to the calculation of the Young's modulus it is necessary to perform the calculation of the lattice cell stress. The resultant lattice stress is finally calculated by an average of all affected element nodes. A second parameter has been implemented for little adjustments in the equation (Eq. 3).

$$\sigma_N = \left[\frac{1}{n}\sum_{i=1}^{n}\left(\frac{\sigma_i}{\sigma}\right)^k\right]^{\frac{1}{k}} \qquad \textbf{Eq. 3}$$

This is the first step into the right direction of generating lattice structures. However, these methods contain also a disadvantage depending on the lattice generation mechanism. The lattice structure can only be generated along existing (FEM-)mesh nodes. Only a mesh dependent (with stress constraint) and not a perfect stress dependent solution (e.g. trabecular growth) can be developed (Fig. 5).

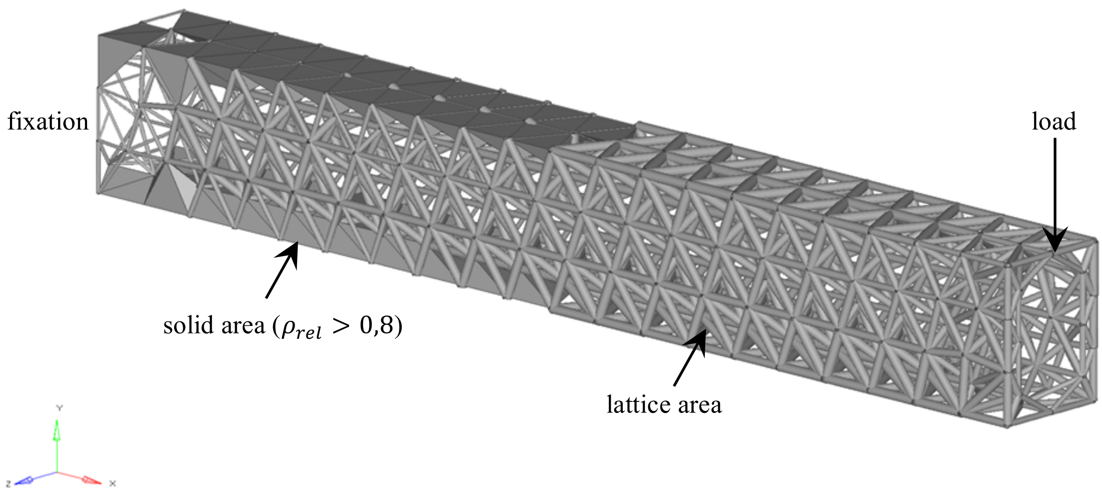

Fig. 5: Optimised cantilever beam (topology and lattice), lattice generation limits $0,2 < \rho_{rel} < 0,8$. Areas with a relative density lower 0,2 are deleted. Areas with a relative density higher than 0,8 are solids. The relative density is realised by different strut diameters.

One sample for lattice generation is provided by Autodesk [10] or Materialise [11]. Autodesk's solution regarding bionic structures is "Autodesk Within". This is a tool designed for additive manufacturing requirements. It is possible to generate load dependent bionic lattice structures with variable strut thicknesses. It is also possible to optimise only the surfaces of products. This case of optimisation is useful to generate porous surfaces on several kinds of implants. The medical industry uses additive manufacturing for years to build dental prosthesis and bone segments made of titanium (Ti-64). For a good intergrowth between bone and implant it is necessary to generate a high specific surface area with a high roughness. This is one of the application fields of additive manufacturing technology - manufacturing of very complex, thin and irregular structures.

3. Optimisation parameters

Every optimisation method needs specific optimisation parameters in order to be successful. Therefore, the next step during the product development is to define the optimisation target. Should the product be stiff against bending, tension or torsion or is there another target to fulfil?

Tab. 1: Method dependent optimisation parameters

No.	OPTIMISATION METHOD	SCOPE OF APPLICATION	OPTIMISATION PARAMETERS
1	topology	• bulky solids and sheet metals • structure roughness depends on the used mesh (hex/quad vs. tet/tria) • subsequent machining necessary • gives possible proposals of the design	• fraction of volume/weight/mass • compliance / stiffness • displacement • stress, strain • fatigue • …
2	topography	• sheet metals only • increase of the moment of inertia • only for out-of-sight surfaces (because of beads) • increase of the stiffness without material addition	• localised or global stress/strain • adjustment boundaries (upper and lower limit) • symmetry (1-plane, 2-plane, cyclic, …) • depth and width of beads
3	shape	• bulky solids (surface) • adjustment of the surface depending on the load onset • reduction of critical areas primary • useful for abrupt geometry change	• localised stress or strain • notch stress • adjustment boundaries (upper and lower limit)
4	size	• sheet metals and composites • optimisation of the sheet thickness • stress dependent	• stress/strain • sheet thickness • composite thickness • frequency
5	lattice	• bulky solids • development of lattices depending on the existing mesh • further lightweight possibility • arbitrary cell structures possible • open/closed cells • structured → lattice • non-structured → foam	• stress dependency • thickness of struts • mesh size (cell size = element size) • mesh type (hex/quad vs. tet/tria) • relative density (upper and lower limit) • increments between density limits (P-value → high, med, low) • sensitivity of normalised stress (k-value)

The result of the data, shown in Tab. 1, indicates that an engineer must be very carefully during the selection of optimisation parameters. Only the right parameters result into a good optimisation proposal. Further it is necessary to take a look on the manufacturability of the resultant optimisation shape. Some topology optimised designs are not fabricable by common manufacturing technologies. In that case the additive manufacturing takes the leadership. By additive manufacturing very complex geometries are producible.

4. Benefit for additive manufacturing

To retrieve a product with a very high functionality it is necessary to combine some of the afore mentioned optimisation methods. For example the lattice optimisation uses topology and size optimisation. The topology optimisation method evaluates the geometry regarding material performance. It will detect high and low stress areas in the whole volume. After that, the low stress areas will be replaced by previously selected lattice structures. The final step is the calibration of the strut thicknesses (as shown in Fig. 5). A topology and size optimised part is the result of these calculations. However, the generated shape of the optimised part looks very complex. The common manufacturing technologies are not able to produce this kind of complex shape. Only the additive manufacturing provides a new possibility to produce the resultant optimised shape. Additive manufacturing is characterised by its specific process. The product is sliced by specific software packages into several cross-sectional layers. During the additive manufacturing process each layer of the sliced part will be exposed by the laser to melt the material (metal powder). After several iterations the whole part will be generated by the layer-by-layer process [12, 13].

Similar to common manufacturing technologies, the additive manufacturing is restricted by specific manufacturing constraints. These manufacturing constraints should be considered during the development and construction process of new products. The design draftsman should know the manufacturing constraints and the design possibilities of this technology. The standardisation of the additive manufacturing process is currently under development by the VDI institution (VDI 3405) and by ASTM. In the first draft of the standardisation sheet, they consider several known design rules for the correct design for additive manufacturing. Design rules such as limitations regarding overhang and sloped walls or diameters of horizontal holes. Furthermore, there are two density measurement procedures defined to determine the relative density (porosity) of the printed part. The first is the density measurement according to the principle of Archimedes (Eq. 4).

$$\rho_{rel} = \frac{m_{air} * (\rho_{H_2O} - \rho_{air})}{\rho_{Al} * (m_{air} - m_{H_2O})} + \frac{\rho_{air}}{\rho_{Al}} \qquad \textbf{Eq. 4}$$

To calculate the relative density it is necessary to determine the weight of the part underwater and the weight of the part in the air. The density of water, air and in this case aluminium are tabular values and temperature dependent. Therefore the measurement of the water temperature is necessary to achieve an adequate result of the relative density.

The second way to determine the relative density is to prepare several polished cross sections of the part. By the help of a microscope it is possible to evaluate the porosity of the sample (Fig. 6). For a good prediction of the over-all relative density it is necessary to make many pictures of several cross-sections. With respect to the manufacturing process conditions it is necessary to consider several building directions of the part. Therefore, the laboratory effort to measure the relative density is higher than the effort for calculation by Archimedes.

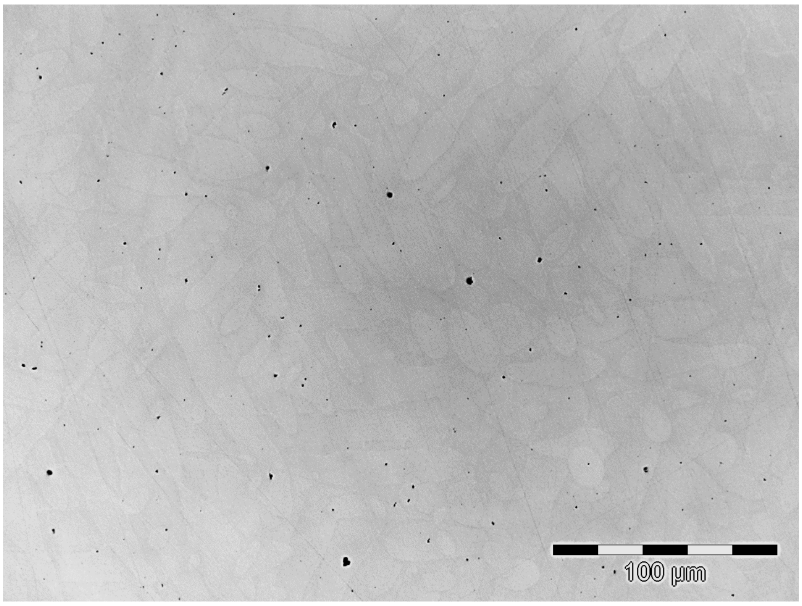

Fig. 6: Polished cross-section of an AlSi10Mg sample to verify process parameters and determine the existing porosity by microscopy. The black spots illustrate almost round pores. This sample has a relative density of about 95%.

By adjusting the parameters of the additive manufacturing process (e.g. laser power, scan speed, hatch distance, layer thickness …) a perfect dataset of parameters would be determined to build parts with a relative density near to 1. With a high relative density it is possible to print lightweight lattice structures without failures. Furthermore, it is possible to characterise the mechanical properties of produced lattice structures. Therefore, for an excessive use of optimisation methods like lattice optimisation and additive manufacturing it is necessary to understand the whole processing route to achieve good results [14, 15, 16].

7. Summary

Since many years, numerical optimisation methods are used to develop lightweight structures for different types of mechanical issues. The additive manufacturing presents, an alternative manufacturing technology to produce the results out of the optimisation tool. Nowadays, a draftsman has to break the "old" borders of construction and to use the full potential of this technology. The complexity of geometries should not be a limit for the development of new products.

The importance of additive manufacturing becomes even more manifested by:

- Combination of different optimisation methods to generate complex shapes
- Correct use of the optimisation methods
- Deep understanding of the additive manufacturing process
- Good knowledge in material science and mechanical guidelines for design
- Evaluate process parameter to validate the process
- Topology optimisation gives an idea of future shapes for additive manufacturing
- Implementation of bionic methods
- Have visions like "build light as a feather"

References

[1] B. Klein: Leichtbau-Konstruktion. Wiesbaden: Springer Fachmedien Wiesbaden 2013
[2] G. Reitter: Leichtbau durch Sicken. http://www.4ming.de/index.php/leichtbau-durch-sicken-fachbuch?start=5, Accessed May 2016
[3] A. Baumgartner, L. Harzheim, C. Mattheck: SKO (soft kill option). The biological way to find an optimum structure topology. International Journal of Fatigue (1992) 14 6, S. 387–393
[4] C. Mattheck, D. Reuschel: Design nach der Natur. Physik in unserer Zeit (1999) 30 6, S. 253–258
[5] C. Mattheck, K. Bethge: Zur Plausibilität der Methode der Zugdreiecke. Materialwissenschaft und Werkstofftechnik (2005) 36 11, S. 748–749
[6] C. Mattheck: Teacher tree. The evolution of notch shape optimization from complex to simple. Engineering Fracture Mechanics (2006) 73 12, S. 1732–1742
[7] Altair: Hyperworks 14. http://www.altairhyperworks.de/hw14/, Accessed May 2016
[8] L.J. Gibson: Biomechanics of cellular solids. Journal of biomechanics (2005) 38 3, S. 377–399
[9] L.J. Gibson, M.F. Ashby: Cellular solids. Structure and properties. Cambridge solid state science series. Cambridge, New York: Cambridge University Press 1999
[10] Autodesk: Within. http://www.autodesk.com/products/within/overview, Accessed May 2016
[11] Materialise: 3-matic. http://software.materialise.com/3-matic, Accessed May 2016
[12] D. Gu., W. Meiners, K. Wissenbach, R. Poprawe: Laser additive manufacturing of metallic components. Materials, processes and mechanisms. International Materials Reviews (2013) 57 3, S. 133–164
[13] G. Adam, D. Zimmer: Design for Additive Manufacturing—Element transitions and aggregated structures. CIRP Journal of Manufacturing Science and Technology (2014) 7 1, S. 20–28
[14] A. Ilin, R. Logvinov, A. Kulikov, A. Prihodovsky, H. Xu, V. Ploshikhin, B. Günther, F. Bechmann: Computer Aided Optimisation of the Thermal Management During Laser Beam Melting Process. Physics Procedia (2014) 56, S. 390–399
[15] A. Wegner, G. Witt: Correlation of Process Parameters and Part Properties in Laser Sintering using Response Surface Modeling. Physics Procedia (2012) 39, S. 480–490
[16] H. Krauss, M.F. Zaeh: Investigations on Manufacturability and Process Reliability of Selective Laser Melting. Physics Procedia (2013) 41, S. 815–822

Marie Cronskär[1], Axel Bergström[1], Karl Neulinger[1]

ADDITIVE MANUFATCURING ON THE BORDER OF CROSSING THE CHASM TO A MAINSTREAM MARKET – CASE STUDIES FROM THE NORTH

Abstract
Additive manufacturing (AM) is constantly getting more attention within industry as it has developed from prototyping to manufacturing. Some claim that it will be the 3:rd industrial revolution but the technology is still in its infancy and huge efforts are needed before it can be utilized in a broad context within industry. The possibilities with the technology are constantly being explored and developed, and some of the business drivers today could be described by for example *"complexity for free"*, *"increased functionality"* and *"customized production"*.

Despite the development of the actual technology, there are more barriers to overcome before the technology truly can be defined as an industrial revolution and one major part of this is to explain and convince the market that the technology can assist in the company growth. So crossing the chasm to a mainstream market is challenging and this paper presents some successful case studies from the company Additive Innovation & Manufacturing Sweden AB (AIM Sweden) where different application experts have cooperated to fully utilize to possibilities of AM in metal, and specifically the Electron Beam Melting ® method.

Electron beam melting, Ti6Al4V, Bionic design, Tooling

[1] AIM Sweden AB

Aziz Huskic [1], Norbert Wild[2]

Use of selective laser melting and laser cladding for the manufacturing of hot stamping tool.

Abstract

Selective Laser Melting (SLM) allows more flexibility and a higher automation level in tool engineering. One of the main advantages of this method is the production of complex geometries. It is possible to directly manufacture complex parts components with integrated functions and undercuts without using tools. The use of injection moulds and tool inserts with complex and conformal cooling channels, which are produced by SLM, increase the productivity and quality of the parts. Another application is the construction of forming tools. The advantage of conformal cooling can also be used for hot stamping tools. Hot stamping is an innovative process by which advanced ultra high strength steel is formed into complex shapes more efficiently than with traditional cold stamping. The process involves the heating of the steel blanks until they are malleable, followed by formation and then rapid cooling in specially designed tools, creating in the process a transformed and hardened material. The tool must be able to achieve a minimum cooling rate of 27 K/s to guarantee a complete martensitic transformation. The die must absorb and evacuate an amount of energy up to 100 kW by means of integrated cooling devices. Therefore hot stamping tools are made of hot work steel with very high thermal conductivity combined with a high wear resistance, for example HTCS 150 and CR7V-L. The processing of these steels with selective laser melting requires the preheating of metal powder. In this paper hot stamping tools are manufactured using SLM and investigated density, strength and toughness. Furthermore, the wear resistance of such hot stamping tools is investigated. In addition, the possibility of repair of hot stamping tools by laser cladding is shown.

[1] University of Applied Sciences Upper Austria, Stelzhammerstr. 23, 4600 Wels, AT
[2] FH OÖ Forschung & Entwicklungs GmbH, AT